KU Leuven
Biomedical Sciences Group
Faculty of Medicine
Department of Development and Regeneration

FORMATION OF ENDOTHELIAL NETWORKS IN HUMAN TISSUE-ENGINEERED SKELETAL MUSCLE

Dacha Gholobova

Dissertation presented in partial fulfilment of the requirements for the degree of
Doctor in Biomedical Sciences

Promoter:	Prof. Dr. Lieven Thorrez
Co-promoters:	Prof. Dr. Pieter Annaert
	Prof. Dr. Maurilio Sampaolesi
Chair:	Prof. Dr. Simon De Meyer
Jury members:	Prof. Dr. Evie Vereecke (secretary)
	Prof. Dr. Hans Van Oosterwyck
	Prof. Dr. Katrien De Bock
	Dr. Heidi Declercq

May 2019

© DACHA GHOLOBOVA
Uitgegeven in eigen beheer, DACHA GHOLOBOVA, GENT-BRUGGE
Cover image by Hanns Schimansky © 2019 Courtesy Galerie Inga Kondeyne

Alle rechten voorbehouden. Niets uit deze uitgave mag worden verveelvoudigd, opgeslagen in een geautomatiseerd gegevensbestand, of openbaar gemaakt, in enige vorm of op enige wijze, hetzij elektronisch, mechanisch, door print-outs, kopieën, of op welke wijze dan ook, zonder voorafgaande schriftelijke toestemming van de uitgever.

All rights reserved. No part of the publication may be reproduced in any form by print, photoprint, microfilm, electronic or any other means without written permission from the publisher.

Table of contents

Table of contents ..... **i**

Summary ..... **v**

Samenvatting ..... **vii**

List of abbreviations ..... **ix**

1 Chapter 1 - General introduction **3**

1.1 Skeletal muscle 3
1.1.1 Structure *3*
1.1.2 Skeletal muscle injury and regeneration *5*
1.2 Clinical significance 7
1.3 Strategies to improve muscle regeneration and repair 9
1.3.1 Growth factors *9*
1.3.2 Stem cells *9*
1.3.2.1 Satellite cells and progenitors *9*
1.3.2.2 Mesenchymal stem cells *10*
1.3.2.3 Vessel-associated stem cells *11*
1.3.2.4 Pluripotent stem cells (PSC) *12*
1.3.2.5 Non-myogenic cells *13*
1.3.3 Skeletal muscle tissue engineering (SMTE) *13*
1.4 Prevascularization 15
1.4.1 Vascularization approaches of tissue engineered constructs: angiogenesis and vasculogenesis *15*
1.4.2 Endothelial cells in prevascularization *17*
1.5 Prevascularization in current SMTE strategies 18
1.5.1 Decellularized tissue as bioscaffold *18*
1.5.2 Hydrogels *19*
1.5.3 Polymer and naturally-derived scaffolds *20*
1.5.4 Scaffold- and hydrogel-free approaches *23*
1.6 Applications of SMTE 23
1.7 References 25

2 Chapter 2 - Aims **39**

3 Chapter 3 - Endothelial network formation within human tissue-engineered skeletal muscle

3.1 Abstract 43
3.2 Introduction 45
3.3 Methods 47
3.3.1 Cell culture *47*
3.3.2 3D tissue construct *47*
3.3.3 Histology *47*
3.3.4 Thickness measurements *48*
3.3.5 Immunocytochemistry *48*
3.3.6 Whole-mount immunofluorescence staining and confocal microscopy *48*
3.3.7 Confocal imaging and data analysis *49*
3.3.8 Statistics *49*
3.4 Results 51
3.4.1 Aligned myofibers are formed in fibrin BAMs cultured in EGM-2 ..... *51*

3.4.2 Formation of aligned myofibers and endothelial networks in fibrin BAMs with a coculture of muscle cells and HUVECs ... *54*
3.4.3 30% HUVECs suffice to induce endothelial networks between aligned myofibers ... *55*
3.4.4 Matrigel impacts myofiber distribution, but does not improve myofiber and endothelial network formation ... *57*
3.5 Discussion ... 61
3.6 Acknowledgments ... 65
3.7 Disclosure Statement ... 65
3.8 Supplementary materials ... 66
3.9 References ... 71

4 Chapter 4 - Functional evaluation of prevascularization in one-stage versus two- stage tissue engineering approach of human bio-artificial muscle

4.1 Abstract ... 77
4.2 Introduction ... 79
4.3 Methods ... 81
4.3.1 Cell culture ... *81*
4.3.2 Tissue-engineering of BAMs ... *82*
4.3.3 Thickness measurements ... *82*
4.3.4 In vivo implantation of BAMs ... *82*
4.3.5 Whole mount immunofluorescence staining ... *83*
4.3.6 Confocal imaging ... *83*
4.3.7 Histology ... *84*
4.3.8 Data analysis ... *84*
4.3.9 Detection of anastomosis ... *84*
4.3.10 Quantitative real-time PCR ... *85*
4.3.11 Statistics ... *86*
4.4 Results ... 87
4.4.1 In vitro BAM formation ... *87*
4.4.2 In vitro myotube formation in prevascularized BAMs ... *87*
4.4.3 In vitro endothelial network formation in BAM-1s and BAM-2s ... *92*
4.4.4 In vivo implantation and explantation ... *94*
4.4.5 In vivo myotube maintenance ... *94*
4.4.6 In vivo vascularization and anastomosis ... *95*
4.4.7 Extracellular matrix remodeling after implantation ... *97*
4.5 Discussion ... 99
4.6 Author Contributions ... 103
4.7 Acknowledgments ... 103
4.8 Disclosure Statement ... 103
4.9 Supplementary materials ... 104
4.10 References ... 107

5 Chapter 5 - Human tissue-engineered skeletal muscle: a novel 3D in vitro model for drug disposition and toxicity after intramuscular injection

5.1 Abstract ... 113
5.2 Introduction ... 115
5.3 Methods ... 119
5.3.1 Cell culture ... *119*
5.3.2 Human muscle strip isolation ... *119*
5.3.3 Bioengineering of BAMs ... *120*
5.3.4 Injected compounds ... *120*
5.3.5 Microinjection ... *121*
5.3.6 CDFDA incubation in 2D cell culture ... *122*

5.3.7 Creatine kinase measurement ... *122*
5.3.8 Detection of CDF fluorescence ... *122*
5.3.9 Detection of NanoLuc® substrate luminescence ... *123*
5.3.10 Immunocytochemistry ... *123*
5.3.11 Whole mount immunofluorescence staining ... *124*
5.3.12 Confocal imaging and data analysis ... *124*
5.3.13 Quantitative real-time PCR ... *124*
5.3.14 Statistics ... *126*
5.3.15 Data Availability ... *126*
5.4 Results ... 127
5.4.1 Optimization of the microinjection procedure ... *127*
5.4.2 Characterization of myoblast (M) and mixed muscle (MM) cell populations ... *128*
5.4.3 Myofiber formation in BAMs ... *129*
5.4.4 Muscle gene expression ... *130*
5.4.5 The 3D BAM model adequately reflects compound toxicity by creatine kinase release 131
5.4.6 Injected CDFDA is released over a time course of 40 hours in BAM ... *132*
5.4.7 Injected pro-NanoLuc® substrate is released over a time course of 40 hours ... *134*
5.5 Discussion ... 137
5.6 Authors' contributions ... 142
5.7 Acknowledgements ... 142
5.8 Declaration of interest ... 142
5.9 Supplementary materials ... 143
5.10 References ... 147

6 Chapter 6 - General discussion

6.1 Bio-artificial muscle ... 153
6.1.1 Prevascularization: introducing endothelial cells to the BAM model ... *155*
6.1.2 In vitro screening ... *158*
6.2 Future perspectives ... 159
6.3 Conclusion ... 162
6.4 References ... 165

APPENDIX

Author affiliations ... 173

Biography ... 175

Bibliography ... 177

Publications ... 177
Oral presentations ... 177
Poster presentations ... 178

Travel grants ... 178

Contribution to teaching ... 178

Courses ... 178
Guidance master students ... 179
Guidance bachelor students ... 179
Guidance summer interns ... 179

Acknowledgments ... 181

Personal contributions ... 185

Summary

Skeletal muscle is a complex tissue with a capacity to regenerate upon injury. However, when skeletal muscle loss is beyond the regenerative capacity of skeletal muscle, the muscle repair process fails and scar tissue replaces the damaged area with resultant functional impairment. Current treatments have several disadvantages and new strategies are being explored, such as skeletal muscle tissue engineering. The aim is to reproduce the native structure and function of muscle *in vitro* and transplant this tissue in the damaged area. Besides applications in regenerative medicine, there are many other applications in which tissue-engineered skeletal muscle can be useful. Some examples are the use as an *in vitro* model for studying myogenesis, myopathology or molecular pathways or implementation as *in vitro* preclinical model for drug-screening and toxicity testing of compounds.

The main goal of this project is development, characterization and optimization of 3D *in vitro* tissue-engineered human skeletal muscle tissue. Existing techniques involve culturing and differentiation of myogenic (stem) cells on natural or synthetic scaffolds. These techniques often result in non-aligned myofibers. Alignment of the myofibers is important for directional force generation, the principal function of skeletal muscle. In our lab, human muscle progenitor cells are engineered in a 3D extracellular fibrin matrix and grown in a custom-made mold with 2 attachment points, serving as artificial tendons. The resulting bio-artificial muscle (BAM) is about one millimeter thick and consists of aligned multinucleated myofibers. However, to create tissue-engineered constructs with a thickness exceeding the millimeter size, perfusion of the construct is essential to avoid cell death by lack of oxygen and nutrients. In this project, we have developed two approaches to introduce vascular networks *in vitro* in the 3D muscle tissue, the so-called prevascularization. To prove functionality of *in vitro* engineered endothelial networks, prevascularized BAMs were implanted subcutaneously in mice for 14 days. *In vivo* anastomosis and perfusion of engineered endothelial networks with host vessels was shown. In addition we have discussed how prevascularization in turn influences the survival and integration of a tissue-engineered construct *in vivo*. Furthermore, the BAM approach has been evaluated as a preclinical model for intramuscular drug injection. We have shown that the BAM is an adequate model to assess compound toxicity, retention, release and compound metabolization. To conclude, the BAM model is a promising tool, but several challenges need to be addressed in order to translate the BAM model into the clinic for regenerative medicine or towards drug development.

Samenvatting

Skeletspierweefsel wordt gekenmerkt door zijn intrinsiek herstelmechanisme bij weefselschade. Echter, wanneer de spierschade te groot is, faalt het spierherstel en wordt er littekenweefsel gevormd, wat resulteert in functie verlies. De huidig toegepaste therapie heeft verscheidene nadelen en er is nood aan nieuwe methodieken. Skeletspierweefsel engineering kan een alternatief bieden. Het doel is aanmaak van skeletspierweefsel *in vitro* dat zo goed mogelijk de structuur en functie weerspiegelt van *in vivo* spier. Naast toepassingen in de regeneratieve geneeskunde zou dit model gebruikt kunnen worden als een *in vitro* model voor de studie van myogenese, myopathologie en als *in vitro* testsysteem voor geneesmiddelen.
Het hoofddoel van dit project is het ontwerpen, karakteriseren en optimaliseren van een *in vitro* 3D model voor humaan skeletspierweefsel. Bestaande technieken voor aanmaak van *in vitro* spierconstructen zijn gebaseerd op de kweek en differentiatie van myogene (stam)cellen op zowel natuurlijke als synthetische (al dan niet biodegradeerbare) draagstructuren. Deze technieken resulteren niet altijd in een structuur waarin de spiervezels eenzelfde lengterichting vertonen. Alignering van spiervezels is belangrijk voor de functie van een spier, namelijk directionele krachtgeneratie. In ons labo wordt alignering bekomen door zelf-organisatie van differentiërende humane primaire myoblasten in een fibrine hydrogel suspensie, in moules met 2 aanhechtingspunten. Het resulterend bio-artificieel spierconstruct is ongeveer één millimeter dik en bevat gealigneerde meerkernige spiervezels. Ze verschillen echter nog van *in vivo* skeletspieren door afwezigheid van (i) innervatie, (ii) aanhechting aan pezen en (iii) een vasculair systeem. De integratie van een vasculair netwerk is van belang om celoverleving en functionaliteit te verzekeren in grotere constructen. In dit onderzoek werden twee strategieën nagegaan om vasculaire netwerken te integreren in het 3D spierconstruct, de zogenaamde prevascularizatie. Om de functionaliteit te testen van de *in vitro* aangemaakte vasculaire netwerken, werden geprevascularizeerde spierconstructen subcutaan geïmplanteerd in muizen voor 14 dagen. Anastomose van de ingebrachte netwerken met de gastheer bloedvaten en perfusie werd aangetoond *in vivo*. Daarbovenop toonde één van de twee weefsel engineering strategieën een betere spiervezelbehoud in het construct te hebben bij implantatie. Daarbovenop werd het spierconstruct geëvalueerd als model voor intramusculair toe te dienen geneesmiddelen. We hebben kunnen aantonen dat het spiermodel geschikt is om toxiciteit, retentie, vrijgave en spierspecifiek metabolisme na intramusculaire (IM) injectie van werkzame stoffen te evalueren.

We kunnen besluiten dat het spierconstruct een veelbelovend model is voor fundamenteel onderzoek maar ook voor regeneratieve toepassingen en geneesmiddelenontwikkeling. Om het spiermodel dichter te brengen bij toepassingen moeten er nog verscheidene uitdagingen worden aangegaan.

List of abbreviations

2D	: two dimensional
3D	: three dimensional
ADSC	: adipose derived stem cell
AP	: alkaline phosphatase
AV	: arterio-venous
BAM	: bio-artificial muscle
BAM-1s	: one stage bio-artificial muscle
BAM-2s	: two stage bio-artificial muscle
BAM-M	: bio-artificial muscle with myoblasts only
BAM-MM	: bio-artificial muscle with a mixed muscle cell population
bFGF	: basic fibroblast growth factor
BM	: bone marrow
BSA	: bovine serum albumin
CD	: cluster of differentiation
CDF	: 5(6)-carboxy-2',7'-dichlorofluorescein
CDFDA	: 5(6)-carboxy-2',7'-dichlorofluorescein diacetate
CK	: creatine kinase
CMV	: cytomegalovirus
DAPI	: 4',6-diamidino-2-phenylindole
DMEM	: dulbecco's modified eagle medium
DNA	: deoxyribose nucleic acid
DPBS	: dulbecco's phosphate-buffered saline
DTT	: dithiothreitol
ECM	: extracellular matrix
EDTA	: ethylenediaminetetraacetic acid
EGM	: endothelial cell growth medium
ECFC	: endothelial colony-forming cell
ELISA	: enzyme linked immunosorbent assay
ESC	: embryonic stem cell
FBS	: fetal bovine serum
FGF	: fibroblast growth factor
GAPDH	: glyceraldehyde-3-Phosphate Dehydrogenase
GFP	: green fluorescent protein
HBSS	: Hank's balanced salt solution
hEGF	: human epidermal growth factor
HGF	: hepatocyte growth factor
HIV	: human immunodeficiency virus
HSP90AB1	: heat shock protein 90 kDA alpha, class B, member 1
HUVEC	: human umbilical vein endothelial cell
IGF	: insulin growth factor
IL	: interleukin
IM	: intramuscular
iPSC	: induced pluripotent stem cell
IVIVE	: in vitro in vivo extrapolation
M	: monoculture of human myoblasts
MAB	: mesoangioblast
MEF	: mouse embryonic fibroblast

MHC : myosin heavy chain
miRFP : monomeric near-infrared fluorescent protein
MM : human mixed muscle cell population
MPC : muscle progenitor cell
MRF : myogenic regulatory factor
MRP : multidrug resistance-associated protein
MSB : martius scarlet blue staining
MSC : mesenchymal stem cell
MTJ : myotendinous junction
MyoG : myogenin
NHDF : normal human dermal fibroblast
NK : natural killer cell
NMJ : neuro-muscular junction
NO : nitric oxide
NOD/SCID : nonobese diabetic/severe combined immunodeficiency
NSAID : non-steroidal anti-inflammatory drug
P/S : penicilin/streptomycin
Pax : paired box
PBPK : physiologically based pharmacokinetic modeling
PBS : phosphate-buffered saline
PCR : polymerase chain reaction
PDGFR : platelet-derived growth factor receptor
PEG : polyethylene glycol
PFA : paraformaldehyde
PFP : platelet free plasma
PGS : poly(glycerol sebacate)
PLGA : poly(lactic-co-glycolic acid)
PLLA : poly(L-lactic acid)
PSC : pluripotent stem cells
RBC : red blood cell
REST : relative expression software tool
RGD : arginine glycine aspartic acid
RIPA : radioimmunoprecipitation assay
RNA : ribonucleic acid
RPL13A : ribosomal protein L13a
RT : room temperature
SC : satellite cell
SCID : severe combined immune deficiency
SIS : small intestinal submucosa
SkFM : skeletal muscle fusion medium
SkGM : skeletal muscle growth medium
SMA : smooth muscle actin
SMTE : skeletal muscle tissue engineering
TA : tibialis anterior (muscle)
TGF : transforming growth factor
TM : tropomyosin
UEA : Ulex Europaeus agglutinin
VEGF : vascular endothelial growth factor
VEGFR : vascular endothelial growth factor receptor

CHAPTER 1

GENERAL INTRODUCTION

Parts of this chapter are adapted from:
Gholobova D, Terrie L, Gérard M, Thorrez L (2019) Vascularization of tissue-engineered skeletal muscle constructs. *Biomaterials* (submitted)

1 General introduction

1.1 Skeletal muscle

1.1.1 Structure

In adult humans, there are roughly 650 skeletal muscles that account for approximately 40 % of the total body weight. The tissue has an important role in body movement, thermoregulation and basal energy metabolism (1, 2). 85 % of the tissue is composed of bundles of aligned multinucleated myofibers, responsible for muscle contraction and thus movement. The other 15 % comprise vasculature, nerves and connective tissue. Myofibers have a cylindrical shape with a diameter varying from 10 to 100 µm, and can reach a length up to 45 cm (2, 3). This elongated shape is determined by the organization of myofibrils, abundantly present in the sarcoplasm (Figure 1.1). The myofibrils are composed of thick and thin myofilaments, myosin and actin respectively, and are arranged repeatedly along the myofiber in sarcomeres, giving the characteristic striation pattern of skeletal muscle. Sarcomeres are the functional units of muscle fibers and are involved in muscle contraction. Besides contractile proteins, the sarcoplasm contains a mitochondrial network and the sarcoplasmic reticulum, close to the sarcolemma transverse tubular system (T-tubule) invaginations. This system is crucial for the conduction of nerve action potential to the myofiber via calcium (1) (Figure 1.1).

The highly organized skeletal muscle connective tissue, the extracellular matrix (ECM), plays an important role in muscle elasticity, force transmission, cell function and regeneration (4–7). The ECM of skeletal muscle is organized hierarchically into three fibrous layers: (i) the endomysium which surrounds a muscle fiber, is in connection with the sarcolemma, the muscle fiber membrane, (ii) the perimysium which surrounds myofiber bundles, the fascicles, and (iii) the epimysium which surrounds the entire muscle (4) (Figure 1.1). The endomysium layer contains capillaries, necessary for nutrient and oxygen supply and metabolic waste removal of myofibers, and nerve branches (Figure 1.1). The perimysium and epimysium are connected with the tendon in the myotendinous junction, which is important in force transmission (Figure

1.1) (4). Forces generated in the myofibers are transmitted from the contractile myofilament apparatus to the muscle ECM by integrins and the dystrophin-glycoprotein complex (8).

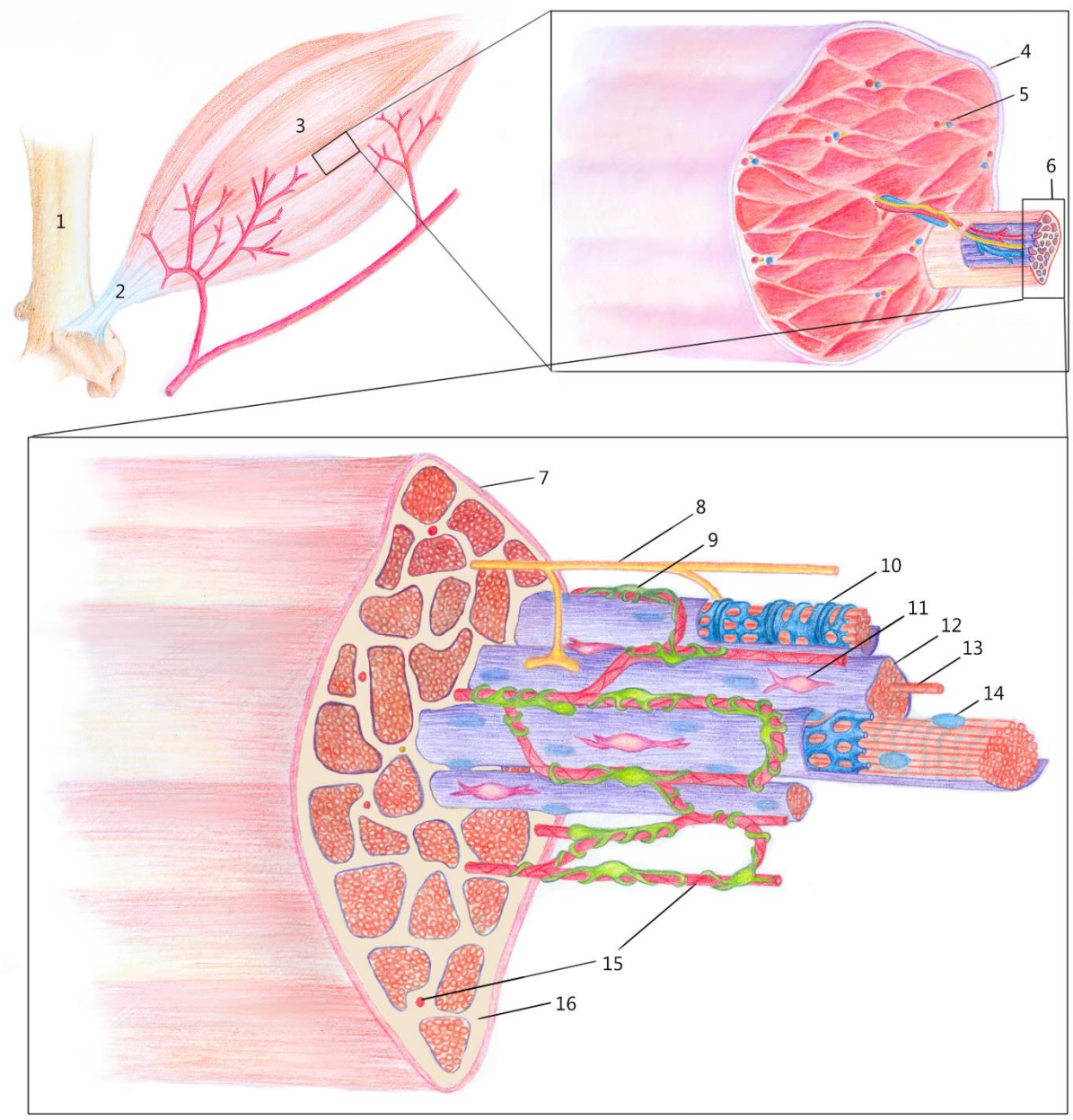


Figure 1.1. Structure of skeletal muscle. 1. bone, 2. tendon, 3. muscle, 4. epimysium, 5. artery (red), vein (blue), nerve (yellow), 6. fascicle, 7. perimysium, 8. nerve, 9. pericyte 10. sarcoplasmic reticulum, 11. satellite cell, 12. sarcolemma, 13. myofibril, 14. muscle cell nucleus 15. capillary 16. endomysium (Figure adapted from (9)).

Collagen is the major structural protein in skeletal muscle ECM. It accounts for 1-10 % of muscle dry weight and the fibrillar types I, III and IV predominate in adult skeletal muscle ECM (4), with type IV mainly in the basal membrane surrounding each muscle fiber (4). Other ECM proteins include fibronectin, laminin, elastin and various proteoglycans (4). Also, ECM binds

non-matrix molecules such as growth factors. Furthermore, native skeletal muscle ECM plays an important role in muscle development during embryogenesis and regeneration. This role during embryogenesis is facilitated by directly influencing cell behaviour through ECM-specific receptors on the cell surface such as integrins (7). However, the storage and postponed release of growth factors by ECM can also indirectly influence cell behaviour through growth factor signalling pathways. Several of these processes occurring during embryonic organogenesis, also take place following injury (8).

1.1.2 Skeletal muscle injury and regeneration

The intrinsic regeneration capacity of skeletal muscle allows repair of damaged muscle tissue in small tissue injuries. The central role in muscle regeneration is played by the muscle stem cells known as satellite cells (SC), adult muscle stem cells situated between the basement membrane of the muscle fiber and the sarcolemma. It is a heterogenous population of stem and progenitor cells that is characterized by early myogenic transcription factors, mainly by Paired box 7 (Pax7) and Pax3, cell receptors such as Tie-2 and c-Met, different adhesion molecules such as CD56 and α7 integrin and others (reviewed in (28)). Satellite cells are in quiescence until required for growth or repair. Upon activation, satellite cells exit quiescence and start to proliferate. Satellite cells divide predominantly asymmetrically to replenish the satellite cell pool or to provide progenitors (10). Activated satellite cells can differentiate into single-nucleated myoblasts, that subsequently can fuse to form multinucleated myotubes and/or fuse with damaged myofibers (8). This differentiation event is defined by the basic helix-loop-helix transcription factors MyoD1, Myf5, myogenin and MRF4, the myogenic regulatory factors (MRF), and recapitulates to a certain level skeletal muscle development (6) (Figure 1.2). Once activated, upregulated Myf5 expression is present in proliferating satellite cells, but not in quiescent state, and decreases with further satellite cell differentiation, followed by MyoD expression committing to myogenic differentiation (6, 11, 12). Downregulation of MyoD at this stage, results in recovery of quiescence and contributes to maintenance of a quiescent satellite cell pool. Upregulation of MyoD promotes myogenin and MRF4 expression, leading to terminal myogenic commitment and fusion (Figure 1.2). Terminal differentiation of regenerating myofibers into mature fibers results in the abundant expression of genes such as myosin and actin (6).

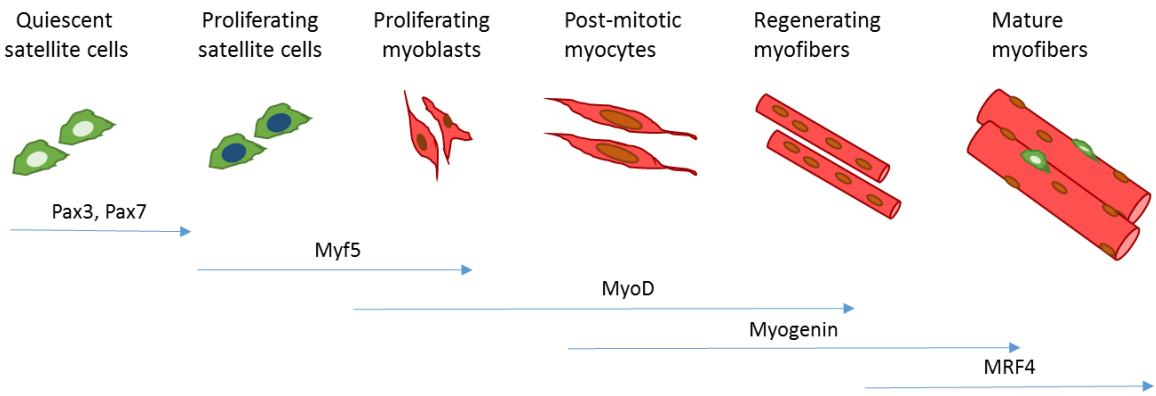


Figure 1.2. Adult myogenesis (Figure adapted from (6)).

Skeletal muscle regeneration is divided into five interrelated and time-dependent phases (Figure 1.3): degeneration and necrosis, inflammation, regeneration, remodeling and maturation (6, 8). Upon damage of myofibers following exercise, injury or disease, myofibers are undergoing necrosis. Release of pro-inflammatory cytokines from the skeletal muscle niche and necrotized tissue recruits inflammatory cells, such as neutrophils and macrophages, which clear damaged cell debris during the inflammatory phase. Recruited inflammatory macrophages (M1) experience a phenotypic and functional switch to pro-remodeling M2 macrophages by a set of cytokines interleukin (IL)-4, IL-10, and IL-13 (13). ECM has been reported to play a crucial role in this transition by providing biologic cues to the macrophages following injury (14). Macrophages stimulate satellite cells to exit the quiescent state and divide asymmetrically (6, 15). Insulin growth factor-1 (IGF-1), secreted by M2 macrophages, initially stimulates SC activation and proliferation, but also induces terminal differentiation of muscle cells to multinucleated myotubes in a later stage of the regeneration phase (16). Moreover, the degradation of the ECM by upregulated matrix metalloproteinases triggers the release of the growth factors stored in the ECM. These growth factors include the hepatocyte (HGF) and fibroblast growth factors (FGF), which act on the satellite cells, inducing their activation and proliferation, while inhibiting their differentiation (13). At the same time, resident fibro-adipogenic progenitors deposit extracellular matrix (ECM) at the injured myofiber region to form connective scar tissue at the site of injury and capillary ingrowth takes place (8). Finally, the two last phases in muscle tissue regeneration, involves scar tissue remodeling and myofiber maturation. In its initial phase, connective scar tissue formation supports skeletal muscle repair serving as scaffold for regenerating myofibers and as guide for the formation of neuromuscular junctions (NMJs), a chemical synapse between a motor neuron and muscle fiber involved in transmission of electrical signals (6). However, uncontrollable collagen deposition by fibroblasts results in fibrosis and loss of function. Transforming growth factor-β (TGF-β) is

known to play an important role in fibrosis and is therefore an interesting target in muscle injury therapies (17, 18). Muscle repair is completed when injured myofibers regain an organized contractile apparatus, when functional recovery is established by innervation and when the blood supply is restored (6, 8). Namely, newly formed NMJs between axons of neurons and the regenerated myofibers are essential for muscle fiber maturation and function, but not for the early phases of regeneration (19). After muscle injury, hypoxia occurs due to damage of blood vessels and initial revascularization takes place, which is essential for muscle regeneration. Newly formed capillaries sprout from uninjured blood vessels and invade the regeneration site to provide oxygen and nutrients. Macrophages, which are important in muscle repair as mentioned above, also have an important role in vascular remodeling (20–22). Furthermore, ECM and its associated growth factors, released upon ECM degradation, (e.g. VEGF-A and platelet-derived growth factor-BB) may also regulate each step of the angiogenic cascade which is needed to form new blood vessels after injury (23, 24). Without the restoration of blood supply, muscle repair is incomplete and results in fibrosis (17).

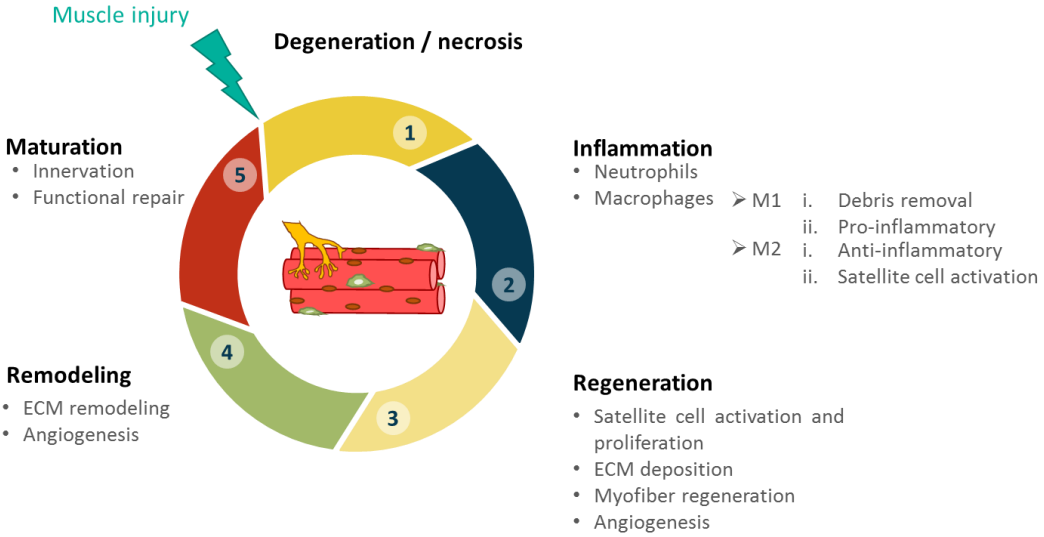


Figure 1.3. Skeletal muscle regeneration upon injury (Figure adapted from (6)).

1.2 Clinical significance

Skeletal muscle is a complex tissue with a capacity to regenerate upon injury. However, when skeletal muscle loss is beyond the regenerative capacity of skeletal muscle, the muscle repair process fails and scar tissue replaces the damaged area with resultant functional impairment (8, 25). This is the case in volumetric muscle loss. Myopathies, traumatic injuries, muscle denervation, sarcopenia and muscle ablation upon surgery are the main causes of muscle loss and function (26). Skeletal muscle injuries are prevalent in sports, in civilian and military

trauma patients. Among 14.5 million evacuated US military personnel from war in 2001 – 2013, an average of 77 % showed musculoskeletal injuries (27, 28), of which a great part was corresponding with soft tissue wounds (29). As for civilians, an average of 150,000 US patients per year has open fractures of which a majority with damage to surrounding soft tissue (28). Despite the clinical importance, no standard surgical or regenerative care exists for volumetric muscle loss. For less severe muscle injuries early mobilization, physical rehabilitation and Non-Steroidal Anti-Inflammatory Drugs (NSAID) therapy result in acceptable functional outcome (30–32). The current procedure for severe volumetric muscle loss injuries involves muscle flap transplantation. An autologous muscle flap, which contains proper vasculature, is excised at a donor site and transplanted to the damaged muscle area. Unfortunately, donor site morbidity and poor survival and integration of donor tissue at the acceptor site is generally observed (33). Attempts are made to enhance the clinical outcome of flap transplantations. Choosing the proper donor site, can reduce donor site complications (34). Another example of improving donor site outcome is the incorporation of a mesh at the donor site after flap excision to prevent hernia (35). Improving vasculature at the site of injury by elongating vasculature from a proximal area by use of vein grafts is another way to promote muscle flap success (36). However, all of these approaches are still based on removal of muscle from a donor site and thus do not solve the problem of donor site morbidity. It is clear that despite the efforts made in recent years, there is a need to develop alternative strategies for muscle flap transplantation in volumetric muscle loss.

Besides volumetric muscle loss, a wide range of myopathies affects the daily life of many people (37, 38). Myopathies are a group of diseases affecting skeletal muscle tissue and are classified as inherited (e.g. muscular dystrophies) or acquired (e.g. inflammatory) myopathies (39, 40). Current therapy focusses mainly on managing symptoms and inflammatory suppression. A lot of research has been conducted to develop therapies that tackle the cause of the disease and the pathophysiology, and further research is required to bring the knowledge from pre-clinical setting to translation into the clinics (39). Development of skeletal muscle models by skeletal muscle tissue engineering mimicking myopathies *in vitro* can facilitate this research process.

1.3 Strategies to improve muscle regeneration and repair

1.3.1 Growth factors

Skeletal muscle regeneration is a highly orchestrated process, in which secreted growth factors play a variety of roles (13). These biologically active molecules, produced by the injured tissue and invading cells at the inflammatory site, influence the regenerative response. Hepatocyte growth factor (HGF), fibroblast growth factor (FGF), platelet-derived growth factor (PDGF) and insulin-like growth factor (IGF), are of particular interest in skeletal muscle repair and regenerative medicine.

HGF, FGF and PDGF are known to regulate satellite cell activation, proliferation and migration, and inhibiting further differentiation (8). Prolonged release of HGF from a fibrin-based scaffold improved skeletal muscle regeneration in a volumetric muscle loss injury model and enhanced the force production of muscle tissue (41). Another growth factor, vascular endothelial growth factor (VEGF), is known to enhance skeletal muscle repair, mainly by stimulating reperfusion of ischemic limbs (42). An injectable hydrogel system can provide a temporal controlled release of VEGF and targeted delivery over 28 days (43). IGF, in particular, is a promising therapeutic agent in skeletal muscle regeneration, since this growth factor stimulates hypertrophy and myogenic differentiation (44). In a mouse model, direct injections of IGF enhanced myogenic healing in lacerated muscles (45). As the healing cascade is complex, it is unlikely a single growth factor can restore regeneration. In this regard, targeting myogenesis and angiogenesis, by simultaneous delivery of IGF and VEGF highly promoted functional outcome in ischemic muscle (46). A drawback of growth factors is that they have short half-lives and their rapid blood clearance. Therefore high concentrations of the factor are typically required. Tunable release by using appropriate scaffolds, can partly overcome these issues.

1.3.2 Stem cells

1.3.2.1 Satellite cells and progenitors

Satellite cells play a prominent role in skeletal muscle regeneration. Transplantation of satellite cells and its progenitors has long been explored as a promising approach for treatment of skeletal muscle disorders. Initially, it was shown that injection of healthy myoblasts could restore dystrophin expression in mdx mice (47). Subsequent clinical trials, in which allogeneic healthy human myoblasts were injected intramuscularly in dystrophic young boys muscles, were less successful (48, 49). Even recently, with improved injection protocols, outcomes of

clinical trials are still disappointing for skeletal muscle disorders (50). These experiments demonstrated the limited migratory and proliferative capacities of human myoblasts, as well as their limited life span *in vivo*. In stress urinary incontinence on the other hand, intrasphincter injection of autologous myoblasts showed functional improvement, increased quality of life and improved incontinence symptoms in woman after 18 months post-injection (51). Also in fecal incontinence treatment in a phase II study, autologous intrasphincter injection of myoblasts demonstrated a functional efficacy after 12 months (52). Use of satellite cells looks promising not only for treatment of incontinence, but in skeletal muscle injuries as well (53, 54). Implantation of single intact myofibers into radiation-ablated muscles in mice or implantation of $CD56^{+}/CD29^{+}$ human satellite cells in myotoxin injured muscle demonstrated skeletal muscle regeneration (53, 54).

Satellite cells are isolated from muscle biopsies by enzymatic digestion or by single fiber explant culture (55). However only a small biopsy would be clinically feasible. To have a sufficient amount of cells for therapy, satellite cell expansion *in vitro* is needed. Unfortunately, SC expansion is limited due to a rapid decrease in myogenic potential and proliferative capacity of SC over time in culture (56). Therefore alternative cell sources with myogenic potential are being explored such as mesoangioblasts, pericytes, mesenchymal-derived stem cells (MSC) or pluripotent stem cell-derived myogenic progenitors (57–60).

1.3.2.2 Mesenchymal stem cells

Mesenchymal stem cells are multipotent stem cells able to differentiate into tissues of mesodermal origin such as cartilage, bone, adipose tissue and skeletal muscle (61). Adipose-derived mesenchymal stem cells (ADSC) are an abundant MSC source, resident in adipose tissue, which is an easy and abundant tissue type to isolate (62). *In vivo* implantation of undifferentiated ADSC in hind limb ischemia induced muscle injury contributed to regenerating muscle fibers (63). Comparing skeletal muscle regeneration in a latissimus dorsi muscle volumetric muscle loss defect upon implantation of decellularized bladder matrices seeded with cultured muscle progenitor cells (MPC) or ADSC resulted in similar regeneration outcome. However, in contrast to MPC, only a small portion of ADSC contributed to new myofiber formation, suggesting other mechanisms are involved in promoting regeneration (64). Bone-marrow (BM) derived MSC (BM-MSC) are another type of MSC. No difference in myogenic potential and proliferation rate was observed between BM-MSC and ADSC *in vitro* (65). Implantation of BM-MSC strongly improved muscle regeneration and functional recovery in

skeletal muscle injuries, but no contribution to newly formed myofibers was observed (66–68). BM-MSC injected at the site of muscle injury was shown to promote angiogenesis, to downregulate TGF-β, which is involved in fibrosis, to suppress inflammatory cytokine production and to upregulate anti-inflammatory cytokines, showing an indirect role in skeletal muscle regeneration (69). ADSC and BM-MSC are both an attractive cell source for transplantations, both having a low expression of major histocompatibility complex class I (MHC I) and lacking MHC II, involved in T-cell mediated rejection (70, 71). BM isolation is a painful procedure and only 0.01% of all cells isolated from BM isolate are MSCs, making ADSC a more attractive cell source for skeletal muscle therapies (72).

MSCs have been evaluated in clinical trials as treatment for fecal incontinence (73, 74). A phase I study demonstrated the safety and tolerability of allogeneic ADSC after injection into the anal sphincter muscles. However, no functional or structural benefits were observed (74). A similar study reported reported no significant functional improvement, but observed structural replacement of scar tissue with myofibers in fecal incontinence patients (73). A phase I clinical study is ongoing for treatment of a supraspinatus muscle lesion (NCT03068988).

1.3.2.3 Vessel-associated stem cells

Pericytes are vessel-associated stem cells with contractile properties, surrounding small blood vessels. They are characterized by markers such as α-smooth muscle actin (α-SMA), NG2, alkaline phosphatase (AP) and PDGFR-α and a lack of endothelial markers (58, 75). Pericytes can be isolated from skeletal muscle, placenta, pancreas and adipose tissue and can be expanded beyond 20 doublings (58, 76). During adult skeletal muscle regeneration, pericytes can differentiate to multinucleated myofibers and generate satellite cells by invading the satellite cell compartment (77). *In vitro*, pericytes formed multinucleated myotubes using myogenic differentiation medium and in coculture with myoblasts (58). *In vivo* intra-muscular administration in dystrophic mice showed engraftment of pericytes in regenerating myofibers, but less efficiently than injected satellite cells (58). The high proliferative capacity of pericytes *in vitro*, their myogenic potential and *in vivo* engraftment, together with the fact that pericytes can be isolated from adipose tissue, an easily accessible biopsy site, makes pericytes an attractive cell source for SMTE.

Mesoangioblasts (MAB) are another type of vessel-associated stem cells, isolated from explants of embryonic dorsal aorta or from juvenile vessels and express early endothelial cell markers such as CD34, Flk-1 and c-kit (78, 79). Adult mesoangioblasts belong to a subgroup of pericytes, lacking endothelial markers but expressing pericyte markers such as SMA, PDGFR-

α, PDGFR- β, NG2, and AP (80, 81). MABs proliferate well *in vitro*, preserving their multipotency and improve muscle function *in vivo* in dystrophic animal models by contributing to muscle regeneration by differentiation into muscle fibers (79, 82). Moreover MABs can be delivered systemically and are able to migrate to the skeletal muscle compartment (79). In the context of SMTE, mesoangioblasts as well as pericytes were mixed with a polyethylene glycol (PEG)-fibrinogen hydrogel and were implanted subcutaneously (59, 60) or intramuscularly (83) without prior *in vitro* culture. All studies showed the potential of pericytes and MABs to form muscle fibers *in vivo*. Implanted MABs even contributed to the reconstitution of a Pax7-positive satellite cell pool in these specific studies (59, 83). In humans, a first phase I/IIa clinical trial demonstrated that intra-arterial injections of human mesoangioblasts are safe, but display only very limited clinical efficacy and myogenic regeneration in Duchenne patients (84).

1.3.2.4 Pluripotent stem cells (PSC)

Pluripotent stem cells (PSC) such as embryonic stem cells (ESC) (85) and induced pluripotent stem cells (iPSC) (86) have an unlimited proliferative capacity and self-renewal and ability to differentiate into any cell type including MPC (87). ESCs are derived from the inner cell mass of blastocyst at an early stage embryo (85). The derivation of ESC raises ethical concerns because isolation requires destruction of an embryo (88). Moreover, immunogenic response (89) and tumorigenicity (90) may hinder their potential in regenerative medicine. To avoid teratoma formation, human ESCs were differentiated into muscle progenitor cells before transplantation in mice, resulting in long-term engraftment and myofiber regeneration (87, 91). The discovery of induced pluripotent stem cells (iPSCs), derived from adult cells (e.g. fibroblasts, adipocytes) and reprogrammed towards an embryonic stem cell (ESC)-like pluripotent state, enables the development of an unlimited source of a patient-specific / disease-specific cell pool for disease modelling and for patient-specific drug screening (86). Efforts are made to develop reproducible differentiation protocols of iPSCs towards skeletal muscle progenitors. Current approaches of myogenic progenitor development include genetic modification to induce overexpression of myogenic transcription factors such as MyoD, Pax 3 or Pax7 transcription factors (92–95). Several approaches were developed without genetic modification by mimicking myogenesis: induction of embryonic mesoderm, followed by myogenic induction with growth factors and small molecules (96, 97). Such PSC derived myogenic progenitors were able to form dystrophin positive muscle fibers in dystrophic animals and show potential in regenerative medicine (98). Also 3D artificial skeletal muscle from

human iPSCs from patients with muscular dystrophies may be promising as a human muscle model for disease modeling and therapy development (57).

1.3.2.5 Non-myogenic cells

During skeletal muscle regeneration, satellite cell dependent myogenesis is influenced by various cellular players (99). Non-myogenic cells play a critical role in myogenic cell differentiation, force generation and matrix remodeling *in vitro* (100, 101) as well as *in vivo* (102). Therefore addition of non-myogenic cells to myogenic progenitors has been explored as an approach to enhance skeletal muscle regeneration. Incorporating tissue-engineered tendons or motor neurons in tissue engineered muscle constructs resulted in the formation of, respectively, myotendinous junctions (103) or NMJs (104, 105). Addition of fibroblasts has been shown to enhance muscle protein expression (106) and myogenic differentiation (107) *in vitro*. A coculture of myoblasts and fibro-adipogenic progenitor cells, cells resident in the skeletal muscle niche, enhanced myogenic differentiation in comparison to a monoculture of myoblasts (108). Also addition of macrophages, that play an important role in muscle repair, showed to stimulate muscle-cell dependent myogenesis *in vitro* and *in vivo* (109). During myogenic regeneration upon injury, capillary sprouting and endothelial cells from circulating progenitor cells rebuild vasculature. *In vitro* coculture studies of endothelial cells and muscle progenitors, have shown that endothelial cells influence muscle cell proliferation and differentiation, mainly through paracrine factor secretion. Examples of paracrine factors are angiopoietin-1, IGF-1, HGF and VEGF (99). A recent study, attempting to explore the cellular crosstalk of these cells *in vivo*, have injected blocking antibodies or inhibitors against factors, secreted by endothelial cells into regenerating skeletal muscle (22). A decrease in myogenesis was observed. However, the blocked factors are not secreted by endothelial cells only, which makes it difficult to attribute the effects solely to endothelial cell secretion of these factors. In tissue engineering, addition of endothelial cells in muscle constructs has shown to improve host vessel ingrowth and muscle cell engraftment and therefore muscle regeneration upon implantation (110, 111).

1.3.3 Skeletal muscle tissue engineering (SMTE)

Scaffolds are suggested as a tool for more efficient stem cell delivery in regenerative medicine. An increased myogenic progenitor cell survival and migration was observed, when seeded on scaffolds compared to cell injections (112, 113). Moreover, a controlled microenvironment of injected myogenic cells demonstrated enhanced muscle regeneration and function (46).

In skeletal muscle tissue engineering (SMTE), cells with myogenic capacities are cultured and differentiated on natural or synthetic biodegradable scaffolds (114, 115). Cell sources with myogenic potential, suited for SMTE, are described in the 'Stem cells' section. SMTE strategies result in 3D skeletal muscle constructs with differentiated myofibers, which often are unaligned. Alignment is needed for force generation upon stimulation and can be achieved, when cells are subjected to a unidirectional force during fusion into myofibers.

The SMTE approach used in our lab is based on previous work of the Vandenburgh lab (116, 117). Satellite cells are isolated from human skeletal muscle biopsies and are expanded to several millions of myoblasts. These myoblasts are cast with a natural hydrogel, e.g. collagen or fibrin, in a silicone mold containing two attachment points. During the course of one week, the cell-gel mix contracts to form a muscle bundle with multinucleated myotubes well-aligned in the direction of the attachment points, the so-called bio-artificial muscle (BAM). The use of attachment points, which induces unidirectional tension during contraction of the hydrogel, is currently a common approach to attain alignment of myofibers (118–122). Alternatively, conductive micro-patterned scaffolds can be used to guide the orientation of the myofibers (123–125). In the study of Takahashi et al., hydrophilic polymer was micropatterned spatio-selectively on a polymer surface, allowing cells to organize themselves in patterned lines, resulting in aligned myofibers (123). Chen et al. have engineered highly aligned and multi-layered 200 µm muscle bundles situated in the microgrooves of a 3D porous collagen scaffold (124). Other tissue engineering approaches include stacking of multiple myoblast cell sheets (126) and scaffold-free approaches (104, 127). However, myofibers formed in this way are small and immature, resulting in a lack of sufficient contractile force to replace native muscle.

In general, SMTE strategies can be categorized based on which scaffold type is used (Figure 1.4). Scaffolds are being used to mimic ECM in SMTE constructs. They're not only important as anchor site, their structure and composition can be crucial in the survival of the tissue-engineered construct and its integration in the (damaged) host tissue. The tissue-engineered construct should provide an optimal niche for wound healing and skeletal muscle regeneration upon implantation in damaged muscle. Approaches towards 3D organization of cells include cell sheet assembly, use of decellularized tissue, hydrogels, synthetic and natural polymer scaffolds (Figure 1.4). In a scaffold-free approach myogenic cell monolayers secrete their own ECM, detach from the culture plate and roll up into a myofiber bundle that mimicks *in vivo* muscle closely (104, 127). Examples of scaffold types, their influence on myogenic regeneration and use in SMTE are discussed in section 1.5.

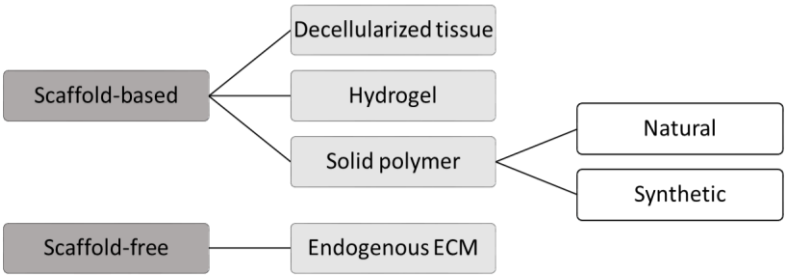


Figure 1.4. SMTE strategies based on scaffold-type.

1.4 Prevascularization

A major shortcoming towards clinical as well as certain *in vitro* testing applications is the limited size of the current engineered constructs. This is due to the lack of a proper vascular network, which is essential for tissue perfusion. The existence of functional blood vessels is critical to ensure delivery of nutrients and oxygen as well as removal of metabolic waste products from all cells throughout the engineered construct. Cell survival becomes limited at a diffusion distance of about 200 μm from a blood vessel or culture medium (128, 129). The presence of a prevascular network in the construct, able to deliver nutrients through the whole tissue, is desirable to ensure a higher survival and prolonged function throughout the organoid both for *in vitro* as well as *in vivo* transplantation studies (130).

1.4.1 Vascularization approaches of tissue engineered constructs: angiogenesis and vasculogenesis

In vivo, vascularization of myooids can be achieved by ingrowth of existing blood vessels. This is achieved by the stimulation of angiogenesis *in vivo*, which is the formation of new capillaries from pre-existing vessels by sprouting of endothelial cells (131). Angiogenesis is relatively slow, approximately 5-17 μm/h (132, 133), and myooids exceeding in any dimension the passive diffusion limit will not receive sufficient nutrients and oxygen during the first days after implantation, resulting in necrosis (134). To stimulate ingrowth of blood vessels in the organoid, growth-factor releasing scaffolds, and/or scaffolds with a specific structure or chemical composition are being used. An example of the first group is the addition of vascular endothelial growth factor (VEGF) in the scaffold (135). This accelerates neoangiogenesis and increases microvessel density in the implanted construct (135, 136). An example of the second group is construct porosity, which also improves capillary ingrowth (137, 138).

As opposed to *in vivo* vascularization by angiogenesis, *in vitro* vascularization by vasculogenesis can also result in vascular networks in the newly-made construct.

Vasculogenesis is the *de novo* assembly of endothelial progenitor cells into capillaries. In contrast to angiogenesis, vasculogenesis is a far less studied and understood process both in general and specifically in the field of tissue engineering (139). In this tissue-engineering strategy, endothelial cells are added in the construct to form an *in vitro* (micro-) vascular network (Figure 1.5B). The advantages of this strategy are threefold. First, the presence of this preformed endothelial network further stimulates host vessel ingrowth upon implantation (140, 141). Second, the presence of endothelial cells in the construct stimulates formation of anastomosis of *in vitro* formed endothelial networks and host vasculature upon implantation (142). And last, prevascularization improves perfusion through and thus also survival of the construct upon implantation (140, 141). It is important to mention that regression of *in vitro* formed networks can occur upon implantation. In such cases anastomosis between *in vitro* formed networks and host vessels will not provide sufficient nutrient supply through the whole implanted constructs. Eventually, angiogenesis through the whole construct should be present to allow long-term survival (143). *In vitro* formation of vascular networks in the construct may be attained through the mechanism of vasculogenesis as mentioned above or angiogenesis (Figure 1.5).

Approaches for vasculogenic prevascularization include co-culturing of target cells and endothelial cells in 3D scaffolds or decellularized matrices, stacking of cell sheets containing endothelial cells and engineering vasculature using microfabrication techniques (e.g. 3D-printing, modular approaches,…) (121, 144–148). Approaches for angiogenic prevascularization use animals as an *in vivo* bioreactor for stimulating blood vessel ingrowth in the construct (Figure 1.5A) (145, 149). An example of angiogenic prevascularization is the use of the arterio-venous (AV) loop model (145, 150). A vein and artery are microsurgically anastomosed to an AV loop and the loop is transferred to an enclosed implantation chamber to create an isolated microenvironment *in vivo*. Upon implantation of the construct in the chamber, new blood vessels sprout from the AV loop into the construct. The AV loop technique is also implemented in clinical practice (36) and been adapted to SMTE (145, 149, 150). After prevascularization of the construct by sprouting vessels from AV, it is possible to transplant the construct in the muscle defect (5) (Figure 1.5A).

Other factors contribute to the success rate of the prevascularization strategy and anastomosis upon implantation. Presence of angiogenic factors, supporting cells such as smooth muscle cells and pericytes, hypoxia and shear stress contribute to a better vascularization outcome (140).

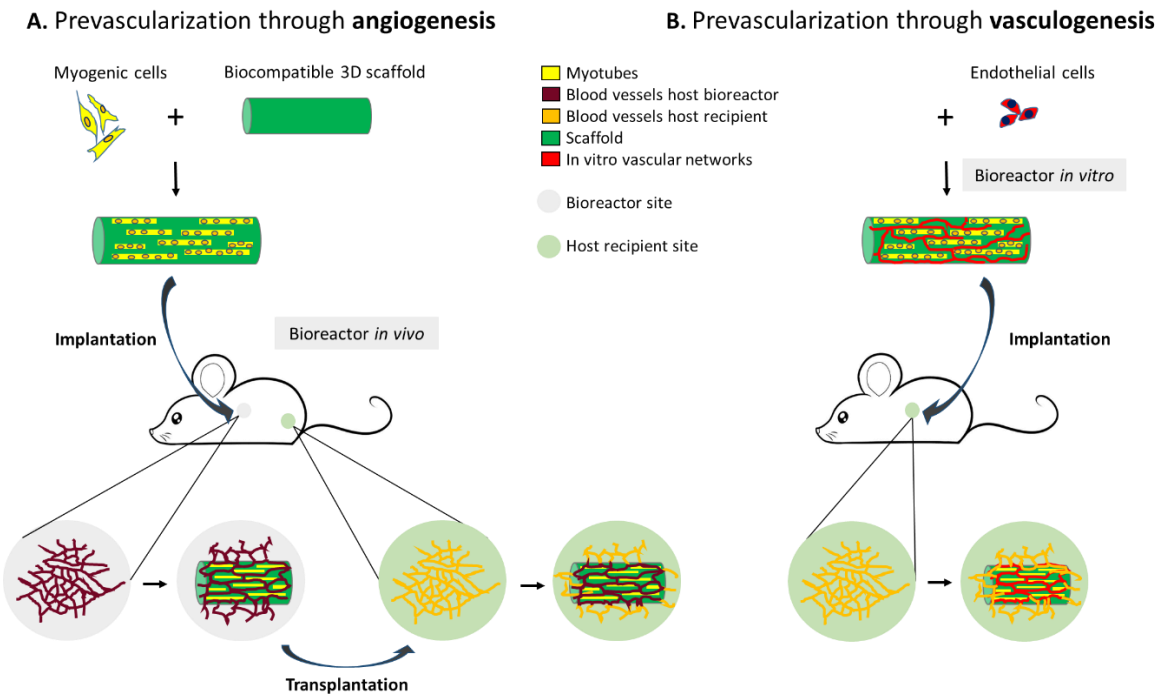


Figure 1.5. Prevascularization strategies of tissue-engineered constructs. (A) In the prevascularization through angiogenesis strategy, a construct with target cells (yellow) is implanted in a bioreactor site in vivo allowing for angiogenesis. Through angiogenesis and ingrowth of host vessels (dark red) the construct is provided by blood vessels. Upon transplantation of the vascularized construct in a host recipient site, a new implantation site or animal, connection between the preformed blood vessels (dark red) and host vessels (orange) takes place. (B) In the prevascularization through vasculogenesis strategy, vascular networks are formed in vitro by de novo formation of vascular networks by endothelial cells (bright red). Upon implantation in the host recipient site, preformed networks (bright red) connect with host vessels (orange), providing perfusion through the whole construct.

1.4.2 Endothelial cells in prevascularization

Endothelial cells are epithelial cells lining blood vessels and capillaries and play a key role in the revascularization process after wound healing (151). Previous studies have demonstrated the positive effects of endothelial cell addition on vascularization, perfusion and survival of myooids *in vitro* and *in vivo* (141, 149). Different types of endothelial cells are available and are implemented in the tissue engineering field (152). It is important to choose the proper endothelial cell source for a specific tissue engineering application. Depending on the tissue microenvironment of the isolated endothelial cells, they will have a different phenotype, gene expression pattern, structure and behavior in vascular network formation (153–155). The most frequently used and studied endothelial cell source are human umbilical cord-derived endothelial cells (HUVECs). These cells are easy to isolate, abundant and well characterized. Furthermore, they are capable of endothelial network formation *in vitro* (121, 141, 149).

However to attain optimal endothelial network formation these cells can be kept in culture only a limited amount of passages (typically less than 10) to ascertain a high differential potential and stable phenotype (156). To address this problem, Fang et al. have suggested vascular endothelial stem cells as cell source for vascular tissue engineering (157). These cells have a high proliferative capacity and can produce tens of millions of endothelial daughter cells *in vitro*. In addition, they are able to differentiate into functional blood vessels upon implantation (157). Other examples of endothelial cell sources include placental isolated endothelial cells (158), tissue-specific microvasculature-derived endothelial cells, embryonic heart cells (159), pluripotent derived endothelial cells (160) and blood outgrowth endothelial cells (161).

1.5 Prevascularization in current SMTE strategies

The choice of scaffold influences (pre)vascularization of the tissue-engineered skeletal muscle and is an important parameter to keep in mind when developing prevascularized SMTE constructs. Also myogenic regeneration is strongly influenced by the scaffold composition.

1.5.1 Decellularized tissue as bioscaffold

The ECM-induced regeneration has sparked research for acellular ECM scaffolds in SMTE. Bioscaffolds composed of ECM can be derived from tissues by removal of cells through chemical, enzymatic or physical methods (162). The use of such scaffold materials has been reported to induce a strong angiogenic response upon scaffold degradation (110, 163–167). Besides the intact angiogenic growth factors, resident in the ECM, the products released after ECM degradation may contribute to this observed angiogenesis *in vivo.* Indeed, the low-molecular-weight peptides released after ECM degradation were found to have a chemoattractant effect for endothelial cells *in vivo* (168). So it seems that these ECM-composed bioscaffolds are an appropriate source to promote neovascularization, making an exogenous growth factor supply superfluous. Next to promoting angiogenesis, the ECM also steers other pathways leading to skeletal muscle regeneration.

The remodelling potential of these bioscaffolds has been demonstrated in the restoration of skeletal muscle damage in animal models as well as in patients (110, 163, 164). Implantation of ECM at the site of injury was associated with attraction of perivascular stem cells and neovascularization (163). However, implantation of ECM alone did not generate a sufficient amount of *de novo* formed multinucleated myofibers to fully restore volumetric loss. A more successful approach involves seeding of myogenic cells on decellularized ECM prior to implantation. Seeding of autologous myoblasts on homologous acellular matrix, obtained from abdominal muscle fragments, has been studied as an approach to repair abdominal wall defects

(167, 169). Addition of endothelial cells to the matrix further stimulated vascularization (164). Eight weeks after implantation of bladder acellular matrix subcutaneously in rats, scaffolds seeded with endothelial cells and muscle progenitor cells (MPCs) displayed enhanced vascularization, striated myofiber formation and innervation as compared to MPC seeding alone. Besides bladder matrices, small intestine submucosa (SIS) bioscaffolds have been used in the context of SMTE as well. In one approach, a triculture system of endothelial cells, myoblasts and fibroblasts was used to construct a muscle graft on SIS derived from the jejunum of pigs (110). The resulting graft, cultured *in vitro* for a period of 3 weeks, was implanted in the site of a full thickness segment of mice abdominal wall. Two weeks post implantation, the grafts were found to be highly integrated with host muscle and were able to generate about 35 % of the intact muscle force.

Once implanted, the *in vivo* degradation of scaffolds is desirable but the timing of this event is crucial. The goal is to gradually integrate the engineered tissue and promote the formation of new host tissue. Furthermore, biodegradation circumvents foreign body reaction, which is a problem occurring with non-degradable biomaterials (170).

1.5.2 Hydrogels

Cell seeding on scaffolds often entails non-homogeneous cell distribution throughout the construct (171). Seeding on scaffolds can give the impression that cells are organized in 3D, while they are actually seeded on 2D surfaces in 3D scaffolds (172). A real 3D environment is necessary for lumen formation in vascular development (173). For homogeneous 'seeding', amorphous hydrogels can be used to encapsulate cells. Another advantage of hydrogels over pre-organized scaffolds is that cells are able to migrate and re-organize easily. The presence of binding and cleavable sites for cells in biological ECM-derived hydrogel materials determines migration and provides molecular cues for proper cell function and organization. Also skeletal muscle differentiation and vascularization events require cell-ECM interaction (133, 174, 175). Next to the molecular properties, the physical properties of hydrogels also play an important role in cell behavior. Hydrogels with an elastic modulus of 12 kPa, mimicking the *in vivo* environment, enhance satellite cell proliferation and self-renewal (119). Also for myotube formation and striation a proper stiffness is required (176). As for vasculogenesis, an inverse relationship exists between the extent of vasculogenesis and hydrogel stiffness (176–178), favoring the use of soft hydrogels for SMTE. Several biomolecules have commonly been used to form a hydrogel for SMTE, such as collagen (117, 179), gelatin (123, 126, 180, 181) and fibrin (121, 182, 183).

Fibrin has an established role in wound healing, where it serves as a provisional matrix for tissue repair. It was assumed that the use of fibrin as a scaffold material for tissue engineering replicates the support during wound healing (184). In the same context of wound healing, fibrin is known for its pro-inflammatory features. However, in the bone regeneration field, there has been a paradigm shift from minimizing the immune response towards modulating inflammation, opening up new possibilities for the use of fibrin (185). From a tissue engineering point of view, the high capacity of fibrin to bind growth factors such as VEGF, FGF and insulin-like growth factor, makes it an intriguing polymer for use as a scaffold for vascular tissue engineering purposes (186). From a clinical point of view, production of autologous fibrin gel from the patient's own blood is possible to minimize immune response (187). Fibrin hydrogels require protection against fibrinolytic enzymes, present in the medium. Also, as occurs naturally in the wound healing process, fibrin is broken down *in vivo*. An approach to prevent degradation of fibrin-based SMTE constructs is to induce remodeling of the fibrin ECM by autologously deposited collagen by included cells (182). Not only inclusion of endothelial cells enhances host vessel invasion, also loading of angiogenesis stimulating growth factors, such as VEGF improves host vessel invasion (188).

However, working with hydrogels alone may not be sufficient to restore large muscle deficits such as volumetric muscle loss due to their weak mechanical properties and rapid degradation *in vivo* (184). A combination between bio-active hydrogels and supportive scaffolds may overcome this problem.

1.5.3 Polymer and naturally-derived scaffolds

Scaffolds provide support and are able to deliver cells and growth factors upon implantation *in vivo*. Several scaffolds are described in the context of prevascularization of skeletal muscle constructs. A distinction can be made between synthetic polymer-based and naturally-derived scaffolds.

Commonly used synthetic polymer scaffolds in SMTE are poly-(L-lactic acid) (PLLA) and polylactic-glycolic acid (PLGA). A 3D biodegradable 50% PLLA and 50% PLGA polymer scaffold with pores of 225 - 500 µm allowed diffusion through the whole construct even in the absence of vascularization. Seeding of endothelial cells (either embryonic stem cell–derived endothelial cells or HUVECs), myoblasts and embryonal fibroblasts resulted in vessel-like structures between partially aligned, multi-nucleated myofibers after 10 days of differentiation *in vitro* (149, 189). After implantation in SCID mice, further maturation of blood vessels and myofibers was observed. The addition of human endothelial cells to the scaffolds resulted in

blood vessels derived from these cells, which significantly improved perfusion and implant survival *in vivo*. Further addition of fibrin (190) resulted in dense vascular networks and improved human cell survival (191). These scaffolds (without fibrin) have also been implanted around a mouse vein and artery anastomosed to an AV loop (149). Newly formed host vessels derived from the AV loop, invaded the scaffold and anastomosed with the implanted endothelial networks. One or two weeks after implantation, the muscle graft with the host vasculature ingrowth and AV loop was transplanted into an abdominal wall defect. Prevascularization with endothelial cells of the construct resulted in improved host integration and vascularization (149). This study is an example of *in vivo* prevascularization (Figure 1.5) of tissue constructs and highlights its beneficial effect on host integration and cell survival.

Compared to PLLA/PLGA polymers with randomly organized pores, scaffolds with engineered microvasculature could further improve cell function and survival in the center of the construct. A microchannel structure has been engineered in a poly(glycerol sebacate) (PGS) elastomer scaffold that allowed perfusion *in vitro* throughout the construct (192). The fabricated microchannels could be perfused and were seeded with HUVECs, but they did not attach well to the PGS. At the outside of the PGS structure, adult human skeletal muscle-derived cells were seeded and permeability of PGS scaffold was demonstrated by perfusion of a myotoxic drug through the channels. As the muscle tissue was the main tissue type, this was called the parenchym site. PGS is degradable and permeable, therefore enabling vascular-parenchymal transport. However, poor myofiber differentiation and survival on the PGS was observed (192). *In vivo* implantation experiments showed elastomer degradation and vascular host invasion one week post-implantation. Considering the abovementioned results, the combination of a pre-fabricated perfusable microvasculature with a hydrogel may be best suited to obtain large well-differentiated myooids.

As an alternative to synthetic polymers, naturally derived and ECM-based biomaterials are also evaluated in vascularization strategies for SMTE. Examples of biomaterials are collagen, fibrin and modified alginate-based scaffolds. They support cell attachment and are susceptible to cell-based remodeling *in vitro* and *in vivo*. The advantage of using naturally derived scaffolds is the presence of biologically active degradation products, that positively affect cell migration and proliferation (193). In contrast, degradation products from synthetic scaffolds typically do not have such positive effect. The main difference of scaffolds versus soft hydrogels, is that scaffolds provide a better initial mechanical support (179, 194).

Collagen scaffolds are biocompatible and allow *in vitro* vasculogenesis when seeded with endothelial cells. To show the vasculogenic potential of collagen scaffolds *in vivo*, cell-free

collagen type I scaffolds with an 80 µm pore size, combined with fibrin hydrogel were implanted and allowed host vessel ingrowth with a higher vascular volume versus fibrin alone (195). Aligned collagen nanofibrillar scaffolds were used to imitate the ECM pattern secreted by vascular cells *in vivo* (196). In this set-up, endothelial cells migrated in the micro-patterning direction of the nanofibrils through integrin α1 binding to collagen (196). Moreover, collagen scaffolds allowed simultaneous differentiation of myogenic cells and endothelial cells into respectively myofibers and tubule-like structures (197).

Other biomaterials such as fibrin scaffolds, not only have pro-angiogenic properties and allow myofiber formation *in vitro*, as mentioned previously, but also support muscle regeneration *in vivo* (41). To decrease the degradation grade by fibrinolysis of fibrin scaffolds a crosslinking strategy such as treatment with 1-ethyl-3-(3-dimethylaminopropyl) carbodiimide can be used (41). Similar to hydrogels, growth factors such as HGF can be incorporated in the scaffold. Implantation in mice of fibrin microthreads loaded with HGF stimulated host myofiber regeneration and enhanced vascular ingrowth (41). Fibrin microthreads were produced by extrusion of fibrinogen and thrombin and support cell alignment (16, 41). Another way to induce myofiber alignment in the construct, is using aligned electrospun fibrin hydrogels, containing additionally 15 % alginate. Seeding mouse C2C12 on fibrin-alginate fibers resulted in highly aligned striated myofibers able to contract spontaneously or upon electrical stimulation (198). Implantation for 4 weeks in tibialis anterior muscle in immunodeficient mice resulted in scaffold degradation, muscle regeneration and ingrowth of host vessels (198).

A less commonly used biomaterial in SMTE and prevascularization approaches is alginate (199–202). *In vitro*, alginate scaffolds supported partial myoblast survival, when modified with an RGD peptide and HGF addition (200). A macroporous alginate scaffold modified with RGD was used as vascular progenitor cell carrier in an ischemic murine hindlimb musculature model (199). The scaffold maintained implanted endothelial cell survival, engraftment and improved angiogenesis in comparison to direct cell injection. However no analysis was performed to assess the effect of the alginate scaffold on muscle regeneration *in vivo* (199). Macroporous alginate scaffolds have shape-memory, allowing to deliver scaffold, cells and growth factors by a minimal invasive procedure through a catheter (202). In a tibialis anterior injury mouse model, the RGD-modified alginate scaffold was used to deliver myoblasts, IGF-1 and VEGF, which lowered scar formation and enhanced muscle function. VEGF addition increased angiogenesis *in vivo* at the injury site (202).

To conclude, skeletal muscle tissues have been engineered *in vitro,* using synthetic and naturally derived scaffolds, which *in vivo* partially support the survival of engineered myofibers and display some evidence of integration with host vasculature.

1.5.4 Scaffold- and hydrogel-free approaches

Scaffold/hydrogel-free SMTE is based on the ability of myofiber monolayers to contract spontaneously resulting in detachment from the substrate and rolling up of the cell sheet (103, 104, 127, 203–205). In general, freshly isolated cells from muscle biopsies from rodents containing SCs, endothelial cells and fibroblasts are used. This heterogenous cell population is then cultured on a low attachment surface such as silicone to form cell sheets. Initial cell adherence is assured by coating the dishes with collagen type I or laminin. Once cell confluence is achieved, growth medium is changed to serum-deprived differentiation medium supporting myocyte fusion into multinucleated myotubes. Simultaneously minutien pins or tissue engineered cell anchors are pinned on the cell monolayer. No ECM is used for initial engineering, but during culture cells secrete their own ECM products. Upon spontaneous cell layer detachment, a muscle bundle is formed in between the anchors (103, 104, 127, 203–205). Such a muscle bundle, which mimicks the organization of mature skeletal muscle with differentiated myofibers, vascular networks and produced ECM shows spontaneous contraction *in vitro* (13). This self-assembling approach provides a stem cell niche with close cell-cell and cell-ECM interactions, necessary for proper regeneration *in vitro*. Pax 7^{+} satellite cells were observed in close association with the myofibers in the muscle bundle, surrounded by laminin, resembling the situation *in vivo* (127). This level of overall maturity of the myooids is achieved by the use of freshly isolated cells, since culturing cells *in vitro* over several passages attributes to change in stem cell behavior (206, 207). In a similar approach, after 28 days *in vivo*, the muscle constructs showed an increased force generation, microvascular ingrowth and functional repair (203, 205). Experiments have only been performed with rodent or avian derived cells. It would be of great interest to evaluate the approach with human derived tissue.

1.6 Applications of SMTE

Besides a need for alternatives in regenerative medicine as reviewed in chapter 1.2, SMTE constructs can be useful in many other applications. Some examples are listed below:

Traditional two-dimensional (2D) monolayers lack the natural cell environment, in specific cell–cell and cell–extracellular matrix (ECM) interactions as well as mechanical and/or chemical cues (208–211). 3D models offer an alternative by improving cell maturation, culture time *in vitro,* proliferation, survival in comparison to 2D models, and providing the ability to

measure functional outcomes (118, 210, 212, 213). For example, commercially available hepatocyte and skin tissue models mimic more accurately the human *in vivo* physiology, which translates in a more representative drug response than 2D cell culture models (212, 214). For these reasons, tissue engineered muscle is preferred to 2D models for *in vitro* studies of myogenesis, myopathology, molecular pathways and muscle physiology (118, 215, 216). Moreover, the use of human cells in such models increases the relevance to study human muscular diseases and to implement the human 3D model as *in vitro* pre-clinical model for drug-screening and toxicity testing of compounds (119, 217, 218).

Nowadays to assess efficacy and safety of candidate drugs, pre-clinical animal models are used, next to 2D cell culture models. Testing in animal models allows evaluation of the route of administration, pharmacokinetics, pharmacodynamics and toxicity (219). Major drawbacks are the high cost of animal models and the fact that animal physiology differs from human physiology (220). These issues together with the ethical considerations demanding for a reduction in the use of animals, the so-called 3R policy (221), have led to a growing interest in creating tissue engineered 3D pre-clinical human tissue models. Tissue engineered skeletal muscle has been evaluated as a pre-clinical model and showed similar responses to compounds as muscle *in vivo* (119, 183, 218, 222). It shows the potential of these *in vitro* assays as a useful tool in drug development of therapeutics for muscle disorders.

Additionally, SMTE is being explored as a 'sustainable' alternative for meat production, which has a negative impact on the environment. Culturing meat *in vitro* as a replacement protein source is based on same SMTE strategies as for clinical applications and has received much attention recently (223). However current technology in producing lab-grown-meat has significant scientific challenges before it can be considered as a sustainable, animal-free, cost-effective and safe alternative for livestock meat (reviewed in (224)).

1.7 References

1. Frontera WR, Ochala J (2015) Skeletal muscle: a brief review of structure and function. *Calcif Tissue Int* 96(3):183–95.
2. Prothero JW (2015) Musculoskeletal system. *The Design of Mammals*, pp 142–156.
3. Dziedzic D, Bogacka U, Ciszek B (2014) Anatomy of sartorius muscle. *Folia Morphol* 73(3):359–362.
4. Gillies AR, Lieber RL (2011) Structure and function of the skeletal muscle extracellular matrix. *Muscle Nerve* 44(3):318–31.
5. Maas H, Sandercock TG (2010) Force transmission between synergistic skeletal muscles through connective tissue linkages. *J Biomed Biotechnol*.
6. Musarò A (2014) The Basis of Muscle Regeneration. *Adv Biol* 2014:1–16.
7. Thorsteinsdóttir S, Deries M, Cachaço AS, Bajanca F (2011) The extracellular matrix dimension of skeletal muscle development. *Dev Biol* 354(2):191–207.
8. Järvinen TA, Järvinen TL, Kääriäinen M, Kalimo H, Järvinen M (2005) Muscle injuries: biology and treatment. *Am J Sports Med* 33(5):745–764.
9. Gholobova D, Terrie L, Gerard M, Thorrez L (2019) Vascularization of tissue-engineered skeletal muscle constructs. (review in submission).
10. Tierney MT, Sacco A (2016) Satellite Cell Heterogeneity in Skeletal Muscle Homeostasis. *Trends Cell Biol* 26(6):434–444.
11. Yablonka-Reuveni Z, Rudnicki MA, Rivera AJ, Primig M, Anderson JE, Natanson P (1999) The transition from proliferation to differentiation is delayed in satellite cells from mice lacking MyoD. *Dev Biol* 210(2):440–455.
12. Cooper RN, Tajbakhsh S, Mouly V, Cossu G, Buckingham M, Butler-Browne GS (1999) In vivo satellite cell activation via Myf5 and MyoD in regenerating mouse skeletal muscle. *J Cell Sci* 112 (Pt 1:2895–901.
13. Karalaki M, Fili S, Philippou A, Koutsilieris M (2009) Muscle regeneration: cellular and molecular events. *In Vivo* 23(5):779–96.
14. Sicari BM, Dziki JL, Siu BF, Medberry CJ, Dearth CL, Badylak SF (2014) The promotion of a constructive macrophage phenotype by solubilized extracellular matrix. *Biomaterials* 35(30):8605–8612.
15. Troy A, Cadwallader AB, Fedorov Y, Tyner K, Tanaka KK, Olwin BB (2012) Coordination of Satellite Cell Activation and Self-Renewal by Par-Complex-Dependent Asymmetric Activation of p38α/β MAPK. *Cell Stem Cell* 11(4):541–553.
16. Cornwell KG, Pins GD (2007) Discrete crosslinked fibrin microthread scaffolds for tissue regeneration. *J Biomed Mater Res Part A* 82A(1):104–112.
17. Laumonier T, Menetrey J (2016) Muscle injuries and strategies for improving their repair. *J Exp Orthop* 3(1):15.
18. Burks TN, Andres-Mateos E, Marx R, Mejias R, Van Erp C, Simmers JL, Walston JD, Ward CW, Cohn RD (2011) Losartan restores skeletal muscle remodeling and protects against disuse atrophy in sarcopenia. *Sci Transl Med* 3(82):1–9.
19. Whalen RG, Harris JB, Butler-Browne GS, Sesodia S (1990) Expression of myosin isoforms during notexin-induced regeneration of rat soleus muscles. *Dev Biol* 141(1):24–40.
20. Dumont N, Frenette J (2010) Macrophages protect against muscle atrophy and promote muscle recovery in vivo and in vitro: a mechanism partly dependent on the insulin-like growth factor-1 signaling molecule. *Am J Pathol* 176(5):2228–2235.
21. Corliss B, Azimi M, Munson J, Peirce SM, Murfee WL (2016) Macrophages: An Inflammatory Link between Angiogenesis and Lymphangiogenesis. 23(2):95–121.
22. Latroche C, et al. (2017) Coupling between Myogenesis and Angiogenesis during Skeletal Muscle Regeneration Is Stimulated by Restorative Macrophages. *Stem Cell Reports* 9(6):2018–2033.
23. Martino MM, et al. (2015) Extracellular Matrix and Growth Factor Engineering for Controlled Angiogenesis in Regenerative Medicine. *Front Bioeng Biotechnol* 3:45.

24. Voytik-Harbin SL, Brightman AO, Kraine MR, Waisner B, Badylak SF (1997) Identification of extractable growth factors from small intestinal submucosa. *J Cell Biochem* 67(4):478–91.
25. Garg K, Ward CL, Hurtgen BJ, Wilken JM, Stinner DJ, Wenke JC, Owens JG, Corona BT (2015) Volumetric muscle loss: Persistent functional deficits beyond frank loss of tissue. *J Orthop Res* 33(1):40–46.
26. Ostrovidov S, Hosseini V, Ahadian S, Fujie T, Parthiban SP, Ramalingam M, Bae H, Kaji H, Khademhosseini A (2014) Skeletal Muscle Tissue Engineering: Methods to Form Skeletal Myotubes and Their Applications. *Tissue Eng Part B Rev* 20(5):403–436.
27. Belmont PJ, McCriskin BJ, Hsiao MS, Burks R, Nelson KJ, Schoenfeld AJ (2013) The Nature and Incidence of Musculoskeletal Combat Wounds in Iraq and Afghanistan (2005–2009). *J Orthop Trauma* 27(5):e107–e113.
28. Corona BT, Wenke JC, Ward CL (2016) Pathophysiology of volumetric muscle loss injury. *Cells Tissues Organs* 202(3–4):180–188.
29. Owens BD, Kragh JF, Macaitis J, Svoboda SJ, Wenke JC (2007) Characterization of Extremity Wounds in Operation Iraqi Freedom and Operation Enduring Freedom. *J Orthop Trauma* 21(4):254–257.
30. Baoge L, Van Den Steen E, Rimbaut S, Philips N, Witvrouw E, Almqvist KF, Vanderstraeten G, Vanden Bossche LC (2012) Treatment of Skeletal Muscle Injury: A Review. *ISRN Orthop* 2012:1–7.
31. Gigante A, Cianforlini M, Manzotti S, Ulisse S (2014) The effects of growth factors on skeletal muscle lesions. *Joints* 1(4):180–6.
32. Greising SM, Warren GL, Southern WM, Nichenko AS, Qualls AE, Corona BT, Call JA (2018) Early rehabilitation for volumetric muscle loss injury augments endogenous regenerative aspects of muscle strength and oxidative capacity. *BMC Musculoskelet Disord* 19(1):173.
33. Lee KT, Mun GH (2014) A Systematic Review of Functional Donor-Site Morbidity after Latissimus Dorsi Muscle Transfer. *Plast Reconstr Surg* 134(2):303–314.
34. Blondeel PN, Vanderstraeten GG, Monstrey SJ, Van Landuyt K, Tonnard P, Lysens R, Boeckx WD, Matton G (1997) The donor site morbidity of free DIEP flaps and free TRAM flaps for breast reconstruction. *Br J Plast Surg* 50(5):322–330.
35. Wan DC, Tseng CY, Anderson-Dam J, Dalio AL, Crisera CA, Festekjian JH (2010) Inclusion of mesh in donor-site repair of free TRAM and muscle-sparing free TRAM flaps yields rates of abdominal complications comparable to those of DIEP flap reconstruction. *Plast Reconstr Surg* 126(2):367–374.
36. Cavadas PC (2008) Arteriovenous vascular loops in free flap reconstruction of the extremities. *Plast Reconstr Surg* 121(2):514–520.
37. Meyer A, Meyer N, Schaeffer M, Gottenberg JE, Geny B, Sibilia J (2014) Incidence and prevalence of inflammatory myopathies: A systematic review. *Rheumatology* 54(1):50–63.
38. Laing NG, Davis MR, Bayley K, Fletcher S, Wilton SD (2011) Molecular diagnosis of duchenne muscular dystrophy: Past, present and future in relation to implementing therapies. *Clin Biochem Rev* 32(3):129–134.
39. Tabebordbar M, Wang ET, Wagers AJ (2013) Skeletal Muscle Degenerative Diseases and Strategies for Therapeutic Muscle Repair. *Annu Rev Pathol Mech Dis* 8(1):441–475.
40. Srinivasan J, Amato AA (2003) Myopathies. *Phys Med Rehabil Clin N Am* 14(2):403–434.
41. Grasman JM, Do DM, Page RL, Pins GD (2015) Rapid release of growth factors regenerates force output in volumetric muscle loss injuries. *Biomaterials* 72:49–60.
42. Shvartsman D, et al. (2014) Sustained delivery of VEGF maintains innervation and promotes reperfusion in ischemic skeletal muscles via NGF/GDNF signaling. *Mol Ther* 22(7):1243–1253.
43. Silva EA, Mooney DJ (2007) Spatiotemporal control of vascular endothelial growth factor delivery from injectable hydrogels enhances angiogenesis. *J Thromb Haemost* 5:590–598.
44. Heszele MFC, Price SR (2004) Insulin-Like Growth Factor I: The Yin and Yang of Muscle Atrophy. *Endocrinology* 145(11):4803–4805.
45. Menetrey J, Kasemkijwattana C, Day CS, Bosch P, Vogt M, Fu FH, Moreland MS, Huard J (2000) Growth factors improve muscle healing in vivo. *J Bone Joint Surg Br* 82(1):131–7.

46. Borselli C, Cezar CA, Shvartsman D, Vandenburgh HH, Mooney DJ (2011) The role of multifunctional delivery scaffold in the ability of cultured myoblasts to promote muscle regeneration. *Biomaterials* 32(34):8905–8914.
47. Partridge T, Morgan E, Coulton G, Hoffmant E, Kunkelt L (1989) Conversion of mdx myofibres from dystrophin-negative to -positive by injection of normal myoblasts. *Nature*:36–39.
48. Law P, Bertorini T, Goodwin T, Chan M, Fang Q, Li H, Kirby D, Florendo J, Herrod H, Golden G (1990) Dystrophin production induced by myoblast transfer therapy in Duchenne muscular dystrophy. *Lancet* 336(8707):114–115.
49. Mendell J, et al. (1995) Myoblast transfer in the treatment of Duchenne's muscular dystrophy. *N Engl J Med* 333(13):832–838.
50. Skuk D, et al. (2007) First test of a "high-density injection" protocol for myogenic cell transplantation throughout large volumes of muscles in a Duchenne muscular dystrophy patient: eighteen months follow-up. *Neuromuscul Disord* 17(1):38–46.
51. Carr LK, Robert M, Kultgen PL, Herschorn S, Birch C, Murphy M, Chancellor MB (2013) Autologous Muscle Derived Cell Therapy for Stress Urinary Incontinence : A Prospective , Dose Ranging Study. *JURO* 189(2):595–601.
52. Giverne C, Aure Ã, Boyer O, Vale Ã, Koning E, Leroi A, Chambon P, De J, Corre S Le, Jacquot S, Bastit ÃD (2018) Autologous Myoblasts for the Treatment of Fecal Incontinence. *Ann Surg* 267(3):443–450.
53. Collins CA, Olsen I, Zammit PS, Heslop L, Petrie A, Partridge TA, Morgan JE (2005) Stem cell function, self-renewal, and behavioral heterogeneity of cells from the adult muscle satellite cell niche. *Cell* 122(2):289–301.
54. Xu X, et al. (2015) Human Satellite Cell Transplantation and Regeneration from Diverse Skeletal Muscles. *Stem Cell Reports* 5(3):419–434.
55. Syverud B, Lee J, VanDusen K, Larkin L (2015) Isolation and Purification of Satellite Cells for Skeletal Muscle Tissue Engineering. *J Regen Med* 03(02).
56. Machida S, Spangenburg EE, Booth FW (2004) Primary rat muscle progenitor cells have decreased proliferation and myotube formation during passages. *Cell Prolif* 37(4):267–277.
57. Maffioletti SM, et al. (2018) Three-Dimensional Human iPSC-Derived Artificial Skeletal Muscles Model Muscular Dystrophies and Enable Multilineage Tissue Engineering. *Cell Rep* 23(3):899–908.
58. Dellavalle A, et al. (2007) Pericytes of human skeletal muscle are myogenic precursors distinct from satellite cells. *Nat Cell Biol* 9(3):255–267.
59. Fuoco C, et al. (2015) In vivo generation of a mature and functional artificial skeletal muscle. *EMBO Mol Med* 7(4):411–422.
60. Fuoco C, et al. (2014) 3D hydrogel environment rejuvenates aged pericytes for skeletal muscle tissue engineering. *Front Physiol* 5(May):1–8.
61. Augello A, De Bari C (2010) The Regulation of Differentiation in Mesenchymal Stem Cells. *Hum Gene Ther* 21(10):1226–1238.
62. Mehrabani D, Mehrabani G, Zare S, Manafi A (2013) Adipose-Derived Stem Cells and Aesthetic Surgery : A Mini Review. *World J Plast Surg* 2(2):65–70.
63. Di Rocco G, Iachininoto MG, Tritarelli A, Straino S, Zacheo A, Germani A, Crea F, Capogrossi MC (2006) Myogenic potential of adipose-tissue-derived cells. *J Cell Sci* 119(14):2945–2952.
64. Kesireddy V (2016) Evaluation of adipose-derived stem cells for tissue-engineered muscle repair construct-mediated repair of a murine model of volumetric muscle loss injury. *Int J Nanomedicine* 11:1461–1473.
65. Bayati V, Hashemitabar M, Gazor R, Nejatbakhsh R, Bijannejad D (2013) Expression of surface markers and myogenic potential of rat bone marrow- and adipose-derived stem cells: a comparative study. *Anat Cell Biol* 46(2):113.
66. Natsu K, Ochi M, Mochizuki Y, Hachisuka H, Yanada S, Yasunaga Y (2004) Allogeneic Bone Marrow-Derived Mesenchymal Stromal Cells Promote the Regeneration of Injured Skeletal Muscle without Differentiation into Myofibers. *Tissue Eng* 10(7–8):1093–1112.

67. Merritt EK, Cannon M V, Hammers DW, Le LN, Gokhale R, Sarathy A, Song TJ, Tierney MT, Suggs LJ, Walters TJ, Farrar RP (2010) Repair of Traumatic Skeletal Muscle Injury with Bone-Marrow-Derived Mesenchymal Stem Cells Seeded on Extracellular Matrix. *Tissue Eng Part A* 16(9):2871–2881.
68. Andrade BM, Baldanza MR, Ribeiro KC, Porto A, Peçanha R, Fortes FSA, Zapata-Sudo G, Campos-De-Carvalho AC, Goldenberg RCS, Werneck-De-Castro JP (2015) Bone marrow mesenchymal cells improve muscle function in a skeletal muscle re-injury model. *PLoS One* 10(6):1–13.
69. Helal MAM, Shaheen NEM, Abu Zahra FA (2016) Immunomodulatory capacity of the local mesenchymal stem cells transplantation after severe skeletal muscle injury in female rats. *Immunopharmacol Immunotoxicol* 38(6):414–422.
70. Jacobs SA, Roobrouck VD, Verfaillie CM, Van Gool SW (2013) Immunological characteristics of human mesenchymal stem cells and multipotent adult progenitor cells. *Immunol Cell Biol* 91(1):32–39.
71. Lin C-S, Lin G, Lue TF (2012) Allogeneic and Xenogeneic Transplantation of Adipose-Derived Stem Cells in Immunocompetent Recipients Without Immunosuppressants. *Stem Cells Dev* 21(15):2770–2778.
72. Pittenger MF, Mackay AM, Beck SC, Jaiswal RK, Douglas R, Mosca JD, Moorman MA, Simonetti DW, Craig S, Marshak DR (1999) Multilineage Potential of Adult Human Mesenchymal Stem Cells. *Science (80-)* 284(5411):143–147.
73. Sarveazad A, Newstead GL, Mirzaei R, Joghataei MT, Bakhtiari M (2017) A new method for treating fecal incontinence by implanting stem cells derived from human adipose tissue : preliminary findings of a randomized double-blind clinical trial. *Stem Cell Res Ther* (8):40.
74. Park EJ, Kang J, Baik SH (2016) Treatment of faecal incontinence using mesenchymal stem cells : a study protocol for a pilot randomised controlled trial. *BMJ Open* (6):e010450.
75. Geevarghese A, Herman IM (2014) Pericyte-endothelial crosstalk: implications and opportunities for advanced cellular therapies. *Transl Res* 163(4):296–306.
76. Crisan M, et al. (2008) A Perivascular Origin for Mesenchymal Stem Cells in Multiple Human Organs. *Cell Stem Cell* 3(3):301–313.
77. Dellavalle A, Maroli G, Covarello D, Azzoni E, Innocenzi A, Perani L, Antonini S, Sambasivan R, Brunelli S, Tajbakhsh S, Cossu Ǵ (2011) Pericytes resident in postnatal skeletal muscle differentiate into muscle fibres and generate satellite cells. *Nat Commun* 2(1):411–499.
78. Minasi MG, et al. (2002) The meso-angioblast: a multipotent, self-renewing cell that originates from the dorsal aorta and differentiates into most mesodermal tissues. *Development* 129(11):2773–2783.
79. Sampaolesi M, et al. (2003) Cell therapy of α-sarcoglycan null dystrophic mice through intra-arterial delivery of mesoangioblasts. *Science (80-)* 301(5632):487–492.
80. Quattrocelli M, Palazzolo G, Perini I, Crippa S, Cassano M, Sampaolesi M (2012) Mouse and Human Mesoangioblasts: Isolation and Characterization from Adult Skeletal Muscles. *Myogenesis*.
81. Berardi E, Annibali D, Cassano M, Crippa S, Sampaolesi M (2014) Molecular and cell-based therapies for muscle degenerations: a road under construction. *Front Physiol* 5(April):1–13.
82. Sampaolesi M, et al. (2006) Mesoangioblast stem cells ameliorate muscle function in dystrophic dogs. *Nature* 444(7119):574–9.
83. Fuoco C, et al. (2012) Injectable polyethylene glycol-fibrinogen hydrogel adjuvant improves survival and differentiation of transplanted mesoangioblasts in acute and chronic skeletal-muscle degeneration. *Skelet Muscle* 2(1):24.
84. Cossu G, et al. (2015) Intra-arterial transplantation of HLA-matched donor mesoangioblasts in Duchenne muscular dystrophy. *EMBO Mol Med* 7(12):1513–1528.
85. Thomson JA, Itskovitz-Eldor J, Shapiro SS, Waknitz MA, Swiergiel JJ, Marshall VS, Jones JM (1998) Embryonic stem cell lines derived from human blastocysts. *Science (80-)* 282(5391):1145–1147.
86. Takahashi K, Yamanaka S (2006) Induction of pluripotent stem cells from mouse embryonic and adult fibroblast cultures by defined factors. *Cell* 126(4):663–676.

87. Barberi T, Bradbury M, Dincer Z, Panagiotakos G, Socci ND, Studer L (2007) Derivation of engraftable skeletal myoblasts from human embryonic stem cells. *Nature* 13(5):642–648.
88. Robertson JA (2010) Embryo Stem Cell Research: Ten Years of Controversy. *J Law, Med Ethics* 38(2):191–203.
89. Preynat-Seauve O, Krause K-H, Villard J (2011) The Immune Barriers of Cell Therapy with Allogenic Stem Cells of Embryonic Origin. *Stem Cell Engineering*, pp 181–197.
90. Ben-David U, Benvenisty N (2011) The tumorigenicity of human embryonic and induced pluripotent stem cells. *Nat Rev Cancer* 11(4):268–277.
91. Zheng JK, Wang Y, Karandikar A, Wang Q, Gai H, Liu AL, Peng C, Sheng HZ (2006) Skeletal myogenesis by human embryonic stem cells. *Cell Res* 16(8):713–722.
92. Maffioletti SM, Gerli MFM, Ragazzi M, Dastidar S, Benedetti S, Loperfido M, Vandendriessche T, Chuah MK, Tedesco FS (2015) Efficient derivation and inducible differentiation of expandable skeletal myogenic cells from human ES and patient-specific iPS cells. *Nat Protoc* 10(7):941–958.
93. Darabi R, Pan W, Bosnakovski D, Baik J, Kyba M, Perlingeiro RCR (2011) Functional Myogenic Engraftment from Mouse iPS Cells. *Stem Cell Rev Reports* 7(4):948–957.
94. Shoji E, Woltjen K, Sakurai H (2015) Directed Myogenic Differentiation of Human Induced Pluripotent Stem Cells. *Vlakna a Textil*, pp 89–99.
95. Darabi R, Gehlbach K, Bachoo RM, Kamath S, Osawa M, Kamm KE, Kyba M, Perlingeiro RCR (2008) Functional skeletal muscle regeneration from differentiating embryonic stem cells. *Nat Med* 14(2):134–143.
96. Chal J, Al Tanoury Z, Hestin M, Gobert B, Aivio S, Hick A, Cherrier T, Nesmith AP, Parker KK, Pourquié O (2016) Generation of human muscle fibers and satellite-like cells from human pluripotent stem cells in vitro. *Nat Protoc* 11(10):1833–1850.
97. Hosoyama T, McGivern J V, Van Dyke JM, Ebert AD, Suzuki M (2014) Derivation of Myogenic Progenitors Directly From Human Pluripotent Stem Cells Using a Sphere-Based Culture. *Stem Cells Transl Med* 3(5):564–574.
98. Chal J, et al. (2015) Differentiation of pluripotent stem cells to muscle fiber to model Duchenne muscular dystrophy. *Nat Biotechnol* 33(August):962–969.
99. Wosczyna MN, Rando TA (2018) Review A Muscle Stem Cell Support Group : Coordinated Cellular Responses in Muscle Regeneration. *Dev Cell* 46(2):135–143.
100. Dennis RG, Kosnik PE, Gilbert ME, Faulkner JA (2001) Excitability and contractility of skeletal muscle engineered from primary cultures and cell lines. *Am J Physiol Physiol* 280(2):C288–C295.
101. Brady MA, Lewis MP, Mudera V (2008) Synergy between myogenic and non-myogenic cells in a 3D tissue-engineered craniofacial skeletal muscle construct. *J Tissue Eng Regen Med* 2:408–417.
102. Ceafalan LC, Popescu BO, Hinescu ME (2014) Cellular Players in Skeletal Muscle Regeneration. *Biomed Res Int* 2014:1–21.
103. Larkin LM, Calve S, Kostrominova TY, Arruda EM (2006) Structure and functional evaluation of tendon-skeletal muscle constructs engineered in vitro. *Tissue Eng* 12(11):3149–3158.
104. Larkin LM, Van der Meulen JH, Dennis RG, Kennedy JB (2007) Functional evaluation of nerve-skeletal muscle constructs engineered in vitro. *In Vitro Cell Dev Biol Anim* 42(3–4):75–82.
105. Morimoto Y, Kato-Negishi M, Onoe H, Takeuchi S (2013) Three-dimensional neuron-muscle constructs with neuromuscular junctions. *Biomaterials* 34(37):9413–9419.
106. Li M, Dickinson CE, Finkelstein EB, Neville CM, Sundback CA (2011) The Role of Fibroblasts in Self-Assembled Skeletal Muscle. *Tissue Eng Part A* 17(21–22):2641–2650.
107. Mackey AL, Magnan M, Chazaud B, Kjaer M (2017) Human skeletal muscle fibroblasts stimulate in vitro myogenesis and in vivo muscle regeneration. *J Physiol* 595(15):5115–5127.
108. Joe AWB, Yi L, Natarajan A, Le Grand F, So L, Wang J, Rudnicki MA, Rossi FMV (2010) Muscle injury activates resident fibro/adipogenic progenitors that facilitate myogenesis. *Nat Cell Biol* 12(2):153–163.
109. Juhas M, Abutaleb N, Wang JT, Ye J, Shaikh Z, Sriworarat C, Qian Y, Bursac N (2018) Incorporation of macrophages into engineered skeletal muscle enables enhanced muscle regeneration. *Nat Biomed Eng* 2(12):942–954.

110. Koffler J, Kaufman-Francis K, Yulia S, Dana E, Daria AP, Landesberg A, Levenberg S (2011) Improved vascular organization enhances functional integration of engineered skeletal muscle grafts. *Proc Natl Acad Sci U S A* 108(36):14789–94.
111. Criswell TL, Corona BT, Wang Z, Zhou Y, Niu G, Xu Y, Christ GJ, Soker S (2013) The role of endothelial cells in myofiber differentiation and the vascularization and innervation of bioengineered muscle tissue in vivo. *Biomaterials* 34(1):140–149.
112. Hill E, Boontheekul T, Mooney DJ (2006) Designing Scaffolds to Enhance Transplanted Myoblast Survival and Migration. *Tissue Eng* 12(5):1295–1304.
113. Boldrin L, et al. (2007) Satellite Cells Delivered by Micro-Patterned Scaffolds : A New Strategy for Cell Transplantation in Muscle Diseases. *Tissue Eng* 13(2):253–262.
114. Fishman JM, Tyraskis A, Maghsoudlou P, Urbani L, Totonelli G, Birchall M, De Coppi P (2013) Skeletal Muscle Tissue Engineering: Which Cell to Use? *Tissue Eng Part B Rev* 44(6):1–46.
115. Klumpp D, Horch RE, Beier JP (2011) Tissue engineering of skeletal muscle. *Tissue Engineering for Tissue and Organ Regeneration.*, ed Eberly PD (InTech).
116. Vandenburgh H, Shansky J, Del Tatto M, Chromiak J (1999) Organogenesis of skeletal muscle in tissue culture. *Methods Mol Med* 18:217–25.
117. Powell CA, Smiley BL, Mills J, Vandenburgh HH (2002) Mechanical stimulation improves tissue-engineered human skeletal muscle. *Am J Physiol Cell Physiol* 283(5):1557–1565.
118. Wang L, Shansky J, Vandenburgh H (2013) Induced formation and maturation of acetylcholine receptor clusters in a defined 3D bio-artificial muscle. *Mol Neurobiol* 48(3):397–403.
119. Madden L, Juhas M, Kraus WE, Truskey GA, Bursac N (2015) Bioengineered human myobundles mimic clinical responses of skeletal muscle to drugs. *Elife* 4:1–14.
120. Heher P, Maleiner B, Prüller J, Teuschl AH, Kollmitzer J, Monforte X, Wolbank S, Redl H, Rünzler D, Fuchs C (2015) A novel bioreactor for the generation of highly aligned 3D skeletal muscle-like constructs through orientation of fibrin via application of static strain. *Acta Biomater* 24:251–265.
121. Gholobova D, Decroix L, Van Muylder V, Desender L, Gerard M, Carpentier G, Vandenburgh H, Thorrez L (2015) Endothelial Network Formation Within Human Tissue-Engineered Skeletal Muscle. *Tissue Eng Part A* 21(19–20):2548–58.
122. Martin NRW, Passey SL, Player DJ, Khodabukus A, Ferguson R a, Sharples AP, Mudera V, Baar K, Lewis MP (2013) Factors affecting the structure and maturation of human tissue engineered skeletal muscle. *Biomaterials* 34(23):5759–65.
123. Takahashi H, Shimizu T, Nakayama M, Yamato M, Okano T (2013) The use of anisotropic cell sheets to control orientation during the self-organization of 3D muscle tissue. *Biomaterials* 34(30):7372–80.
124. Chen S, Nakamoto T, Kawazoe N, Chen G (2015) Engineering multi-layered skeletal muscle tissue by using 3D microgrooved collagen scaffolds. *Biomaterials* 73:23–31.
125. Sun Y, Duffy R, Lee A, Feinberg AW (2013) Optimizing the structure and contractility of engineered skeletal muscle thin films. *Acta Biomater* 9:7885–7894.
126. Haraguchi Y, Shimizu T, Sasagawa T, Sekine H, Sakaguchi K, Kikuchi T, Sekine W, Sekiya S, Yamato M, Umezu M, Okano T (2012) Fabrication of functional three-dimensional tissues by stacking cell sheets in vitro. *Nat Protoc* 7(5):850–858.
127. Carosio S, Barberi L, Rizzuto E, Nicoletti C, Del Prete Z, Musarò A (2013) Generation of eX vivo-vascularized Muscle Engineered Tissue (X-MET). *Sci Rep* 3:1420.
128. Folkman J, Hochberg M (1973) Self-regulation of growth in three dimensions. *J Exp Med* 138(4):745–53.
129. Thorrez L, Shansky J, Wang L, Fast L, VandenDriessche T, Chuah M, Mooney D, Vandenburgh H (2008) Growth, differentiation, transplantation and survival of human skeletal myofibers on biodegradable scaffolds. *Biomaterials* 29(1):75–84.
130. Costa-Almeida R, Granja PL, Soares R, Guerreiro SG (2014) Cellular strategies to promote vascularisation in tissue engineering applications. *Eur Cells Mater* 28:51–67.
131. Carmeliet P, Jain RK (2011) Molecular mechanisms and clinical applications of angiogenesis. *Nature* 473(7347):298–307.
132. Blinder YJ, Freiman A, Raindel N, Mooney DJ, Levenberg S (2016) Vasculogenic dynamics in 3D engineered tissue constructs. *Sci Rep* 5(1):17840.

133. Laschke MW, Menger MD (2012) Vascularization in tissue engineering: angiogenesis versus inosculation. *Eur Surg Res* 48(2):85–92.
134. Tremblay PL, Hudon V, Berthod F, Germain L, Auger FA (2005) Inosculation of tissue-engineered capillaries with the host's vasculature in a reconstructed skin transplanted on mice. *Am J Transplant* 5(5):1002–1010.
135. Lindhorst D, et al. (2010) Effects of VEGF loading on scaffold-confined vascularization. *J Biomed Mater Res Part A* 95(3):783–792.
136. Laschke MW, Rücker M, Jensen G, Carvalho C, Mülhaupt R, Gellrich N-C, Menger MD (2008) Incorporation of growth factor containing Matrigel promotes vascularization of porous PLGA scaffolds. *J Biomed Mater Res A* 85(2):397–407.
137. Chiu YC, Cheng MH, Engel H, Kao SW, Larson JC, Gupta S, Brey EM (2011) The role of pore size on vascularization and tissue remodeling in PEG hydrogels. *Biomaterials* 32(26):6045–6051.
138. Wake MC, Patrick CW, Mikos AG (1994) Pore morphology effects on the fibrovascular tissue growth in porous polymer substrates. *Cell Transplant* 3(4):339–43.
139. Kaully T, Kaufman-Francis K, Lesman A, Levenberg S (2009) Vascularization-the conduit to viable engineered tissues. *Tissue Eng Part B Rev* 15(2):159–69.
140. Laschke MW, Menger MD (2015) Prevascularization in tissue engineering: Current concepts and future directions. *Biotechnol Adv* 34(2):112–121.
141. Levenberg S, Rouwkema J, Macdonald M, Garfein ESS, Kohane DSS, Darland DCC, Marini R, Van Blitterswijk CAA, Mulligan RCC, D'Amore PAA, Langer R (2005) Engineering vascularized skeletal muscle tissue. *Nat Biotechnol* 23(7):879–84.
142. Chen X, Aledia AS, Ghajar CM, Griffith CK, Putnam AJ, Hughes CCW, George SC (2009) Prevascularization of a fibrin-based tissue construct accelerates the formation of functional anastomosis with host vasculature. *Tissue Eng Part A* 15(6):1363–1371.
143. Hanjaya-Putra D, Shen Y-I, Wilson A, Fox-Talbot K, Khetan S, Burdick JA, Steenbergen C, Gerecht S (2013) Integration and regression of implanted engineered human vascular networks during deep wound healing. *Stem Cells Transl Med* 2(4):297–306.
144. Sekine H, Shimizu T, Sakaguchi K, Dobashi I, Wada M, Yamato M, Kobayashi E, Umezu M, Okano T (2013) In vitro fabrication of functional three-dimensional tissues with perfusable blood vessels. *Nat Commun* 4:1399.
145. Bach AD, Arkudas A, Tjiawi J, Polykandriotis E, Kneser U, Horch RE, Beier JP (2006) A new approach to tissue engineering of vascularized skeletal muscle. *J Cell Mol Med* 10(3):716–726.
146. Takei T, Kitazono Z, Ozuno Y, Yoshinaga T, Nishimata H, Yoshida M (2016) Vascular-like network prepared using hollow hydrogel microfibers. *J Biosci Bioeng* 121(3):336–340.
147. Miller JS, et al. (2012) Rapid casting of patterned vascular networks for perfusable engineered three-dimensional tissues. *Nat Mater* 11(9):768–774.
148. Quint C, Kondo Y, Manson RJ, Lawson JH, Dardik A, Niklason LE (2011) Decellularized tissue-engineered blood vessel as an arterial conduit. *Proc Natl Acad Sci U S A* 108(22):9214–9219.
149. Shandalov Y, Egozi D, Koffler J, Dado-Rosenfeld D, Ben-Shimol D, Freiman A, Shor E, Kabala A, Levenberg S (2014) An engineered muscle flap for reconstruction of large soft tissue defects. *Proc Natl Acad Sci U S A* 111(16):6010–6015.
150. Bitto FF, Klumpp D, Lange C, Boos AM, Arkudas A, Bleiziffer O, Horch RE, Kneser U, Beier JP (2013) Myogenic Differentiation of Mesenchymal Stem Cells in a Newly Developed Neurotised AV-Loop Model. *Biomed Res Int* 2013:1–11.
151. Polverini PJ (2013) Angiogenesis and Wound Healing: Basic Discoveries, Clinical Implications And Therapeutic Opportunities. *Oral Wound Heal Cell Biol Clin Manag*:175–193.
152. Baldwin J, Antille M, Bonda U, De-Juan-Pardo EM, Khosrotehrani K, Ivanovski S, Petcu EB, Hutmacher DW (2014) In vitro pre-vascularisation of tissue-engineered constructs A co-culture perspective. *Vasc Cell* 6(1):13.
153. Khan OF, Sefton M V (2011) Endothelialized biomaterials for tissue engineering applications in vivo. *Trends Biotechnol* 29(8):379–387.
154. Chi JT, Chang HY, Haraldsen G, Jahnsen FL, Troyanskaya OG, Chang DS, Wang Z, Rockson SG, van de Rijn M, Botstein D, Brown PO (2003) Endothelial cell diversity revealed by global expression profiling. *Proc Natl Acad Sci* 100(19):10623–10628.

155. Au P, et al. (2008) Differential in vivo potential of endothelial progenitor cells from human umbilical cord blood and adult peripheral blood to form functional long-lasting vessels. *Blood* 111(3):1302–1305.
156. Liao H, He H, Chen Y, Zeng F, Huang J, Wu L, Chen Y (2014) Effects of long-term serial cell passaging on cell spreading, migration, and cell-surface ultrastructures of cultured vascular endothelial cells. *Cytotechnology* 66(2):229–238.
157. Fang S, Wei J, Pentinmikko N, Leinonen H, Salven P (2012) Generation of functional blood vessels from a single c-kit+ adult vascular endothelial stem cell. *PLoS Biol* 10(10):e1001407.
158. Lang I, Pabst MA, Hiden U, Blaschitz A, Dohr G, Hahn T, Desoye G (2003) Heterogeneity of microvascular endothelial cells isolated from human term placenta and macrovascular umbilical vein endothelial cells. *Eur J Cell Biol* 82(4):163–73.
159. Van der Schaft DW, Van Spreeuwel AC, Van Assen HC, Baaijens FP (2011) Mechanoregulation of Vascularization in Aligned Tissue-Engineered Muscle: A Role for Vascular Endothelial Growth Factor. *Tissue Eng Part A* 17(21–22):2857–2865.
160. Sriram G, Tan JY, Islam I, Rufaihah AJ, Cao T (2015) Efficient differentiation of human embryonic stem cells to arterial and venous endothelial cells under feeder- and serum-free conditions. *Stem Cell Res Ther* 6(1):261.
161. Van Beem RT, Verloop RE, Kleijer M, Noort WA, Loof N, Koolwijk P, Van der Schoot CE, Van Hinsbergh VWM, Zwaginga JJ (2009) Blood outgrowth endothelial cells from cord blood and peripheral blood: angiogenesis-related characteristics in vitro. *J Thromb Haemost* 7(1):217–26.
162. Crapo PM, Gilbert TW, Badylak SF (2011) An overview of tissue and whole organ decellularization processes. *Biomaterials* 32(12):3233–43.
163. Sicari BM, et al. (2014) An acellular biologic scaffold promotes skeletal muscle formation in mice and humans with volumetric muscle loss. *Sci Transl Med* 6(234):234ra58.
164. Criswell TL, Corona BT, Wang Z, Zhou Y, Niu G, Xu Y, Christ GJ, Soker S (2013) The role of endothelial cells in myofiber differentiation and the vascularization and innervation of bioengineered muscle tissue in vivo. *Biomaterials* 34:140–149.
165. Sandusky GE, Lantz GC, Badylak SF (1995) Healing Comparison of Small Intestine Submucosa and ePTFE Grafts in the Canine Carotid Artery. *J Surg Res* 58(4):415–420.
166. Badylak SF, Kropp B, McPherson T, Liang H, Snyder PW (1998) Small intestinal submucosa: a rapidly resorbed bioscaffold for augmentation cystoplasty in a dog model. *Tissue Eng* 4(4):379–387.
167. Conconi MT, Coppi P De, Bellini S, Zara G, Sabatti M, Marzaro M, Franco Zanon G, Gamba PG, Parnigotto PP, Nussdorfer GG (2005) Homologous muscle acellular matrix seeded with autologous myoblasts as a tissue-engineering approach to abdominal wall-defect repair. *Biomaterials* 26(15):2567–2574.
168. Li F, Li W, Johnson SA, Ingram DA, Yoder MC, Badylak SF (2004) Low-Molecular-Weight Peptides Derived from Extracellular Matrix as Chemoattractants for Primary Endothelial Cells. *Endothelium* 11(3–4):199–206.
169. Merritt EK, Hammers DW, Tierney M, Suggs LJ, Walters TJ, Farrar RP (2010) Functional Assessment of Skeletal Muscle Regeneration Utilizing Homologous Extracellular Matrix as Scaffolding. *Tissue Eng Part A* 16(4):1395–1405.
170. Chapple CR, Raz S, Brubaker L, Zimmern PE (2013) Mesh Sling in an Era of Uncertainty: Lessons Learned and the Way Forward. *Eur Urol* 64(4):525–529.
171. Sachlos E, Czernuszka JT (2003) Making tissue engineering scaffolds work. Review: the application of solid freeform fabrication technology to the production of tissue engineering scaffolds. *Eur Cell Mater* 5:29–40.
172. Billiet T, Vandenhaute M, Schelfhout J, Van Vlierberghe S, Dubruel P (2012) A review of trends and limitations in hydrogel-rapid prototyping for tissue engineering. *Biomaterials* 33(26):6020–41.
173. Davis GE, Stratman AN, Sacharidou A, Koh W (2011) Molecular Basis for Endothelial Lumen Formation and Tubulogenesis During Vasculogenesis and Angiogenic Sprouting. *Int Rev Cell Mol Biol* 288:101–165.

174. Osses N, Brandan E (2002) ECM is required for skeletal muscle differentiation independently of muscle regulatory factor expression. *Am J Physiol Cell Physiol* 282(2):383–394.
175. Davis GE, Bayless KJ (2003) An integrin and Rho GTPase-dependent pinocytic vacuole mechanism controls capillary lumen formation in collagen and fibrin matrices. *Microcirculation* 10(1):27–44.
176. Engler AJ, Griffin M a, Sen S, Bönnemann CG, Sweeney HL, Discher DE (2004) Myotubes differentiate optimally on substrates with tissue-like stiffness: pathological implications for soft or stiff microenvironments. *J Cell Biol* 166(6):877–87.
177. Blatchley MR, Gerecht S (2015) Acellular implantable and injectable hydrogels for vascular regeneration. *Biomed Mater* 10(3):034001.
178. Rao RR, Peterson AW, Ceccarelli J, Putnam AJ, Stegemann JP (2012) Matrix composition regulates three-dimensional network formation by endothelial cells and mesenchymal stem cells in collagen/fibrin materials. *Angiogenesis* 15(2):253–264.
179. Pollot BE, Rathbone CR, Wenke JC, Guda T (2018) Natural polymeric hydrogel evaluation for skeletal muscle tissue engineering. *J Biomed Mater Res - Part B Appl Biomater* 106(22):672–679.
180. Hosseini V, Ahadian S, Ostrovidov S, Camci-Unal G, Chen S, Kaji H, Ramalingam M, Khademhosseini A (2012) Engineered Contractile Skeletal Muscle Tissue on a Microgrooved Methacrylated Gelatin Substrate. *Tissue Eng Part A* 18(23–24):2453–2465.
181. Nagamori E, Ngo TX, Takezawa Y, Saito A, Sawa Y, Shimizu T, Okano T, Taya M, Kino-oka M (2013) Network formation through active migration of human vascular endothelial cells in a multilayered skeletal myoblast sheet. *Biomaterials* 34(3):662–8.
182. Thorrez L, DiSano K, Shansky J, Vandenburgh H (2018) Engineering of human skeletal muscle with an autologous deposited extracellular matrix. *Front Physiol* Aug(9):1076.
183. Vandenburgh H, Shansky J, Benesch-Lee F, Barbata V, Reid J, Thorrez L, Valentini R, Crawford G (2008) Drug-screening platform based on the contractility of tissue-engineered muscle. *Muscle Nerve* 37(4):438–47.
184. Janmey PA, Winer JP, Weisel JW (2009) Fibrin gels and their clinical and bioengineering applications. *J R Soc Interface* 6(30):1–10.
185. Vasconcelos DM, et al. (2016) Fibrinogen scaffolds with immunomodulatory properties promote in vivo bone regeneration. *Biomaterials* 111:163–178.
186. Sahni A, Khorana AA, Baggs RB, Peng H, Francis CW (2006) FGF-2 binding to fibrin(ogen) is required for augmented angiogenesis. *Blood* 107(1):126–31.
187. Dietrich M, Heselhaus J, Wozniak J, Weinandy S, Mela P, Tschoeke B, Schmitz-Rode T, Jockenhoevel S (2013) Fibrin-based tissue engineering: comparison of different methods of autologous fibrinogen isolation. *Tissue Eng Part C Methods* 19(3):216–26.
188. Sacchi V, et al. (2014) Long-lasting fibrin matrices ensure stable and functional angiogenesis by highly tunable, sustained delivery of recombinant VEGF164. *Proc Natl Acad Sci* 111(19):6952–6957.
189. Levenberg S, Rouwkema J, Macdonald M, Garfein ESS, Kohane DSS, Darland DCC, Marini R, van Blitterswijk C a a, Mulligan RCC, D'Amore P a a, Langer R (2005) Engineering vascularized skeletal muscle tissue. *Nat Biotechnol* 23(7):879–84.
190. Morin KT, Tranquillo RT (2013) In vitro models of angiogenesis and vasculogenesis in fibrin gel. *Exp Cell Res* 319(16):2409–17.
191. Lesman A, Koffler J, Atlas R, Blinder YJ, Kam Z, Levenberg S (2011) Engineering vessel-like networks within multicellular fibrin-based constructs. *Biomaterials* 32:7856–7869.
192. Ye X, Lu L, Kolewe ME, Park H, Larson BL, Kim ES, Freed LE (2013) A biodegradable microvessel scaffold as a framework to enable vascular support of engineered tissues. *Biomaterials* 34(38):10007–10015.
193. Vorotnikova E, et al. (2010) Extracellular matrix-derived products modulate endothelial and progenitor cell migration and proliferation in vitro and stimulate regenerative healing in vivo. *Matrix Biol* 29(8):690–700.

194. Porzionato A, Sfriso M, Pontini A, Macchi V, Petrelli L, Pavan P, Natali A, Bassetto F, Vindigni V, De Caro R (2015) Decellularized Human Skeletal Muscle as Biologic Scaffold for Reconstructive Surgery. *Int J Mol Sci* 16(7):14808–14831.
195. Chan EC, Kuo S-M, Kong AM, Morrison WA, Dusting GJ, Mitchell GM, Lim SY, Liu G-S (2016) Three Dimensional Collagen Scaffold Promotes Intrinsic Vascularisation for Tissue Engineering Applications. *PLoS One* 11(2):e0149799.
196. Nakayama KH, Hong G, Lee JC, Patel J, Edwards B, Zaitseva TS, Paukshto M V, Dai H, Cooke JP, Woo YJ, Huang NF (2015) Aligned-Braided Nanofibrillar Scaffold with Endothelial Cells Enhances Arteriogenesis. *ACS Nano* 70(12):773–779.
197. Chen S, Kawazoe N, Chen G (2017) Biomimetic Assembly of Vascular Endothelial Cells and Muscle Cells in Microgrooved Collagen Porous Scaffolds. *Tissue Eng Part C Methods* 23(6):367–376.
198. Gilbert-Honick J, Iyer SR, Somers SM, Lovering RM, Wagner K, Mao HQ, Grayson WL (2018) Engineering functional and histological regeneration of vascularized skeletal muscle. *Biomaterials* 164:70–79.
199. Silva EA, Kim E-S, Kong HJ, Mooney DJ (2008) Material-based deployment enhances efficacy of endothelial progenitor cells. *Proc Natl Acad Sci* 105(38):14347–14352.
200. Hill E, Boontheekul T, Mooney DJ (2006) Designing Scaffolds to Enhance Transplanted Myoblast Survival and Migration. *Tissue Eng* 12(5):1295–1304.
201. Pumberger M, et al. (2016) Synthetic niche to modulate regenerative potential of MSCs and enhance skeletal muscle regeneration. *Biomaterials* 99:95–108.
202. Wang L, Cao L, Shansky J, Wang Z, Mooney D, Vandenburgh H (2014) Minimally invasive approach to the repair of injured skeletal muscle with a shape-memory scaffold. *Mol Ther* 22(8):1441–1449.
203. VanDusen KW, Syverud BC, Williams ML, Lee JD, Larkin LM (2014) Engineered skeletal muscle units for repair of volumetric muscle loss in the tibialis anterior muscle of a rat. *Tissue Eng Part A* 20(21–22):2920–30.
204. Shansky J, Chromiak J, Del Tatto M, Vandenburgh H (1997) A simplified method for tissue engineering skeletal muscle organoids in vitro. *Vitr Cell Dev Biol - Anim* 33(9):659–661.
205. Rodriguez BL, Florida SE, VanDusen KW, Syverud BC, Larkin LM (2018) The Maturation of Tissue-Engineered Skeletal Muscle Units Following 28-Day Ectopic Implantation in a Rat. *Regen Eng Transl Med*.
206. Quarta M, et al. (2016) An artificial niche preserves the quiescence of muscle stem cells and enhances their therapeutic efficacy. *Nat Biotechnol* 34(7):752–759.
207. Fu X, et al. (2015) Combination of inflammation-related cytokines promotes long-term muscle stem cell expansion. *Cell Res* 25(6):655–673.
208. Discher DE, Janmey P, Wang Y-L (2005) Tissue cells feel and respond to the stiffness of their substrate. *Science* 310(5751):1139–43.
209. Falkenberg N, Höfig I, Rosemann M, Szumielewski J, Richter S, Schorpp K, Hadian K, Aubele M, Atkinson MJ, Anastasov N (2016) Three-dimensional microtissues essentially contribute to preclinical validations of therapeutic targets in breast cancer. *Cancer Med* 5(4):703–710.
210. Bell CC, et al. (2016) Characterization of primary human hepatocyte spheroids as a model system for drug-induced liver injury, liver function and disease. *Sci Rep* 6(1):25187.
211. Schmeichel KL, Bissell MJ (2003) Modeling tissue-specific signaling and organ function in three dimensions. *J Cell Sci* 116(12):2377–88.
212. Spielmann H, Hoffmann S, Liebsch M, Botham P, Fentem J (2007) The ECVAM international validation study on in vitro tests for acute skin irritation: report on the validity of the EPISKIN and EpiDerm assays and on the Skin Integrity Function Test. *Altern Lab Anim* 35(6):559–601.
213. Anton D, Burckel H, Josset E, Noel G (2015) Three-dimensional cell culture: A breakthrough in vivo. *Int J Mol Sci* 16(3):5517–5527.
214. Hendriks DFG, Fredriksson Puigvert L, Messner S, Mortiz W, Ingelman-Sundberg M (2016) Hepatic 3D spheroid models for the detection and study of compounds with cholestatic liability. *Sci Rep* 6(1):35434.

215. Rao L, Qian Y, Khodabukus A, Ribar T, Bursac N (2018) Engineering human pluripotent stem cells into a functional skeletal muscle tissue. *Nat Commun* 9(1):126.
216. Martin NRW, Turner MC, Farrington R, Player DJ, Lewis MP (2017) Leucine elicits myotube hypertrophy and enhances maximal contractile force in tissue engineered skeletal muscle in vitro. *J Cell Physiol* 232(10):2788–2797.
217. Vandenburgh H (2010) High-content drug screening with engineered musculoskeletal tissues. *Tissue Eng Part B Rev* 16(1):55–64.
218. Gholobova D, Gerard M, Decroix L, Desender L, Callewaert N, Annaert P, Thorrez L (2018) Human tissue-engineered skeletal muscle: a novel 3D in vitro model for drug disposition and toxicity after intramuscular injection. *Sci Rep* 8(1):12206.
219. Dambach DM, Uppal H (2012) Improving risk assessment. *Sci Transl Med* 4(159):1–6.
220. Olson H, et al. (2000) Concordance of the toxicity of pharmaceuticals in humans and in animals. *Regul Toxicol Pharmacol* 32(1):56–67.
221. Cozigou G, Crozier J, Hendriksen C, Manou I, Ramirez-hernandez T (2015) The European Partnership for Alternative Approaches to Animal Testing (EPAA): Promoting Alternative Methods in Europe and Beyond. *J Am Assoc Lab Anim Sci* 54(2):209–213.
222. Vandenburgh H, Shansky J, Benesch-Lee F, Skelly K, Spinazzola JM, Saponjian Y, Tseng BS (2009) Automated drug screening with contractile muscle tissue engineered from dystrophic myoblasts. *FASEB J* 23(10):3325–34.
223. Dance A (2017) Engineering the animal out of animal products. *Nat Biotechnol* 35(8):704–707.
224. Thorrez L, Vandenburgh H (2019) The Quest for 'Clean Meat' – Significant Scientific Challenges Still Exist. *Nat Biotechnol* (in submission).

CHAPTER 2

AIMS

2 Aims

The main objective of this thesis is to further elaborate a current *in vitro* model for human skeletal muscle, mimicking more closely the *in vivo* situation. A common shortcoming of current tissue engineered constructs is the lack of a functional vasculature, limiting their size and *in vivo* functionality. Therefore, we have evaluated different approaches for prevascularization of skeletal muscle construct.

AIM 1. Develop a human prevascularized skeletal muscle construct.

Since endothelial cells are able to form vascular networks through vasculogenesis, we hypothesized, that introduction of endothelial cells to the existing BAM model would result in a muscle construct with well aligned myotubes interspersed with vascular structures. A fibrin BAM model containing human muscle cells and HUVECs was developed, the so called coculture BAM or the one stage approach. Different medium conditions for coculturing both cell types were evaluated, to ensure an optimal myoblast differentiation and endothelial cell survival. Moreover, different myoblast-HUVEC ratios and total cell numbers were assessed to warrant a BAM construct with well differentiated myotubes and endothelial networks. The first approach is discussed in **Chapter 3** and has been published as 'Gholobova D et al. (2015) Endothelial Network Formation Within Human Tissue-Engineered Skeletal Muscle. Tissue Eng Part A 21(19–20):2548–2558'. To further improve prevascularization with minimal loss of myotube formation in the BAM a two stage prevascularization approach was developed and evaluated *in vitro*. In the two-stage approach, a one week old BAM containing differentiated myotubes was coated with a fibrin hydrogel containing endothelial cells. Since differentiation of each cell type occurs in its own specialized medium, we predicted a better survival and morphology of each cell type. This approach is discussed in **Chapter 4** and is submitted to Biomaterials: 'Gholobova et al. (2019) Functional evaluation of prevascularization in one-stage versus two- stage tissue engineering approach of human bio-artificial muscle'.

AIM 2. Evaluate whether prevascularization improves BAM engraftment *in vivo.*

To define which SMTE approach supported better myotube survival and maturation on the one hand, and perfusion throughout the implanted construct on the other hand, prevascularized BAMs were implanted in NOD/SCID mice for 14 days. Myotube and endothelial network formation were evaluated before and after implantation by confocal microscopy and image analysis. Perfusion was evaluated by Ulex europaeus agglutinin-I (UEA-I) tail vein injection

and presence of red blood cells in engineered endothelial networks. Since endothelial networks and myotube formation were more developed in the two stage approach, we hypothesized that the two stage BAM would have better engraftment *in vivo*. The second aim is discussed in **Chapter 4** and is submitted to Biomaterials: 'Gholobova et al. (2019) Functional evaluation of prevascularization in one-stage versus two- stage tissue engineering approach of human bio-artificial muscle'.

AIM 3. Evaluate the BAM model as an *in vitro* model for intramuscular drug injections.

To further decrease and complement the use of *in vivo* animal studies, we have evaluated engineered human muscles as a pre-clinical model for intramuscular drug injection. Since BAMs contain differentiated human myotubes in an organized 3-dimensional structure, we hypothesized BAMs are able to reflect compound toxicity and pharmacokinetics better than currently possible with 2-dimensional cell culture. Therefore a customized micro injection set-up was developed. We evaluated BAMs engineered with myoblasts only and BAMs with a mixed muscle cell population and compared to 2-dimensional muscle cell culture and human muscle biopsies. To assess whether BAMs are able to evaluate pharmacokinetics and metabolism after intra-muscular injection, we injected several compounds; a dye, a hydrolysable compound and a reducible substrate. Direct reflux, release and metabolism were assessed over time. Furthermore, to explore whether the BAM reflects compound toxicity, we have injected a wasp venom toxin and evaluated creatine kinase release in the medium. This aim and results are discussed in **Chapter 5** and have been published as 'Gholobova D et al. (2018) Human tissue-engineered skeletal muscle: a novel 3D in vitro model for drug disposition and toxicity after intramuscular injection. Sci Rep 8(1):12206.'

CHAPTER 3

ENDOTHELIAL NETWORK FORMATION WITHIN HUMAN TISSUE-ENGINEERED SKELETAL MUSCLE

Published as:
Gholobova D, Decroix L, Van Muylder V, Desender L, Gerard M, Carpentier G, Vandenburgh H, Thorrez L (2015) Endothelial Network Formation Within Human Tissue-Engineered Skeletal Muscle. *Tissue Engineering Part A* 21(19–20):2548–2558.

3.1 Abstract

The size of *in vitro* engineered skeletal muscle tissue is limited due to the lack of a vascular network *in vitro*. In this article, we report tissue-engineered skeletal muscle consisting of human aligned myofibers with interspersed endothelial networks. We extend our bioartificial muscle (BAM) model by coculturing human muscle progenitor cells with human umbilical vein endothelial cells (HUVECs) in a fibrin extracellular matrix (ECM). First, the optimal medium conditions for coculturing myoblasts with HUVECs were determined in a fusion assay. Endothelial growth medium proved to be the best compromise for the coculture, without affecting the myoblast fusion index. Second, both cell types were cocultured in a BAM maintained under tension to stimulate myofiber alignment. We then tested different total cell numbers containing 50% HUVECs and found that BAMs with a total cell number of 2.10^6 resulted in well-aligned and densely packed myofibers while allowing for improved interspersed endothelial network formation. Third, we compared different myoblast-HUVEC ratios. Including higher numbers of myoblasts improved endothelial network formation at lower total cell density; however, improvement of network characteristics reached a plateau when 1.10^6 or more myoblasts were present. Finally, addition of Matrigel to the fibrin ECM did not enhance overall myofiber and endothelial network formation. Therefore, in our BAM model, we suggest the use of a fibrin extracellular matrix containing 2.10^6 cells of which 50-70% are muscle cells. Optimizing these coculture conditions allows for a physiologically more relevant muscle model and paves the way toward engineering of larger *in vitro* muscle constructs.

3.2 Introduction

Skeletal muscle tissue has a capacity for self-renewal upon muscle injury, but when this is impaired, non-functional scar tissue replaces the damaged or lost muscle. Current therapeutic interventions include autologous muscle transpositions, but these are associated with donor site morbidity and poor tissue survival and integration (1). As an alternative for autologous muscle transpositions, human skeletal muscle organoids can be created *in vitro* by tissue engineering. Next to potential applications in regenerative medicine, muscle organoids may also be used as an *in vitro* model for myogenesis or myopathology. Culture and differentiation of myogenic progenitor cells on natural and synthetic biodegradable scaffolds result in differentiated myofibers, which are often unaligned (2,3). Parallel alignment of the myofibers can be induced when cells are subjected to a unidirectional force during differentiation and results in functional bioartificial muscles (BAMs), which can be electrically and mechanically stimulated (4-6). However, the size of *in vitro* created skeletal muscle tissue is limited due to the lack of a vascular network *in vitro*. Coculturing endothelial cells and myoblasts, muscle precursor cells, might overcome this problem. This way, the newly formed muscle can be prevascularized, meaning that an endothelial network is formed *in vitro* in the tissue-engineered muscle. The goal is to anastomose this network to the host vasculature after transplantation. Although prevascularization of tissue-engineered muscle has been described on scaffolds (7,8), myofibers do not align in one direction on these scaffolds, precluding muscle contractility. Other tissue engineering approaches such as the use of soft hydrogels, the combination of endothelial cell sheets with myoblast cell sheets, and microfabrication techniques such as 3D printing may be more suitable to obtain aligned myofibers (7,9–13). Engineering muscle precursor cells in a soft hydrogel such as fibrin allows the myofibers to align in one direction while fibrin behaves as a proangiogenic, making it a good scaffold for both the formation of myofibers and endothelial networks. Prevascularization of aligned tissue-engineered muscle tissue has been described for murine muscle based on coculture of C2C12 murine myoblasts and embryonic heart endothelial cells (14). Another report describes the engineering of aligned, functional rat muscle with postimplantation vascular integration in mice (15). To our knowledge, however, prevascularization of human aligned myofibers has not been described. In this work, we aimed to determine suitable culture conditions allowing both aligned myofiber formation and endothelial network formation as a first step toward a human vascularized BAM. Therefore, we used a coculture of human muscle cells, containing both myoblasts and fibroblasts, and human umbilical vein endothelial cells (HUVECs) in a fibrin extracellular matrix (ECM).

3.3 Methods

3.3.1 Cell culture

HUVECs labeled with green fluorescent protein (GFP) (Angio-proteomie) were cultured in gelatin-coated culture flasks (0.1% gelatin, Millipore, preincubated for 1 h at 37°C) in endothelial growth medium (EGM-2 with bullet kit; Lonza). GFP-HUVECs were split at 90% confluence and used in the experiment at passage 7. Human muscle cells (gift from H. Vandenburgh, Brown University, USA) were isolated by needle biopsy on a 27-year-old male volunteer from a muscle biopsy (vastus lateralis) according to procedures approved by the Institutional Clinical Review Board of the Miriam Hospital (Providence, RI). For muscle satellite cell isolation, muscle tissue was digested for 2 h at 37 °C in DMEM containing 0.1 % collagenase II (Worthington Biochemical Corp.) and 4 mg/ml dispase II (Roche). Cells were plated on 0.1% gelatin-coated T25 tissue culture flask for expansion. They were cultured in skeletal muscle growth medium (SkGM; Lonza) supplemented with 15% fetal bovine serum (FBS; Lonza). Muscle cells were split at 60–70% confluence and used in experiments at 21 doublings.

3.3.2 3D tissue construct

Muscle cells and GFP-HUVECs were mixed with 500 mL thrombin (4 U/mL, Tissucol) and cast into 25-mm-long silicone rubber molds with end attachment sites. Then, 500 mL fibrinogen (2 mg/mL; Tissucol), with or without the addition of 20% Matrigel (BD Biosciences), was added and the cell–gel mix was mixed by quickly pipetting up and down to form a fibrin gel (1 mg/mL, with or without 10% Matrigel), including both cell types. Following 2h of incubation at 37°C, EGM-2 or SkGM supplemented with fibrinolysis inhibitors, aprotinin (92.5 µg/mL; Carl Roth) and tranexamic acid (400µM; Sigma), was added and replaced every two days. For BAMs containing only muscle cells, the medium was switched to differentiation medium two days after casting (SkFM; DMEM with 10ng/mL hEGF, 10mg/mL insulin, 50mg/mL BSA, and 50mg/mL gentamicin). BAMs were made with different cell type ratios and numbers. The medium was replaced every 2 days and BAMs were kept in culture for 7 days before thickness measurement and fixation.

3.3.3 Histology

4% formaldehyde fixed BAMs were dehydrated through an alcohol series and embedded in paraffin. Tissue was sectioned at a thickness of 5 µm with a microtome (Leica RM2125 RTS). Tissue slices were stained with Hematoxylin & Eosin.

3.3.4 Thickness measurements

Cross-sectional thickness of BAMs in culture was measured with a sterile micrometer at day 7 after casting.

3.3.5 Immunocytochemistry

Immunocytochemistry was performed to (i) determine the amount of myoblasts and fibroblasts in the cell population and (ii) to characterize the fusion index of the myoblasts. For desmin staining, muscle cells were cultured in SkGM in 12-well dishes for 2–3 days until 60–70% confluent. For determination of fusion index, the cells were cultured to 80% confluence in SkGM, and then switched to SkFM for 4 days to induce fusion into myofibers. Fixation was performed in a 1:1 methanol–acetone mix at -20°C for 10 min. Next, cells were permeabilized in blocking buffer containing 0.2% Triton X-100 (Sigma) and 1% bovine serum albumin (BSA; Sigma) in PBS (30 min, RT). Subsequently, cells were incubated for 2 h (RT) with a monoclonal mouse antibody against desmin (Sigma; D1033, 1:200 in blocking buffer) or tropomyosin (Sigma, T9283, 1:100 in blocking buffer) to determine the myoblast percentage and the fusion index, respectively. Cells were labeled with a polyclonal goat anti-mouse secondary antibody (Alexa Fluor 568, A11004; Invitrogen) for 30 min in the dark and subsequently incubated with DAPI (0.1 mg/mL in PBS; Life Technologies) for 1 h. The percentage of myoblasts in a muscle cell population was defined as the ratio of desmin-positive cells to the total amount of cells (identified by the DAPI- stained nuclei). Fusion index was defined as the ratio of tropomyosin-positive cells to the total amount of myoblasts in the population.

3.3.6 Whole-mount immunofluorescence staining and confocal microscopy

Constructs were washed (3 x 15 min in PBS), and then removed from the attachment sites. Then, they were pinned on styrofoam to preserve their original shape while fixing in 4% formaldehyde (Merck) for 1 h and stored at 4°C in PBS. Immediately before whole-mount staining, samples were fixed a second time in -20°C methanol for 10 min and permeabilized in blocking buffer for 1 h. Subsequently, BAMs were incubated overnight at 4°C with a monoclonal mouse antibody against tropomyosin (Sigma; T9283, 1:100 in blocking buffer). Next, BAMs were washed and incubated with a polyclonal goat anti-mouse secondary antibody (Alexa Fluor 568, A11004, Invitrogen, 1:200) for 30 min in the dark, followed by incubation with DAPI (Life Technologies; 0.1 mg/mL in PBS) for 1 h. BAMs were stored in PBS in the dark until visualized.

3.3.7 Confocal imaging and data analysis

BAMs were placed on coverslips and visualized by confocal microscopy (Zeiss LSM710) within 48 h. Per BAM, 5 z-stacks were acquired, each containing 20–40 images (depending on the intensity of the signal at various depths) every 5 µm toward the center of the BAM. For myofiber analysis, each 20-µm z-projection (image grouping performed by the ImageJ software (16)) was manually analyzed for different parameters of myofiber formation: myofiber alignment, length, and diameter, as well as number of myofibers per microscopic field. Myofiber alignment was determined by the standard deviation of the angles of the myofibers. A lower number thus indicates better alignment. For endothelial network analysis, each 60-µm z-projection was automatically analyzed by a customized version of the Angiogenesis Analyzer, an ImageJ plugin created by Gilles Carpentier (17). This tool quantifies endothelial networks in an objective manner by extracting characteristic information of the network. Parameters to define endothelial networks were junctions (group of joined nodes, pixels with at least three neighbors), branches (elements delimited by a junction and one extremity), isolated segments (binary lines, which are not branched), total length of endothelial network (interconnected segments, branches, and isolated segments), % branching length (length of interconnected segments and branches divided by total network length), and meshes (areas enclosed by segments) (Supplementary Figure S3.1).

3.3.8 Statistics

Number of replicates refers to number of analyzed images for microscopic analyses or to number of BAMs for thickness analyses. D'Agostino and Pearson normality test and Bartlett's test were used to verify normality of the data and equality of variances, respectively. Normally distributed data with equal variances were analyzed by an unpaired Student t-test when two groups were compared. For comparing several normally distributed groups, a one-way ANOVA was used with a Bonferroni multiple comparison post-test. For groups that were not normally distributed and/or had unequal variances, a non-parametric Mann–Whitney test was used for comparison between two groups, while the Kruskal–Wallis test followed by Dunn's post-test was performed for multiple comparisons. All values are expressed as mean ± standard deviation. *$p < 0.05$, **$p < 0.01$, ***$p < 0.001$, NS = not significant.

3.4 Results

3.4.1 Aligned myofibers are formed in fibrin BAMs cultured in EGM-2

We first characterized the cells expanded from human muscle biopsy. The myogenic progenitor population (further referred to as muscle cells) contained 92.1% ± 4.0% (n = 15) myoblasts and 7.9% ± 4.0% fibroblasts as assessed by desmin staining. Myoblasts had a fusion index of 70.0% ± 5.7% (n = 20) as determined by tropomyosin staining. To make BAMs, 1.10^6 of these cells were mixed in a fibrin ECM (1 mg/mL) and cultured in growth medium (SkGM) for 2 days, followed by differentiation medium (SkFM) for 5 days. The cell-ECM mix contracted around 2 attachment sites and formed 2-cm-long muscle organoids (Figure 3.1, inset) containing aligned myofibers (Figures 3.1A, B, and 3.2A).

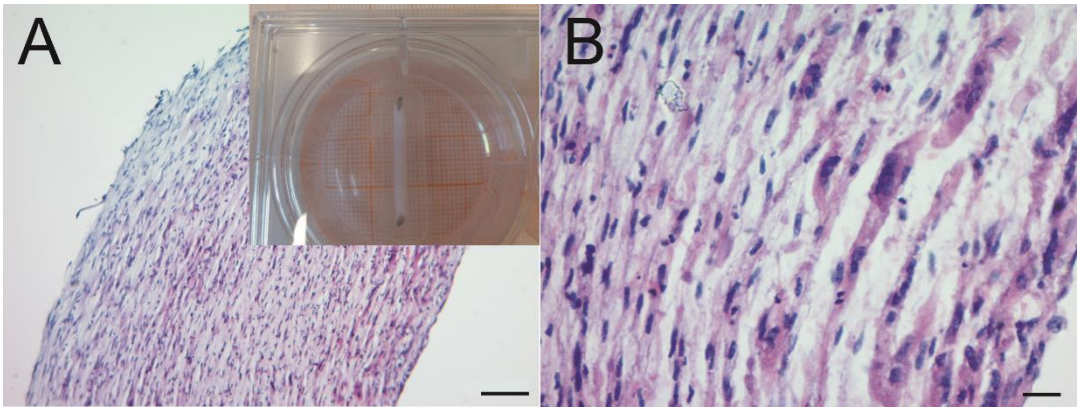


Figure 3.1. H&E staining of a bioartificial muscle (BAM) with 1.10^6 muscle cells in a fibrin extracellular matrix shown with a 10 x (A) and 40 x (B) objective. Inset shows a seven-day-old BAM in a six-well plate, fixed to two attachment sites, which are 2 cm apart. Myofibers are aligned and homogeneously distributed over the entire BAM. Scale bars represent 50 (A) and 10 µm (B).

Aiming at the formation of endothelial networks and aligned myofibers in BAMs, cocultures of HUVECs and muscle cells were mixed in a fibrin ECM in a 50:50 ratio.They are further referred to as coculture BAMs, in contrast to regular BAMs that do not contain endothelial cells. To investigate if endothelial networks can be formed in these organoids, we first applied the same tissue engineering procedure to cocultures of the muscle cells and endothelial cells. However, culturing 5.10^5 muscle cells and 5.10^5 GFP-HUVECs under these culture conditions resulted in poor survival of HUVECs as assessed by confocal fluorescence microscopy (data not shown). Since HUVECs are cultured in EGM-2, muscle cell survival and proliferation in this medium were examined in 2D. Muscle cells proliferated in EGM-2, although significantly slower (doubling time 39.71 – 1.59 h, n = 9) compared with SkGM (30.34 – 0.55 h, n = 9). Optimal differentiation conditions for 2D cultures are obtained by growing the muscle cells for

2–3 days in SkGM until 80% confluency, followed by 3–4 days in SkFM (SkGM-SkFM). Performing the differentiation in EGM-2 for 5 days resulted in myofibers with significantly less nuclei per fiber (2.49 ± 0.10 nuclei per fiber, n = 29) compared with SkGM-SkFM differentiation (7.06 ± 0.58 nuclei per fiber, n = 18). However, the fusion index does not differ significantly between EGM-2 (0.61 ± 0.012, n = 29) and SkGM- SkFM (0.67 ± 0.01, n = 18).

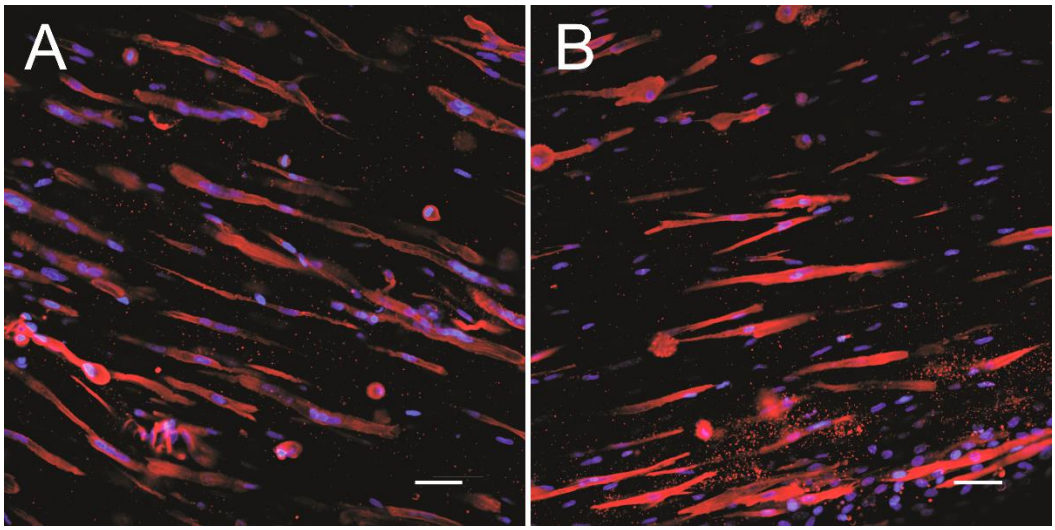


Figure 3.2. Multinucleated myofibers in BAMs with 1.10^6 muscle cells, cultured in (A) SkGM-SkFM and (B) EGM-2. Blue: nuclei stained with DAPI; red: myofibers stained with tropomyosin immunofluorescence.

Next, we compared myofiber formation in the 3D organoid with 1.10^6 muscle cells cultured in EGM-2 versus SkGM- SkFM. Whole-mount tropomyosin staining was performed to visualize the formation of myofibers. Multinucleated myofibers formed in both EGM-2 and SkGM-SkFM. However, myofibers cultured in EGM-2 contained a significantly lower number of nuclei per myofiber (2.29± 0.10, n=10) compared with those cultured in SkGM-SkFM (3.09± 0.15, n=10) (Figure 3.2). Culturing BAMs in EGM-2 also decreased the diameter of the formed myofibers. On the other hand, there was no significant difference between the use of the two media in the number and length of myofibers and the alignment factor (Table 3.1 columns A and D). In addition, the total thickness of the fibrin BAMs with 1.10^6 muscle cells was similar in SkGM-SkFM (2.48 ± 0.224 mm, n= 3) versus EGM-2 (2.76 ± 0.159 mm, n= 3). Since EGM-2 allowed culturing of muscle cells and HUVECs with formation of myofibers while enabling an optimal survival of the HUVECs, we further optimized coculture BAMs in EGM-2.

	A (n=12)	B (n=8)	C (n=11)	D (n=10)	E (n=34)	F (n=11)	G (n=75)	A-D	B-C	D-E	C-E	B-D	D-F	D-G
# Myoblasts	**1.10^6**	**5.10^5**	**5.10^5**	**1.10^6**	**1.10^6**	**1.10^6**	**1.10^6**							
# HUVECs	**0**	**0**	**5.10^5**	**0**	**1.10^6**	**0**	**0**							
Medium	**SkGM/SkFM**	**EGM-2**	**EGM-2**	**EGM-2**	**EGM-2**	**EGM-2**	**EGM-2**							
						+10% matrigel outer 20 µm	**+10% matrigel inner 140 µm**							
Number/microscopic field	42.20 ± 7.64	21.51 ± 2.34	25.63 ± 10.02	39.96 ± 5.75	40.48 ± 10.25	37.09 ± 17.14	35.21 ± 8.24	NS	NS	NS	**	*	NS	NS
Alignment	10.34 ± 4.95	11.36 ± 4.00	16.24 ± 5.96	8.04 ± 1.89	5.09 ± 1.33	7.51 ± 3.76	14.07 ± 4.45	NS	NS	NS	***	NS	NS	***
Length (µm)	147.60 ± 14.11	118.7 ± 16.30	118.90 ± 6.93	126.30 ± 7.02	127.4 ± 37.56	176.30 ± 52.45	113.40 ± 21.21	NS	NS	NS	NS	NS	***	NS
Diameter (µm)	15.34 ± 3.78	10.81 ± 4.26	12.79 ± 4.60	12.20 ± 3.00	13.26 ± 3.69	14.27 ± 3.22	13.75 ± 3.67	*	NS	NS	NS	NS	NS	NS

Table 3.1. Columns A–E are discussed and compared in the 'Aligned myofibers are formed in fibrin BAMs cultured in EGM-2' section, columns F–G are discussed in the 'Matrigel impacts myofiber distribution, but does not improve myofiber and endothelial network formation' section. In the last seven columns, statistical significances are shown for comparisons of indicated groups. Multiple comparisons were made by a Kruskal–Wallis test followed by Dunn's post-test, except for the parameter diameter where a parametric ANOVA followed by a Bonferroni post-test was used. BAM: bioartificial muscle, EGM: endothelial growth medium, HUVEC: human umbilical vein derived endothelial cell.

3.4.2 Formation of aligned myofibers and endothelial networks in fibrin BAMs with a coculture of muscle cells and HUVECs

Coculture BAMs with 50% endothelial cells were further studied in EGM-2 with different total cell numbers (Figure 3.3). The thickness of the BAM was inversely proportional with the total number of cells used both in BAMs with and without HUVECs (Table 3.2 column A). BAMs and coculture BAMS, containing the same number of muscle cells (5.10^5 or 1.10^6), showed similar myofiber formation and alignment (Table 3.1 columns B-C and D-E, Supplementary Figure S3.2). Myofibers were better aligned and more densely packed in coculture BAMs with a higher total cell number of $2 .10^6$ versus 1.10^6 (Figure 3.3). Compared with coculture BAMs with a total number of 1.10^6, coculture BAMs with 2.10^6 cells showed a significant increase in myofiber density and alignment (Table 3.1 columns C and E, Supplementary Figure S3.2 and Supplementary Video S3.1). We hypothesized that also endothelial network formation would be enhanced. Indeed, the endothelial networks were significantly improved in the coculture BAMs with $2 .10^6$ cells (Figure 3.4, Table 3.3 columns A and D, Supplementary Figure S3.3 and Supplementary Video S3.2). The presence of meshes was detected in coculture BAMs and confirms formation of extended endothelial networks (Figures 3.3 and 3.4).

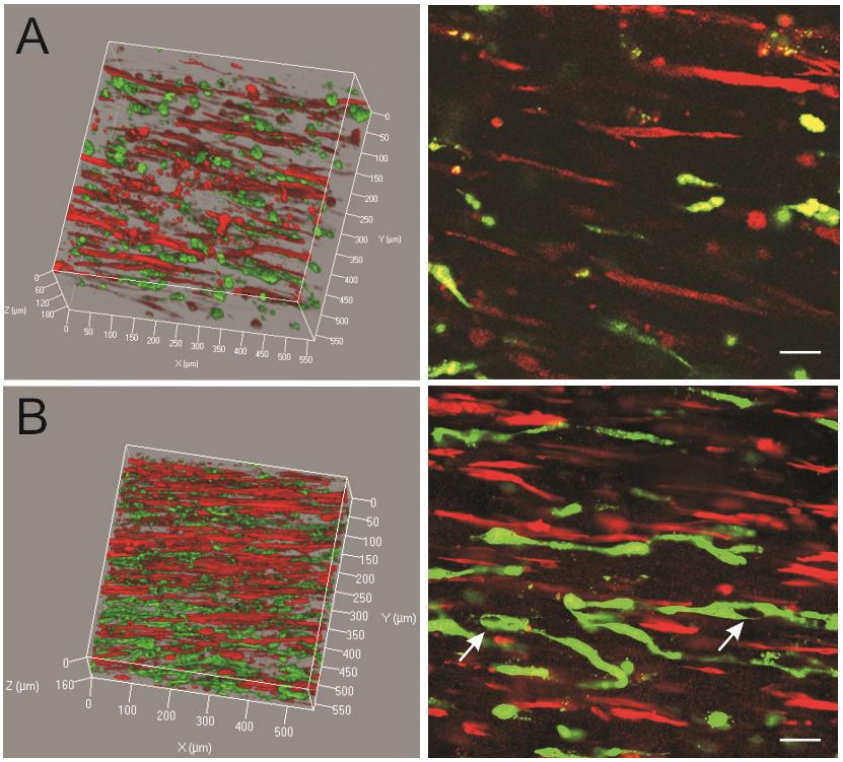


Figure 3.3. Fluorescent confocal images of coculture BAM with 50% human umbilical vein endothelial cells (HUVECs) and 50% muscle cells and a total cell number of 1.10^6 cells (A) and 2.10^6 cells (B). Endothelial networks (green) between aligned myofibers (red) in 3D (left) and an xy-cross section in 2D (right). Scale bars represent 50 µm, meshes are indicated by arrows.

Table 3.2. Thickness (in mm) of Different Fibrin BAMs Cultured for 7 Days in EGM-2

	A. Fibrin ECM	***B. Fibrin + 10% matrigel ECM***
5.10^5 muscle cells	3.20 ± 0.07 (n=3)	3.23 ± 0.35 (n=3)
1.10^6 muscle cells	2.48 ± 0.39 (n=3)	3.32 ±0.13 (n=3)
5.10^5 muscle cells + 5.10^5 GFP-HUVECs	2.20 ± 0.36 (n=3)	2.20 ±0.18 (n=3)
1.10^6 muscle cells + 1.10^6 GFP-HUVECs	1.27 ± 0.22 (n=12)	ND
12.10^5 muscle cells + 8.10^5 GFP HUVECs	1.30 ± 0.03 (n=4)	ND
14.10^5 muscle cells + 6.10^5 GFP HUVECs	1.28 ± 0.21 (n=4)	ND

3.4.3 30% HUVECs suffice to induce endothelial networks between aligned myofibers

Based on our previous findings and on research from other groups (7,9,18), we started experiments with coculture BAMs with a ratio of 50% muscle cells and 50% HUVECs to obtain myofiber and endothelial network formation. To optimize this ratio, BAMs with a total of 1.10^6 or $2. 10^6$ cells were made with different ratios, ranging from 50–70% muscle cells and 50–30% HUVECs. In coculture BAMs with a total of 1.10^6 cells, a muscle cell:HUVEC ratio of 60:40

or 70:30 showed significantly better endothelial network formation compared with coculture BAMs with a 50:50 ratio (Table 3.3 columns A-C, Figure 3.4 and Supplementary Fig. S3.3). Although there was a trend toward further improvement of the endothelial network formation in the 70:30 ratio compared with the 60:40 ratio, this was not significantly different. In the condition with a high percentage of HUVECs (50%), dense clusters of HUVECs occurred at certain places on the surface of the BAMs, which could not be analyzed by the Angiogenesis Analyzer. When a total number of 2.10^6 cells were used, all ratios performed equally well (Table 3.3 columns D–F). However, when compared with the same ratio in BAMs with 1.10^6 cells, there was a significant improvement in endothelial network formation for each ratio, indicating that increasing the total cell number to 2.10^6 is beneficial for all ratios studied (Supplementary Video S3.2). The dense clusters of HUVECs mentioned above were not observed in BAMs with a total cell count of 2.10^6 cells. In coculture BAMs with a total of 1.10^6 cells, a ratio of 60:40 or 70:30 also showed significantly better myofiber formation compared with coculture BAMs with a 50:50 ratio: there was a significant increase in myofiber density and alignment (Table 3.4 columns A-C and Supplementary Figure S3.4). When a total cell number of 2.10^6 was used, no major changes toward improvement of myofiber formation could be detected with increasing ratios of myoblasts (Table 3.4 columns D-F and Supplementary Figure S3.4). When comparing the same ratios in BAMs with 1.10^6 versus 2.10^6 cells, there only was a consistent improvement in alignment of myofibers for the BAMs with 2.10^6 cells.

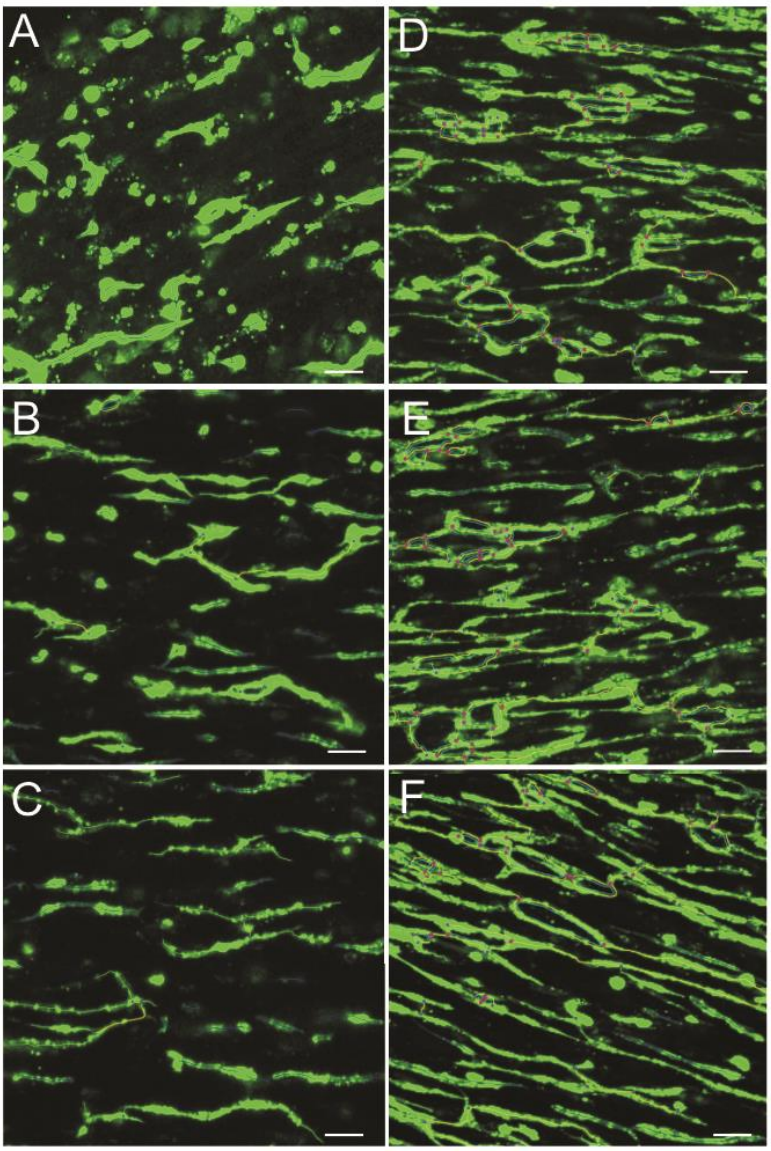


Figure 3.4. (A) Analysis by Angiogenesis Analyzer ImageJ's plugin, visualizing endothelial network formation of 60-µm z-projection images of fibrin BAMs with a total of 1.10^6 cells with 50% (A), 40% (B), and 30% (C) HUVECs or with a total of 2.10^6 cells with 50% (D), 40% (E), and 30% (F) HUVECs. Angiogenesis Analyzer indicates master junctions (pink dots), master segments (yellow), meshes (light blue), branches (green), and isolated segments (blue). Scale bar represents 50 µm.

3.4.4 Matrigel impacts myofiber distribution, but does not improve myofiber and endothelial network formation

In tissue engineering, Matrigel is often used as a (component of) hydrogel because it contains a complex mixture of ECM components and growth factors and has a beneficial impact on tissue growth *in vitro* (1,14). We hypothesized that addition of Matrigel to the fibrin ECM might enhance myofiber and endothelial network formation. We assessed the addition of 10% Matrigel to the ECM of fibrin. This did not significantly change the thickness of the BAMs,

neither in BAMs with 1.10^6 muscle cells nor in coculture BAMs with 5.10^5 muscle cells and 5.10^5 HUVECs (Table 3.2). While in BAMs with 1.10^6 muscle cells in fibrin only, myofibers are evenly distributed throughout the BAM, the addition of 10% Matrigel to the ECM causes an uneven distribution and formation of myofibers. An outer region of 20–30 µm was observed, containing densely packed and highly aligned myofibers and a core with lower cell density containing significantly lower length and alignment of myofibers (Table 3.1, compare columns F-G with column D and Supplementary Figure S3.5). Compared with the homogeneously distributed fibrin BAMs, the outer densely packed region shows significantly longer myofibers, but there is no significant difference in alignment, fiber diameter, or number of myofibers (Table 3.1, column F versus D). The inner region contains myofibers that are less well aligned with no significant difference in the other parameters (Table 3.1, column G versus D). To conclude, the addition of 10% Matrigel does not result in a better myofiber formation throughout the entire BAM, but only in a small outer region of the BAM. In contrast, a decreased myofiber alignment is observed in the inner region. Overall, myofiber formation is heterogeneous throughout the BAM in the presence of Matrigel in the ECM.

	A (n=37)	B (n=8)	C (n=5)	D (n=219)	E (n=65)	F (n=50)	A-B	A-C	A-D	B-E	C-F
Total # cells in BAM	**1.10^6**	**1.10^6**	**1.10^6**	**2.10^6**	**2.10^6**	**2.10^6**					
# Muscle cells	**5.10^5**	**6.10^5**	**7.10^5**	**10.10^5**	**12.10^5**	**14.10^5**					
# HUVECs	**5.10^5**	**4.10^5**	**3.10^5**	**10.10^5**	**8.10^5**	**6.10^5**					
% branching length	20.96 ± 13.28	39.05 ± 15.67	48.29 ± 8.19	76.36 ± 11.84	79.21 ± 8.01	75.92 ± 11.05	**	***	***	***	***
Number of isolated segments	51.24 ± 14.29	36.00 ± 8.40	29.60 ± 2.70	18.72 ± 9.89	15.37 ± 4.78	16.44 ± 5.41	**	***	***	***	***
Number of junctions	3.62 ± 2.64	7.63 ± 4.03	8.60 ± 2.61	47.43 ± 21.61	50.13 ± 13.54	49.64 ± 28.78	**	**	***	***	***
Number of branches	7.78 ± 4.92	15.13 ± 6.47	15.40 ± 5.37	45.96 ± 13.84	48.33 ± 9.68	46.14 ± 17.55	**	**	***	***	***
Total length (µm)	16422 ± 3591	20349 ± 5295	21488 ± 4574	38262 ± 7147	39920 ± 4942	40165 ± 8298	*	*	***	***	***
Number of meshes	0.49 ± 0.8035	0.75 ± 0.71	1.00 ± 0.70	10.50 ± 7.14	12.35 ± 5.182	12.38 ± 8.82	NS	NS	***	***	***

Table 3.3. In the last five columns, statistical significances are shown for comparisons of indicated groups. Comparisons B–C, D–E, D–F, and E–F were also made, but did not result in statistically significant differences for any of the parameters. For multiple comparisons within groups [1.10^6 total cell count (A–C) or 2.10^6 total cell count (D–F)], a nonparametric Kruskal–Wallis test with Dunn's post- test was used. For pairwise comparisons between groups (A-D, B-E and C-F), a Mann Whitney test was performed.

	A (n=11)	B (n=24)	C (n=19)	D (n=34)	E (n=20)	F (n=15)	A-B	A-C	B-C	D-E	D-F	E-F	A-D	B-E	C-F
Total # cells in BAM	**1.10^6**	**1.10^6**	**1.10^6**	**2.10^6**	**2.10^6**	**2.10^6**									
# Muscle cells	**5.10^5**	**6.10^5**	**7.10^5**	**10.10^5**	**12.10^5**	**14.10^5**									
# HUVECs	**5.10^5**	**4.10^5**	**3.10^5**	**10.10^5**	**8.10^5**	**6.10^5**									
Number/ microscopic field	25.63 ±10.02	47.08 ±15.41	48.68 ± 12.56	40.48 ± 10.25	48.29 ± 13.62	49.16 ± 7.26	**	***	NS	NS	**	NS	**	NS	NS
Alignment	16.24 ± 5.96	6.25 ± 0.84	7.72 ± 4.30	5.09 ± 1.33	3.65 ± 0.79	4.912 ± 1.12	***	*	NS	***	NS	**	***	***	***
Length (µm)	118.90 ± 6.93	123.4 ± 13.9	119.7 ± 15.9	127.4 ± 37.56	121.3 ± 15.37	119.2 ± 13.18	NS	NS	NS	NS	NS	NS	NS	NS	NS
Diameter (µm)	12.79 ± 4.60	16.88 ± 8.82	24.05 ± 7.18	13.26 ± 3.69	12.22 ± 2.88	11.96 ± 1.058	NS	***	**	NS	NS	NS	NS	*	***

Table 3.4. In the last nine columns, statistical significances are shown for comparisons of indicated groups. For multiple comparisons within groups [1.10^6 total cell count (A–C) or 2.10^6 total cell count (D–F)], a nonparametric Kruskal-Wallis test with Dunn's post test was used. For pairwise comparisons between groups (A-D, B-E and C-F), a Mann Whitney test was performed.

3.5 Discussion

Obtaining thicker tissue-engineered constructs is one of the important goals in the field of tissue-engineering. To succeed, vascularization is essential for obtaining viable constructs with increased survival time *in vitro* and improved engraftment upon transplantation (7,9,18). To do this, networks of endothelial cells, which form the innermost layer of blood vessels, must be established within the tissue-engineered muscle. The current BAM model consists of aligned multinucleated myofibers, without endothelial cells, starting from a population of human myoblasts and fibroblasts cast in ECM (19). We used the natural hydrogel fibrin as a scaffold for the cells rather than collagen or other alternatives. This choice was made because of its stiffness characteristics and angiogenic properties (20–24). The formation of 3D tissue-engineered human muscle in a fibrin ECM was already described in detail before; however, endothelial cells were not present in these 3D cultures (24).

In our work, HUVECs were added to the muscle cell–fibrin mix to obtain endothelial networks between the myofibers. HUVECs are relatively easy to obtain from the umbilical cord, are robust in culture, and are capable of endothelial cell tube formation *in vitro* (25,26). Adding multiple cell types in an organoid presents a challenge regarding culture conditions (27). In addition, in our system, culture conditions needed to be modified to sustain growth and differentiation of both cell types. We observed that endothelial cells fail to survive and form networks in the optimal culture condition for fibrin BAMs in skeletal muscle growth and differentiation medium. Therefore, we analyzed myofiber formation in BAMs cultured in EGM-2, a growth medium optimized for endothelial cells. This resulted in thinner myofibers with fewer nuclei per fiber compared with the original medium. This may be explained both by a decreased proliferation of myoblasts during the first 2 days in EGM-2 versus SkGM, resulting in a lower cell density and a decreased myoblast fusion in EGM-2 as observed by a lower number of nuclei per myofiber. Nevertheless, aligned myofibers were still formed in BAMs cultured in EGM-2 while allowing the survival of HUVECs, making it the preferred medium for sustaining coculture BAMs.

Next, we investigated varying total cell numbers per BAM and different ratios of HUVECs versus muscle cells to determine the impact on endothelial network formation as well as myofiber formation. For BAMs with 1.10^6 total cells and 50% HUVECs, limited branching and mesh formation were observed. Network characteristics could be improved in cocultures with 40% or even 30% HUVECS. These endothelial networks have a higher number of branches and junctions and a lower number of isolated segments compared with the 50% HUVEC BAMs.

The biggest improvement, however, was observed when a total cell number of 2.10^6 was used instead of 1.10^6 (Supplementary Video S3.2). In these BAMs, the total length of the endothelial network doubled, concurrent with a higher number of meshes, branches, and junctions and a lower number of isolated segments. For 2.10^6 cells, there was no further improvement when the muscle cell:HUVEC ratio was increased from 50:50 to 60:40 or 70:30. This suggests that for the given system and conditions tested, a maximal endothelial network formation was reached when 2.10^6 cells were used, independent of the muscle cell:HUVEC ratio. In addition, for myofiber formation, the 30% and 40% HUVEC BAMs with a total cell number of 1.10^6 contained a higher number of myofibers that were thicker and better aligned than in the 50% HUVEC BAMs. Moreover, in the 50% HUVEC BAMs, HUVECs were unequally distributed throughout the BAM with denser layers toward the surface. These dense layers of HUVECs were not observed in the conditions with 2.10^6 cells, pointing to a better distribution of the HUVECs within the BAM. Overall, parameters of myofiber formation performed equally well or better when using 2.10^6 cells versus 1.10^6 cells. Similar to endothelial network formation, changing the muscle cell:HUVEC ratio did not further influence myofiber formation for 2.10^6 total cells. These and the above findings suggest an optimal combination of myofiber and endothelial network formation in coculture BAMs with 2.10^6 cells and a minimum of 50% muscle cells (Supplementary Video S3.3). The presence of 1.10^6 muscle cells (both in BAMs with or without endothelial cells) has a double advantage over BAMs with only 5.10^5 muscle cells. First, as can be expected when using more muscle cells, myofiber density is higher. Second, a concurrent positive effect is observed in the alignment of myofibers. At the tissue level, BAMs with a higher total cell number have a significantly smaller thickness regardless of the type of cells. This may be explained by an augmented cell-mediated contraction of the ECM. We can conclude that the presence of HUVECs does not impair the formation of myofibers.

In addition to a better endothelial network formation when doubling total cell number per BAM, an increased amount of muscle cells has an important effect on endothelial network formation in the presence of similar amounts of HUVECs (compare Table 3.4 column A vs column F). It has been described that vascular endothelial growth factor (VEGF) is also produced by myoblasts and this expression is enhanced when myofibers are kept under uniaxial tension (14). In the experiments described in this article, we used EGM-2, which contains 0.5 ng/mL VEGF. Addition of VEGF in constructs with only endothelial cells leads to a more organized growth pattern of the endothelial cells (14). Although the amount of VEGF secreted by the myofibers in the cell culture medium (<0.3 ng/mL) (14) was much lower than the amount of VEGF present

in EGM-2, local VEGF concentrations in our extracellular fibrin matrix may be much higher because of VEGF binding to fibrin (28). This is consistent with the observation that even lower total amounts of HUVECs still result in better endothelial network formation when the total cell number is kept at 1.10^6 since the total amount of myofibers is higher.

In none of the myofibers we visualized, we could detect cross-striations. These have been described *in vitro* both in 2D (29) as well as in 3D muscle cultures (1,30). We performed confocal microscopy at day 7 of cocultures, whereas cross- striations were reported only after 14 days of culture. Next to a prolonged culture time, supplementing EGM-2 with specific growth factors to stimulate myoblast fusion, such as MAGIC-F1 protein, IGF-1, and follistatin (31), can be explored in the future. In addition, subjecting BAMs to electrical and/ or mechanical stimulation has been described to further improve several muscle characteristics, such as viscoelastic properties, protein synthesis, myofiber diameter, and density, thus improving the level of maturation of myofibers (32,33). Next to HUVECs, other endothelial cell populations may be worthwhile for further investigation. In particular, endothelial colony-forming cells (ECFCs), also termed blood outgrowth endothelial cells, are able to perform *de novo* tube formation and are proangiogenic *in vitro* and *in vivo* (34). Human peripheral blood and umbilical cord blood ECFCs form *de novo* functional blood vessels when seeded into a matrix and implanted *in vivo* (35). Microvessel density was similar for ECFCs and HUVECs, indicating a robust vasculogenic potential for both cell types (36). Adult peripheral blood ECFCs formed unstable vessels, while umbilical cord blood-derived ECFCs transiently formed vessels when implanted alone and were stable for four months when coimplanted with fibroblasts in an immunodeficient recipient (37). Our muscle cell population also contains fibroblasts. These have been described to provide support for endothelial cells as well as modulate their migration, viability, and network formation (38). Optimizing fibroblast ratios and/or using other cell populations such as pericytes to stabilize endothelial networks may also further improve the cocultures (39). It remains to be seen though if the type of endothelial cells, which are used *in vitro*, is a critical factor once the construct is implanted since the implanted endothelial network may be replaced by the host. Engineered human vascular networks, which were transplanted into third-degree burns, connected with the host vessels during the first week, but during a remodeling phase in the second week after transplantation, the transplanted vessels regressed (40) and were replaced by host vessels. Transformation into mature blood vessels occurs through an inflammation-mediated process of vascular remodeling (41).

As described by others (7,9,11,18), prevascularization of tissue-engineered muscle improves vascularization, blood perfusion, and survival of the muscle constructs upon transplantation.

Specifically, Koffler et al. (18) have shown that the degree of prevascularization *in vitro*, which highly depends on ECM, cell types, cell number, culture conditions, and duration of *in vitro* culture, determines the *in vivo* vascularization. The goal of our study was to optimize experimental conditions to obtain maximal endothelial network formation in coculture BAMs. These findings open perspectives toward culture of larger prevascularized BAMs with potential for human muscle transplantations as well as a physiologically relevant *in vitro* model for studying diseases and therapies (5,42,43). Host blood vessels are able to invade avascular muscle bundles (15); however, this still limits the size of muscle bundles that can be kept in culture preimplantation. Ideally, anastomosis of the preimplantation network with host vessels occurs. Anastomosis between HUVEC-derived vessels and host (mouse) vessels has been detected (8) and this occurs as early as 1 day after implantation (18), although it is not clear to what extent anastomosis occurs. Whether our prevascularized BAMs survive *in vivo* and allow for anastomosis will be assessed by future implantation experiments.

We also tested the addition of 10% Matrigel in coculture BAMs. Matrigel has been used in combination with collagen type I to form BAMs (19). It is a gelatinous protein mixture obtained from mouse sarcoma cells containing many ECM proteins and growth factors. Fibrin (1 mg/mL) without Matrigel supports a homogenous formation of myofibers. In contrast, in the BAMs with 10% Matrigel, the myofibers in the exterior 20 µm of the BAM are longer than in the condition without Matrigel. In the center of the BAM, the myofibers are less well aligned compared with the fibrin-only ECM. To conclude, we do not suggest using Matrigel as part of the ECM of BAMs with a fibrin-based ECM to obtain homogeneously distributed and formed myofibers. Moreover, the composition of Matrigel is not fully characterized.

In addition, different gel formulations and gelation conditions can strongly influence fibrin biochemistry and ultrastructure, which in turn has an important effect on its angiogenic properties and on cell behavior (44). Fibrin ultrastructure (and cell behavior) is also affected by fibrinogen and thrombin concentrations, calcium ion content, ionic strength, temperature, and pH during gelation. For both thrombin and fibrinogen, there is not only a difference between brands but also within one brand, depending on the source of the fibrin (44). Therefore, a direct comparison of these results with previous results in literature is difficult since different research groups not only use different types of fibrin but also different cell types, cell numbers, and volumes of ECM in tissue engineering of BAMs (5,7,9,12,18–20).

To create muscle tissue similar to that in the adult body, still other hurdles need to be overcome. A major one is the formation of neuromuscular synapses. Therefore, myofibers should express functional nicotinic acetylcholine receptors (AchRs) capable of generating acetylcholine-

induced action potentials. Acetylcholine receptor expression increases sharply just before myoblast fusion (45), but is distributed randomly along the surface. During later phases of myogenesis, these receptors cluster at the motor endplates. In the absence of neural cells, BAMs have been shown to form mature AchR clusters by the addition of agrin and laminin (46). In the absence of mature AchR clusters, BAMs can still be stimulated by electrical current, which results in increased protein synthesis, increased force production, and excitability (5,47). The introduction of neural cells to a monolayer of myotubes resulted in the formation of neuromuscular-like junctions with clustering of acetylcholine receptors (48). It is not known whether endothelial cells could affect the expression of muscle nicotinic receptors and/or induce clustering of AchRs. This could be further studied with our coculture system. Furthermore, BAMs should remain under tension *in vivo* to avoid atrophy. Therefore, another issue to be addressed is the integration of BAMs with bioartificial tendons. Our model system allows for extensive biochemical, physical, cellular, and electrical characterization of the effect of adding different cell types to muscle cells during myofiber formation. It thus bridges the gap between 2D culture systems and *in vivo* transplantation of exogenous muscle tissue.

To our knowledge, we have tissue engineered for the first time a human BAM containing advanced endothelial cell networks by coculturing HUVECs and human muscle cells in a fibrin ECM.

3.6 Acknowledgments

The authors thank Petra D'hooge for technical assistance with confocal microscopy and Sigrid Vanryckeghem for administrative support. This work was funded by the Research Fund KU Leuven (CREA/12/034). L.T. is a Postdoctoral Fellow of the Research Foundation-Flanders (FWO).

3.7 Disclosure Statement

No competing financial interests exist.

3.8 Supplementary materials

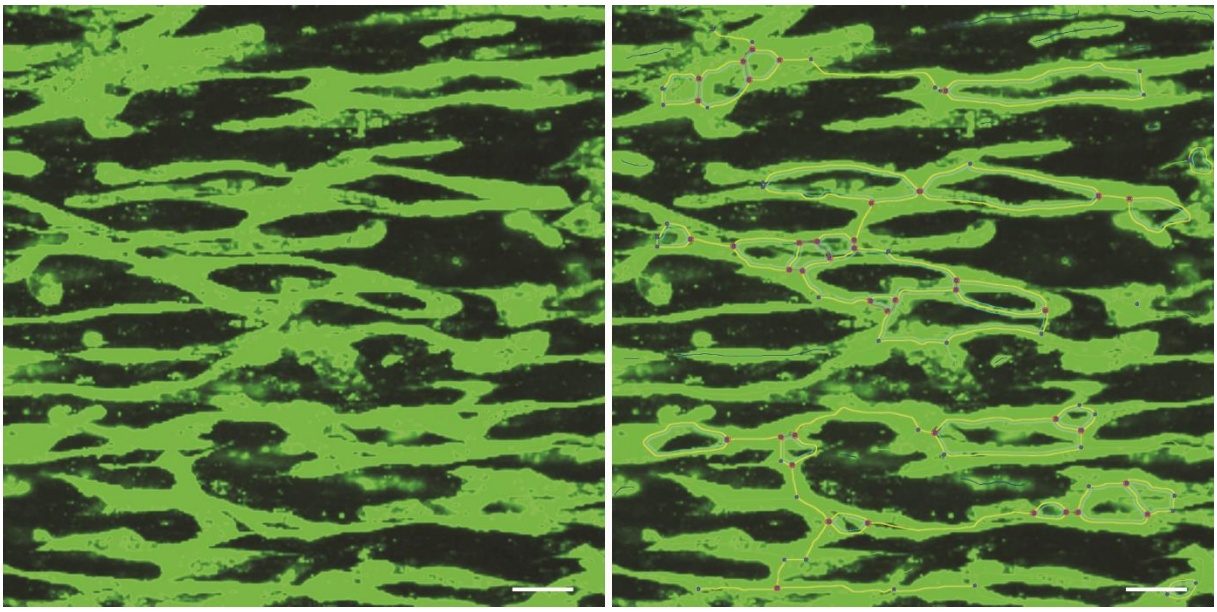


Figure S3.1. Quantification by Angiogenesis Analyzer (right) and original image (left) of endothelial network formation in a coculture BAM. In the right image, there is an indication of master junctions (pink dots), master segments (yellow), meshes (light blue), branches (green) and isolated segments (blue). Scale bar indicates 50 µm.

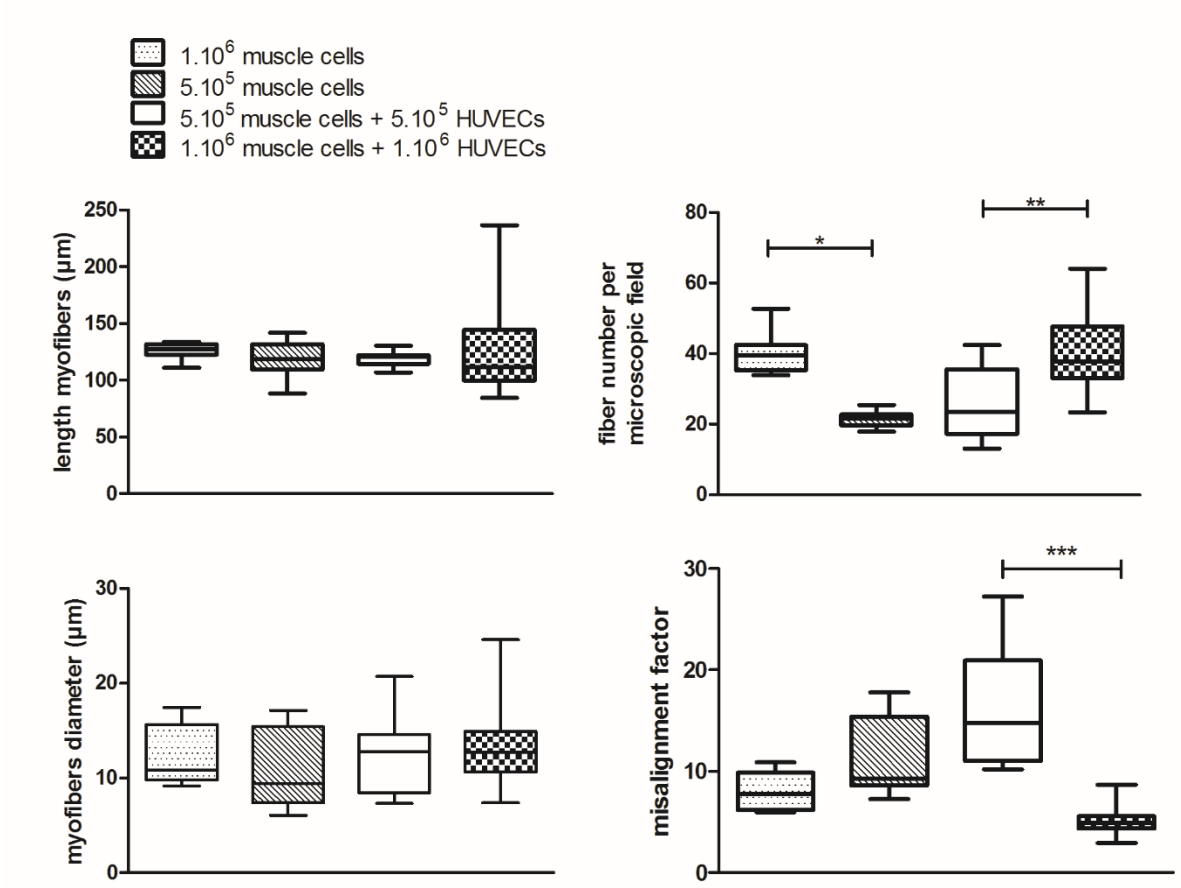


Figure S3.2. Myofiber formation in fibrin BAMs with 0.5 or 1.10^6 muscle cells with or without 0.5 or 1.10^6 HUVECs, respectively.

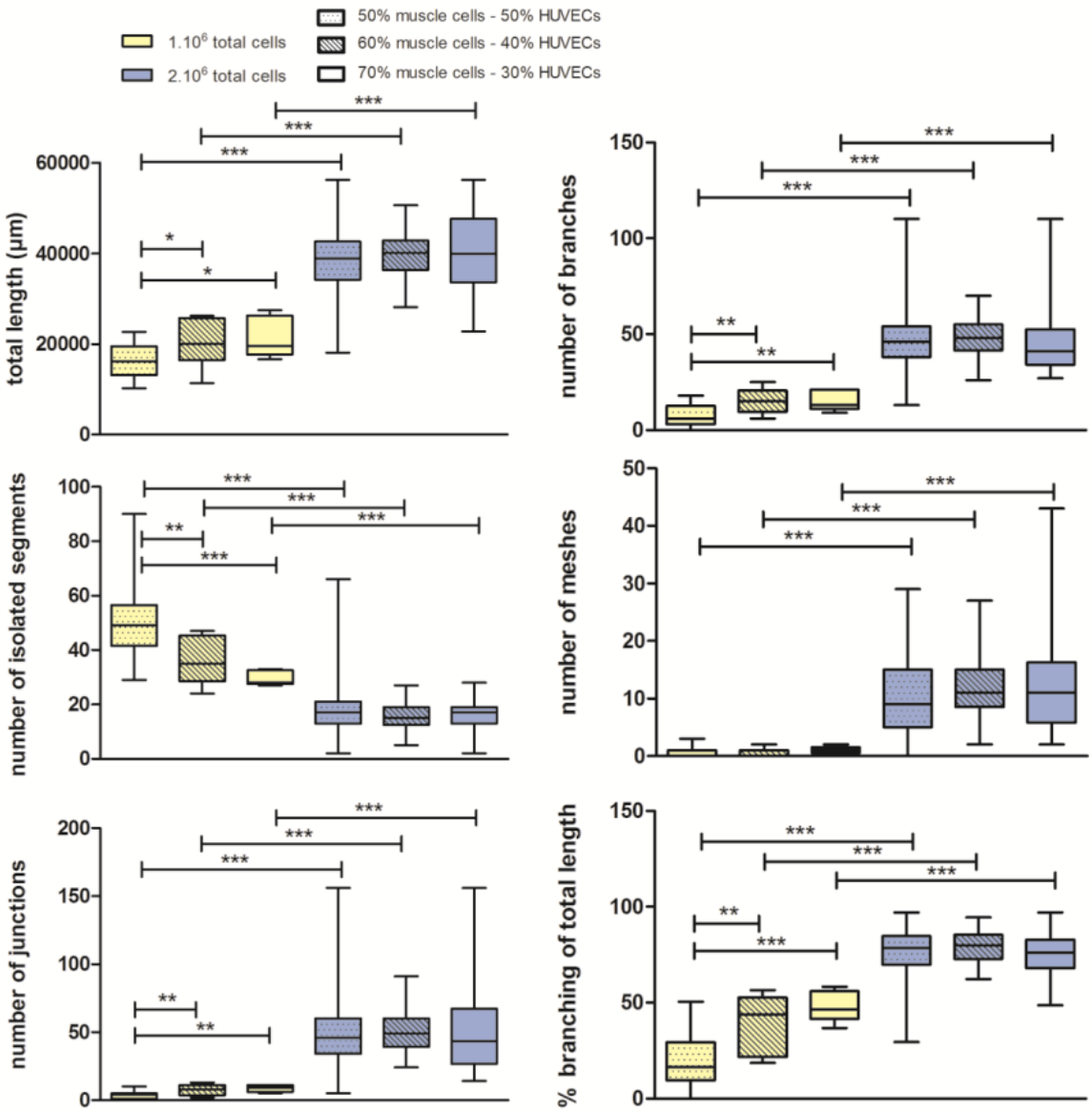


Figure S3.3. Endothelial network formation in coculture BAMs with different ratios of muscle cells and HUVECs in a total of 1.10^6 or 2.10^6 cells. This figure is a graphical representation of Table 3.3.

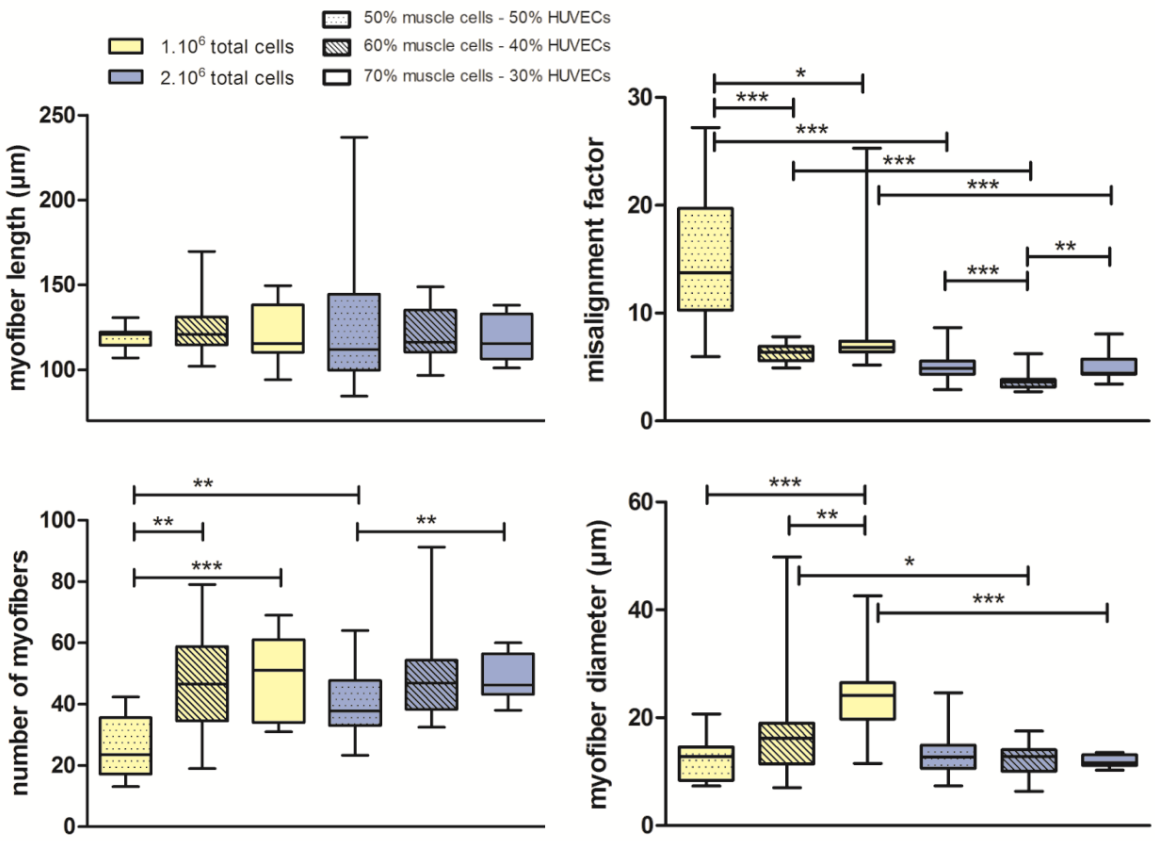


Figure S3.4. Myofiber formation in coculture BAMs with different ratios of muscle cells and HUVECs in a total of 1.10^6 or 2.10^6 cells. This figure is a graphical representation of Table 3.4.

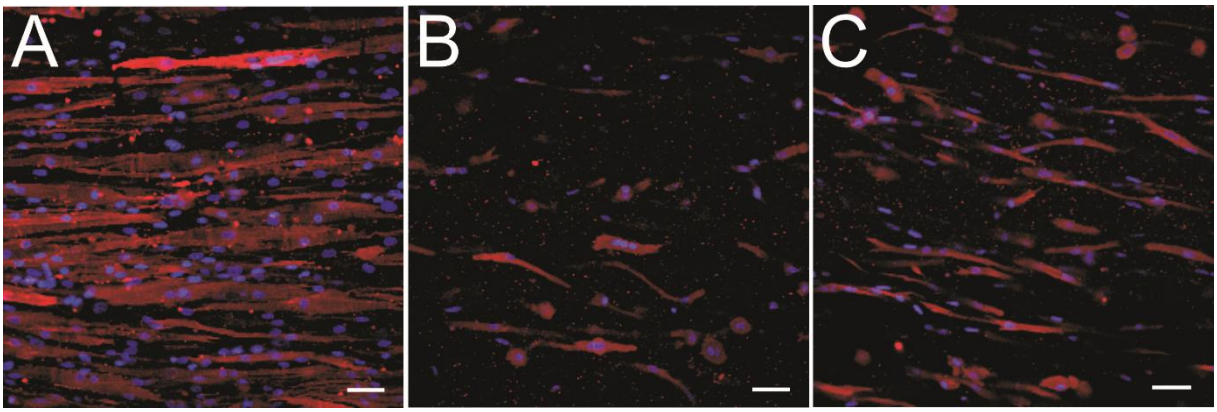


Figure S3.5. BAM with 1.10^6 muscle cells in an ECM of fibrin +10% matrigel (A and B show outer and inner zone respectively) and in a fibrin ECM without matrigel (C). The outer zone of 20 – 30 µm with matrigel (A) shows well aligned myofibers which are longer than in the condition without matrigel (C) whereas the inner zone (B) shows less well aligned myofibers compared to the condition shown in (C). Tropomyosin staining (red) shows myofibers, DAPI (blue) shows cell nuclei.

Video S3.1. Fluorescent confocal z-stack of aligned myofibers in coculture BAM with 50% HUVECs and 50% muscle cells and a total cell number of 2.10^6 cells. This video is a rotating 3D reconstruction of Figure 3.3B.
https://www.liebertpub.com/doi/suppl/10.1089/ten.tea.2015.0093

Video S3.2. Fluorescent confocal z-stack of endothelial networks in coculture BAM with 50% HUVECs and 50% muscle cells and a total cell number of 2.10^6 cells. This video is a rotating 3D reconstruction of Figure 3.3B.
https://www.liebertpub.com/doi/suppl/10.1089/ten.tea.2015.0093

Video S3.3. Fluorescent confocal z-stack of coculture BAM with 50% HUVECs and 50% muscle cells and a total cell number of 2.10^6 cells. Endothelial networks (green) between aligned myofibers (red) in 3D. This video is a rotating 3D reconstruction of Figure 3.3B.
https://www.liebertpub.com/doi/suppl/10.1089/ten.tea.2015.0093

3.9 References

1. Hinds S, Bian W, Dennis RG, Bursac N (2011) The role of extracellular matrix composition in structure and function of bioengineered skeletal muscle. *Biomaterials* 32(14):3575–83.
2. Fishman JM, Tyraskis A, Maghsoudlou P, Urbani L, Totonelli G, Birchall M, De Coppi P (2013) Skeletal Muscle Tissue Engineering: Which Cell to Use? *Tissue Eng Part B Rev* 44(6):1–46.
3. Klumpp D, Horch RE, Beier JP (2011) Tissue engineering of skeletal muscle. *Tissue Engineering of Skeletal Muscle, Tissue Engineering for Tissue and Organ Regeneration*, ed Eberly PD (InTech).
4. Thorrez L, Shansky J, Wang L, Fast L, VandenDriessche T, Chuah M, Mooney D, Vandenburgh H (2008) Growth, differentiation, transplantation and survival of human skeletal myofibers on biodegradable scaffolds. *Biomaterials* 29(1):75–84.
5. Vandenburgh H, Shansky J, Benesch-Lee F, Barbata V, Reid J, Thorrez L, Valentini R, Crawford G (2008) Drug-screening platform based on the contractility of tissue-engineered muscle. *Muscle Nerve* 37(4):438–47.
6. Shansky J, Chromiak J (1997) A simplified method for tissue engineering skeletal muscle organoids in vitro. *In Vitro Cell Dev Biol Anim* 33(5):659–661.
7. Levenberg S, Rouwkema J, Macdonald M, Garfein ES, Kohane DS, Darland DC, Marini R, van Blitterswijk C a, Mulligan RC, D'Amore P a, Langer R (2005) Engineering vascularized skeletal muscle tissue. *Nat Biotechnol* 23(7):879–84.
8. Shandalov Y, Egozi D, Koffler J, Dado-Rosenfeld D, Ben-Shimol D, Freiman A, Shor E, Kabala A, Levenberg S (2014) An engineered muscle flap for reconstruction of large soft tissue defects. *Proc Natl Acad Sci U S A* 111(16):6010–6015.
9. Lesman A, Koffler J, Atlas R, Blinder YJ, Kam Z, Levenberg S (2011) Engineering vessel-like networks within multicellular fibrin-based constructs. *Biomaterials* 32(31):7856–69.
10. Nagamori E, Ngo TX, Takezawa Y, Saito A, Sawa Y, Shimizu T, Okano T, Taya M, Kino-oka M (2013) Network formation through active migration of human vascular endothelial cells in a multilayered skeletal myoblast sheet. *Biomaterials* 34(3):662–8.
11. Carosio S, Barberi L, Rizzuto E, Nicoletti C, Del Prete Z, Musarò A (2013) Generation of eX vivo-vascularized Muscle Engineered Tissue (X-MET). *Sci Rep* 3:1420.
12. Criswell TL, Corona BT, Wang Z, Zhou Y, Niu G, Xu Y, Christ GJ, Soker S (2013) The role of endothelial cells in myofiber differentiation and the vascularization and innervation of bioengineered muscle tissue in vivo. *Biomaterials* 34:140–149.
13. Miller JS, et al. (2012) Rapid casting of patterned vascular networks for perfusable engineered three-dimensional tissues. *Nat Mater* 11(7):1–7.
14. Van der Schaft DWJ, Van Spreeuwel ACC, Van Assen HC, Baaijens FPT (2011) Mechanoregulation of vascularization in aligned tissue-engineered muscle: a role for vascular endothelial growth factor. *Tissue Eng Part A* 17(21–22):2857–65.
15. Juhas M, Engelmayr GC, Fontanella AN, Palmer GM, Bursac N (2014) Biomimetic engineered muscle with capacity for vascular integration and functional maturation in vivo. *Proc Natl Acad Sci U S A* 111(15):5508–13.
16. Rasband W ImageJ. U. S. National Institutes of Health, Bethesda, Maryland, USA. http://imagej.nih.gov/ij/
17. Carpentier G (2012) Gilles carpentier research web site: computer image analysis. Angiogenesis Analyzer for ImageJ.
18. Koffler J, Kaufman-Francis K, Yulia S, Dana E, Daria AP, Landesberg A, Levenberg S (2011) Improved vascular organization enhances functional integration of engineered skeletal muscle grafts. *Proc Natl Acad Sci U S A* 108(36):14789–94.

19. Thorrez L, Vandenburgh H, Callewaert N, Mertens N, Shansky J, Wang L, Arnout J, Collen D, Chuah M, Vandendriessche T (2006) Angiogenesis enhances factor IX delivery and persistence from retrievable human bioengineered muscle implants. *Mol Ther* 14(3):442–451.

20. Rosso F, Marino G, Giordano A, Barbarisi M, Parmeggiani D, Barbarisi A (2005) Smart materials as scaffolds for tissue engineering. *J Cell Physiol* 203(3):465–70.

21. Morin KT, Tranquillo RT (2011) Guided sprouting from endothelial spheroids in fibrin gels aligned by magnetic fields and cell-induced gel compaction. *Biomaterials* 32(26):6111–8.

22. Morin KT, Smith AO, Davis GE, Tranquillo RT (2013) Aligned human microvessels formed in 3D fibrin gel by constraint of gel contraction. *Microvasc Res* 90:12–22.

23. Morin KT, Dries-Devlin JL, Tranquillo RT (2013) Engineered Microvessels with Strong Alignment and High Lumen Density Via Cell-Induced Fibrin Gel Compaction and Interstitial Flow. *Tissue Eng Part A* 20. doi:10.1089/ten.TEA.2013.0262.

24. Chiron S, Tomczak C, Duperray A, Lainé J, Bonne G, Eder A, Hansen A, Eschenhagen T, Verdier C, Coirault C (2012) Complex interactions between human myoblasts and the surrounding 3D fibrin-based matrix. *PLoS One* 7(4):e36173.

25. Nakatsu MN, Sainson RCA, Aoto JN, Taylor KL, Aitkenhead M, Pérez-del-Pulgar S, Carpenter PM, Hughes CCW (2003) Angiogenic sprouting and capillary lumen formation modeled by human umbilical vein endothelial cells (HUVEC) in fibrin gels: the role of fibroblasts and Angiopoietin-1. *Microvasc Res* 66(2):102–12.

26. Arnaoutova I, George J, Kleinman HK, Benton G (2009) The endothelial cell tube formation assay on basement membrane turns 20: State of the science and the art. *Angiogenesis* 12:267–274.

27. Baldwin J, Antille M, Bonda U, De-Juan-Pardo EM, Khosrotehrani K, Ivanovski S, Petcu EB, Hutmacher DW (2014) In vitro pre-vascularisation of tissue-engineered constructs A co-culture perspective. *Vasc Cell* 6:13.

28. Sahni A, Francis CW (2000) Vascular endothelial growth factor binds to fibrinogen and fibrin and stimulates endothelial cell proliferation. *Blood* 96(12):3772–8.

29. Engler AJ, Griffin M a, Sen S, Bönnemann CG, Sweeney HL, Discher DE (2004) Myotubes differentiate optimally on substrates with tissue-like stiffness: pathological implications for soft or stiff microenvironments. *J Cell Biol* 166(6):877–87.

30. Martin NRW, Passey SL, Player DJ, Khodabukus A, Ferguson R a, Sharples AP, Mudera V, Baar K, Lewis MP (2013) Factors affecting the structure and maturation of human tissue engineered skeletal muscle. *Biomaterials* 34(23):5759–65.

31. Cassano M, et al. (2008) Magic-factor 1, a partial agonist of Met, induces muscle hypertrophy by protecting myogenic progenitors from apoptosis. *PLoS One* 3(9):e3223.

32. Powell C, Smiley BL, Mills J, Vandenburgh HH (2002) Mechanical stimulation improves tissue-engineered human skeletal muscle. *Am J Physiol Cell Physiol* 283(5):1557–1565.

33. Rangarajan S, Madden L, Bursac N (2014) Use of Flow, Electrical, and Mechanical Stimulation to Promote Engineering of Striated Muscles. *Ann Biomed Eng* 42(7):1391–405.

34. van Beem RT, Verloop RE, Kleijer M, Noort W a, Loof N, Koolwijk P, van der Schoot CE, van Hinsbergh VWM, Zwaginga JJ (2009) Blood outgrowth endothelial cells from cord blood and peripheral blood: angiogenesis-related characteristics in vitro. *J Thromb Haemost* 7(1):217–26.

35. Yoder MC, Mead LE, Prater D, Krier TR, Mroueh KN, Li F, Krasich R, Temm CJ, Prchal JT, Ingram DA (2007) Redefining endothelial progenitor cells via clonal analysis and hematopoietic stem/progenitor cell principals. *Blood* 109(5):1801–1809.

36. Melero-Martin JM, Khan Z a., Picard A, Wu X, Paruchuri S, Bischoff J (2007) In vivo vasculogenic potential of human blood-derived endothelial progenitor cells. *Blood* 109(11):4761–4768.

37. Au P, Daheron LM, Duda DG, Cohen KS, Tyrrell J a, Lanning RM, Fukumura D, Scadden DT, Jain RK (2008) Differential in vivo potential of endothelial progenitor cells from human umbilical cord blood and adult peripheral blood to form functional long-lasting vessels. *Blood* 111(3):1302–1305.

38. Kunz-Schughart L a, Schroeder J a, Wondrak M, van Rey F, Lehle K, Hofstaedter F, Wheatley DN (2006) Potential of fibroblasts to regulate the formation of three-dimensional vessel-like structures from endothelial cells in vitro. *Am J Physiol Cell Physiol* 290:C1385–C1398.

39. Sampaolesi M, et al. (2006) Mesoangioblast stem cells ameliorate muscle function in dystrophic dogs. *Nature* 444(7119):574–9.

40. Hanjaya-Putra D, Shen Y-I, Wilson A, Fox-Talbot K, Khetan S, Burdick JA, Steenbergen C, Gerecht S (2013) Integration and regression of implanted engineered human vascular networks during deep wound healing. *Stem Cells Transl Med* 2(4):297–306.

41. Roh JD, et al. (2010) Tissue-engineered vascular grafts transform into mature blood vessels via an inflammation-mediated process of vascular remodeling. *Proc Natl Acad Sci U S A* 107(10):4669–74.

42. Vandenburgh H, Shansky J, Benesch-Lee F, Skelly K, Spinazzola JM, Saponjian Y, Tseng BS (2009) Automated drug screening with contractile muscle tissue engineered from dystrophic myoblasts. *FASEB J* 23(10):3325–34.

43. Vandenburgh H (2010) High-content drug screening with engineered musculoskeletal tissues. *Tissue Eng Part B Rev* 16(1):55–64.

44. Morin KT, Tranquillo RT (2013) In vitro models of angiogenesis and vasculogenesis in fibrin gel. *Exp Cell Res* 319(16):2409–17.

45. Krause RM, Hamann M, Bader CR, Liu JH, Baroffio a, Bernheim L (1995) Activation of nicotinic acetylcholine receptors increases the rate of fusion of cultured human myoblasts. *J Physiol* 489(3):779–790.

46. Wang L, Shansky J, Vandenburgh H (2013) Induced formation and maturation of acetylcholine receptor clusters in a defined 3D bio-artificial muscle. *Mol Neurobiol* 48(3):397–403.

47. Donnelly K, Khodabukus A, Philp A, Deldicque L, Dennis RG, Baar K (2010) A novel bioreactor for stimulating skeletal muscle in vitro. *Tissue Eng Part C Methods* 16(4):711–8.

48. Larkin LM, Van der Meulen JH, Dennis RG, Kennedy JB (2007) Functional evaluation of nerve-skeletal muscle constructs engineered in vitro. *In Vitro Cell Dev Biol Anim* 42(3–4):75–82.

CHAPTER 4

FUNCTIONAL EVALUATION OF PREVASCULARIZATION IN ONE-STAGE VERSUS TWO-STAGE TISSUE ENGINEERING APPROACH OF HUMAN BIO-ARTIFICIAL MUSCLE

Submitted as:
Gholobova D, Mackova K, Desender L, Carpentier G, Terrie L, Gerard M, Hympanova L, Deprest J, Thorrez L (2019) Functional evaluation of prevascularization in one-stage versus two- stage tissue engineering approach of human bio-artificial muscle. *Biomaterials*

4.1 Abstract

A common shortcoming of current tissue engineered constructs is the lack of a functional vasculature, limiting their size and functionality. Prevascularization is a possible strategy to introduce vascular networks in these constructs. It includes among others co-culturing target cells with endothelial (precursor) cells that are able to form endothelial networks through vasculogenesis. In this paper, we compared two different prevascularization approaches of bio-artificial skeletal muscle tissue (BAM*) in vitro* and *in vivo*. In the one-stage approach, human muscle cells were directly cocultured with endothelial cells in 3D. In the two-stage approach, a one week old BAM containing differentiated myotubes was coated with a fibrin hydrogel containing endothelial cells. The obtained endothelial networks were longer and better interconnected with the two-stage approach. We evaluated whether prevascularization had a beneficial effect on *in vivo* perfusion of the BAM and improved myotube survival by implantation in the *latissimus dorsi* muscle of NODSCID mice for 5 or 14 days. Also *in vivo*, the two-stage approach displayed the highest vascular density. At day 14 anastomosis of implanted endothelial networks with the host vasculature was apparent. BAMs without endothelial networks contained longer and thicker myotubes *in vitro*, but their morphology degraded *in vivo*. In contrast, maintenance of myotube morphology was well supported in the two-stage prevascularized BAMs. To conclude, a two-stage prevascularization approach for muscle engineering improved the vascular density in the construct and supported myotube maintenance *in vivo*.

4.2 Introduction

Skeletal muscle tissue has a high regenerative capacity that is able to replace damaged muscle tissue upon injury (1, 2). A central role in muscle regeneration is played by the muscle progenitor cells known as satellite cells. However in cases of volumetric muscle loss, a failure of muscle repair and scar tissue formation is often observed, resulting in functional muscle impairment (2). The current treatment strategy for localized skeletal muscle repair includes muscle flap transplantation. Therefore, autologous muscle tissue is transplanted from a donor site to the damaged muscle. Unfortunately, this is associated with donor site morbidity and poor flap survival (3). To limit this problem, microsurgery is used to include vasculature to allow the reconstitution of blood supply in the tissue. In turn, this provides oxygen and nutrients, and removes waste products throughout the transplanted tissue (4, 5). To avoid the need of donor site tissue and related injuries, tissue engineered skeletal muscle holds promise as an alternative treatment. Skeletal muscle tissue engineering (SMTE) aims to create *in vitro* muscle tissue that mimics the structure and function of *in vivo* muscle, and thus offers the potential to repair the damaged muscle area. Similar to muscle flaps, clinically relevant SMTE constructs should include vascular networks to improve cell survival deeper than a few hundred micrometer within the tissue, which is the limit of passive diffusion (4, 6, 7). Prevascularization is the formation of capillary-like networks before implantation and is aimed to overcome this diffusion limit. It is an important hurdle to take if the aim is to increase the size of engineered tissue constructs. As for engineering (immature) blood vessels in *in vitro* skeletal muscle constructs, a few *in vitro* approaches have been described, such as co-culturing endothelial cells (EC) and myogenic progenitors on different scaffolds and hydrogels, combining endothelial cell sheets with myoblast cell sheets and engineering vasculature using microfabrication techniques (4, 5, 8, 9). Besides applications in regenerative medicine, such a vascularized muscle model can be used to study mechanisms underlying myogenesis, vasculogenesis and vasculo-myogenic interactions.

Prevascularization is based on *de novo* blood vessel formation known as vasculogenesis. It was shown to be advantageous in SMTE *in vivo* transplantation studies by supporting a higher survival and prolonged functionality of the implanted skeletal muscle construct (10, 11). The SMTE approach used in these prevascularization studies was based on the use of solid scaffolds. The SMTE approach used in our lab is based on previous work of the Vandenburgh lab and uses hydrogels, allowing cells to self-organize and migrate (12, 13). In this approach, cells isolated from a human muscle biopsy are expanded to several millions of muscle cells

(myoblasts and a minority of fibroblasts) and then cast in silicone molds in the presence of a natural hydrogel. After one week, this results in the formation of a bio-artificial muscle containing multinucleated myotubes well-aligned in the direction of the attachment points, so called bio-artificial muscle (BAM). The resulting construct is limited in size (2cm long, ± 1mm thick) due to the absence of a vascular network. To increase the size of the BAM, which would expand its applications and utility, we already succeeded in prevascularizing a BAM *in vitro* in a previous study (9). This was done by seeding human umbilical vein-derived endothelial cells (HUVECs) together with muscle cells in a fibrin hydrogel followed by one week of tissue contraction and cell differentiation. This is a direct 3D co-culture approach, defined as one-stage prevascularization approach in this manuscript (BAM-1s). Despite detailed *in vitro* analysis, no functionality of the preformed endothelial networks was tested *in vivo*. In this follow-up study we aim to (i) further improve the prevascularization with minimal loss of myotube formation in the BAM based on a novel two-stage BAM prevascularization approach (BAM-2s) and (ii) to assess *in vivo* behaviour of prevascularized BAMs in a mouse model.

4.3 Methods

4.3.1 Cell culture

Green Fluorescent Protein (GFP)-labeled HUVECs (GFP-HUVECs, Angio-proteomie) were seeded in cell culture flasks which were precoated for 1 h at 37°C with gelatin (0.1% gelatin, Millipore) and cultured in endothelial growth medium (EGM-2 with bullet kit, Lonza). HUVECs were split at 90% confluence and used in the experiment at passage 7.

Human skeletal muscle cells were isolated from fresh human muscle tissue (vastus lateralis) biopsies obtained from the Human Body Donation programme of KU Leuven University as described in (14). For muscle satellite cell isolation, muscle tissue was digested for 2 h at 37 °C in DMEM containing 0.1 % collagenase II (Worthington Biochemical Corp.) and 4 mg/ml dispase II (Roche). Cells were plated on 0.1% gelatin-coated T25 tissue culture flask for expansion. They were cultured in Ultroser-based skeletal muscle growth medium (SkGM): DMEM high glucose with Glutamax and pyruvate supplemented with 10% fetal bovine serum (Thermo Fisher), 50 µg/ml gentamicin (Thermo Fisher) and 1% Ultroser solution (Pall corporation). Muscle cells were split at 60-70% confluence and used in experiments at 12 doublings. In the isolated muscle cell population, myoblast percentage and fusion index were determined exactly as described before (9, 14).

Muscle cells that were used for tissue engineering of BAMs, and subsequently for implantation, expressed the far-red fluorescent protein miRFP670 (15). The expression of miRFP670 was obtained by transducing $5x10^5$ muscle cells in 3.15 ml SkGM for 48 h with 350 µl $1.21x10^6$ pg p24/ml CMV-miRFP670 cDNA-containing HIV1-derived retroviral particles. Retroviral vectors were produced as previously described by the Leuven Viral Vector Core (Full description in (16) and with improvements in (17)). The transfer plasmid pCH-CMV-miRFP670-3xflag-IRES-blasti was made by cloning the miRFP670 sequence (RefSeq KX421097.1) into an already present pCH-CMV-eGFP-3xflag-Ires-blasti plasmid. All cloning steps were verified by sequencing. This resulted in the expression of triple flag-tagged miRFP670 under the control of a cytomegalovirus (CMV) promotor and with simultaneous expression of a blasticidin resistance cDNA. Lentiviral vector particle number was estimated by quantifying the surface protein p24 with enzyme linked immunosorbent assay (ELISA) (HIV-1 core profile ELISA, DuPont), which was determined to be $1.21x10^6$ pg p24/ml.

4.3.2 Tissue-engineering of BAMs

Three different types of BAMs were used: BAMs with $2x10^6$ muscle cells, cultured for 2 weeks in SkGM/SkFM (BAM), BAMs with $1,4x10^6$ muscle cells and $0,6x10^6$ HUVECs (BAM-1s), cultured for 1 week in EGM-2 and BAMs with $2x10^6$ muscle cells cultured for 1 week in SkGM/SkFM after which the construct was embedded in a fibrin hydrogel with $2x10^6$ GFP labeled HUVECs (BAM-2s) (schematic representation in Figure 4.1).

Tissue-engineering of BAMs was described in (9, 14). Briefly, cells were mixed with 500 µl thrombin (4 U/ml, Bio Phar Laboratories LLC). The mixture was cast into 25-mm-long silicone rubber molds with end attachment sites spaced 20 mm. Then, to form a fibrin hydrogel (1 mg/ml) containing the cells, 500 µl fibrinogen (2 mg/ml, Merck Chemicals) was added and the cell-gel mix was mixed. Following 2 h incubation at 37°C, SkGM (for BAM) or EGM-2 medium (for BAM-1s) supplemented with fibrinolysis inhibitors aprotinin (92.5 µg/ml Carl Roth) and tranexamic acid (400 µM, Sigma) was added. For BAM, the medium was switched to differentiation medium (SkFM, DMEM with 10 ng/ml hEGF, 10 µg/ml insulin, 50 µg/ml BSA and 50 µg/ml gentamicin) two days after casting. To obtain the third type of BAM, BAM-2s, 1 week old BAMs were embedded in 1 ml fibrin (created similar as above) hydrogel containing $2x10^6$ HUVECs and cultured for another week in EGM-2. Medium was replaced every 2 days and BAMs were kept in culture for 7 or 14 days prior to thickness measurement and fixation.

4.3.3 Thickness measurements

Cross-sectional thickness of BAMs in culture and post-implantation was measured with a sterile micrometer at day 7 or day 14 after casting.

4.3.4 In vivo implantation of BAMs

All animal experiments were evaluated and approved by the Animal Ethics Committee of the KU Leuven (P099/2017) and were performed according to international guidelines. BAMs were implanted subcutaneously on the *latissimus dorsi* muscle for a period of 14 days in 6-7 weeks old non-obese diabetic severe combined immunodeficiency (NOD/SCID) mice (Janvier) (n=12 for BAM, n=8 for BAM-1s and n=4 for BAM-2s). All animals were anesthetized and maintained with isoflurane (0.5-2 %, 3-5 L/min) and oxygen while being kept warm on a heating pad during surgery and recovery. The *latissimus dorsi* muscle and its fascia were scraped with a sterile scalpel until minor bleeding was observed. Both sides of the BAM were secured to the muscle with non-resorbable polypropylene suture (Ethicon) parallel to the spine.

After implantation, meloxicam (2 mg/kg; Meloxidyl CEVA) and buprenorphine (0.1 mg/kg; Vetergesic) (for 2 days) were administered subcutaneously. Animals were euthanized 5 or 14 days later. Construct and underlying host tissue was explanted. Host muscle was explanted each time, which served as a negative control. Explants were washed in PBS for 5 min and fixed using 4 % formaldehyde solution (w/v) for 6 h at room temperature (RT).

4.3.5 Whole mount immunofluorescence staining

To assess *in vitro* BAM formation, the 3 types of BAM (BAM, BAM-1s, BAM-2s) were washed (3 x 5 min in PBS) and then removed from the attachment sites. Then, they were pinned on Styrofoam to preserve their original shape during fixation in 4% formaldehyde for 1 h at room temperature (RT) and stored at 4°C in PBS. Explanted constructs from the *in vivo* implantation study were fixed for 6 h at RT in 4% formaldehyde and stored at 4°C in PBS in the dark. For tropomyosin immunohistochemical staining, samples were fixed a second time, in methanol (-20°C, 20 min) immediately prior to staining. Next, the samples were permeabilized in blocking buffer containing 0.2% Triton-X-100 (Sigma) and 1% bovine serum albumin (BSA, Sigma) in PBS for 3 h at RT. Subsequently, the samples were incubated overnight at 4°C with a monoclonal mouse antibody against tropomyosin (Sigma, T9283, 1:100 in blocking buffer) or with polyclonal rabbit antibody against collagen IV (Abcam, ab6586, 1:400 in blocking buffer). To stain capillaries, the explanted BAM constructs were incubated overnight at 4°C with a polyclonal rabbit antibody against CD 31 (Invitrogen, PA16301, 1:30 in blocking buffer). Next, the human BAMs and explants were washed and incubated with a polyclonal goat anti-mouse secondary antibody (Alexa Fluor 633, A-11059 or A-21063, Invitrogen, 1:200), a polyclonal goat anti-rabbit secondary antibody (Alexa Fluor 633, A21070, Thermo Fisher) or a polyclonal donkey anti-rabbit secondary antibody (Alexa Fluor 488, A-21206, Life Technologies) for 3 h in the dark, followed by incubation with DAPI (Life Technologies, 0.1 µg/ml in PBS) for 1 h at RT. Samples were stored in PBS in the dark until visualized.

4.3.6 Confocal imaging

Confocal imaging and data analysis of *in vitro* BAMs and *in vivo* BAMs were performed as described in (9). Briefly, BAMs and explanted tissue were visualized by confocal microscopy (Zeiss LSM710). Per BAM, 5 z-stacks were acquired with Plan-Apochromat 25x/0.8, WD 0.57 mm objective every 5 µm. Since explanted BAMs at day 14 were surrounded by host tissue, the distance to the construct exceeded the working distance of the objective. Therefore 200 µm sections were cut with a vibrotome (Microm HM 650 V, VWR) to allow visualization within

the whole explanted tissue (in collaboration with Prof. Veerle Baekelandt, KU Leuven). More detailed images were acquired with Plan-Apochromat 63x/1.2, WD 0.49 mm. Three dimensional reconstructions of stacked images were generated with Imaris 9.2.0.

4.3.7 Histology

4% formaldehyde fixed BAMs and explanted constructs were dehydrated through an alcohol series and embedded in paraffin. Tissue was sectioned at a thickness of 5 µm with a microtome (Leica RM2125 RTS). Tissue slices were stained with Martius Scarlet Blue (MSB) staining (18) to evaluate the extracellular matrix deposition in BAMs before and after implantation. Murine muscle was used as positive control.

4.3.8 Data analysis

Myotube analysis and endothelial network analysis in *in vitro* constructs and after implantation was performed as previously reported in Gholobova et. al (9). For myotube formation 20 µm z-projections were manually analyzed for different parameters of myotube formation: myotube alignment, length, density and diameter. Myotube alignment was represented as the mean of the standard deviation of the angles of the myotubes. A lower number thus indicates better alignment. For endothelial network analysis, 60 µm z-projections were automatically analyzed by a customized version of the "Angiogenesis Analyzer", an ImageJ plugin created by Gilles Carpentier (9, 19). Moreover, a customized algorithm was developed that was able to detect non-perfused and perfused vessels. This tool is able to measure several parameters of endothelial networks of which we used: total length of endothelial network (master segments, branches and isolated segments), % master segments (length of master segments, longest elements giving origin to branches, divided by total network length) % branching length (length of interconnected segments and branches, elements delimited by two junctions, or a junction and one extremity, divided by total network length) and % isolated segments (length of isolated segments, binary lines which are not branched, divided by total network length.

4.3.9 Detection of anastomosis

Two different approaches were used to evaluate anastomosis and perfusion of the implanted endothelial networks with host vessels; in the first approach 1.25 µg/g body mass rhodamine-labelled Ulex europaeus agglutinine-I (UEA-I; Vectorlabs) was injected intravenously in the tail vein, circulation was allowed for 2 min, whereafter the animal was euthanized by cervical dislocation. UEA-I specifically targets human endothelial cells. Presence of UEA-I positive human endothelial networks was confirmed with confocal imaging of explanted constructs. In

the second approach, human GFP labeled endothelial networks in the explanted constructs were examined for the presence of auto-fluorescent red blood cells by confocal microscopy.

4.3.10 Quantitative real-time PCR

RT-qPCR was performed to determine the expression of the different myosin heavy chain isoforms (*MYH1, MYH3, MYH8*) and myogenin (*MyoG*) in the 3 types of human BAMs to reflect the developmental state of the myotubes in the tissue-engineered constructs. To normalize for the amount of cells, 3 reference genes were used: *GAPDH, HSP90AB1* and *RPL13A*. RT-qPCR was performed as described previously (20). Briefly, BAMs were washed with PBS and lyzed by sonication. After centrifugation (5 min, 2600 g), high quality total RNA was isolated from supernatant using the PureLink RNA Mini Kit (Ambion #12183018A) as evaluated by A260/A280. 2 µg of isolated RNA was reverse transcribed with the qScript cDNA SuperMix (Quantabio #95048-100). PCR was performed with GeneAmp® PCR System 9700 (Applied Biosystems). Gene-specific primers (Table 4.1) were designed using NCBI/Primer-Blast and Primer3plus. Primer efficiency was determined by serial dilution of cDNA during RT-qPCR and verified to be > 90%. RT-qPCR was performed with the LightCycler® 480 Instrument (Roche) using Perfecta Sybr Green Supermix (Quantabio #95054-500). All samples, 10 µl reaction volume, were run in technical duplicates. 40 cycles were run with a DNA dissociation step (95°C, 15 s), a primer annealing step and an amplification step (60°C, 45 s). Melting curve analysis was performed to verify the amplification product. Relative mRNA expression was statistically analyzed with relative expression software tool (REST 2009, Qiagen). The REST software calculates whether gene expression is significantly different between the sample and control group using bootstrap randomization (21).

Table 4.1. List of primers used for RT-qPCR

Gene	Orientation	Primer sequence (5' - 3')	Amplicon size (bp)
MYH1	Forward	GGG AGA CCT AAA ATT GGC TCA A	106
	Reverse	TTG CAG ACC GCT CAT TTC AAA	
MYH3	Forward	CTT GTG GGC GGA GGT CTG G	119
	Reverse	AGC TAT GCC GAA CAC TTC CAT	
MYH8	Forward	ACA TTA CTG GCT GGC TGG AC	143
	Reverse	ACC TTT CTT CGC GCT GCT AT	
MyoG	Forward	GTG TGT AAG AGG AAG TCG GTG TC	90
	Reverse	GAA GGC CTC ATT CAC CTT CTT	
GAPDH	Forward	TCA AGA AGG TGG TGA AGC AGG	168
	Reverse	ACC AGG AAA TGA GCT TGA CAA A	
HSP90AB1	Forward	AGA AAT TGC CCA ACT CAT GTC C	75
	Reverse	ATC AAC TCC CGA AGG AAA ATC TC	
RPL13A	Forward	CCT GGA GGA GAA GAG GAA AGA GA	126
	Reverse	TTG AGG ACC TCT GTG TAT TTG TCA A	

4.3.11 Statistics

Number of replicates refers to number of analyzed images for microscopic analyses or to number of BAMs for thickness analyses. D'Agostino & Pearson normality test and Bartlett's test were used to verify normality of the data and equality of variances, respectively. Normally distributed data with equal variances were analyzed by an unpaired student t-test when two groups were compared. For comparing several normally distributed groups, a one-way ANOVA was used with a Bonferroni multiple comparison post test. For groups that were not normally distributed and/or had unequal variances, a non-parametric Mann-Whitney test was used for comparison between two groups while Kruskal-Wallis test followed by a Dunn's post test was performed for multiple comparisons. All values of analyzed images and relative expression data were displayed in Whisker boxplots and thickness analyses as mean ± standard deviation. *,$ $p < 0.05$, **,$$ $p < 0.01$, ***,$$$ $p < 0.001$.

4.4 Results

4.4.1 In vitro BAM formation

First, cells isolated from a human muscle biopsy were expanded and characterized. This muscle cell population, previously described in (20) contained 82 ± 5 % desmin-positive myoblasts (n=6) at 12 doublings. Myoblasts had a fusion index of 80 ± 15 % (n=6) as determined by tropomyosin staining, forming myotubes with 10 ± 4 nuclei per myotube (Figure S4.1). To make bio-artificial muscle with only muscle cells (BAM), $2x10^6$ muscle cells were mixed in a fibrin extracellular matrix (1mg/ml) and cultured in skeletal muscle growth medium (SkGM) for 2 days, followed by skeletal muscle differentiation medium (SkFM) for 12 days. The cell-fibrin hydrogel mix contracted around 2 attachment points and formed a 2-cm long muscle bundle (schematic representation in Figure 4.1, macroscopic image in Figure 4.2a & 4.2d), containing aligned multinucleated myotubes (Figure 4.3a) with a thickness of 1.25 ± 0.2 mm (n=21).

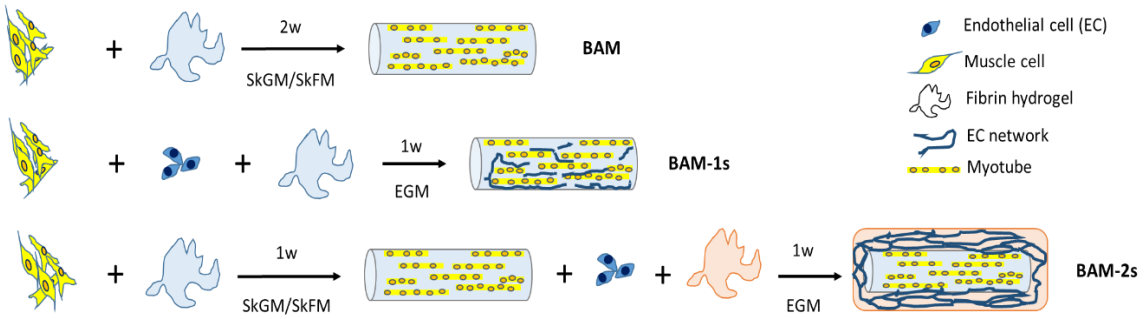


Figure 4.4. Schematic representation of tissue engineering strategies. BAM represents bio-artificial muscle with aligned myotubes differentiated for 2 weeks in SkGM and SkFM medium. BAM-1s is a prevascularization strategy based on coculture of endothelial and muscle cells, cultured for 1 week in EGM medium which results in aligned myotubes with interspersed endothelial networks. BAM-2s is a prevascularization strategy by embedding a BAM cultured for 1 week in SkGM/SkFM in a fibrin hydrogel containing endothelial cells (EC). Culturing this construct for an additional week in EGM medium, results in a myotube bundle surrounded by an endothelial coat containing highly interconnected endothelial networks.

4.4.2 In vitro myotube formation in prevascularized BAMs

Two different prevascularization strategies of BAMs were evaluated. The first approach was previously evaluated in vitro and described in (9). This co-culture strategy, here termed the 1-stage prevascularization (or BAM-1s) was made by coculturing muscle cells with endothelial cells (HUVECs) in a 70:30 ratio and a total number of 2x106 cells in fibrin hydrogel (schematic representation in Figure 4.1, macroscopic image in Figure 4.2a right side). As we described

previously, culturing HUVECs in skeletal muscle media results in poor HUVEC survival, therefore we cultured BAM-1s in EGM-2, an optimized medium for endothelial cells (9). After 1 week in culture, the cell – fibrin hydrogel contracted to a muscle bundle with interspersed endothelial network and a total thickness of 1.34 ± 0.15 mm (n=16) (Figure 4.2a right side). No significant difference in BAM thickness was present in comparison to BAM.

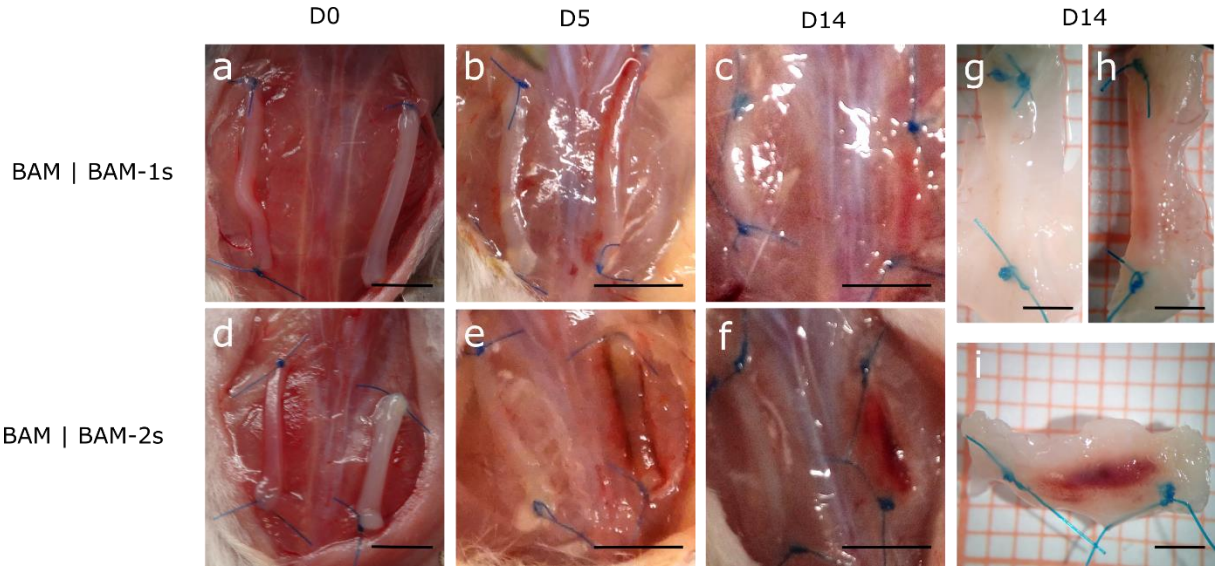


Figure 4.2. Implantation of BAM, BAM-1s and BAM-2s constructs. Macroscopic images of BAM, BAM-1s and BAM-2s at day 0 of implantation (a & d), at day 5 (b & e) and 14 (c & f) of post-implantation. BAM constructs were sutured on the left latissimus dorsi muscle, BAM-1s or BAM-2s on the right latissimus dorsi muscle. G, h and i show enlarged images of explanted constructs with surrounding host tissue at day 14 post-implantation. Scale bars represent 0.5 cm (a-f) and 0.2 cm (g-i).

However, as reported before (9), myotube formation in BAM-1s is compromised in the EGM medium resulting in decreased myotube diameter and density compared to BAM (compare Figure 4.3a with 4.3b and Figure 4.4c & 4.4d). No difference in myotube length and myotube alignment was observed (Figure 4.4a & b). RT-qPCR analysis for myosin heavy chain (MYH) isoform expression showed a presence of less mature myotubes (Figure 4.5) in BAM-1s compared to BAM reflected by a 2.5 and 4.7-fold lower expression level of respectively the adult isoform MYH1 and the perinatal isoform MYH8. Also, a respectively 3-fold and 1.4-fold lower expression level was observed for the embryonic isoform MYH3 and myogenin, indicating a lower myogenic differentiation in BAM-1s.

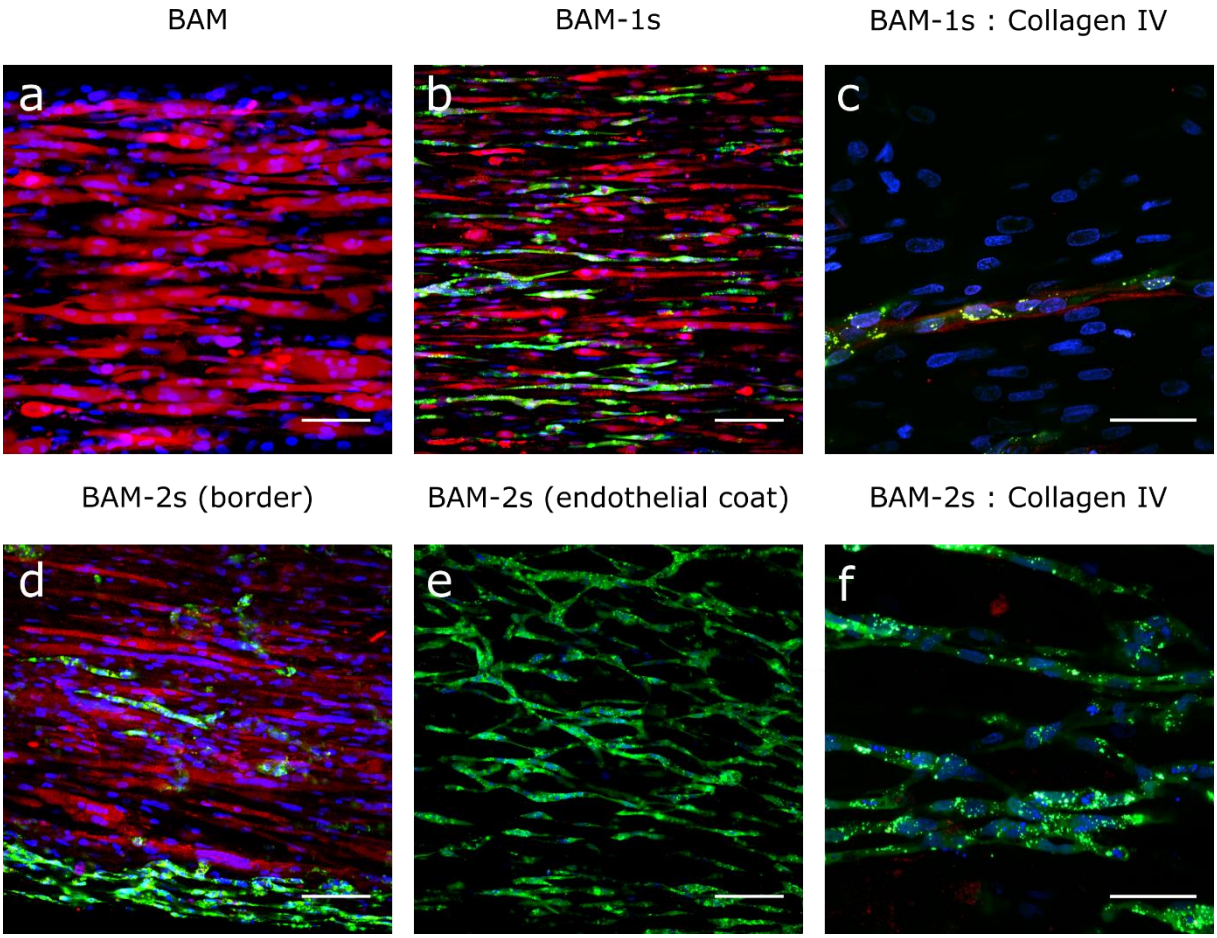


Figure 4.3. *In vitro* myotube formation and prevascularization. Fluorescent confocal images of *in vitro* tissue-engineered skeletal muscle (BAM) with only muscle cells (BAM), a coculture BAM with GFP labeled HUVECs (green) (BAM-1s) and a BAM with an endothelial coat (BAM-2s). The 3 types of BAM show presence of aligned multinucleated (DAPI, blue) myotubes (red) (a, b and d). In the coculture BAM-1s additional endothelial networks (green) are interspersed between the aligned myotubes (b). These endothelial networks (green) are positive for collagen IV (c, in red). In BAM-2s interconnected endothelial networks are located in the endothelial coat and surround the myotube bundle (d, e) and are negative for collagen IV (f). Scale bars represent 100 µm (a, b, d and e) and 50 µm (c & f).

To circumvent this compromised myotube formation, we also explored a two-stage prevascularization approach (BAM-2s). First, $2x10^6$ muscle cells were mixed with a fibrin hydrogel (1 mg/ml) to engineer a one-week old BAM as described before (9). Then, we embedded the BAM in a fibrin hydrogel containing $2x10^6$ HUVEC cells, further referred to as the endothelial coat. This construct was cultured for another week in EGM-2 to stimulate endothelial network formation (schematic representation in Figure 4.1, macroscopic image in Figure 4.2d right side). Endothelial cells in this coat layer spontaneously formed endothelial networks, and this layer was 117 ± 12 µm thick (n=6) one week after casting (Figure 4.3e). The advantage of this procedure is that differentiation of each cell type occurred in its own

specialized medium, resulting in better survival and morphology of each cell type. The resulting BAM-2s was 1.5 ± 0.15 mm (n=16) thick (Figure 4.2d), which was significantly thicker than BAM and BAM-1s . After 14 days in culture, we visualized myotube formation using confocal microscopy (Figure 4.3d). Myotube density was significant higher in BAM-2s compared to BAM-1s and similar to BAM (Figure 4.4d, $). Myotube diameter *in vitro* was highest in BAM (Figure 4.4c, $). No differences were observed for myotube length and alignment between the 3 different BAM types (Figure 4.4a & 4.4b). Regarding MYH isoform expression in BAM-2s, no difference with BAM was observed for *MYH1*. A lower expression of *MYH3, MYH8* and myogenin was observed, respectively 45, 3.2 and 3.3-fold lower than in myotubes in BAM (Figure 4.5). Comparing *MYH* expression in BAM-2s vs BAM-1s, showed a significantly 4.4-fold higher expression of *MYH1* in BAM-2s and a 10 and 2-fold lower expression level of *MYH3* and myogenin respectively (Figure 4.5), an indication of a higher maturity grade of the myotubes in BAM-2s.

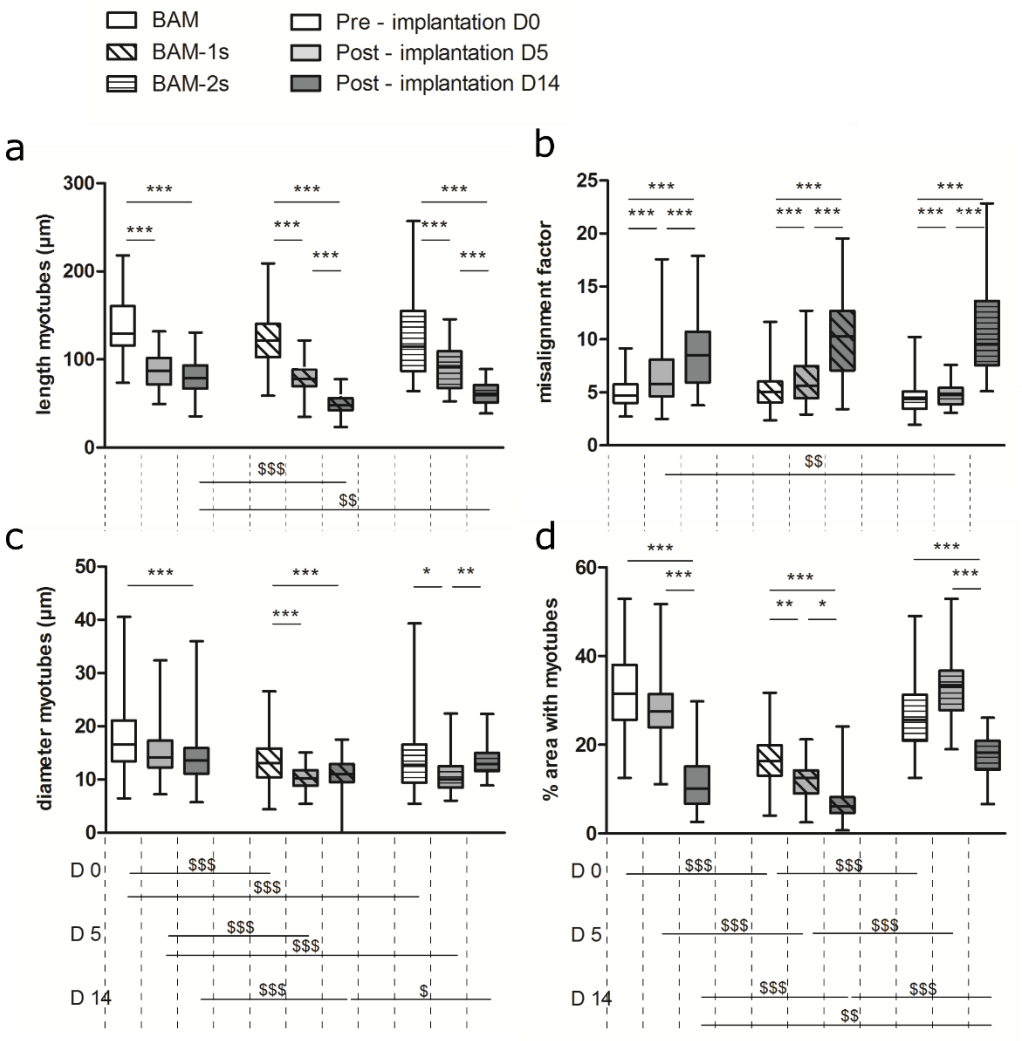


Figure 4.4. Morphological analysis of myotubes in BAMs *in vitro* and *in vivo*. Parameters, such as myotube length (a), alignment (b), diameter (c) and myotube density (d) characterizing the formation and morphology of myotubes in BAM with only muscle cells (BAM), in a coculture BAM with HUVECs (BAM-1s) and in BAM with an endothelial coat (BAM-2s) at day 0 of implantation and 5, 14 days post-implantation. Statistical significances for comparisons in a BAM condition between different time points are indicated with * and for comparisons between different conditions at a specific time point are indicated with $. For multiple comparisons a nonparametric Kruskal-Wallis test with Dunn's post test was used. * or $ $p < 0.05$, ** or $$ $p < 0.01$, *** or $$$ $p < 0.001$.

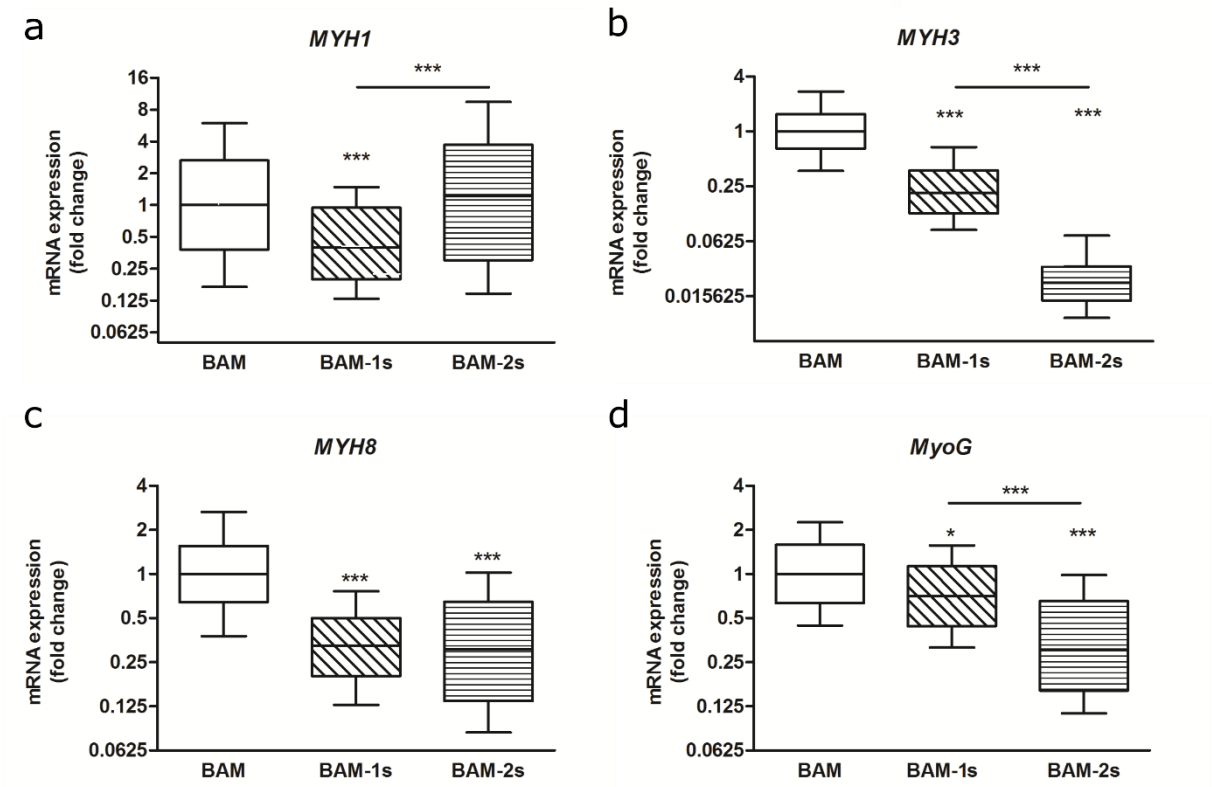


Figure 4.5. Myogenic gene expression. Relative expression of MYH isoforms and myogenin in coculture BAMs (BAM-1s) and BAMs with an endothelial coat with HUVECs (BAM-2s). Expression levels of these genes were quantified by RT-qPCR as the fold changes relative to gene expression in BAMs with only muscle cells. Relative expression in BAM1s was compared to relative expression in BAM-2s as well (comparing line with significance level). Relative expression is depicted as Whisker boxplots. *p < 0.05, **p < 0.01, ***p < 0.001.

4.4.3 In vitro endothelial network formation in BAM-1s and BAM-2s

Endothelial networks were formed through self-assembly and self-organization in BAM-1s and BAM-2s fibrin constructs (Figure 4.3 b, d & e). In BAM-1s, endothelial networks were interspersed between aligned myotubes. In BAM-2s, the endothelial network (Figure 4.3e) penetrated the myotube bundle occasionally in the transition area between the BAM and the endothelial coat (Figure 4.3d). When comparing endothelial networks in BAM-1s and BAM-2s, a higher network complexity could be observed in BAM-2s (Figure 4.3b & e, Figure 4.6). Endothelial network branching and the percentage of master segments, longest elements giving origin to branches, was significantly higher in BAM-2s compared to endothelial networks in BAM-1s (Figure 4.6). Also, total endothelial network length was higher in BAM-2s. Additionally, the number of isolated segments was lower in BAM-2s, showing that networks in BAM-2s were more interconnected than in BAM-1s (Figure 4.6). Although the endothelial network characteristics were better in BAM-2s than BAM-1s, they were negative for collagen

IV, a basement membrane protein important in vascular maturity and stabilization (22) (Figure 4.3f). This in contrast to networks in BAM-1s, where the endothelial network basement membrane contained collagen IV (Figure 4.3c). However, networks of BAM-1s regressed after one week *in vitro* (Figure S4.2).

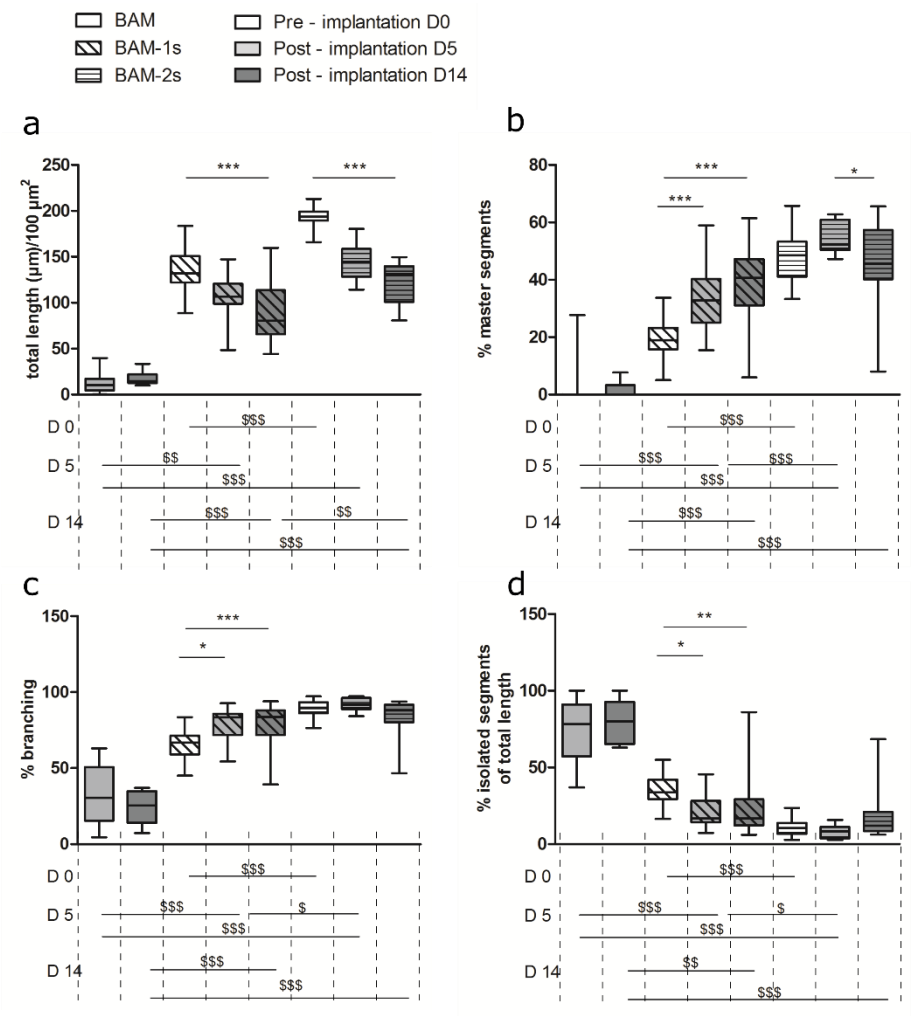


Figure 4.6. Morphological analysis of endothelial networks *in vitro* and *in vivo* in BAMs. Parameters, such as (a) total length/100 µm^2 , (b) % master segments, (c) % branching and (d) % isolated segments and characterizing the formation and morphology of ingrowing host vessels in BAM with only muscle cells (BAM; host endothelial cells labeled with CD31), of endothelial networks *in vitro* and *in vivo* in a coculture BAM with endothelial cells (BAM-1s) and in BAM with an endothelial coat (BAM-2s) at day 0 of implantation and 5, 14 days post-implantation. Statistical significances for comparisons in a BAM condition between different time points, are indicated with * and for comparisons between different conditions at a specific time point are indicated with $. * or $ $p < 0.05$, ** or $$ $p < 0.01$, *** or $$$ $p < 0.001$.

4.4.4 In vivo implantation and explantation

Next, we wanted to evaluate whether different strategies of prevascularization affect the implanted construct in terms of (i) myotube survival, (ii) myotube maturation and (iii) whether the *in vitro* engineered endothelial networks are functional and improve construct perfusion. Therefore, we implanted the three BAM types on *latissimus dorsi* muscle on the back of NOD/SCID mice. The prevascularized constructs were implanted on the right *latissimus dorsi* muscle, while BAMs (without prevascular networks) were implanted on the left *latissimus dorsi* (Figure 4.2a & d) as a reference. Both on explantation day 5 and 14, differences in vascularization between constructs could be observed macroscopically (Figure 4.2b & e, c & f, h & i). While the appearance of the muscle cell only BAM construct remained similar to before implantation (white), BAM-1s and BAM-2s were red, pointing to the presence of blood (Figure 4.2 b,c & e,f; right side). In contrast to day 5, the different types of BAM were integrated with host tissue at day 14. Therefore, BAM constructs were explanted together with surrounding host tissue at day 14. To visualize myotube presence in day 14 explanted constructs by confocal microscopy, the tissue was cut into 200 µm sections with a vibratome.

4.4.5 In vivo myotube maintenance

Myotube survival and maturation *in vivo* were evaluated morphologically at 5 and 14 days after implantation. Myotubes were still present at day 14 of implantation in all conditions (Figure 4.6). However, compared to pre-implantation, a reduction in myotube length in all conditions was shown at day 5 which was even more prominent at day 14 (Figure 4.4a). At the latest time point, myotube length was decreased by 40 % (BAM), 61 % (BAM-1s) and 47 % (BAM-2s). Similarly, myotube alignment decreased over 14 days, depicted in Figure 4.4b as an increase in misalignment. On the other hand, myotube diameter decreased in BAM and BAM-1s conditions, but stayed constant in BAM-2s over 14 days. While *in vitro* BAM had the thickest myotubes, no such difference was present after 14 days implantation compared to BAM-2s (Figure 4.4c). Finally, myotube density decreased in all conditions although this effect was least prominent in the BAM-2s condition (67.8 % (BAM), 61 % (BAM-1s) and 33,4 % (BAM-2s), Figure 4.4d). At day 14, BAM-1s had the lowest myotube density while BAM-2s had the highest (Figure 4.7d,e & f).

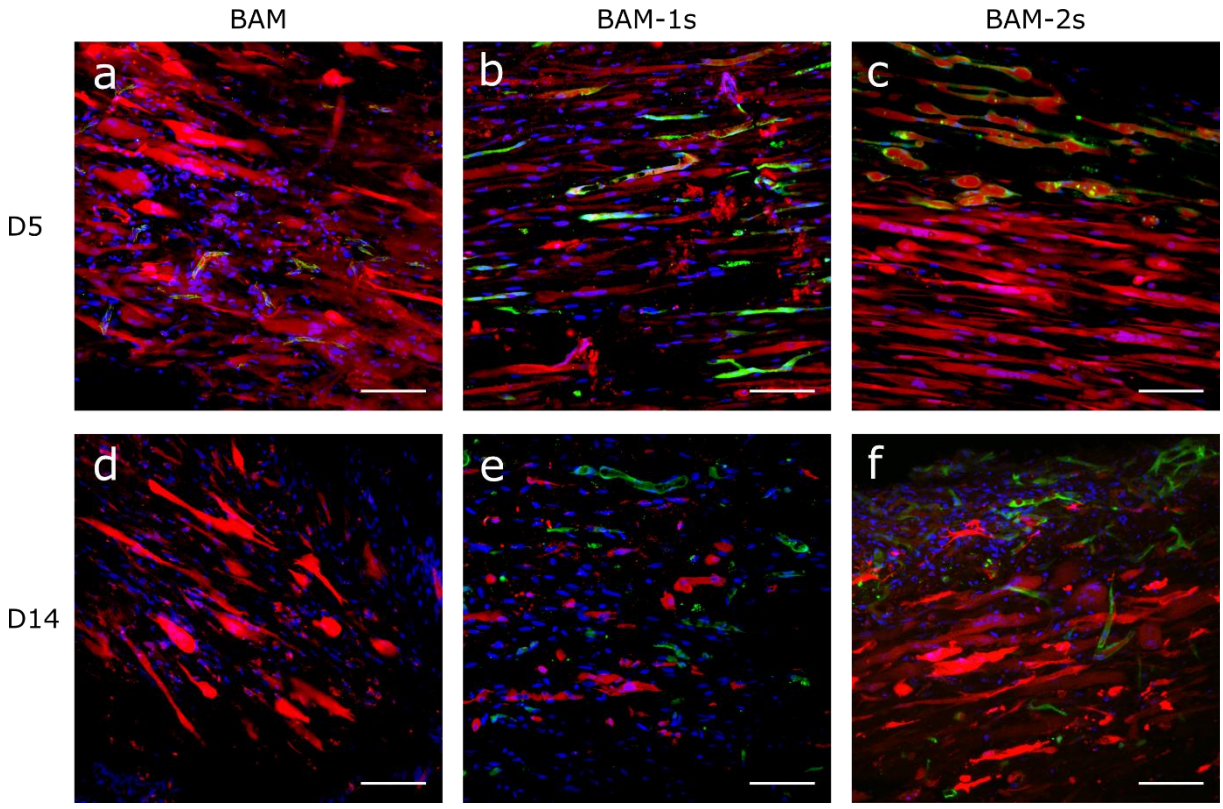


Figure 4.7. Confocal images of myotube and endothelial network presence in BAMs post-implantation. Fluorescent confocal images of BAMs explanted after 5 or 14 days *in vivo* with only muscle cells (BAM) and CD 31 positive capillaries (green) (a & d), of BAM-1s with GFP labeled HUVECs (green) (b & e) and BAM-2s (c & f). The 3 types of BAM show presence of aligned multinucleated (DAPI, blue) myotubes (red) (a-f) at day 5 and day 14. Scale bars represent 100 µm.

4.4.6 In vivo vascularization and anastomosis

In vivo vascularization of BAMs was assessed 5 and 14 days after implantation. Many GFP labeled endothelial vessels, which originated from the HUVECs, were present in BAM-1s and BAM-2s at day 5 and 14 (Figures 4.6, 4.7, 4.8), as indicated by the vascular density determined by total network length per 100 µm^2, in contrast to BAM where a low vascular density of CD31-positive vessels per 100 µm^2 was observed (Figures 4.6, 4.7). A significantly higher vascular density was observed for BAM-2s in comparison to BAM-1s at day 14 (Figure 4.6). After 5 days *in vivo*, the location of the endothelial vessels remained similar as to the situation *in vitro* for BAM-1s and BAM-2s: while interspersed between myotubes in BAM-1s, endothelial vessels in BAM-2s surrounded the myotube bundle (Figure 4.7b & c). However, at day 14, vascular structures derived from HUVECs were also observed between myotubes in BAM-2s (Figure 4.7f). The vascular density decreased significantly in both BAM-1s and BAM-2s over 14 days in prevascularized BAMs (Figure 4.6a). The percentage of master segments increased in BAM-1s, concomitant with a decrease in isolated segments, indicating a preferential pruning

of isolated segments (Figure 4.6b,d). In BAM-2s, isolated segments were already rare and this remained similar *in vivo*, consistent with a high percentage of master segments and nearly all networks displaying branching (Figure 4.6b,c, d). A human endothelial cell specific agglutinin (UEA-I), rhodamine labelled, was injected intravenously to determine whether the implanted vascular networks in BAM-1s and BAM-2s were anastomosed with host vessels and were perfused and functional (5). The latter was also verified by the presence of red blood cells in the GFP labeled networks. At day 5, in both BAM-1s and BAM-2s, a lot of endothelial vessels contained red blood cells, while only sparse presence of UEA-I-positive endothelial networks was observed (figure 4.8 b & c), showing early anastomosis, but little perfusion. At day 14, a part of the GFP-labeled endothelial vessels in BAM-1s and BAM-2s were UEA-I positive (Supplementary Videos S4.1 and S4.2), showing functionality of implanted networks (8 e & f) and contained red blood cells (Supplementary Video S4.3).

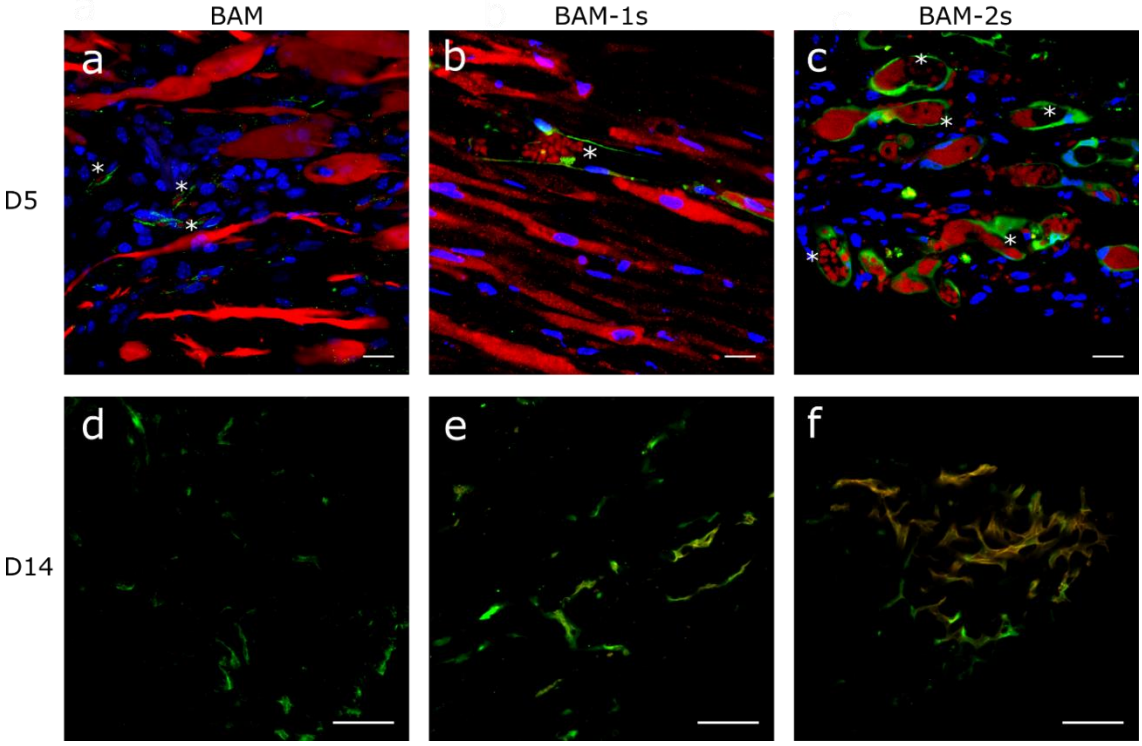


Figure 4.8. *In vivo* perfusion of prevascularized endothelial networks at 5 and 14 days post-implantation. Fluorescent confocal images of implanted BAM at day 5 and day 14 with only muscle cells (BAM) and CD 31 positive capillaries (green) (a & d), of a coculture BAM with GFP labeled HUVECs (BAM-1s) (green) (b & e) and a BAM with an endothelial coat containing GFP labeled HUVECs (green) (BAM-2s) (c & f). At day 5 post-implantation prevascularized BAMs contain GFP labeled endothelial vessels (green) that are perfused with red blood cells (red dots, asterisk (b & c)). At day 14 GFP labeled endothelial vessels (green) are UEA-I positive (orange) (e & f), showing anastomosis between host vessels and implanted networks and perfusion. Muscle cell only BAM contains CD31 positive capillaries (green) at day 5 (a) and at day 14 (d), perfused with red blood cells at day 5 (a). Scale bars represent 20 µm (a-c) and 100 µm (d-f).

4.4.7 Extracellular matrix remodeling after implantation

Extracellular matrix (ECM) remodeling *in vivo* was evaluated by Martius Scarlet Blue (MSB) which stains muscle tissue red, fibrin pink/purple, collagen blue and red blood cells orange. *In vitro* BAM ECM mainly consists of fibrin (Figure 4.9 a-c) while BAM and BAM-2s also showed limited deposition of collagen *in vitro* (Figure 4.9 a, c). At day 5, little ECM remodeling was observed, with limited collagen deposition in BAM (Figure 4.9 d-f). Presence of myotubes as seen with confocal microscopy (Figure 4.7) was confirmed with MSB staining (Figure 4.9 d-f). The presence of blood vessels in BAM-1s and BAM-2s constructs was also confirmed with MSB staining; red blood cells stained in orange are clearly detectable and located within the BAM-1s or surrounding the BAM-2s (Figure 4.9 e, f, h & i). After 14 days *in vivo*, fibrin ECM in BAM and BAM-1s was remodeled into a collagen ECM (Figure 4.9g & h). In BAM-2s, a difference could be observed between the inner myotube part containing mainly fibrin ECM and the endothelial coat which showed primarily collagen (Figure 4.9i).

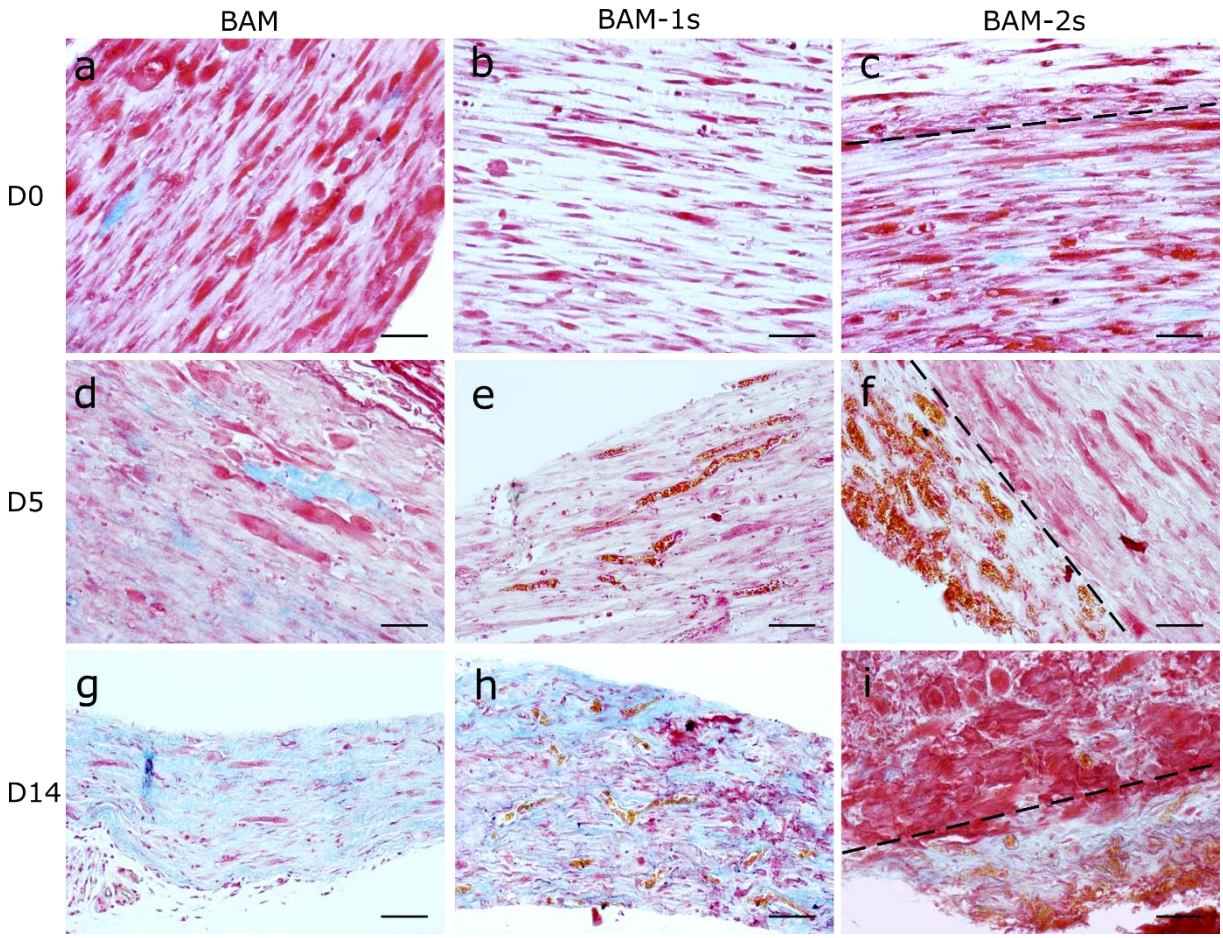


Figure 4.9. Extracellular matrix remodeling in BAMs. Martius Scarlet Blue (MSB staining) of fibrin BAM with only myotubes (BAM), coculture BAM with interspersed endothelial networks (BAM-1s) and BAM with endothelial coat with endothelial networks (BAM-2s) at day 0 of implantation and day 5 and 14 post-implantation. *In vitro* BAMs consist of fibrin (light pink) (a-c) with collagen deposition (blue) in BAM (a) and BAM-2s (c) and aligned myotubes (dark pink/red). At day 5 post-implantation *in vivo* BAMs consist mainly of fibrin, while at day 14 post-implantation BAM fibrin extracellular matrix (ECM) is remodeled to collagen (g), BAM-1s ECM is partly remodeled and in BAM-2s only the endothelial coat (dashed line indicates the border between endothelial coat and muscle bundle) shows remodeling. Red blood cells are stained in orange and are present in capillaries at day 5 and day 14 in BAM-1s and BAM-2s (e-f, h-i). Scale bars represent 20 µm.

4.5 Discussion

At present, the use of muscle flaps to treat volumetric muscle loss has significant drawbacks (2). Tissue engineered skeletal muscle holds promise for an alternative treatment. The tissue-engineering approach used in this paper further builds on a muscle tissue engineering approach, called Bio-Artificial Muscle (BAM) containing aligned myotubes (13, 23). Still, many challenges towards clinical as well as *in vitro* testing applications remain. One of them is the limited size of the constructs, imposed by the limit of passive diffusion of nutrients and gases. Prevascularization is being explored as a method to allow *in vitro* perfusion and to enhance *in vivo* survival and engraftment of tissue-engineered constructs (10, 24, 25). In this paper, we have evaluated two prevascularization strategies of tissue-engineered bio-artificial muscle (BAM) to tackle the limitation.

The first approach, a one-stage approached (BAM-1s), was previously evaluated *in vitro* (9). In this approach a direct coculture of endothelial cells and muscle cells results in aligned multinucleated myotubes with interspersed endothelial networks. The natural hydrogel fibrin is used as a scaffold, because of its pro-angiogenic and stiffness characteristics (26). However, data on functionality of these networks were lacking. BAM-1s constructs were cultured in endothelial cell growth medium. Based on our findings this supports endothelial network formation as well as myotube formation (9). However, as can be expected, myotube formation is not optimal in endothelial medium when compared to culture in skeletal muscle specific media (9). The impaired myotube formation in endothelial medium was also described by others (10) and confirmed in the present study. Endothelial medium allowed only for 2% of muscle cells to undergo terminal differentiation, marked by myogenin expression (10). Additionally, a lower number of muscle cells are used in BAM-1s ($1.4x10^6$ muscle cells) compared to BAM with only muscle cells (BAM, $2x10^6$ muscle cells). Furthermore, BAMs were cultured for 2 weeks compared to 1 week for BAM-1s. A prolonged culture time generally results in enhanced myogenic differentiation and in increased myotube diameter and myogenic gene expression as reported elsewhere (27). However, culturing BAM-1s longer than 1 week resulted in endothelial network degradation and was therefore not compatible with the aims of prevascularizing the BAMs and may require addition of other cell types to stabilize the networks.

To support optimal myotube formation, we established another prevascularization strategy, consisting of two stages, termed BAM-2s. In the first stage, BAMs were cultured for one week as before, without endothelial cells and then in a second stage, an endothelial cell coat was added in which endothelial networks formed during the second week. This strategy bypassed

the issues mentioned for BAM-1s. Together with the prolonged culture time, culturing muscle cells the first week in skeletal muscle media resulted in better myotube formation. Consequently, myotubes in BAM-2s were indeed thicker and had a higher myotube density compared to myotubes in BAM-1s. Only regarding myotube diameter, BAMs without endothelial cells were still superior to BAM-2s.

Characterization of endothelial networks *in vitro* indicated that the most interconnected networks with the highest vascular density were observed in BAM-2s. Indeed, an increased endothelial cell density in fibrin hydrogel was already described to result in an enhanced number of branches and total vessel length (28), and this is consistent with the high endothelial cell density in the coat of the BAM-2s approach. Also our previous study showed improved endothelial network formation *in vitro* when a higher density of endothelial cells was used (9). A well-organized endothelial network *in vitro* is important for the *in vivo* vascularization and tissue integration as shown in the study of Koffler et al., where a more structured vascular network *in vitro* improved the *in vivo* engraftment (11). Besides analysis of morphological parameters, collagen IV deposition was assessed. Collagen IV is the main component of the vascular basement membrane matrix. Basement membrane matrix assembly is a critical step in vessel maturation and vessel stability as observed in *in vitro* and developmental studies (22, 29–31). Endothelial networks in BAM-1s were surrounded by a thin layer that contained collagen IV, suggesting the presence of a basement membrane, in contrast to endothelial networks in BAM-2s. In BAM-1s endothelial cells were mixed with muscle cells containing both myoblasts and fibroblasts (32, 33), in contrast to BAM-2s where only endothelial cells were present in the coat region. Several groups have successfully shown that addition of mesenchymal-derived cells, such as fibroblasts, pericytes and/or smooth muscle cells improves endothelial network maturation and *in vitro/in vivo* network stabilization in tissue engineered constructs (34–36). These cells are able to differentiate into supportive mural cells around newly formed endothelial networks in coculture settings with endothelial cells (34, 37, 38). Pericytes for example are known for their role in stimulating basement membrane matrix deposition by endothelial cells (22). Optimizing fibroblast – endothelial cell ratios and/or evaluation of other mesenchymal-derived cells as mural cells may still improve prevascularization outcome. In this study we have used HUVECs as endothelial cell source. HUVECs are easy to isolate, abundant and well characterized. Furthermore, they are capable of endothelial network formation *in vitro* (5, 9, 10). Other examples of endothelial cell sources able to form endothelial networks are microvascular endothelial cells (39), embryonic heart endothelial cells (40), pluripotent cell derived endothelial cells (41) and blood outgrowth

endothelial cells (42) and are worthwhile for further investigation in prevascularization strategies.

To evaluate whether prevascularization improves *in vivo* myotube survival and tissue perfusion we implanted BAMs with and without endothelial networks on the *latissimus dorsi* muscle of NODSCID mice for 5 or 14 days. In all conditions, myotubes were still observed at day 14 of implantation in the construct. However, myotube length, density and alignment decreased in all conditions *in vivo*. Myotube length was decreased by 40 % (BAM), 61 % (BAM-1s) and 47 % (BAM-2s) over 14 days. At day 14, myotube density was decreased by 67.8 % (BAM), 61 % (BAM-1s) and 33,4 % (BAM-2s). The BAM-2s thus outperformed the other BAM types in maintenance of myotube density. Moreover, myotube diameter remained constant over 14 days in BAM-2s, while a decrease was observed in BAM and BAM-1s. Taken together, this proved that the prevascularization strategy of BAM-2s improved myotube maintenance *in vivo*. An implantation time exceeding 14 days may even improve myotube maturation as reported previously (43).

Despite early anastomosis at day 5 of implanted endothelial networks with host vessels and thus tissue perfusion, a decrease in myotube density was observed in all conditions. This may be due to a more limited supply of nutrients and oxygen in the first days *in vivo* as compared to the *in vitro* situation where constructs are completely submerged in a nutrient rich medium. Furthermore, the decrease may also be explained by the occurrence of xenogeneic rejection. Although NOD/SCID mice lack functional T and B cells, have impaired macrophage function and lack the complement system (44), a low level of natural killer (NK) cell activity was still observed in NOD/SCID mice (45–47). Also macrophage, neutrophil and mast cell invasion may be responsible for the rejection, as seen with implantation of human mesenchymal stem cells on poly(ε-caprolactone) in a NOD/SCID model (47). Immunodeficient animal models are also deprived of pro-regenerative effects of the immune response during skeletal muscle repair (48–50). Inflammatory cells, such as macrophages and neutrophils, are recruited and start producing growth factors and cytokines important in satellite cell activation, proliferation and differentiation and capillary ingrowth to injured muscle (2). For clinical application, use of human autologous muscle and endothelial cells will eliminate xenogeneic responses.

Next to examination of the effect of prevascularization on myotube maintenance *in vivo*, also the effect on *in vivo* vascularization was evaluated. Prevascularized BAMs showed a significantly higher vascular density *in vivo* compared to BAMs with only muscle cells, as reported previously by others in tissue-engineered constructs (10, 11). In this study, already at day 5 of implantation anastomosis of the implanted networks with host vessels was observed

by the presence of red blood cells in the human endothelial networks. Similar to our findings, Chen et al. found evidence of anastomosis of endothelial networks in a fibrin gel (without muscle cells) at day 5 (28). This anastomosis speed may not be sufficient for oxygen-sensitive tissues such as cardiomyocytes causing ischemia that leads to cell death (51). Improving the structure and maturation of *in vitro* networks and optimizing the mesenchymal-derived cell – endothelial cell ratio as proposed before (11, 24, 34, 36), addition of exogenous growth factors (e.g. VEGF, FGF and PDGF) to promote *in vivo* vascularization (52) and optimizing fibrin concentration, type and ultrastructure (26, 53) may reduce anastomosis time and increase vascularization. Despite anastomosis of HUVEC endothelial vessels, shown by red blood cell presence, no perfusion of intravenously injected agglutinin was observed at day 5, suggesting a restricted perfusion. It has been observed with laser speckle imaging that thrombi occurred early after anastomosis of implanted endothelial vessels with host vessels (54). By day 7 however, functional perfused vessels were reported (54). In our experiments, onset of full perfusion as demonstrated with fluorescent agglutinin occurred between day 5 and 14 after implantation and showed functionality of the networks.

Fibrin BAMs maintained structural integrity over 14 days. Fibrin ECM was remodeled to collagen as shown by MSB staining over 14 days of implantation. This is similar to previous studies where fibrin degradation was observed over two weeks in acellular fibrin clots (55) and tissue engineered skeletal muscle with fibrin ECM (43) and where collagen deposition was also shown. Enhancement of ECM remodeling *in vitro* has recently been described to improve visco-elastic properties of BAMs (56). Fibroblasts together with immune cells, such as neutrophils and macrophages, are an important cell source during ECM remodeling upon injury (57, 58). The elimination of an inflammatory trigger and resolution of inflammation are important for preventing fibrosis (57). Characterizing the presence of invading immune cells could help understand the evolution of ECM remodeling and engraftment (59, 60). At day 14 no sign of fibrotic tissue was observed around implanted BAMs on histological sections. Together with the high vascular density and perfusion at day 14 this proves successful engraftment in BAM-1s and BAM-2s, but not in BAM where a very low vascular density was seen.

In conclusion, we tested two prevascularization strategies of bio-artificial skeletal muscle and evaluated construct survival and engraftment in the host tissue after implantation *in vivo.* The two stage approach resulted in a prevascularization which became functional *in vivo* and supported best myotube survival. Although further improvements can still be done, this opens perspectives for engineering of larger skeletal muscle constructs.

4.6 Author Contributions

DG and LTh contributed to conception and designed the project. DG performed *in vitro* experiments. DG, KM, LH, LTe, JD were responsible for *in vivo* experiments. DG, LD, LTe performed data collection. DG and GC performed data analysis. DG performed interpretation and statistical analysis. DG wrote the manuscript with input from all authors. LTh supervised the project. All authors read and approved the manuscript.

4.7 Acknowledgments

The authors are grateful to Stephanie De Vleeschauwer, Erna Dewil and Marleen Lox, Aernout Luttun, Sander Craps, Greetje Vande Velde, Veerle Baekelandt and Joris Van Asselberghs for technical assistance, Rik Gijsbers for miRFP670 cDNA-containing HIV1-derived retroviral vector, Evie Vereecke for human muscle samples, Laurens Willaert and Rune Peyskens for myotube morphological analysis and Sigrid Vanryckeghem for administrative support. This work was funded by Fonds Wetenschappelijk Onderzoek – Vlaanderen (1.5.298.17 N); and AFM-Telethon trampoline grant (19802) .

4.8 Disclosure Statement

No competing financial interests exist.

4.9 Supplementary materials

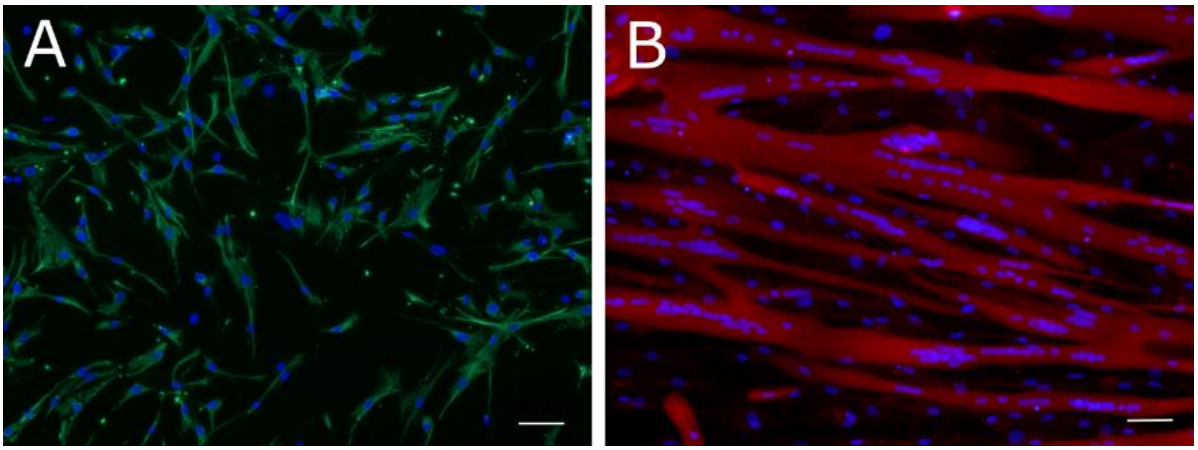


Figure S4.1.**Characterization of muscle cell population.** The muscle cell population cultured *in vitro* contains at 12 doublings 82 ± 5% myoblasts as shown by desmin immunofluorescence staining (green) and nuclear staining (DAPI, blue) (a). After four days in fusion medium, positive tropomyosin staining (red) and multinucleated cells indicate efficient differentiation to muscle fibers (b). Scale bars represent 50 µm.

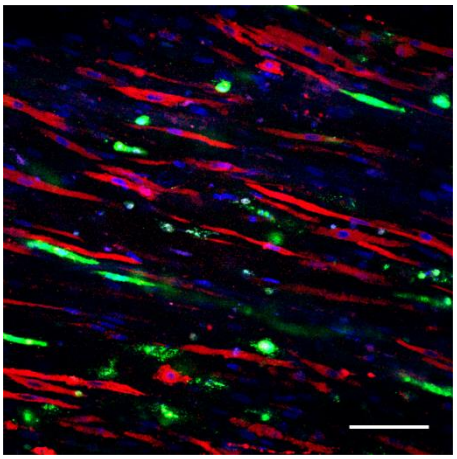


Figure S4.2. Degradation of endothelial networks of 10 days *in vitro* BAM-1s. Fluorescent confocal image of 1 week and 3 days old *in vitro* BAM-1s with GFP labeled HUVECs (green) and multinucleated (DAPI, blue) myotubes (red), showing endothelial network degradation (green spheres). Scale bar represents 100 µm.

Video S4.1. 3D reconstruction with ZEN Black software of agglutinin (orange) perfused GFP labeled endothelial vessels (green) in BAM-1s 14 days post-implantation.

https://www.dropbox.com/s/bgpbag8zam0l458/Supplementary%20Video%201.mp4?dl=0

Video S4.2. 3D reconstruction with ZEN Black software of agglutinin (orange) perfused GFP labeled endothelial vessels (green) in BAM-2s 14 days post-implantation.

https://www.dropbox.com/s/rl6fj9z87of2ipj/Supplementary%20Video%202.mp4?dl=0

Video S4.3. 3D reconstruction with IMARIS software of red blood cell (red) perfused GFP labeled endothelial vessels (green) in BAM-1s 14 days post-implantation.

https://www.dropbox.com/s/qny6w3bwcny7grg/Supplementary%20Video%203.mp4?dl=0

4.10 References

1. Musarò A (2014) The Basis of Muscle Regeneration. *Adv Biol* 2014:1–16.
2. Järvinen TA, Järvinen TL, Kääriäinen M, Kalimo H, Järvinen M (2005) Muscle injuries: biology and treatment. *Am J Sports Med* 33(5):745–764.
3. Lee KT, Mun GH (2014) A Systematic Review of Functional Donor-Site Morbidity after Latissimus Dorsi Muscle Transfer. *Plast Reconstr Surg* 134(2):303–314.
4. Cittadella Vigodarzere G, Mantero S (2014) Skeletal muscle tissue engineering: strategies for volumetric constructs. *Front Physiol* 5(9):362.
5. Shandalov Y, Egozi D, Koffler J, Dado-Rosenfeld D, Ben-Shimol D, Freiman A, Shor E, Kabala A, Levenberg S (2014) An engineered muscle flap for reconstruction of large soft tissue defects. *Proc Natl Acad Sci U S A* 111(16):6010–6015.
6. Thorrez L, Shansky J, Wang L, Fast L, VandenDriessche T, Chuah M, Mooney D, Vandenburgh H (2008) Growth, differentiation, transplantation and survival of human skeletal myofibers on biodegradable scaffolds. *Biomaterials* 29(1):75–84.
7. Folkman J, Hochberg M (1973) Self-regulation of growth in three dimensions. *J Exp Med* 138(4):745–53.
8. Cerino G, Gaudiello E, Grussenmeyer T, Melly L, Massai D, Banfi A, Martin I, Eckstein F, Grapow M, Marsano A (2016) Three dimensional multi-cellular muscle-like tissue engineering in perfusion-based bioreactors. *Biotechnol Bioeng* 113(1):226–36.
9. Gholobova D, Decroix L, Van Mulyder V, Desender L, Gerard M, Carpentier G, Vandenburgh H, Thorrez L (2015) Endothelial network formation within human tissue-engineered skeletal muscle. *Tissue Eng Part A* 21(19–20):2548–58.
10. Levenberg S, Rouwkema J, Macdonald M, Garfein E, Kohane D, Darland D, Marini R, van Blitterswijk C, Mulligan R, D'Amore P, Langer R (2005) Engineering vascularized skeletal muscle tissue. *Nat Biotechnol* 23(7):879–84.
11. Koffler J, Kaufman-Francis K, Yulia S, Dana E, Daria AP, Landesberg A, Levenberg S (2011) Improved vascular organization enhances functional integration of engineered skeletal muscle grafts. *Proc Natl Acad Sci U S A* 108(36):14789–94.
12. Vandenburgh H, Shansky J, Del Tatto M, Chromiak J (1999) Organogenesis of skeletal muscle in tissue culture. *Methods Mol Med* 18:217–25.
13. Powell CA, Smiley BL, Mills J, Vandenburgh HH (2002) Mechanical stimulation improves tissue-engineered human skeletal muscle. *Am J Physiol Cell Physiol* 283(5):1557–65.
14. Gholobova D, Gerard M, Terrie L, Desender L, Shansky J, Vandenburgh H, Thorrez L (2019) Coculture Method to Obtain Endothelial Networks Within Human Tissue-Engineered Skeletal Muscle. *Myogenesis*, pp 169–183.
15. Shcherbakova D, Baloban M, Emelyanov A, Brenowitz M, Guo P, Verkhusha V (2016) Bright monomeric near-infrared fluorescent proteins as tags and biosensors for multiscale imaging. *Nat Commun* 7:1–12.
16. Geraerts M, Micheils M, Baekelandt V, Debyser Z, Gijsbers R (2005) Upscaling of lentiviral vector production by tangential flow filtration. *J Gene Med* 7(10):1299–1310.
17. Ibrahimi A, et al. (2009) Highly Efficient Multicistronic Lentiviral Vectors with Peptide 2A Sequences. *Hum Gene Ther* 20(8):845–860.
18. Lendrum AC, Fraser DS, Slidders W, Henderson R (1962) Studies on the character and staining of fibrin. *J Clin Pathol* 15:401–413.
19. Carpentier G (2012) Angiogenesis Analyzer for ImageJ - Gilles Carpentier Research Web Site: Computer Image Analysis.
20. Gholobova D, Gerard M, Decroix L, Desender L, Callewaert N, Annaert P, Thorrez L (2018) Human tissue-engineered skeletal muscle: a novel 3D in vitro model for drug disposition and toxicity after intramuscular injection. *Sci Rep* (12):1–14.
21. Pfaffl MW, Horgan GW, Dempfle L (2002) Relative expression software tool (REST) for group-wise comparison and statistical analysis of relative expression results in real-time PCR. *Nucleic Acids Res* 30(9):36.

22. Stratman AN, Malotte KM, Mahan RD, Davis MJ, Davis GE (2009) Pericyte recruitment during vasculogenic tube assembly stimulates endothelial basement membrane matrix formation. *Blood* 114(24):5091–5101.
23. Vandenburgh H, Shansky J, Benesch-Lee F, Barbata V, Reid J, Thorrez L, Valentini R, Crawford G (2008) Drug-screening platform based on the contractility of tissue-engineered muscle. *Muscle Nerve* 37(4):438–47.
24. Costa-Almeida R, Granja PL, Soares R, Guerreiro SG (2014) Cellular strategies to promote vascularisation in tissue engineering applications. *Eur Cells Mater* 28:51–67.
25. Laschke MW, Menger MD (2012) Vascularization in tissue engineering: angiogenesis versus inosculation. *Eur Surg Res* 48(2):85–92.
26. Morin KT, Tranquillo RT (2013) In vitro models of angiogenesis and vasculogenesis in fibrin gel. *Exp Cell Res* 319(16):2409–2417.
27. Madden L, Juhas M, Kraus WE, Truskey GA, Bursac N (2015) Bioengineered human myobundles mimic clinical responses of skeletal muscle to drugs. *Elife* 4:1–14.
28. Chen X, Aledia AS, Ghajar CM, Griffith CK, Putnam AJ, Hughes CCW, George SC (2009) Prevascularization of a fibrin-based tissue construct accelerates the formation of functional anastomosis with host vasculature. *Tissue Eng Part A* 15(6):1363–1371.
29. Jain RK (2003) Molecular regulation of vessel maturation. *Nat Med* 9(6):685–693.
30. Kalluri R (2003) Basement membranes: Structure, assembly and role in tumour angiogenesis. *Nat Rev Cancer* 3(6):422–433.
31. Poschl E, Brachvogel, Ursula Schlötzer-Schrehardt B, Saito K, Ninomiya Y, Mayer U (2004) Collagen IV is essential for basement membrane stability but dispensable for initiation of its assembly during early development. *Development* 131(7):1619–1628.
32. Brady MA, Lewis MP, Mudera V (2008) Synergy between myogenic and non-myogenic cells in a 3D tissue-engineered craniofacial skeletal muscle construct. *J Tissue Eng Regen Med* 2:408–417.
33. Carosio S, Barberi L, Rizzuto E, Nicoletti C, Del Prete Z, Musarò A (2013) Generation of eX vivo-vascularized Muscle Engineered Tissue (X-MET). *Sci Rep* 3:1420.
34. Jeon JS, Bersini S, Whisler J a, Chen MB, Dubini G, Charest JL, Moretti M, Kamm RD (2014) Generation of 3D functional microvascular networks with human mesenchymal stem cells in microfluidic systems. *Integr Biol* 6(5):555–63.
35. Sacharidou A, Stratman AN, Davis GE (2011) Molecular mechanisms controlling vascular lumen formation in three-dimensional extracellular matrices. *Cells Tissues Organs* 195(1–2):122–143.
36. Gökçinar-Yagci B, Uçkan-Çetinkaya D, Çelebi-Saltik B (2015) Pericytes: Properties, Functions and Applications in Tissue Engineering. *Stem Cell Rev Reports* 11(4):549–559.
37. Ding R, Darland DC, Parmacek MS, Amore PAD (2004) Endothelial-mesenchymal interactions in vitro reveal molecular mechanisms of smooth muscle/pericyte differentiation. *Stem Cells Dev* 13(5):509–520.
38. Lesman A, Koffler J, Atlas R, Blinder YJ, Kam Z, Levenberg S (2011) Engineering vessel-like networks within multicellular fibrin-based constructs. *Biomaterials* 32:7856–7869.
39. Nör JE, Peters MC, Christensen JB, Sutorik MM, Linn S, Khan MK, Addison CL, Mooney DJ, Polverini PJ (2001) Engineering and characterization of functional human microvessels in immunodeficient mice. *Lab Invest* 81(4):453–463.
40. Van der Schaft DWJ, Van Spreeuwel ACC, Van Assen HC, Baaijens FPT (2011) Mechanoregulation of Vascularization in Aligned Tissue-Engineered Muscle: A Role for Vascular Endothelial Growth Factor. *Tissue Eng Part A* 17(21–22):2857–2865.
41. Sriram G, Tan JY, Islam I, Rufaihah AJ, Cao T (2015) Efficient differentiation of human embryonic stem cells to arterial and venous endothelial cells under feeder- and serum-free conditions. *Stem Cell Res Ther* 6(1):261.
42. Van Beem RT, Verloop RE, Kleijer M, Noort W a, Loof N, Koolwijk P, Van der Schoot CE, Van Hinsbergh VWM, Zwaginga JJ (2009) Blood outgrowth endothelial cells from cord blood and peripheral blood: angiogenesis-related characteristics in vitro. *J Thromb Haemost* 7(1):217–26.

43. Gilbert-Honick J, Iyer SR, Somers SM, Lovering RM, Wagner K, Mao HQ, Grayson WL (2018) Engineering functional and histological regeneration of vascularized skeletal muscle. *Biomaterials* 164:70–79.
44. Shultz L, et al. (2010) Multiple defects in innate and adaptive immunologic function in NOD / LtSz-scid mice. *J Immunol* 154:180–191.
45. Christianson S (1997) Enhanced human CD4+ T cell engraftment in beta2-microglobulin-deficient NOD-scid mice. *J Immunol* 158(8):3578–3586.
46. Yoshino H, Ueda T, Kawahata M, Kobayashi K, Ebihara Y, Manabe A, Tanaka R, Ito M, Asano S, Nakahata T, Tsuji K (2000) Natural killer cell depletion by anti-asialo GM1 antiserum treatment enhances human hematopoietic stem cell engraftment in NOD/Shi-scid mice. *Bone Marrow Transplant* 26(11):1211–1216.
47. Xia Z, Ye H, Choong C, Ferguson DJP, Platt N, Cui Z, Triffitt JT (2004) Macrophagic response to human mesenchymal stem cell and poly(ε-caprolactone) implantation in nonobese diabetic/severe combined immunodeficient mice. *J Biomed Mater Res - Part A* 71(3):538–548.
48. Laumonier T, Menetrey J (2016) Muscle injuries and strategies for improving their repair. *J Exp Orthop* 3(1):15.
49. Juhas M, Abutaleb N, Wang JT, Ye J, Shaikh Z, Sriworarat C, Qian Y, Bursac N (2018) Incorporation of macrophages into engineered skeletal muscle enables enhanced muscle regeneration. *Nat Biomed Eng* 2(12):942–954.
50. Sadtler K, et al. (2016) Developing a pro-regenerative biomaterial scaffold microenvironment requires T helper 2 cells. *Science* 352(6283):366–370.
51. Zhang M, Methot D, Poppa V, Fujio Y, Walsh K, Murry CE (2001) Cardiomyocyte grafting for cardiac repair: Graft cell death and anti-death strategies. *J Mol Cell Cardiol* 33(5):907–921.
52. Kaully T, Kaufman-Francis K, Lesman A, Levenberg S (2009) Vascularization-the conduit to viable engineered tissues. *Tissue Eng Part B Rev* 15(2):159–69.
53. Kaijzel EL, Koolwijk P, Van Erck MGM, Van Hinsbergh VWM, De Maat MPM (2006) Molecular weight fibrinogen variants determine angiogenesis rate in a fibrin matrix in vitro and in vivo. *J Thromb Haemost* 4(9):1975–1981.
54. White S, Pittman C, Hingorani R, Arora R, Esipova T, Vinogradov S, Hughes C, Choi B, George S (2014) Implanted Cell-Dense Prevascularized Tissues Develop Functional Vasculature That Supports Reoxygenation After Thrombosis. *Tissue Eng Part A* 20(17–18):2316–2328.
55. Wolbank S, Pichler V, Crawford JF, Meinl A, van Griensven M, Goppelt A, Redl H (2015) Non-invasive in vivo tracking of fibrin degradation by fluorescence imaging. *J Tissue Eng Regen Med* 9:973–976.
56. Thorrez L, DiSano K, Shansky J, Vandenburgh H (2018) Engineering of human skeletal muscle with an autologous deposited extracellular matrix. *Front Physiol* 9(Aug):1–11.
57. Van Linthout S, Miteva K, Tschöpe C (2014) Crosstalk between fibroblasts and inflammatory cells. *Cardiovasc Res* 102(2):258–269.
58. Brown B, Badylak SF (2014) Extracellular matrix as an inductive scaffold for functional tissue reconstruction. *Transl Res* 163(4):268–285.
59. Bloise N, et al. (2018) Ether-Oxygen Containing Electrospun Microfibrous and Sub-Microfibrous Scaffolds Based on Poly(butylene 1,4-cyclohexanedicarboxylate) for Skeletal Muscle Tissue Engineering. *Int J Mol Sci* 19(10):3212.
60. Yuan T, Xiao Y, Fan Y, Liang J, Zhang X (2017) The degradation and local tissue effects of collagen hydrogel and sponge implants in muscle. *Polym Test* 62:348–354.

CHAPTER 5

HUMAN TISSUE-ENGINEERED SKELETAL MUSCLE: A NOVEL 3D IN VITRO MODEL FOR DRUG DISPOSITION AND TOXICITY AFTER INTRAMUSCULAR INJECTION

Published as:
Gholobova D, Gerard M, Decroix L, Desender L, Callewaert N, Annaert P, Thorrez L (2018) Human tissue-engineered skeletal muscle: a novel 3D in vitro model for drug disposition and toxicity after intramuscular injection. *Scientific Reports* 8(1):12206.

5.1 Abstract

The development of laboratory-grown tissues, referred to as organoids, bio-artificial tissue or tissue-engineered constructs, is clearly expanding. We describe for the first time how engineered human muscles can be applied as a pre- or non-clinical model for intramuscular drug injection to further decrease and complement the use of *in vivo* animal studies. The human bio-artificial muscle (BAM) is formed in a seven day tissue engineering procedure during which human myoblasts fuse and differentiate to aligned myofibers in an extracellular matrix. The dimensions of the BAM constructs allow for injection and follow-up during several days after injection. A stereotactic setup allows controllable injection at multiple sites in the BAM. We injected several compounds; a dye, a hydrolysable compound, a reducible substrate and a wasp venom toxin. Afterwards, direct reflux, release and metabolism were assessed in the BAM constructs in comparison to 2D cell culture and isolated human muscle strips. Spectrophotometry and luminescence allowed to measure the release of the injected compounds and their metabolites over time. A release profile over 40 hours was observed in the BAM model in contrast to 2D cell culture, showing the capacity of the BAM model to function as a drug depot. We also determined compound toxicity on the BAMs by measuring creatine kinase release in the medium, which increased with increasing toxic insult. Taken together, we show that the BAM is an injectable human 3D cell culture model that can be used to measure release and metabolism of injected compounds *in vitro*.

5.2 Introduction

When testing drug candidates non-clinically, adequate model systems are crucial for a high success rate in clinical trials. Currently, 2D cell culture models are widespread as one of the model systems for high-throughput screening since they are very accessible. However, they lack the natural cell environment. The latter may include cell–cell and cell–extracellular matrix (ECM) interactions as well as mechanical and/or chemical cues (1–4). Moreover in 2D cell culture, compounds added to the cell culture medium can easily access the target cells and are exposed homogenously to all cells, in contrast to drug exposure to tissues *in vivo* (5, 6). These limitations are well-known and therefore the next step is drug testing in animal models. This allows evaluation of the route of administration, pharmacokinetics and pharmacodynamics. Major drawbacks are the cost of animal experiments and the fact that animal physiology differs from human physiology. Ninety percent of compounds declared safe and effective in animal models subsequently failed in clinical trials, 29 % was attributable to toxicity (7, 8). Moreover, current policy promotes replacement, refinement and reduction of animal experiments, the so-called 3R principle (9, 10). These issues have led to a growing interest in creating 3D non-clinical human tissue models using tissue engineering. In tissue engineering, cells are used with natural or synthetic scaffolds to create *in vitro* bio-artificial tissue that can replace *in vivo* tissue in various applications (11). Three-dimensional tissue can also be created by differentiation from stem cells. Tissues derived by orchestrated *in vitro* stem cell differentiation are referred to as organoids. Different tissues such as cartilage, bone, heart and skeletal muscle, skin, liver and nerve are being developed (12–18). Most of the approaches are still in research phase, but some products are already used in clinical practice. For example skin replacement products are already used in burn wound treatment (reviewed in (19)). Besides the use of human *in vitro* grown tissues in regenerative medicine, they can also be used as models for disease aetiology, study of development or for drug testing purposes (20). For example, commercially available hepatocyte and skin tissue models were described to more accurately reflect the human *in vivo* physiology and have a more representative drug response than 2D cell culture models (21, 22). Despite the increased interest, many tissue engineering hurdles remain to be tackled. Most of the *in vitro* tissues have relatively small dimensions (often submillimeter) and when used for drug testing they are incubated in a medium containing the drug. Nowadays 12 % of the drug formulations from the Belgian drug data base are administered through injection, of which one third intramuscularly (23). Other injection routes include subcutaneous, intravenous or intradermal (23). Intramuscular injections deliver medication deep into the muscles, serving as

a depot, allowing the medication to be gradually released in the blood. There are several reasons to prefer intramuscular drug administration over oral, subcutaneous or intravenous administration; physicochemical and pharmacokinetic properties of the drug, onset, intensity and duration of the effect and patient's compliance. When looking at the onset of effect after administration, IV injections produce the most rapid onset of effect, followed by IM and SC injections (24). So, although the IM route administration is not the fastest way to deliver a drug, it is preferred for drugs that require a longer efficacy. The injection creates a drug depot in the muscle tissue and the drug is released slowly over a certain period of time (25). For example, longer term low plasma levels were found for the IM administrated antipsychotic drug haloperidol decanoate in contrast to orally administrated haloperidol in schizophrenia patients, limiting side effects (26, 27).

Due to lack of alternatives, candidate drugs and drug formulations for intramuscular administration are tested using methods developed for oral drug administration. *In vitro* dissolution testing of candidate drugs is used to predict *in vivo* drug release profiles (28–31). But *in vitro* results obtained from these studies cannot adequately predict *in vivo* behavior of intramuscular drug formulations, due to a lack of good representation of the complex muscle physiology. To obtain pharmacokinetic and toxicity data that can be predictive for human drug responses, we studied micro-injection of compounds into a previously developed human bio-artificial muscle (BAM) model (32–34). The BAM is a muscle bundle consisting of aligned myofibers, able to contract upon electrical and/or mechanical stimulation that has been developed in the Vandenburgh group (34, 35). This model system could bridge the gap between 2D cell culture and animal models, while immediately using human instead of animal tissue. Injection of drugs in engineered tissues has not been described thus far and could be a valuable non-clinical model to assess compound toxicity, metabolism and release profile.

BAMs are formed by mixing muscle cells, isolated from muscle biopsies, in a natural hydrogel in a silicone mold containing two attachment points. Over a one week period, the cell-gel mix contracts to form multinucleated myofibers well-aligned in the direction of the attachment points. Such a model can be used to study mechanisms underlying muscle development, skeletal muscle innervation and vascularization (33, 36). Furthermore this model can be used as an *in vitro* disease model for muscular disorders and drug screening. By using muscular dystrophic muscle cells in the BAM model, Vandenburgh et al. were able to establish an *in vitro* assay that could predict the behavior of potential treatments for muscle weakness in Duchenne muscular dystrophy and other muscle disorders (37). Another example of the potential of the BAM model for drug screening purposes describes the positive effect of insulin-like growth factor 1 and the

negative effect of a statin on the morphology and contractility of the human BAM. These effects are also observed in human muscle *in vivo* and show the predictive behavior of the BAM model for skeletal muscle drug screening (38). While this BAM model has also been evaluated in *ex vivo* gene therapy studies (39), this model has never been implemented in the context of IM injections. The use of human cells in this 3D muscle model can improve the predictability of the human response on candidate drugs. This would increase the success rate of the compound in later clinical trials and at the same time reduce the cost of the drug discovery process (5). In this paper we have evaluated myofiber formation in BAMs with myoblasts only (BAM-M) and BAMs with a mixed muscle cell population (BAM – MM), mainly consisting of myoblasts and fibroblasts. We show that several parameters such as compound toxicity, retention, release and metabolism of injected test compounds can be measured in this model system. The effect of myofiber composition in the BAM model on the release profile and metabolism was assessed as well. Two compounds were chosen for injection in the BAMs with an in-house micro-injection system based on the ability to measure the amounts of both released parent compounds and their corresponding metabolites. The first compound; 5(6)-carboxy-2',7'-dichlorofluorescein diacetate (CDFDA) is hydrolyzed by cellular esterases to 5(6)-carboxy-2',7'-dichlorofluorescein (CDF), which is a fluorescent compound. The second compound, pro-NanoLuc® substrate, can be reduced by cellular reductases to a NanoLuc® substrate which can subsequently be processed by a NanoLuc® enzyme to produce light. The metabolic reactions that are quantified in the tests, namely hydrolysis and reduction, are two reactions that can occur during drug metabolism. We also determined compound toxicity on the BAMs by measuring creatine kinase release in the medium, which clearly increased with increasing toxic insult. In short, we show that the BAM is an injectable human 3D cell culture model which can reflect compound toxicity and release from muscle-like tissue and is capable of metabolizing the injected compounds, a process that is also relevant to the *in vivo* situation.

5.3 Methods

5.3.1 Cell culture

Human skeletal muscle myoblasts (M) from a skeletal muscle biopsy from the abdomen of a 28-year old Caucasian man were acquired from Tebu-Bio, 088SKB-F (lot SKM070512A), certified to contain 94.8 % CD56-positive cells at passage 3. Cells were expanded from passage 3 to 4 in a T75 cell culture flask (Elscolab) and from passage 4 to 7 in T175 cell culture flasks in Skeletal muscle Growth Medium (SkGM, Lonza), supplemented with 15% Fetal bovine serum (FBS, Fisher Scientific #10500064). Cells were split [4000 cells/cm2] at approximately 70% confluence with 0.125% trypsin/EDTA (Thermo Fisher Scientific #25200056). A human skeletal muscle cell population was isolated from a biopsy from the vastus lateralis muscle of a 60-year old Caucasian man 2 days post-mortem (Human Body Donation programme of KU Leuven University, Prof. E. Vereecke) as described in (40). In the mixed muscle (MM) cell population, myoblast percentage and fusion index were determined as described in (33). Cells were expanded until 12 doublings in T175 cell culture flasks in SkGM, supplemented with 15 % FBS and split (4000 cells/cm^2) at approximately 70 % confluence with 0.125 % trypsin/EDTA. C2C12 mouse myoblast cell line was acquired from Sigma. Cells were expanded in C2C12 growth medium: DMEM Glutamax (Thermo Fisher #31966021), 10% FBS, 1% Penicilin/Streptomycin (P/S, Thermo Fisher #15070063). Cells were split at approximately 90% confluency with 0.125 % trypsin/EDTA.

5.3.2 Human muscle strip isolation

A human muscle tissue biopsy, 307 mg wet weight, from the vastus lateralis muscle of a 60-year old Caucasian woman was isolated 1 day post-mortem (Human Body Donation programme of KU Leuven University, Prof. E. Vereecke). Muscle tissue was transferred to a 50 ml tube with chilled 20 ml DMEM Glutamax + 1% P/S. Working in a biological safety cabinet, muscle tissue was transferred to a 60 mm petri dish with 2 ml DMEM Glutamax + 1% P/S. Using sterile forceps and scalpel, excess connective tissue and fat was removed from the tissue sample. Then, the muscle tissue was cut into approximately 2 mm x 10 mm strips. Using 1.2 cm long sterile stainless steel insect pins (Vermandel #20.051), muscle strips were pinned into sterile sylgard coated 6-well plate wells under tension, with one pin at each end of strip. Strips were cultured for 1 day in DMEM Glutamax + 1% P/S until injection.

5.3.3 Bioengineering of BAMs

BAMs were engineered as previously described (33, 41). Briefly, C2C12 mouse myoblasts, human myoblasts (M) or human mixed muscle (MM) cells were trypsinized with 0.125% trypsin/EDTA, counted and mixed with 500 µl human thrombin (Bio Pharm Laboratories LLC #SKU 93-050 , 4 U/ml in DPBS ($+Ca^{2+}$, $+Mg^{2+}$) (Gibco #14040-083)). The mixture was cast into 25-mm-long silicone rubber molds with end attachment sites spaced 20 mm. Then, 500 µl fibrinogen (Merck Chemicals #341576, 2 mg/ml in DPBS (with Ca^{2+} and Mg^{2+})) was added and the cell-gel mix was mixed by quickly pipetting up and down, to form a fibrin hydrogel (1 mg/ml) containing the M or MM cells. Following two hours incubation at 37°C, SkGM medium for human M and MM cells and C2C12 growth medium for C2C12 cells supplemented with fibrinolysis inhibitors aprotinin (92.5 µg/ml in PBS (Gibco #10010-015, Carl Roth #A162.3) and tranexamic acid (400 µM in PBS, Sigma #857653-10G) was added. Two days after casting, the medium was switched to differentiation medium, SkFM, in the case of human M and MM cells: DMEM GlutaMax with 10 ng/ml hEGF (Peprotech #AF-100-15), 10 µg/ml insulin (Sigma-Aldrich #I9278), 50 µg/ml BSA (Sigma-Aldrich #A2153) and 50 µg/ml gentamicin (Thermo Fisher #15750037), also containing fibrinolysis inhibitors. For C2C12 cells the C2C12 growth medium was switched to C2C12 fusion medium containing DMEM Glutamax, 2% Horse serum, 1% P/S, fibrinolysis inhibitors and Cytosine β-D-arabinofuranoside (Sigma #C1768). Medium was replaced every 2 days and BAMs were kept in culture for 7 days prior to microinjection.

5.3.4 Injected compounds

5(6)-carboxy-2'7'-dichlorofluorescein diacetate (CDFDA, Sigma Aldrich #*21884*) was freshly dissolved in DMSO (Sigma Aldrich, #D2650) to 100 mM and further diluted in 30% polyethylene glycol-400 (Sigma Aldrich #202398) in HBSS without Ca^{2+} and Mg^{2} (Thermo Fisher # 14175053) to a final concentration of 500 µM for microinjection. 5(6)-carboxy-2'7'-dichlorofluorescein (CDF, Sigma Aldrich # 21882) was freshly dissolved in DMSO (100 mM) and diluted to a final concentration of 250 µM in HBSS. The pro-NanoLuc® substrate of the RealTime-Glo™ MT Cell Viability Assay (Promega #G9711) was used as a luminescent micro-injectable substrate. Mastoparan (Sigma Aldrich #M-5280), a wasp venom peptide, was dissolved to 1 mg/ml in PBS.

5.3.5 Microinjection

Two hours before injection, BAMs or human muscle strips were washed twice with 1 ml HBSS and further incubated in HBSS for two hours. Immediately before injection, BAMs or strips were washed again with 1 ml HBSS. Next, HBSS was removed to perform the injection. An in-house microinjection system was built using a syringe (Hamilton® Syringe 75RN 5.0 µL) fitted with a glass capillary using a 1 mm compression fitting (Dual Ferrule RN adaptor, Hamilton). The 1 mm glass capillary (VWR #612-2804) was pulled by hand and cut at the end to have an external diameter of 10 – 30 µm. The syringe with glass capillary could be exactly positioned using a 3D stereotactic system. Visual monitoring of penetration of the capillary in the BAM was performed with a stereomicroscope (Wild MSB, Heerbrugg Switzerland) (Figure 5.1a). Each BAM or strip was injected 1 to 4 times with 0.5 - 1 µl per sample (Figure 5.1b and 5.1c). For visualization and optimization of the injection procedure, Trypan blue (Thermo Fisher) was used. In case of multiple injections, different areas of the BAM were injected. Immediately after injection, 800 µl HBSS was added to the mold, completely submerging the BAM or muscle strip in HBSS. The tissue was washed twice with 800 µl HBSS, each time with a fixed time interval between washes (respectively 1 and 1.5 min) after which again 800 µl HBSS was added. All compounds in the washing steps were considered to be direct reflux. Effectively injected compound was calculated by subtracting the amount of refluxed compound from the total amount of compound that was recovered. At 5 min, 1.5 h, 16 h and 40 h 800 µl samples were taken and 800 µl fresh HBSS was added. The HBSS samples were stored for further processing at 4°C for pro-NanoLuc® substrate injections and at 4°C in acidic conditions for CDFDA injections (addition of 15 mM HCl per sample) or -20°C for HBSS and mastoparan injections. Measurements of CDF and NanoLuc® substrate occurred within 48 hours after collection of the final samples.

After the experiment, the BAM diameter was measured with a micrometer, each BAM was removed from its attachment sites, dried for 1 min on a tissue and frozen at -20°C. To determine whether residual compound could be found in the BAMs, they were disrupted using a tip sonicator (Branson, 5 – 10 cycles of 12 micron, 10 s each) in 800 µl RIPA buffer (25 mM Tris pH 7.4, 150mM NaCl, 1% Nonidet^{TM} P40 (Igepal)) while kept on ice. This 800 µl sample was further processed as the HBSS samples mentioned above.

5.3.6 CDFDA incubation in 2D cell culture

50,000 M or MM cells were cultured in SkGM in 6-wells to 80 % confluence and then switched to SkFM medium to induce myofiber formation. Cells were washed twice with 1 ml HBSS. 800 µl of 625 nM CDFDA solution in HBSS was added to cells. At 5 min, 1.5 h, 16 h and 40 h, 800 µl samples were taken and the same volume of HBSS was added.

5.3.7 Creatine kinase measurement

The toxicity of an injected compound was determined by measuring creatine kinase (CK) release. For toxicity measurements, the 3 types of BAM (mouse C2C12, human BAM-M and human BAM-MM) were injected as mentioned above with mastoparan at a myotoxic concentration of 1 mg/ml (42) or with HBSS. After injection, 800 µl of HBSS was added to the silicone mold of the BAM. The plates containing the BAMs were incubated at room temperature for 5 minutes after which the HBSS, containing the CK that was released by the BAMs, was stored at -20°C until CK measurement. As a positive control, BAMs were crushed in a cell homogenizer (Kimble Kontes) in 800 µl HBSS. CK concentration was measured on a Roche Cobas c501 chemistry analyzer with the CKL test kit (Roche Diagnostics #04524977) by measuring NADPH absorbance proportional to CK concentration. The lower quantification limit of this assay is 7 U/l.

5.3.8 Detection of CDF fluorescence

A calibration curve was prepared by serial 2x dilution of CDF and CDFDA in HBSS, starting at 250 µM. 150 µl of all samples was added in duplicate in a white 96-well plate (Roche #004729692001). The plate was shaken for 30 seconds and CDF fluorescence was measured using an excitation wavelength of 490 nm, emission was captured between 510 and 570 nm (GloMax®-Multi Microplate Multimode Reader, Promega) three times for each sample. For CDFDA determination, in half of the samples, 6 µl of NaOH (2M) was added to increase the pH above 11 and the plate was shaken for 30 seconds. This induces rapid and complete conversion of all CDFDA to CDF (data not shown). After 30 min incubation at room temperature, CDF fluorescence was recorded again as specified above. The amount of CDFDA was calculated as the total amount of CDF after forced hydrolysis minus the amount of CDF before hydrolysis.

5.3.9 Detection of NanoLuc® substrate luminescence

The pro-NanoLuc® substrate (Promega, #N1110) is supplied as a 1000x concentrated solution, to be diluted to a 1x solution for use in cell culture as advised by the manufacturer. Absolute concentration is proprietary so all concentrations are indicated as an x-times concentrated solution. As a calibration curve, a 2x dilution series was made of the pro-NanoLuc® substrate in HBSS, starting with a 0.5x concentration. 100 µl of each sample was pipetted in the white 96-well plate. All samples were added in duplicate and a 0.25x concentration of the NanoLuc® enzyme was added to each well. In one half of the samples and in the wells of the calibration curve, 20 mM dithiothreitol (DTT) (AppliChem #A2948) was added to induce forced reduction of the pro-NanoLuc® substrate in the sample. The plate was shaken for 30s and then incubated at 37°C for 2h. Luminescence occurs by conversion of the reduced Nanoluc® substrate by the NanoLuc® enzyme and is proportional to the amount of reduced substrate. Luminescence was recorded with an integration time of 1s on a GloMax®-Multi Microplate Multimode Reader (Promega).

5.3.10 Immunocytochemistry

Immunocytochemistry was performed in order to characterize the myoblast (M) and mixed muscle cell (MM) population used in the injected BAMs. The percentage of myoblasts and their fusion index was determined by a desmin and tropomyosin immunofluorescence staining. For desmin staining, myoblasts were cultured in SkGM in 24-well dishes for 2-3 days until ~70% confluent. Fixation was performed in a 1:1 methanol-aceton mix at -20°C for 10 min. For determination of fusion index, the cells were cultured to 80% confluence in SkGM and then switched to SkFM for 4 days to induce fusion into myofibers. Fixation was performed in 4% formaldehyde freshly prepared from paraformaldehyde (Merck # 1040031000) at RT for 10 min. Next, cells were permeabilized in blocking buffer containing 0.2% Triton-X-100 (Sigma #X100) and 1% bovine serum albumin (BSA, Sigma # A2153) in PBS (30 min, RT). Subsequently, cells were incubated overnight at 4°C with a monoclonal mouse antibody against desmin (Sigma, D1033, 1:200 in blocking buffer) or tropomyosin (Sigma, T9283, 1:100 in blocking buffer) to determine the myoblast percentage and the fusion index respectively. Cells were labeled with a polyclonal goat anti-mouse secondary antibody (Alexa Fluor 568, Invitrogen # A11004, 1:200 in PBS) for 30 minutes in the dark and subsequently incubated with DAPI (0.1 µg/ml in PBS, Life Technologies) for 1 hour. Images were acquired with Zeiss Zen software by AxioCam ICc 1 camera mounted on a Zeiss Axiovert 10 microscope. The

percentage of myoblasts in a muscle cell population was defined as the ratio of desmin positive cells to the total number of cells (identified by the DAPI-stained nuclei). For each replicate 150 – 300 cells were counted. Fusion index was defined as the ratio of nuclei in tropomyosin positive cells to the total number of myoblast nuclei in the population.

5.3.11 Whole mount immunofluorescence staining

The 3 types of BAMs (mouse GFP-labeled C2C12, human BAM-M and human BAM-MM) and the human muscle strips were washed (3x 5 min in PBS) and then removed from the attachment sites. Then, they were pinned on Styrofoam to preserve their original shape during fixation in 4% formaldehyde for 1 h and stored at 4°C in PBS. Immediately before whole-mount staining, samples were fixed a second time in -20°C methanol for 10 minutes and permeabilized in blocking buffer for 3 hours. Subsequently, the human BAMs and muscle strip were incubated overnight at 4°C with a monoclonal mouse antibody against tropomyosin (Sigma, T9283, 1:100 in blocking buffer) and MF20 (DSHB), recognizing all myosin heavy chain (MHC) isoforms. Next, the human BAMs and muscle strips were washed and incubated with a polyclonal goat anti-mouse secondary antibody (Alexa Fluor 633, A-11059 or A-21063 , Invitrogen, 1:200) for 30 minutes in the dark, followed by incubation with DAPI (Life Technologies, 0.1 µg/ml in PBS) for 1 hour. Samples were stored in PBS in the dark until visualized.

5.3.12 Confocal imaging and data analysis

Fixed GFP-labeled C2C12 BAMs, fixed and stained human BAMs or muscle strips were placed on coverslips and visualized by confocal microscopy (Zeiss LSM710) within 48 hours. Per sample, 2-5 z-stacks were acquired, each containing 20-40 images (depending on the intensity of the signal at various depths) every 5 µm towards the center of the tissue. For myofiber analysis in C2C12 BAMs, z-projections of 20 µm were created in ImageJ (43). The 20 µm z-projections were analyzed for different parameters of myofiber formation: myofiber alignment, length and myofiber density per microscopic field. Myofiber alignment was determined by the standard deviation of the angles of the myofibers compared to the mean alignment direction. A lower number thus indicates better alignment. In human BAMs number of nuclei per fiber were counted on 2D images.

5.3.13 Quantitative real-time PCR

RT-PCR was carried out to determine the expression of the different myosin heavy chain isoforms (*MYH1, MYH3, MYH8*) and myogenin (*MyoG*) in the 2 types of human BAM and muscle strip to compare the developmental state of the myofibers in the tissue-engineered

constructs to mature human muscle. To normalize for the amount of cells, 3 reference genes were used: *GAPDH, HSP90AB1* and *RPL13A*. Therefore BAMs or muscle strips were washed twice with PBS for 5 min and removed from the attachment sites. Per sample, 1 ml lysis buffer (Invitrogen #46-6001) with 1% 2-mercaptoethanol (Janssen Chimica #1254734) was added for 5 minutes at room temperature. The samples were stored at -80°C until further processing. The samples were disrupted using a tip sonicator (Branson, 5 – 10 cycles of 12 micron, 10 s each) while kept on ice and then centrifuged for 5 min at 2600 g. Total RNA was isolated from supernatans using the PureLink RNA Mini Kit (Ambion #12183018A). 2 µg of isolated RNA was reverse transcribed with the qScript cDNA SuperMix (Quantabio #95048-100) in 20 µl. PCR was performed with GeneAmp® PCR System 9700 (Applied Biosystems). Gene-specific primers (Table 5.1) were designed using NCBI/Primer-Blast and Primer3plus. Primer efficiency was determined by running a qRT-PCR for each specific gene primer pair with a serial dilution of cDNA. QRT PCR was performed with the LightCycler® 480 Instrument (Roche) using Perfecta Sybr Green Supermix (Quantabio #95054-500). All samples were run in duplicate. 40 cycles were run with a DNA dissociation step (95°C, 15 sec''), a primer annealing step and an amplification step (60°C, 45 sec''). After each cycle, Sybr Green fluorescence was recorded. After 40 cycles, a melting curve was recorded in which the temperature was increased at 1°C per sec'' from 60°C to 95°C while the Sybr Green fluorescence was recorded continuously.

Table 5.1. List of primers used for qRT-PCR

Gene	Orientation	Primer sequence (5' - 3')	Amplicon size (bp)
MYH1	Forward	GGG AGA CCT AAA ATT GGC TCA A	106
	Reverse	TTG CAG ACC GCT CAT TTC AAA	
MYH3	Forward	CTT GTG GGC GGA GGT CTG G	119
	Reverse	AGC TAT GCC GAA CAC TTC CAT	
MYH8	Forward	ACA TTA CTG GCT GGC TGG AC	143
	Reverse	ACC TTT CTT CGC GCT GCT AT	
MyoG	Forward	GTG TGT AAG AGG AAG TCG GTG TC	90
	Reverse	GAA GGC CTC ATT CAC CTT CTT	
GAPDH	Forward	TCA AGA AGG TGG TGA AGC AGG	168
	Reverse	ACC AGG AAA TGA GCT TGA CAA A	
HSP90AB1	Forward	AGA AAT TGC CCA ACT CAT GTC C	75
	Reverse	ATC AAC TCC CGA AGG AAA ATC TC	
RPL13A	Forward	CCT GGA GGA GAA GAG GAA AGA GA	126
	Reverse	TTG AGG ACC TCT GTG TAT TTG TCA A	

5.3.14 Statistics

Number of replicates refers to number of analyzed images for microscopic analyses, to the number of wells containing 2D cells treated with a compound, to the number of biological samples for quantitative real-time PCR analysis or to the number of BAMs for thickness analyses and microinjections. D'Agostino & Pearson normality test and Bartlett's test were used to verify normality of the data and equality of variances, respectively. Normally distributed data with equal variances were analyzed by an unpaired Student's t-test when two groups were compared. For comparing several normally distributed groups, a one-way ANOVA was used with a Bonferroni multiple comparison post test. When taking into account the factor time and cell type, a two-way ANOVA was used when comparing several groups. For groups that were not normally distributed and/or had unequal variances, a non-parametric Mann-Whitney test was used for comparison between two groups while Kruskal-Wallis test followed by a Dunn's post test was performed for multiple comparisons. All values were expressed as mean ± standard deviation. Relative mRNA expression was statistically analyzed with relative expression software tool (REST 2009, Qiagen). The REST software calculates whether gene expression is significantly different between the sample and control group using bootstrap randomization (44). Relative expression data were displayed in Whisker boxplots. * $p < 0.05$, ** $p < 0.01$, *** $p < 0.001$.

5.3.15 Data Availability

The datasets generated and analysed during the current study are available from the corresponding author on request.

5.4 Results

5.4.1 Optimization of the microinjection procedure

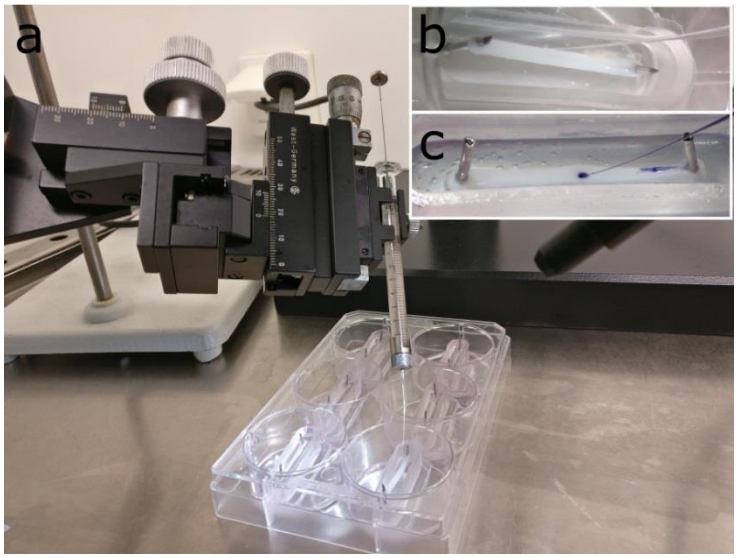


Figure 5.1. Microinjection setup. (a) In-house micro-injection setup. A pulled glass needle is attached to a 10 µl Hamilton syringe which can be accurately positioned in X-, Y- and Z-direction with a stereotactic device. Inlay images (b and c) show the enlarged view as seen through the stereomicroscope of the injection of pro-NanoLuc® substrate (b) or two trypan blue injections (c) in BAMs.

BAMs and muscle strips were injected with microliter quantities using a custom-built injection device (Figure 5.1A-1B). In order to obtain a 3D microinjection system, we characterized and optimized different parameters. First, the thickness of the BAM can influence the injection. The thicker the BAM, the easier the injection can be performed and the higher the maximal injection volume. Increasing the thickness of the BAM is possible by increasing the amount of extracellular matrix protein used when casting the cell-hydrogel mix in the mold. However, increasing the concentration of fibrinogen to 2 mg/ml in C2C12 mouse BAMs, caused a decrease in the quality and the amount of muscle fibers, especially in the center of the BAM (supplementary Figure S5.1); therefore, 1 mg/ml fibrin was further used throughout experiments. Using 4.10^6 C2C12 cells per BAM instead of 2.10^6 cells did not further improve the myofiber quality (Figure S5.1). The thickness of BAMs engineered with 2.10^6 human cells in 1mg/ml fibrin was 1.78 mm ± 0.18 mm (BAM-M) and 1.45 ± 0.14 mm (BAM-MM). Muscle strips used for toxicity testing and CDFDA injections were 1.41 ± 0.31 mm thick. Due to these thickness restrictions, glass capillary needles with a small outer diameter were preferable for injection to commercial stainless steel needles, which have an outer diameter of > 100 µm. Hand-pulled glass capillary needles with different outer diameters were fitted on a 5 µl syringe.

Initial experiments to monitor the injection process were performed with Trypan blue dye (Figure 5.1C). Using a capillary needle with an outer diameter of 10 – 30 µm ensured efficient injection without clogging the needle and allowed easy penetration into the elastic tissue-engineered muscle. Using Trypan blue, we determined that the injected volume should be smaller than or equal to 1 µl to avoid leakage of the dye from the BAM during injection. However, to increase the injected amount of compound/dye, we were able to inject each BAM up to 5 times without creating physically overlapping injection sites. In Figure 5.1A, the microinjection setup is shown. When injecting with Trypan blue, we could also observe an amount of dye immediately exiting the BAM when removing the needle. Therefore, the BAM was washed twice after each injection to remove this refluxed compound. Finally, when analyzing the release behavior of one of the studied compounds, CDFDA, we also determined that a fraction of the CDFDA adhered to the silicone mold (Supplementary Table S5.1), indicating an influence of the used materials on the recovered amount.

5.4.2 Characterization of myoblast (M) and mixed muscle (MM) cell populations

The cell population with only human skeletal muscle myoblasts (M) was characterized by desmin staining at passage 4, showing that the population contained 98 ± 2% desmin positive cells, consistent with 95 % $CD56^+$ cells at passage 3 as described in the datasheet, both CD56 and desmin being myogenic markers. The cells were further expanded in growth medium and used for tissue engineering at passage 7. At this passage, cells were 100% desmin positive (Figure 5.2a) and had a fusion index of 64 ± 3%, forming muscle fibers with 8 ± 1 nuclei per fiber (n=5) (Figure 5.2c). The mixed muscle (MM) cell population, obtained when the isolated muscle cell population is not further selected, contained 82 ± 5 % desmin positive myoblasts (n=6) (Figure 5.2b). Non-myogenic cells, which were previously reported to be mainly fibroblasts (45, 46), contributed to the remaining 18 %. The myoblasts in the MM cell population had a fusion index of 80 ± 15 % , forming muscle fibers with 10 ± 4 nuclei per fiber (n=6) (Figure 5.2d).

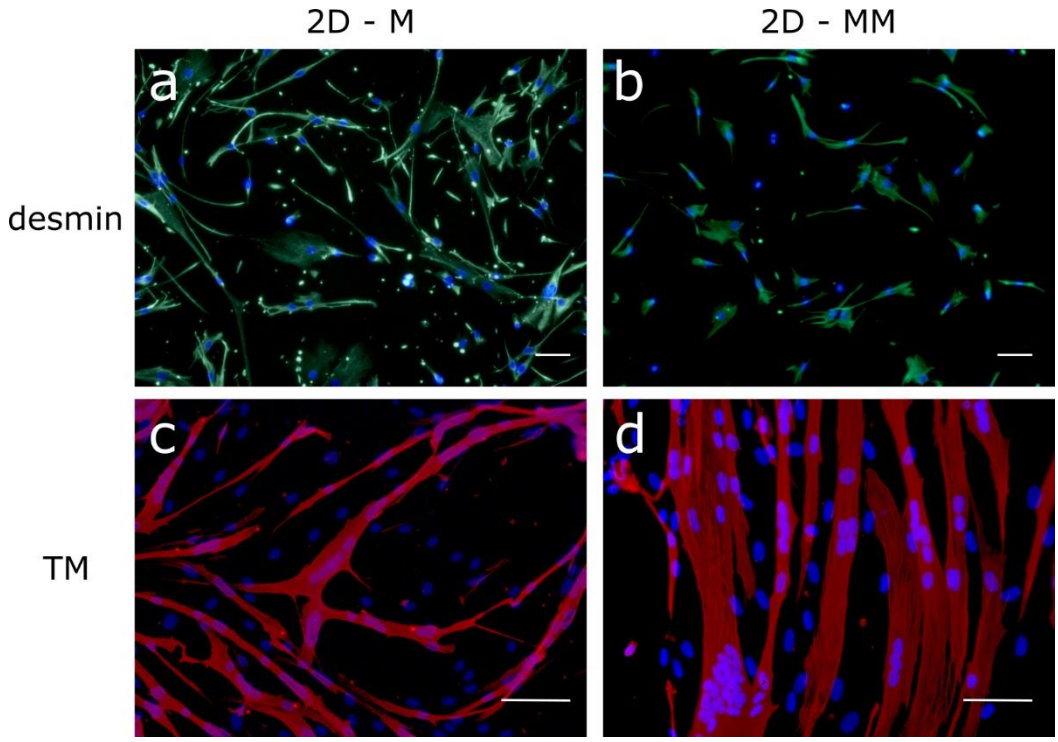


Figure 5.2. Human cells used for microinjection are highly myogenic and capable of differentiation into muscle fibers. (a-b) The cell population with only myoblasts (M) and mixed muscle cell population (MM) contains 100% and 82 ± 5 % myoblasts respectively as shown by desmin immunofluorescence staining (green) and nuclear staining (DAPI, blue) (a and b respectively). (c-d) After four days in SkFM, positive tropomyosin staining (red) and cell fusion indicates efficient differentiation to muscle fibers in the M and MM cell populations. Scale bars represent 50 µm.

5.4.3 Myofiber formation in BAMs

BAMs were formed by mixing $2x10^6$ cells in a 1 mg/ml fibrin matrix in a silicone mold containing 2 attachment points. During the course of 1 week, the cell-gel mix contracted to form BAMs. Myofiber formation was assessed with tropomyosin (TM) and myosin heavy chain (MHC) immunofluorescence in BAMs with myoblasts only (BAM-M) and in BAMs with a mixed muscle cell population (BAM – MM) in comparison to human muscle strips. In both BAM conditions, TM (Figure 5.3 a-d) and MHC (Figure 5.3 g-h) positive muscle fibers were observed, well-aligned in the direction of the attachment points (Figure 5.3). Presence of striated myofibers indicates an organized contractile aparatus as shown in human muscle strips (Figure 5.3 f and j). Striation was also observed in the BAMs although to a lesser extent (Figure 5.3 b and d). In human muscle strips nuclei were at the periphery (Figure 5.3 e and i), while in the tissue engineered constructs in the middle of the myotubes (Figure 5.3 a, c, g, h).

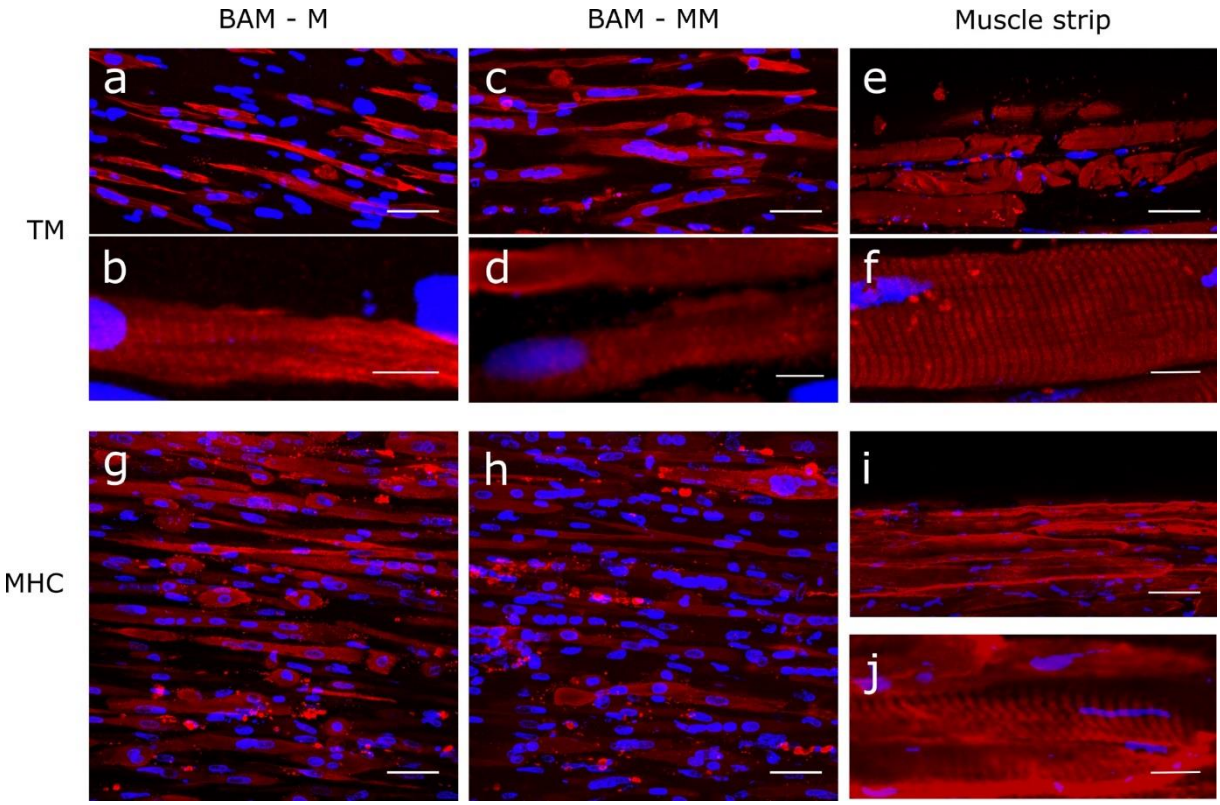


Figure 5.3. Myofibers within BAM-M and BAM-MM are well-aligned, multinucleated and occasionally striated. (a-f) Confocal microscopy images of tropomyosin (TM) immunofluorescence stained myofibers in 1 week old 3D BAMs with myoblasts only (BAM-M) (a-b), in 1 week old BAMs with mixed muscle cell population (BAM-MM) (c-d) and isolated human muscle strips (e-f). (g-j) Confocal image of MHC immunofluorescence stained myofibers in BAM-M (g), 1 week old BAM-MM (h) and muscle strips (i-j). The BAMs contain well-aligned, multinucleated (DAPI, blue), occasionally striated myofibers (b,d and f). Scale bars represent 50 µm (a, c, e, g, h and i) and 10 µm (b, d, f and j).

5.4.4 Muscle gene expression

Quantitative real-time PCR was used to analyze relative expression levels of *MYH1*, *MYH3*, *MYH8* and myogenin in human BAMs in comparison to human muscle. In comparison to mature muscle (n=5), BAM-M (n=4) and BAM-MM (n=5) expressed relatively lower levels of *MYH1* (5 times lower for both BAM-M and BAM-MM) and *MYH8* (4 and 2.2 times lower for respectively BAM-M and BAM-MM), showing a rather high expression of the mature *MYH1* and perinatal *MYH8* isoforms. Furthermore, myofibers within tissue engineered BAMs have significantly higher levels of embryonic *MYH3* and myogenin than in mature muscle (Figure 5.4). When comparing BAM-M to BAM-MM myofibers (Figure 5.4), we observe that BAM-MM shows a slightly higher expression of *MYH8, MYH3* and myogenin, suggestive for a more active myofiber formation in the BAM-MM.

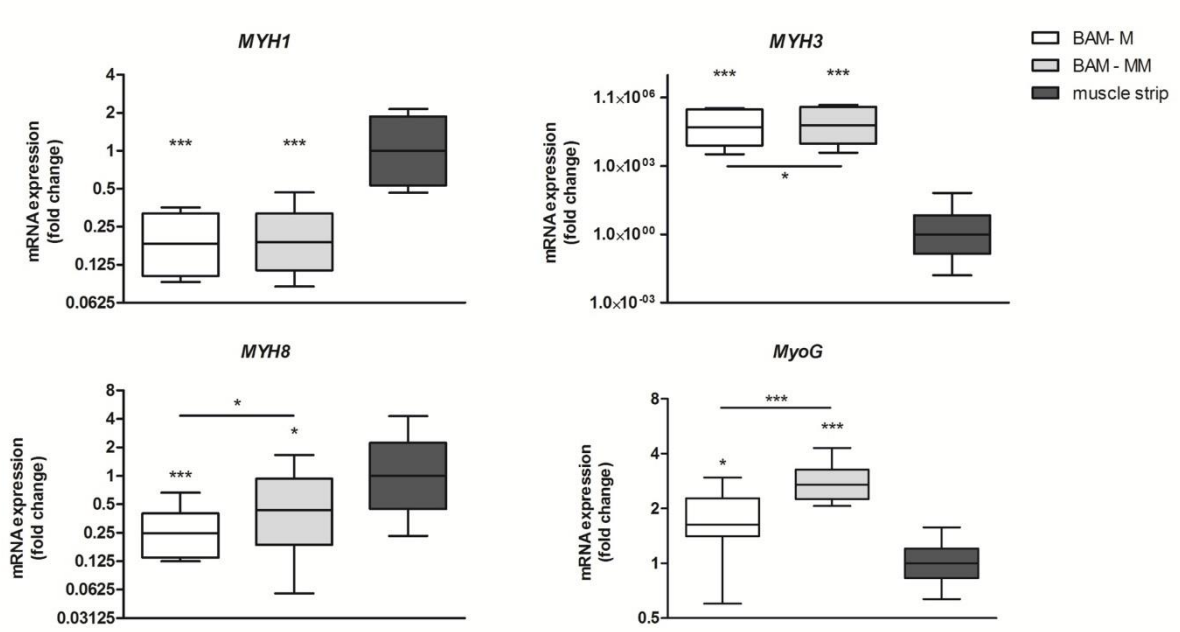


Figure 5.4. Relative myogenic gene expression in BAM-M and BAM-MM in comparison to human muscle. Relative expression of MYH isoforms and myogenin in 1 week old BAMs with myoblasts only (BAM-M) and in BAMs with a mixed muscle cell population (BAM-MM). Expression levels of these genes were quantified by quantitative real-time PCR as the fold changes relative to gene expression in muscle strips. *GAPDH, HSP90AB1 and RPL13A* were used as reference genes to normalize for the amount of cells. Relative expression in BAM-M was compared to relative expression in BAM-MM as well. Relative expression is depicted as Whisker boxplots. * p< 0.05, ** p< 0.01, *** p< 0.001.

5.4.5 The 3D BAM model adequately reflects compound toxicity by creatine kinase release

Creatine kinase is an intracellular enzyme abundant in skeletal muscle and is released upon cell damage. In the 3D injection model creatine kinase (CK) will be released into the medium due to cellular damage, when an injected compound is toxic. As a toxic compound, we used mastoparan, a wasp venom peptide with proven myotoxic effects (42). In the proposed 3D BAM model system, toxicity was increased as follows. Injection of HBSS (4 times 1 µl) was used to control for the possibly damaging effect of the injection procedure. Second, 1 µl mastoparan (1 mg/ml) was injected once or four times in a BAM to increase the toxic effect. Finally BAMs were crushed with a cell homogenizer in order to release a maximal amount of CK. A dose-dependent increase of CK release was observed both in BAM-M and in BAM-MM when inducing increasing amounts of damage to the BAMs (Figure 5.5, n=3 for BAM-M and n=4 for BAM-MM for each condition). Similar results were obtained in a pilot experiment in which mouse BAMs were injected (supplementary Figure S5.2). A significant higher CK content was observed in BAM-MM in comparison to BAMs with myoblasts only upon crushing. CK levels

measured in 800 µl HBSS incubated for 5 minutes with non-injected BAMs were below detection limit (<7 U/L, data not shown).

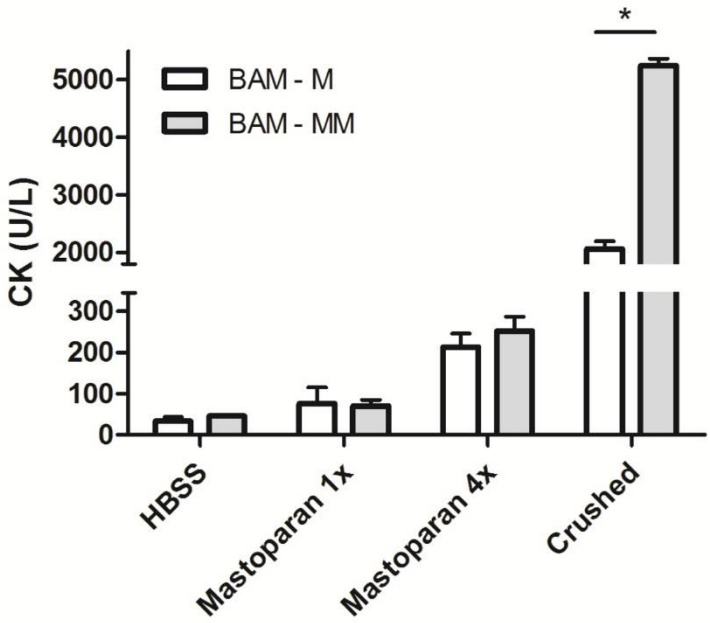


Figure 5.5. Creatine kinase release from the BAM-M and BAM-MM reflects increasing toxicity caused by increased damage from injected compounds to the BAM. Micro-injection of HBSS (1x 1µl) and mastoparan (1mg/ml, 1x 1µl and 4x 1µl) as well as crushing the BAM were used to inflict an increasing amount of damage to the BAM. The creatine kinase (CK) released from the BAM during 5 minutes is a measure for toxicity/damage. Error bars depict standard deviations.

5.4.6 Injected CDFDA is released over a time course of 40 hours in BAM

Many drugs are metabolized in the human body and a reaction that often occurs is (ester) hydrolysis. As a model compound for this reaction, we used the fluorogenic probe substrate CDFDA. This compound is hydrolyzed by intracellular esterases to the fluorescent CDF. Any unchanged CDFDA that is released by the BAM can also be measured by increasing the pH of the sample, which induces forced hydrolysis.

Before performing our experiments, we optimized the assay protocol. First, we confirmed that CDF and CDFDA were completely soluble in 30% PEG-400 in HBSS at the concentrations used for injection (500 µM). Second, we determined the detection limit and concentration range of CDF in which a linear increase of the fluorescence was recorded (0.5 – 100 nM, Supplementary Figure S5.3A). Third, the time to obtain complete forced hydrolysis of CDFDA to CDF was determined (Supplementary Figure S5.3B). Finally, we evaluated the occurrence of spontaneous hydrolysis of CDFDA during the experimental conditions (Supplementary

Figure S5.3C). Since performing a freeze-thaw cycle of CDFDA samples resulted in complete hydrolysis due to a temporary increase in pH, all samples were stored in the dark in acid conditions at 4°C until analysis.

CDF fluorescence of samples taken at different time points (5 min, 1.5h, 16h, 40h) after injection of CDFDA was measured before and after forced hydrolysis. Retention and release in BAM-M (n=3) and BAM-MM (n=8) were analyzed in comparison to human muscle strips (n=7). In Figure 5.6b, the release of CDF and CDFDA per time point is shown as a percentage of the total amount of effectively injected compound. It can be seen that the injected CDFDA is released into the medium over a time course of 40 hours in all conditions (Figure 5.6b). Furthermore, incubation of CDFDA in 2D cell cultures does not give a release profile over time in contrast to injection in 3D BAMs (Figure 5.6a). Figure 5.6c shows for each time point which percentage of CDFDA was hydrolyzed to CDF by the BAM-M (n=3), BAM-MM (n=8) and muscle strip (n=7) at that time point. The tissue-engineered constructs are able to metabolize the injected CDFDA. The muscle strips have in general a higher metabolic capacity at each time point (Figure 5.6c). At 40 hours the amount of metabolized CDFDA was below detection limit (< DL in Figure 5.6c) for BAM-MM and muscle strips. CDF and CDFDA were assessed in a cell lysate after sonicating the BAMs after 40h, but were not detectable.

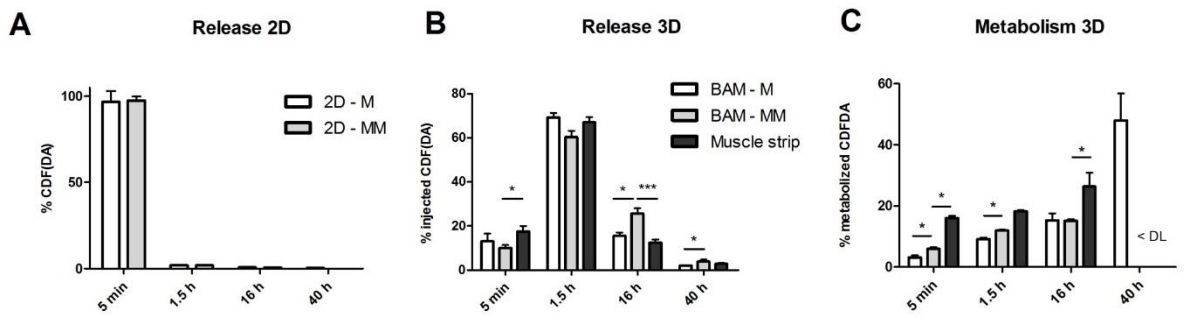


Figure 5.6. CDFDA injected in human BAMs is released in the incubation buffer (HBSS) over a time course of 40 hours. (a) In 2D cell culture 625 nM CDFDA solution (800 µl) was added to the differentiated myoblast only (2D-M) or mixed muscle cell population (2D-MM). Thereafter, CDFDA solution was replaced by 800 µl HBSS at 5 minutes, 1.5 h, 16 h and 40 h and CDF(DA) concentration was measured. (b-c) 500 µM CDFDA (1 µl) was injected in BAMs with myoblasts only (M), BAMs with mixed muscle cell population (MM) and human muscle strips. The release of CDF and CDFDA from BAM-M, BAM-MM and human muscle strips is shown per time point as a percentage of the total amount of effectively injected compound. (c) Percentage of CDFDA metabolized to CDF by the BAM. < DL indicates below detection limit. Error bars depict standard deviations. * $p< 0.05$, ** $p< 0.01$, *** $p< 0.001$.

5.4.7 Injected pro-NanoLuc® substrate is released over a time course of 40 hours

Another reaction in the body aimed to neutralize toxins or process drugs is reduction. As a model compound for this reaction we injected the pro-NanoLuc® substrate. This compound is a substrate of the NanoLuc® luciferase, but only after it gets reduced. During the resulting enzymatic reaction, light is produced that can be detected by a luminescence plate reader. Any pro-NanoLuc® substrate that is released without reduction by the BAM in the medium can also be measured by adding a strong reducing agent such as DTT. Samples are again taken at different time points after injection (5 min, 1.5h, 16h, 40h) in BAMs with myoblast only (n=3). Immediately before the measurement, the NanoLuc® luciferase is added to the samples and the luminescence is recorded. In the samples where DTT is added, both pro-NanoLuc® substrate and NanoLuc® substrate in the sample are measured. In Figure 5.7A, the release of the (pro-)NanoLuc® substrate per time point is shown as a percentage of the total amount of effectively injected compound. The latter was measured to be 61.4 ± 7.2% of the injected amount of pro-NanoLuc® substrate. In Figure 5.7B the percentage of pro-NanoLuc® substrate that was reduced by the BAM to NanoLuc® substrate is shown per time point. (Pro-)NanoLuc® substrate was assessed in a cell lysate of sonicated BAMs after 40h, but was not detectable.

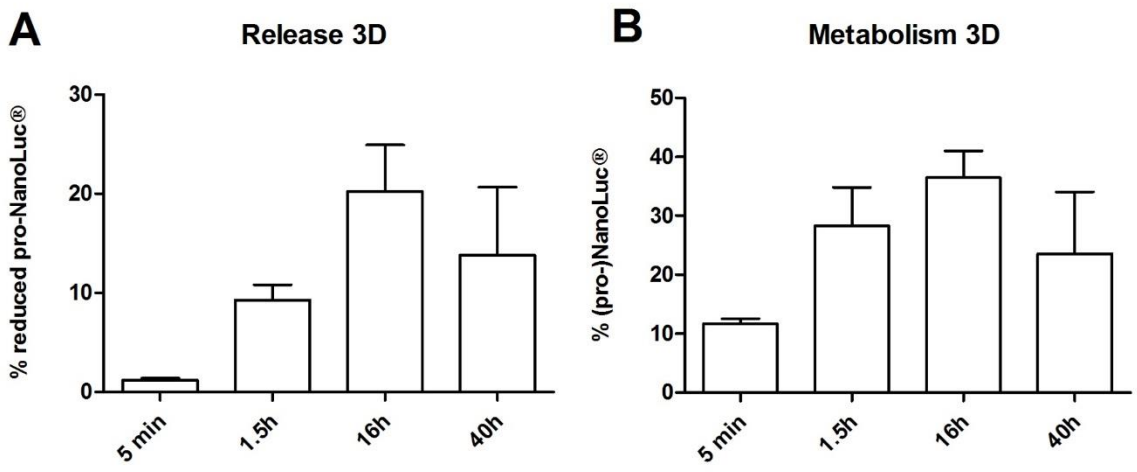


Figure 5.7. Injected pro-NanoLuc® substrate is released over a time course of 40 hours while the BAM is able to metabolize the substrate to a reduced form. 4x 0.5 µl pro-NanoLuc® substrate was injected in 3 BAMs with myoblasts only. In (a), the measured release of pro-NanoLuc® substrate and NanoLuc® substrate is shown per time point as a percentage of the total amount of effectively injected compound while in (b) the percentage of the substrate reduced by the BAM is shown. Error bars depict standard deviations.

5.5 Discussion

Increasingly 3D organoids, tissue engineered constructs and related model systems are developed for drug discovery research. A search on Pubmed with the combined subjects ‘tissue engineering’ and ‘drug’, shows 150 papers published in the year 2000 versus 2468 publications in 2016. We investigated the use of a human 3D muscle model for intramuscular injections of drugs. Drug metabolism, release and toxicity are complex processes, which are up until today mainly studied in animal models. Although animals are still needed for a full understanding of the intramuscular injection of a drug and its effects on the whole-body physiology, some important aspects may be modeled in tissue engineered constructs.

After intramuscular injection of a compound it will often be metabolized by oxidation, reduction and/or hydrolysis, mainly in the liver, but also in muscle or other tissues. About 5-7% of drugs are administered as a prodrug and need to be metabolized in order to obtain the active compound (47). We selected two model compounds that are metabolized in two different ways in the muscle, by intracellular esterase or reductase enzymes. These were CDFDA and pro-NanoLuc® substrate, of which the hydrolyzed or reduced form can easily be measured. Although CDF is easily retained in the cell due to its negative charges, it is subject to transporter-mediated efflux typically by transporters of the multidrug resistance-associated protein (MRP) family (48, 49). This qualifies CDF as a suitable probe for our study. Depending on the nature of the injected drugs and desired sensitivity, other bioanalytical methods such as liquid chromatography coupled to tandem mass spectrometry (LC-MS/MS) or other forms of spectroscopy can be envisioned.

In the process of optimizing the micro-injection of BAMs, several parameters were evaluated. First, the thickness of the BAMs was varied. We hypothesized that thicker BAMs may allow for injection of larger volumes. Therefore we investigated increased concentrations of extracellular matrix proteins (in this case, fibrinogen) and increased numbers of embedded muscle cells. However, if the BAMs became too thick, differentiation capacity decreased, muscle fibers were less well aligned and the presence of muscle fibers in the center of the BAM decreased (Supplemental Figure S5.1). Based on these data, we continued working with BAMs made with 1 mg/ml fibrin, having a thickness of just below 2 mm at the time of injection. In these BAMs, we were able to inject volumes up to 1 µl per injection site. Second, we optimized the concentration of injected compound and its metabolite in order to be detectable by readily available methods. A third factor was minimizing the impact on the release profile of direct reflux of the compound in the surrounding medium while removing the needle. This

immediately refluxed compound could clearly be visualized when injecting a colored compound such as Trypan blue (Figure 5.1c). Therefore, we performed two washing steps after injection (resp. 1 and 2.5 min after injection) to remove refluxed compound. Since the injection volume is limited to 1 µl, injecting up to 5 times in a single BAM allowed to increase the total amount of compound injected in the BAM. Fourth, tissue exerts an elastic resistance to injection. By decreasing the outer diameter of the capillary needle from 100 µm to 10-30 µm, less resistance and better penetration into the muscle tissue was obtained. Finally, spontaneous hydrolysis of CDFDA which occurs more rapidly at alkaline pH (48), was avoided by keeping samples at 4°C in acidic conditions (Figure S5.3). A freeze-thaw cycle was also avoided because a temporary increase in pH can occur during thawing of a sample. Spontaneous reduction of the pro-NanoLuc® substrate was not observed.

After optimizing the injection procedure, we evaluated 2 different cell populations as source for myofiber formation in BAMs: a monoculture of human myoblasts (M) and an isolated human mixed muscle cell population (MM), containing 82 ± 5 % desmin positive myoblasts. The remaining 18 % are non-myogenic cells, mainly fibroblasts (45, 46). The presence of fibroblasts is important during myogenesis as shown in a fibroblast ablation study in mice *in vivo* (50). For *in vitro* muscle formation, non-myogenic cells play a critical role in myogenic cell differentiation, force generation and matrix remodeling (45, 51). In 2D, myofiber formation was better in the mixed muscle cell population compared to myoblasts only. A fusion index of 64 % and 80 % was observed in respectively M and MM cells. Additionally when comparing M and MM cells for the number of nuclei per myofiber, we could observe 8 and 10 nuclei respectively. To better characterize the myofiber formation in BAMs, myosin heavy chain (MHC) and tropomyosin (TM) immunofluorescence stainings were performed on whole tissue. Both proteins play important roles in muscle force generation (52). Myofibers present in both BAM-M and BAM-MM are MHC and TM-positive showing presence of occasionally striated myofibers, although to a lesser extent than in mature muscle (Figure 5.3b and d). Another characteristic of skeletal muscle maturity is the presence of nuclei at the periphery of the myofibers. In our tissue-engineered human BAMs nuclei have a central location in the myofibers (Figure 5.3 a, c, g, h), an indication of the early myotube stage (53).

Furthermore quantitative real-time PCR was used to study myogenic gene expression in the 2 types of BAMs in comparison to gene levels in mature human muscle. Relative expression levels of *MYH1*, *MYH3*, *MYH8* and myogenin were analyzed. Myosin heavy chain isoforms reflect the developmental state of muscle fibers (36). *MYH3*, *MYH8* and *MYH1* are expressed in embryonic, perinatal and adult stages, respectively. Analysis of isoforms and expression

levels estimates the level of maturation of myofibers present in BAMs. Myogenin expression is indicative for early myogenic differentiation and myofiber formation. Analysis showed that myofibers present in the 2 types of BAM express 5 times lower levels of *MYH1* compared to myofibers in adult muscle and 4 and 2.2 times lower levels of *MYH8* for respectively BAM-M and BAM-MM, indicating that myofibers are not as mature as in adult muscle. High expression of *MYH3* and myogenin in BAMs shows early myotube formation resulting in more embryonic myofibers. Comparing BAM-MM to BAM-M, the significantly higher *MYH8*, *MYH3* and myogenin levels indicate a more active myofiber formation in BAM-MM. Also significant higher CK content was observed in BAM-MM. Creatin kinase expression is highly increased during myogenesis and reflects the maturity grade of myofibers (54, 55). From the above, we can conclude that both BAM-M and BAM-MM have clear myogenic features but are less mature than adult muscle and that BAM-MM shows more pronounced differentiation than BAM-M.

The release kinetics of the two injected compounds was clearly different. While already ~80% of effectively injected CDFDA was released after 1.5 hours for BAM-M, this was only ~40% in the case of the pro-NanoLuc® substrate (Figure 5.6 and 5.7). This could be due to the fact that the pro-NanoLuc® substrate was a suspension instead of a solution as was the case with CDFDA. In a suspension, undissolved particles are present, and gradual dissolution typically causes a slower release of the compound. A suspension for injection represents an interesting dosage form for certain drugs. For example, a slow-release version of antipsychotic drugs such as paliperidone may decrease the number of individual injections needed, leading to a better therapy compliance (56). Furthermore we could clearly show the utility of our 3D model to follow release kinetics over time, in constrast to a 2D cell culture model (Figure 5.6a and b), emphasizing the benefits of the BAM model. The release of CDF(DA) in BAMs and human muscle strip was highest at 1.5 hours and had a similar release profile over time. Overall, release kinetics from the muscle can indeed be an important parameter in drug development, which can be simulated in this *in vitro* model.

The metabolic turnover was similar between the two compounds, up to 16 hours after injection. The longer the compounds were present in the BAM, the higher the ratio of metabolite over parent compound. The muscle strips with mature myofibers had in general a higher metabolic capacity per time point. It is well-known that intracellular aspecific esterases can hydrolyze compounds such as CDFDA (57) while reductases play a role in the reduction of the pro-

NanoLuc® substrate, as shown for prodrugs that are activated by reduction (58–60). Part of the hydrolyzed CDFDA was due to spontaneous hydrolysis as shown in Figure S5.3C.

The next step in drug development is translating the *in vitro* results to corresponding *in vivo* exposures in the body. This can be achieved by *in vitro in vivo* extrapolation (IVIVE) linked to physiologically based pharmacokinetic (PBPK) modeling (61). IVIVE-PBPK allows to predict the *in vivo* exposure profiles in the target tissue, relying on all relevant processes related to the absorption, distribution, metabolism and excretion of the drug of interest. Furthermore, this so-called 'bottom-up' modelling and simulation approach, based on data obtained in *in vitro* tests, enables to determine adequate drug doses yielding desired target concentrations *in vivo* (62). To apply an IVIVE approach to the BAM model also scaling factors between *in vitro* and *in vivo* muscle tissue (e.g. amount of muscle tissue *in vitro*/*in vivo*) are required, in addition to the *in vitro* data on drug release and metabolism after BAM injections. At the PBPK level, muscle physiological parameters such as muscle blood perfusion rates need to be taken into account. *In vivo* pharmacokinetic data for IM haloperidol decanoate administration are available (27), and could be used as reference data to evaluate the value of a retrospective prediction based on IVIVE-PBPK. Such an exercise will support the validation of the BAM model as a suitable representation of the *in vivo* muscle environment.

Some challenges regarding the use of tissue-engineered constructs for drug research remain (63). First, the need to reflect complex organ functions. Regarding skeletal muscle, this encompasses the coculture of different tissue types such as nerve tissue, connective tissue and blood vessels. Coculturing these different tissue types and obtaining functionality is currently still a challenge (33, 64–66). The BAM models described in this paper only consist of a monoculture of myoblasts or a mixed muscle cell population and are able to evaluate the effects of injected compounds on myofibers. To better reflect the whole-muscle physiology, we aim to include multiple cell types in the BAM model. We are developing a skeletal muscle model in which endothelial precursor cells are added to induce a vascular network in the BAM (33). The presence of a vascular network and blood flow determines the local drug absorption and therefore the corresponding drug concentration and release time in the muscle. For example, the difference in blood flow between muscle groups resulted in different plasma concentrations and release time of intramuscular injected lidocaine (67, 68). To address this challenge one could use a bio-reactor to obtain flow perfusion in the construct and mimic blood flow (64, 69). Second, *in vivo* tissues are stimulated by chemical, electrical and mechanical stimuli from their environment to differentiate/mature into physiologically relevant tissues. Our *in vitro* tissue-

engineered skeletal muscle could also benefit from mechanical and electrical stimulation resulting in more mature striated skeletal muscle tissue (34, 70, 71). Third, an inherent characteristic of this model is the absence of other organs, such as the liver or the immune system. Influence of immune cells on pharmacokinetics and –dynamics may be important e.g. for vaccine testing. It has been shown that macrophages are capable of *in vivo* (pro)drug biotransformation (72). Approaches to integrate such responses are under development, typically on a microscale for screening purposes and are referred to as organ-on-a-chip systems. These are micro-engineered 3D models of the functional units of human organs that are connected with microfluidic channels and mimic organ-organ interactions (5). An important application of these model systems is testing a more realistic and overall effect of new drugs on several organs of the human body simultaneously (73). Although animal experiments can still be justified to monitor complex interactions, tissue model systems can partially reduce this need. Finally, since producing tissue-engineered constructs is labor intensive and time consuming, there is a need for automated procedures. An automated drug screening setup, as described previously to assess force of engineered muscle (37), with an additional micro-injection apparatus and sampling, would allow for higher throughput and decreased variability.

To conclude we can state that, using our *in vitro* 3D tissue engineered model for intramuscular injection, we are able to evaluate different parameters such as compound toxicity, release and biotransformation. The proposed system addresses the need to minimize animal experimentation.

5.6 Authors' contributions

LD and LT conceived and initiated the project. DG, MG, LD, LDS, NC designed and performed experiments. PA and LT supervised the project. DG, MG, PA and LT prepared and wrote the manuscript. All authors read and approved the final manuscript.

5.7 Acknowledgements

The authors thank Sigrid Vanryckeghem for administrative support, prof. Frank Martens for initial creatine kinase measurements, Maudi Sannen, Stijn Desnijder and Lisanne Terrie for technical assistance, Elise Lesage and prof. E. Vereecke for muscle biopsies and prof. Herman Vandenburgh for critical reading.
Funding: Research Fund KU Leuven (CREA/12/034); Fonds Wetenschappelijk Onderzoek – Vlaanderen (1.5.298.17N); and AFM-Telethon trampoline grant (19802).

5.8 Declaration of interest

Declarations of interest: none.

5.9 Supplementary materials

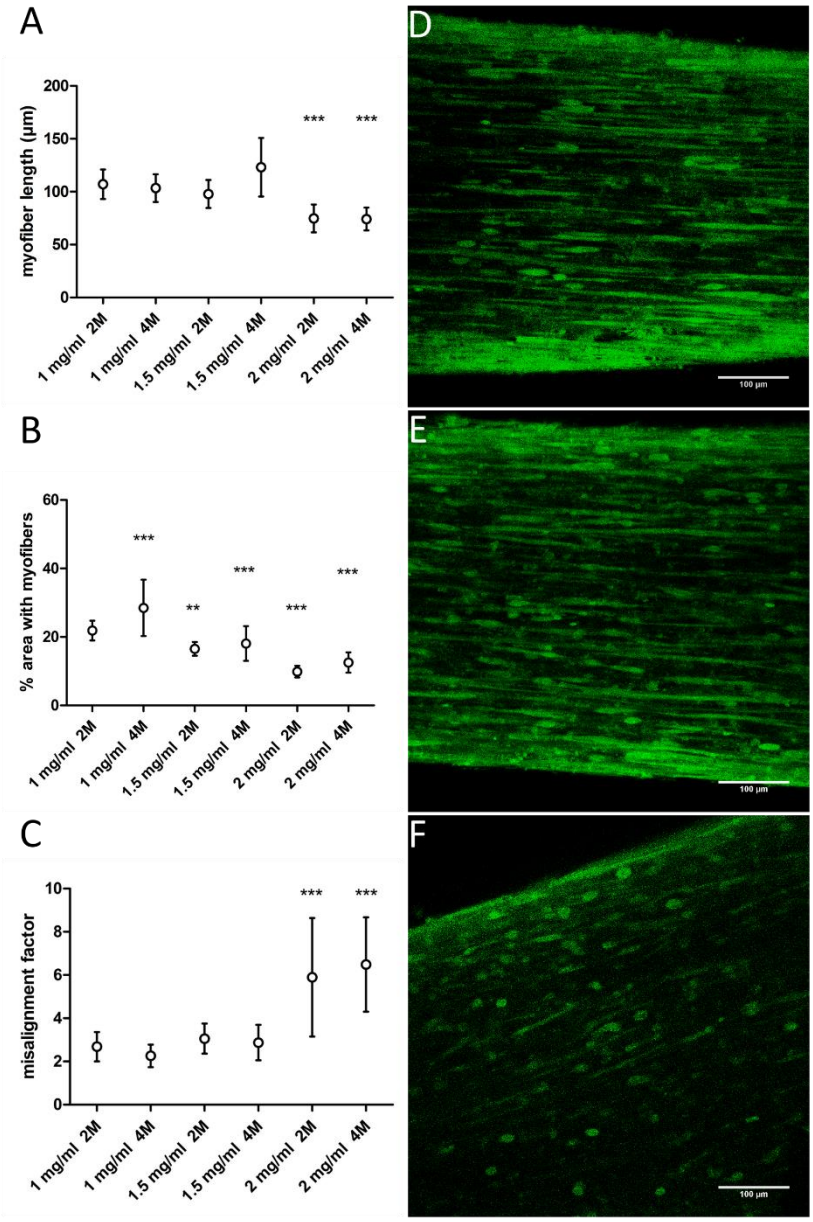


Figure S5.1. Myofiber formation in C2C12 BAMs with different fibrin concentration and cell numbers. (A-C) Parameters characterizing the formation of myofibers in C2C12 fibrin BAMs with different fibrin concentrations (1 mg/ml, 1.5 mg/ml or 2 mg/ml) and total cell numbers (2.10^6 or 4.10^6). Multiple comparisons were made by a Kruskal Wallis test followed by a Dunn's post test against the condition with 1 mg/ml fibrin and 2.10^6 total cell number condition. All values were expressed as mean ± standard deviation. * $p< 0.05$, ** $p< 0.01$, *** $p< 0.001$ (D-F). Fluorescent confocal 2D images of GFP labeled myofibers in C2C12 BAMs containing a constant total cell number (4.10^6) and an increasing fibrin concentration (1 mg/ml (D), 1.5 mg/ml (E) and 2 mg/ml (F)). Scale bars represent 100 µm.

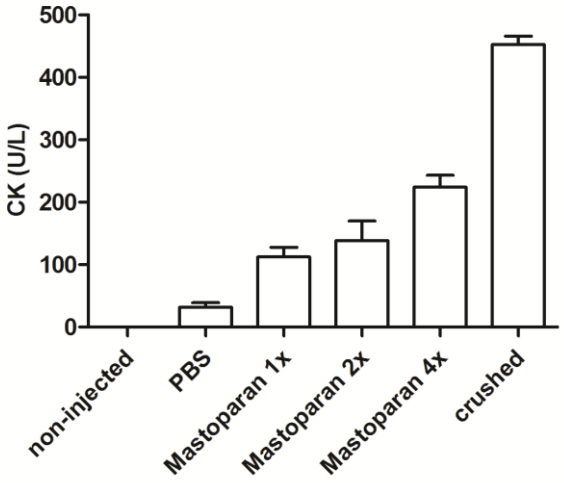


Figure S5.2. Creatine kinase release from the C2C12 BAM reflects increasing toxicity caused by increased damage from injected compounds to the BAM. Micro-injection of PBS (1x 0.8 µl, n = 4) or mastoparan (1mg/ml, 1x (n = 5), 2x (n = 3) or 4x (n = 2) 0.8 µl) as well as crushing the BAM (n = 6) were used to inflict an increasing amount of damage to the mouse BAM. After injection(s), the mouse BAMs were submerged in 800 µl PBS. After 5 minutes, the HBSS was removed and stored at -21°C. The creatine kinase released from the BAM during these 5 minutes or after crushing, is a measure for toxicity/damage. Creatine levels measured in 800 µl HBSS incubated for 5 minutes with non-injected mouse BAMs (n = 6) is shown as a negative control. Error bars depict standard deviations.

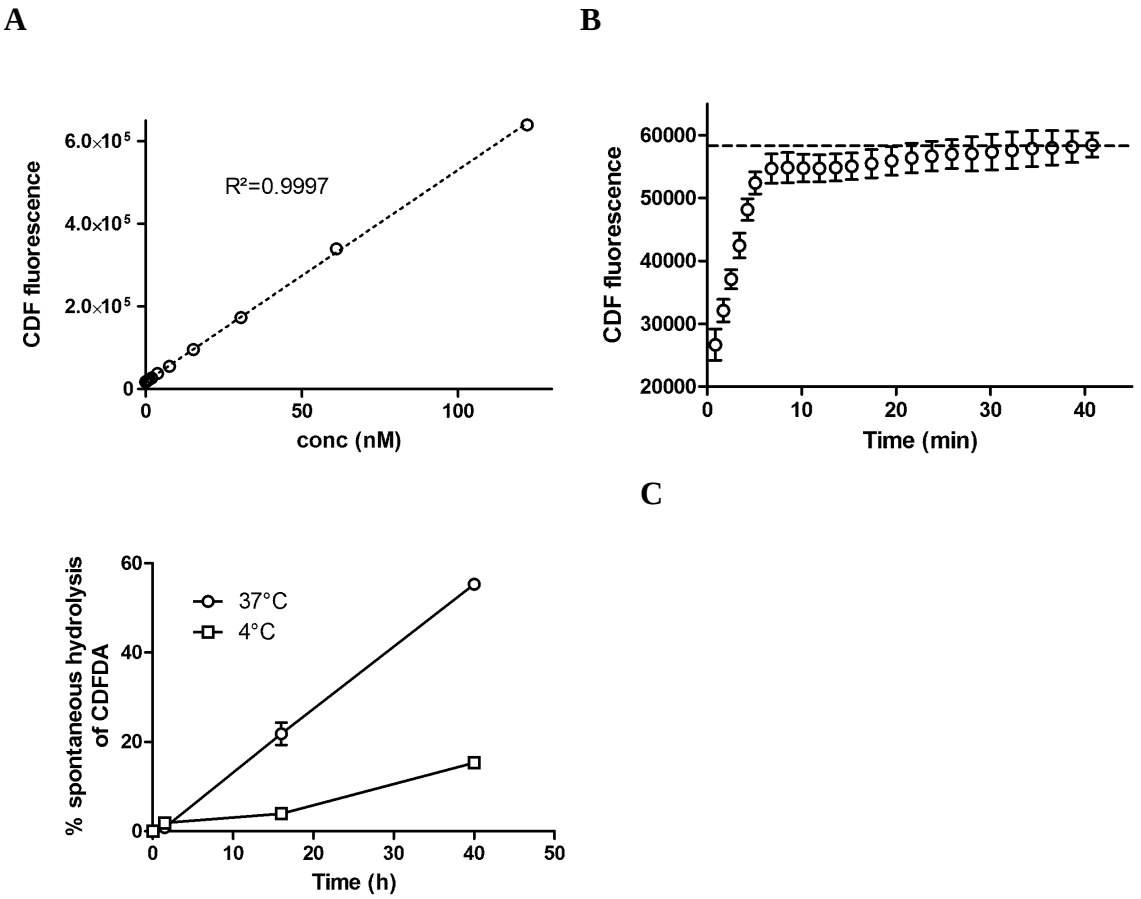


Figure S5.3. Experimental conditions of CDF detection and CDFDA hydrolysis. (A) Calibration curve of CDF fluorescence versus its concentration in nM. Every data point is an average of 3 measurements (SD shown but invisible due to small variation). A linear relationship between the two parameters can be seen between 0.5 and 100 nM. In (B), the time to obtain complete hydrolysis of CDFDA to CDF was measured at room temperature. CDFDA was diluted to a concentration of 200 nM and 6 wells were filled with 150 µl of this solution. To each well, 3 µl NaOH (2M) was added to obtain a pH ≥ 11 and the plate was shaken for 30 sec. Thereafter, the plate was measured each 25 seconds for 100 times. After 30 minutes, the plateau of CDF fluorescence is reached (dotted line). For clarity reasons, not all data points are shown on the graph. (C) Spontaneous hydrolysis of CDFDA (100 nM) during incubation (37°C, 5% CO_2) and storage in HBSS at 4°C during 40 hours.

	[CDF] measured	% recovery
A. 625 nM non-hydrolyzed CDFDA	10.5 ± 1.9	1.7 ± 0.3
	10.3± 2.2	1.6 ± 0.4
B. 625 nM non-hydrolyzed CDFDA, washed with 0,5% Triton-X 100	< det lim	< det lim
	< det lim	< det lim
C. 625 nM CDFDA hydrolyzed to CDF	344.6 ± 3.0	55.1± 0.5
	347.0 ± 21.5	55.5± 3.4
D. 625 nM CDFDA hydrolyzed to CDF, washed with 0,5% Triton-X 100	542.5± 33.7	86.8± 5.4
	515.9± 20.2	82.5± 3.2

Table S5.1. Characterization of CDFDA adherence to silicone mold. A CDFDA solution of 625 nM (800 µl) was incubated in a silicone mold in a 6-well plate for 6 hours at room temperature. Condition A: the concentration of CDF in the CDFDA solution was measured after 6 hours. This is the spontaneously hydrolyzed CDFDA. Condition B: Identical to condition A, but the mold was washed with 800 µl HBSS with 0.5% Triton-X-100 to remove any CDFDA that adhered to the silicone mold. Condition C: the CDFDA recovered from the mold was hydrolyzed to CDF using a pH jump to 11. This is the total concentration of CDFDA and CDF that was present in the sample. Condition D: Identical to condition C, but the mold was washed with 800 µl HBSS with 0.5% Triton-X-100. All numbers are the average of three technical replicates with their standard deviation. Two replicate samples were measured and are shown for each condition.

5.10 References

1. Discher DE, Janmey P, Wang Y-L (2005) Tissue cells feel and respond to the stiffness of their substrate. *Science* 310(5751):1139–43.
2. Falkenberg N, Höfig I, Rosemann M, Szumielewski J, Richter S, Schorpp K, Hadian K, Aubele M, Atkinson MJ, Anastasov N (2016) Three- dimensional microtissues essentially contribute to preclinical validations of therapeutic targets in breast cancer. *Cancer Med*:703–710.
3. Schmeichel KL (2003) Modeling tissue-specific signaling and organ function in three dimensions. *J Cell Sci* 116(12):2377–2388.
4. Bell CC, et al. (2016) Characterization of primary human hepatocyte spheroids as a model system for drug-induced liver injury, liver function and disease. *Sci Rep* 6(1):25187.
5. Esch MB, King TL, Shuler ML (2011) The role of body-on-a-chip devices in drug and toxicity studies. *Annu Rev Biomed Eng* 13:55–72.
6. Kola I, Landis J (2004) Can the pharmaceutical industry reduce attrition rates? *Nat Rev Drug Discov* 3(8):711–715.
7. Olson H, et al. (2000) Concordance of the toxicity of pharmaceuticals in humans and in animals. *Regul Toxicol Pharmacol* 32(1):56–67.
8. Duyk G (2003) Attrition and translation. *Science* 302(5645):603–605.
9. Cozigou G, Crozier J, Hendriksen C, Manou I, Ramirez-hernandez T (2015) The European Partnership for Alternative Approaches to Animal Testing (EPAA): Promoting Alternative Methods in Europe and Beyond. *J Am Assoc Lab Anim Sci* 54(2):209–213.
10. Yum K, Hong SG, Lee LP (2015) Physiologically relevant organs on chips. *Biotechnol J* 9(1):16–27.
11. Langer R, Vacanti J (1993) Tissue engineering. *Science (80-)* 260(5110):920–926.
12. Makris EA, Gomoll AH, Malizos KN, Hu JC, Athanasiou KA (2014) Repair and tissue engineering techniques for articular cartilage. *Nat Rev Rheumatol* 11(1):21–34.
13. Zhang BGX, Quigley AF, Myers DE, Wallace GG, Kapsa RMI, Choong PFM (2014) Recent advances in nerve tissue engineering. *Int J Artif Organs* 37(4):277–291.
14. Weinberger F, Mannhardt I, Eschenhagen T (2017) Engineering Cardiac Muscle Tissue. *Circ Res* 120(9):1487–1500.
15. Klumpp D, Horch RE, Beier JP (2011) Tissue engineering of skeletal muscle. *Tissue Engineering of Skeletal Muscle, Tissue Engineering for Tissue and Organ Regeneration*, ed Eberly PD (InTech).
16. Klar AS, Zimoch J, Biedermann T (2017) Skin Tissue Engineering: Application of Adipose-Derived Stem Cells. *Biomed Res Int*:1–12.
17. Palakkan AA, David H, Anil K, Kumary T, James R (2013) Liver tissue engineering and cell sources: Issues and challenges. *Liver Int* 33(5):666–676.
18. Henkel J, Woodruff MA, Epari DR, Steck R, Glatt V, Dickinson IC, Choong PFM, Schuetz MA, Hutmacher DW (2013) Bone Regeneration Based on Tissue Engineering Conceptions — A 21st Century Perspective. *Bone Res* 1(3):216–248.
19. Chua AWC, Khoo YC, Tan BK, Tan KC, Foo CL, Chong SJ (2016) Skin tissue engineering advances in severe burns: review and therapeutic applications. *Burn Trauma* 4(1):3.
20. Benam KH, et al. (2015) Engineered In Vitro Disease Models. *Annu Rev Pathol Mech Dis* 10(1):195–262.
21. Spielmann H, Hoffmann S, Liebsch M, Botham P, Fentem J (2007) The ECVAM international validation study on in vitro tests for acute skin irritation: report on the validity of the EPISKIN and EpiDerm assays and on the Skin Integrity Function Test. *Altern Lab Anim* 35(6):559–601.
22. Hendriks DFG, Puigvert LF, Messner S, Mortiz W (2016) Hepatic 3D spheroid models for the detection and study of compounds with cholestatic liability. *Nat Publ Gr* (July):1–12.
23. Gecommentarieerd Geneesmiddelenrepertorium (2018) Available at: http://www.bcfi.be/nl/download [Accessed March 20, 2018].
24. DiPiro JT, Talbert RL, Yee GC, Matzke GR, Wells BG, Posey ML (2014) *Pharmacotherapy: a pathophysiologic approach.* ed Stamford CA& L (McGraw-Hill Medical). 9th Ed.
25. Nicoll LH, Hesby A (2002) Intramuscular injection: an integrative research review and guideline for evidence-based practice. *Appl Nurs Res* 15(3):149–62.

26. Gelders YG (1986) Pharmacology, pharmacokinetics and clinical development of haloperidol decanoate. *Int Clin Psychopharmacol* 1:1–11.
27. Nayak RK, Doose DR, Nair NP (1987) The bioavailability and pharmacokinetics of oral and depot intramuscular haloperidol in schizophrenic patients. *J Clin Pharmacol* 27:144–150.
28. Simon A, de Almeida Borges VR, Cabral LM, de Sousa VP (2013) Development and validation of a discriminative dissolution test for betamethasone sodium phosphate and betamethasone dipropionate intramuscular injectable suspension. *AAPS Pharm Sci Tech* 14(1):425–34.
29. Gray V, Kelly G, Xia M, Butler C, Thomas S, Mayock S (2009) The science of USP 1 and 2 dissolution: present challenges and future relevance. *Pharm Res* 26(6):1289–302.
30. Seidlitz A, Weitschies W (2012) In-vitro dissolution methods for controlled release parenterals and their applicability to drug-eluting stent testing. *J Pharm Pharmacol* 64(7):969–85.
31. Alam A, Ahuja A, Baboota S, Gidwani SK, Ali J (2009) Formulation and evaluation of pharmaceutically equivalent parenteral depot suspension of methyl prednisolone acetate. *Indian J Pharm Sci* 71(1):30–4.
32. Vandenburgh H, Del Tatto M, Shansky J, Lemaire J, Chang A, Payumo F, Lee P, Goodyear A, Raven L (1996) Tissue-engineered skeletal muscle organoids for reversible gene therapy. *Hum Gene Ther* 7(17):2195–2200.
33. Gholobova D, Decroix L, Van Muylder V, Desender L, Gerard M, Carpentier G, Vandenburgh H, Thorrez L (2015) Endothelial Network Formation Within Human Tissue-Engineered Skeletal Muscle. *Tissue Eng Part A* 21(19–20):2548–58.
34. Powell CA, Smiley BL, Mills J, Vandenburgh HH (2002) Mechanical stimulation improves tissue-engineered human skeletal muscle. *Am J Physiol - Cell Physiol* 283(5). Available at: http://ajpcell.physiology.org/content/283/5/C1557 [Accessed May 24, 2017].
35. Vandenburgh, H; Shansky, J; Del Tatto MC (1999) Organogenesis of Skeletal Muscle in Tissue Culture. *Methods Mol Med* 18:217–225.
36. Wang L, Shansky J, Vandenburgh H (2013) Induced formation and maturation of acetylcholine receptor clusters in a defined 3D bio-artificial muscle. *Mol Neurobiol* 48(3):397–403.
37. Vandenburgh H, Shansky J, Benesch-Lee F, Skelly K, Spinazzola JM, Saponjian Y, Tseng BS (2009) Automated drug screening with contractile muscle tissue engineered from dystrophic myoblasts. *FASEB J* 23(10):3325–34.
38. Vandenburgh H, Shansky J, Benesch-Lee F, Barbata V, Reid J, Thorrez L, Valentini R, Crawford G (2008) Drug-screening platform based on the contractility of tissue-engineered muscle. *Muscle Nerve* 37(4):438–47.
39. Thorrez L, Vandenburgh H, Callewaert N, Mertens N, Shansky J, Wang L, Arnout J, Collen D, Chuah M, Vandendriessche T (2006) Angiogenesis enhances factor IX delivery and persistence from retrievable human bioengineered muscle implants. *Mol Ther* 14(3):442–51.
40. Shansky J, Vandenburgh H, Hennessey J, Ferland P, McGuire S, Powell C, DelTatto M, Nackman M (2006) *Tissue Engineering Human Skeletal Muscle for Clinical Applications* ed Gordana Vunjak-Novakovic IF.
41. Decroix L, Van Muylder V, Desender L, Sampaolesi M, Thorrez L (2015) Tissue clearing for confocal imaging of native and bio-artificial skeletal muscle. *Biotech Histochem* 90(6):424–431.
42. Rocha T, de Souza BM, Palma MS, da Cruz-Höfling MA (2007) Myotoxic effects of mastoparan from Polybia paulista (Hymenoptera, Epiponini) wasp venom in mice skeletal muscle. *Toxicon* 50(5):589–99.
43. Rasband W ImageJ.
44. Pfaffl MW, Horgan GW, Dempfle L (2002) Relative expression software tool (REST) for group-wise comparison and statistical analysis of relative expression results in real-time PCR. *Nucleic Acids Res* 30(9):36.
45. Brady MA, Lewis MP, Mudera V (2008) Synergy between myogenic and non-myogenic cells in a 3D tissue-engineered craniofacial skeletal muscle construct. *J Tissue Eng Regen Med* 2:408–417.
46. Carosio S, Barberi L, Rizzuto E, Nicoletti C, Del Prete Z, Musarò A (2013) Generation of eX vivo-vascularized Muscle Engineered Tissue (X-MET). *Sci Rep* 3:1420.
47. Abet V, Filace F, Recio J, Alvarez-Builla J, Burgos C (2017) Prodrug approach: An overview of recent cases. *Eur J Med Chem* 127:810–827.

48. Zamek-gliszczynski MJ, Xiong HAO, Patel NJ, Turncliff RZ, Pollack GM, Brouwer KIMLR (2003) Dichlorofluorescein and Its Diacetate Promoiety in the Liver. *Pharmacology* 304(2):801–809.
49. Dive C, Cox H, Watson J V, Workman P (1988) Polar fluorescein derivatives as improved substrate probes for flow cytoenzymological assay of cellular esterases. *Mol Cell Probes* 2(2):131–45.
50. Murphy MM, Lawson JA, Mathew SJ, Hutcheson DA, Kardon G (2011) Satellite cells, connective tissue fibroblasts and their interactions are crucial for muscle regeneration. *Development* 138(17):3625–3637.
51. Dennis RG, Kosnik PE, Gilbert ME, Faulkner JA (2001) Excitability and contractility of skeletal muscle engineered from primary cultures and cell lines. *Am J Physiol Cell Physiol* 280(2):C288-95.
52. Frontera WR, Ochala J (2015) Skeletal muscle: a brief review of structure and function. *Calcif Tissue Int* 96(3):183–95.
53. Roman W, Gomes ER (2017) Nuclear positioning in skeletal muscle. *Semin Cell Dev Biol*. 54. Chamberlain JS, Jaynes JB, Hauschka SD (1985) Regulation of creatine kinase induction in differentiating mouse myoblasts. *Mol Cell Biol* 5(3):484–92.
55. Zuurveld JG, Wirtz P, Loermans HM, Veerkamp JH (1985) Postnatal growth and differentiation in three hindlimb muscles of the rat. Characterization with biochemical and enzyme-histochemical methods. *Cell Tissue Res* 241(1):183–92.
56. Darville N, van Heerden M, Mariën D, De Meulder M, Rossenu S, Vermeulen A, Vynckier A, De Jonghe S, Sterkens P, Annaert P, Van den Mooter G (2016) The effect of macrophage and angiogenesis inhibition on the drug release and absorption from an intramuscular sustained-release paliperidone palmitate suspension. *J Control Release* 230:95–108.
57. Breeuwer P, Drocourt JL, Bunschoten N, Zwietering MH, Rombouts FM, Abee T (1995) Characterization of uptake and hydrolysis of fluorescein diacetate and carboxyfluorescein diacetate by intracellular esterases in Saccharomyces cerevisiae, which result in accumulation of fluorescent product. *Appl Environ Microbiol* 61(4):1614–9.
58. Sartorelli AC, Hodnick WF, Belcourt MF, Tomasz M, Haffty B, Fischer JJ, Rockwell S (1994) Mitomycin C: a prototype bioreductive agent. *Oncol Res* 6(10–11):501–8.
59. Siegel D, Beall H, Senekowitsch C, Kasai M, Arai H, Gibson NW, Ross D (1992) Bioreductive activation of mitomycin C by DT-diaphorase. *Biochemistry* 31(34):7879–7885.
60. Neve EPA, Köfeler H, Hendriks DFG, Nordling Å, Gogvadze V, Mkrtchian S, Näslund E, Ingelman-Sundberg M (2015) Expression and Function of mARC: Roles in Lipogenesis and Metabolic Activation of Ximelagatran. *PLoS One* 10(9). doi:10.1371/journal.pone.0138487.
61. Chen Y, Jin JY, Mukadam S, Malhi V, Kenny JR (2012) Application of IVIVE and PBPK modeling in prospective prediction of clinical pharmacokinetics: strategy and approach during the drug discovery phase with four case studies. *Biopharm Drug Dispos* 33(2):85–98.
62. Yoon M, Campbell JL, Andersen J, Melvin ME, Clewell H (2012) Quantitative in vitro to in vivo extrapolation of cell-based toxicity assay results. *Crit Rev Toxicol* 42(8):633–652.
63. Pacheco DP, Reis RL, Correlo VM, Marques AP (2015) The Crosstalk between Tissue Engineering and Pharmaceutical Biotechnology: Recent Advances and Future Directions. *Curr Pharm Biotechnol* 16(11):1012–23.
64. Cerino G, Gaudiello E, Grussenmeyer T, Melly L, Massai D, Banfi A, Martin I, Eckstein F, Grapow M, Marsano A (2015) Three dimensional multi-cellular muscle-like tissue engineering in perfusion-based bioreactors. *Biotechnol Bioeng* 113(1). doi:10.1002/bit.25688.
65. Levenberg S, Rouwkema J, Macdonald M, Garfein ES, Kohane DS, Darland DC, Marini R, van Blitterswijk C a, Mulligan RC, D'Amore P a, Langer R (2005) Engineering vascularized skeletal muscle tissue. *Nat Biotechnol* 23(7):879–84.
66. Coupin G, Warter J, Poindron P (2000) Cell Types Required to Efficiently Innervate Human Muscle Cells in Vitro Se. 212:204–212.
67. Cohen LS, Rosenthal JE, Horner DW, Atkins JM, Matthews OA, Sarnoff SJ (1972) Plasma levels of lidocaine after intramuscular administration. *Am J Cardiol* 29(4):520–523.
68. Evans EF, Proctor JD, Fratkin MJ, Velandia J, Wasserman a J (1975) Blood flow in muscle groups and drug absorption. *Clin Pharmacol Ther* 17(1):44–47.

69. Yum K, Hong SG, Healy KE, Lee LP (2014) Physiologically relevant organs on chips. *Biotechnol J* 9(1):16–27.
70. Ito A, Yamamoto Y, Sato M, Ikeda K, Yamamoto M, Fujita H, Nagamori E, Kawabe Y, Kamihira M (2014) Induction of functional tissue-engineered skeletal muscle constructs by defined electrical stimulation. *Sci Rep* 4:4781.
71. Rangarajan S, Madden L, Bursac N (2014) Use of flow, electrical, and mechanical stimulation to promote engineering of striated muscles. *Ann Biomed Eng* 42(7):1391–405.
72. Wickramasinghe SN (1987) Evidence of drug metabolism by macrophages: possible role of macrophages in the pathogenesis of drug-induced tissue damage and in the activation of environmental procarcinogens. *Clin Lab Haematol* 9(3):271–80.
73. Caplin JD, Granados NG, James MR, Montazami R, Hashemi N (2015) Microfluidic Organ-on-a-Chip Technology for Advancement of Drug Development and Toxicology. *Adv Healthc Mater* 4(10):1426–50.

CHAPTER 6

GENERAL DISCUSSION

6.1 Bio-artificial muscle

Skeletal muscle tissue accounts for a great part of the human body and is essential for locomotion, metabolism, respiration and thermoregulation (1, 2). Traumatic injuries, muscle denervation, sarcopenia and muscle ablation upon surgery can cause muscle loss and concomitant loss of function (3). Current treatment strategies have several disadvantages (4, 5), therefore alternatives are being explored such as skeletal muscle tissue engineering (SMTE). Satellite cells and progenitor cells with myogenic properties from different sources have been cultured on natural and synthetic biodegradable scaffolds or hydrogels to create skeletal muscle *in vitro*. A key challenge in SMTE, as well as in tissue engineering in general, is the establishment of an efficient vascularization for constructs, guaranteeing survival and function *in vitro,* but also *in vivo* in transplantation studies.

We have further refined the SMTE approach developed in the Vandenburgh lab, as already published in the context of *ex vivo* gene therapy and drug screening applications (6, 7). To engineer bio-artificial muscle (BAM) isolated satellite cells from human muscle biopsies are expanded, mixed with an extracellular matrix (ECM) hydrogel and cast in a mold with end attachment sites. During the course of one week, the cell-gel mix contracts and detaches from the mold to form a muscle bundle with multinucleated myotubes aligned in the direction of the attachment points (7–9). The use of such a hydrogel allows the cells to migrate, align and self-organize. Obtaining aligned muscle fibers is a key feature of engineering functional skeletal muscle tissue. Alignment allows force transduction upon electrical or mechanical stimulation. Besides the SMTE approach using hydrogels and attachment sites to achieve alignment (10–15), conductive micro-patterned scaffolds can be used to guide the orientation of the myofibers (16–18). However myofibers formed in this way are relatively small and immature resulting in a lack of sufficient contractile force to replace native muscle (6).

Since collagen is the main structural protein of skeletal muscle ECM, collagen type I was previously evaluated as a hydrogel for SMTE (6–8). To further improve myofiber formation in BAMs, collagen gels were often combined with Matrigel, a complex mixture of ECM components and growth factors (6, 8, 19). However, since the main goal of this thesis was to induce construct vascularization, we have evaluated fibrin as ECM in our BAM model. This choice was made because of its pro-angiogenic properties (20). Fibrin hydrogels were evaluated previously in BAM formation and support myogenesis *in vitro* (10, 21), but were not evaluated yet in prevascularization strategies of BAMs. In our BAM setting, fibrin did allow myotube formation as well as endothelial network formation (14). Addition of 10% Matrigel to fibrin

BAMs resulted in longer myofibers, but only in the exterior 20 µm of the BAM as shown in Chapter 3. To obtain myofibers with similar morphology and homogeneous distribution throughout the BAM, an ECM composed of only fibrin was used for further experiments.

Our current approach, similar to other SMTE approaches, results in immature myotubes, as discussed in Chapter 5. Myotube immaturity was demonstrated morphologically by the central location of myotube nuclei and the absence of striation in most of the tissue-engineered myotubes (22). Furthermore, to assess the maturation status of the myotubes in the tissue-engineered constructs expression of different myosin heavy chain isoforms (*MYH1, MYH3, MYH8*) and myogenin (*MYOG*) was determined and compared to expression in mature biopsied human muscle strips. Analysis of isoforms and expression levels showed presence of embryonic-like myotubes in BAMs (21).

In this dissertation, we have used human commercially available and biopsy isolated myoblasts as a myogenic cell source for tissue engineering. Regarding commercially acquired myoblast primary cell lines, we have observed some issues such as a low myogenic potential, low myogenic cell percentages and very high doubling times. Therefore we have used mainly primary myoblast cell lines, isolated in-house by digestion of human post-mortem vastus lateralis muscle. There was a high donor variability regarding the percentage isolated muscle, myogenic potential and proliferative capacity as was shown previously (23). It seemed that these parameters were also dependent on the digestion method used to isolate cells from the biopsy. We evaluated different satellite cell isolation protocols (unpublished data) and found that the collagenase – dispase method (24) provided the highest cell yield and myoblast percentage. An inherent characteristic of using muscle biopsies from deceased donors is high age (all over 60 years), often concomitant with cachexia, which negatively impacts cell yield and myoblast expansion potential. We characterized the isolated cell populations and made selections based on expansion and myogenic potential to ensure cell quality. A younger donor age would likely be beneficial for a prolonged proliferative and myogenic capacity during *in vitro* expansion and upon *in vivo* implantation. In ageing mice models it was shown that in advanced geriatric life stages, satellite cells enter a state of irreversible cell proliferation arrest, called senescence (25). Using muscle cells with long expansion potential is important for both *in vivo* as well as *in vitro* applications, ensuring sufficient cell supply for more high-throughput tests. Moreover, ageing satellite cells have an intrinsic regenerative decline and impaired self-renewal potential *in vivo* (25, 26). Efforts are made to restore the regenerative capacity of aged satellite cells, the so-called rejuvenation process (27). Return to quiescence is essential for satellite cell pool reconstitution after tissue damage. Using satellite cells with a high self-

renewal potential in implantation studies may provide a stem cell source, that can contribute to later regeneration upon injury (28).

Skeletal muscle is not only composed of myofibers but also contains non-myogenic cells such as endothelial cells, neural cells, fibroblasts, pericytes and stromal cells, reviewed in (29). Non-myogenic cells play a critical role in myogenic cell differentiation, force generation and matrix remodeling *in vitro* (30, 31) as well as *in vivo* (29). In Chapter 5, a mixed muscle cell population versus a pure myoblast population was evaluated and compared for myotube formation in BAM. The mixed muscle cell population contained 82% desmin positive myoblasts. Non-myogenic cells contributed to the remaining 18% and were previously reported to be mainly fibroblasts (31, 32). BAMs with a mixed muscle cell population showed a higher myogenic protein expression and creatine kinase content compared to BAMs with only myoblasts. Presence of non-myogenic cells may explain the difference in myotube formation, however the pure myoblast population in BAMs with only myoblasts was derived from a donor with obesity, which is known to affect muscle regeneration (33).

6.1.1 Prevascularization: introducing endothelial cells to the BAM model

In vivo, capillaries surrounding muscle fibers not only play an important role in nutrient and oxygen supply, but also in skeletal muscle regeneration, in particular the endothelial cells surrounding the capillaries (29, 34). To better mimic skeletal muscle and to stimulate perfusion throughout the construct we have explored prevascularization of BAMs. A coculture BAM model containing human muscle cells and HUVECs was developed, the so called coculture BAM. Different medium conditions for coculturing both cell types were evaluated, to ensure an optimal myoblast differentiation and endothelial cell survival. Moreover, different myoblast-HUVEC ratios and total cell numbers were assessed to warrant a BAM construct with well aligned myotubes interspersed with endothelial networks. Coculturing muscle cells with endothelial cells in the BAM model resulted in formation of aligned multinucleated myotubes interspersed by endothelial networks as documented in Chapter 3 and is referred to as the one stage approach in Chapter 4. The soft fibrin hydrogel allowed for migration and self-organization of endothelial cells into vascular networks, a process called vasculogenesis. In 3D cultures, where endothelial networks are seeded adjacent to microchannels and connect with those channels, function of formed networks is evaluated by perfusion of fluorescent microbeads through the microchannels. If the endothelial networks are lumenized, presence of microbeads is observed in those networks (35). Alternatively, the presence of lumina is evaluated on microscopic images by the presence of hollow tubes (34, 36). No clear evidence

of lumen formation *in vitro* was observed in the coculture BAM. *In vivo* functionality of implanted endothelial networks and anastomosis with host vessels is tested by intravenous injection of fluorescent labeled lectins (37) or dextran (38). *In vivo* functionality of endothelial networks in coculture BAM was confirmed at 14 days post-implantation in NODSCID mice by the presence of perfused lectins.

Culturing multiple cell types in an organoid presents its own unique challenges regarding culture conditions. Myofiber formation *in vitro* is triggered by a low serum concentration (11, 39), but culturing endothelial cells usually requires high serum conditions (40, 41). To culture and differentiate muscle cells and endothelial cells together we established a trade-off in myotube formation by culturing both cell types in endothelial cell specific growth medium (EGM). The observed impaired myotube formation in endothelial medium was also described by others (42). Moreover, different total cell numbers and myoblast-HUVEC ratios were assessed to warrant a BAM construct with well aligned myotubes interspersed with endothelial networks. BAMs ,containing 2.10^6 cells, resulted in well aligned and densely packed myofibers compared to the BAMs with a total cell number of 1.10^6. Total cell number also had an effect on endothelial network formation: the number of junctions, meshes, branches and total length increased in 2.10^6 total cell number condition, while number of isolated segments decreased. To further improve prevascularization with minimal loss of myotube formation in the BAM, a two stage tissue-engineering approach was developed and is discussed in Chapter 4. The two stage prevascularized BAM was created by embedding a BAM, cultured for one week in myogenic medium, in a fibrin hydrogel containing endothelial cells and cultured in endothelial growth medium for another one week. The advantage of this procedure is that each cell type could be cultured in its own specialized medium, resulting in better survival and behavior of each cell type. This two stage approach, with sequential use of different culture media strongly improved the myotube and endothelial network formation in the BAM compared to the one stage approach. Also the two stage prevascularization strategy was evaluated *in vivo* in a mouse model and showed lectin perfused endothelial vessels at day 14. The two stage tissue-engineering approach is promising, since myotube maintenance *in vivo* was higher in comparison to non-prevascularized BAMs and the one stage approach.

A way to improve network maturation, stabilization and function of blood vessels is by the addition of pericytes, mesenchymal precursor cells, fibroblasts and/or smooth muscle cells in tissue engineered constructs prior to implantation (35, 43, 44). These cells are often used in coculture settings with endothelial cells due to their capacity to differentiate into supportive mural cells around newly formed endothelial networks. Expression of smooth muscle actin is

characteristic for this differentiation into mural cells (35, 37, 42, 45, 46). Their presence supports *in vitro* and *in vivo* stabilization, endothelial network formation and prevents blood vessel regression (42, 47–51). In our cocultures, fibroblasts were present, but addition of other cell types may further enhance formation and stability of the prevascular network. We have observed a general decrease in myofiber formation after 14 days of implantation in all BAM types. The hypothesis is that insufficient blood supply causes this deterioration. We only have evaluated host vessel ingrowth in non-prevascularized BAMs and observed very little invasion and very high grade of myofiber degradation. No evaluation of host vessel ingrowth has been performed in prevascularized constructs due to limited time and technicalities. It would be of interest to determine in future experiments whether host vessel ingrowth is stimulated in prevascularized BAMS or whether the vessels are derived from the implanted endothelial networks. A way to improve ingrowth of host blood vessels is the incorporation of angiogenic growth factors in the fibrin construct such as VEGF, HGF, PDGF-BB and FGF (52, 53). Incorporation of growth factors in fibrin hydrogel may not only be beneficial for angiogenesis, but also for myogenic regeneration (54). This adjusted fibrin should be evaluated as well *in vitro* on myofiber and endothelial network formation, as *in vivo* on host vessel ingrowth and myogenesis.

Furthermore we have performed the implantation for two weeks only. Towards clinical translation, it will be interesting to monitor long-term outcome of implanted BAMs (55). It will be of interest to assess the contribution of host muscle versus implanted muscle at the site of injury after implantation. In our study, we have performed subcutaneous implantation to evaluate endothelial network functionality. However the ultimate goal is the restoration of a volumetric muscle defect. Therefore the next step is implantation in injured skeletal muscle.

6.1.2 In vitro screening

Tissue engineered skeletal muscle can also be developed for *in vitro* disease models or pre-clinical *in vitro* models for drug screening to complement traditional 2D cell culture and animal models. In comparison to 2D cell cultures, 3D engineered muscle have a prolonged culture duration (11, 56), increased protein content (57) and a more mature myosin heavy chain isoform expression (56). Additionally, 3D muscle constructs allow assessment of electrically or chemically stimulated contractile force generation (6, 11, 56). To increase relevance for pre-clinical drug development, 3D engineered muscle ideally should contain human cells, mimic the structure, function and regenerative capacity of native muscle and be applicable for high throughput screening.

The BAM model has already been described in the context of an *in vitro* disease model and drug screening (6, 15), but has never been implemented in the context of intramuscular (IM) injections. Currently candidate drugs and drug formulations for intramuscular administration are tested using methods for oral drug administration (58, 59), but these models don't reflect the physiology of muscle. To measure compound absorption, distribution and release after intramuscular injection, injectable 3D tissue is needed (21). Therefore, we evaluated the technical feasibility and suitability of using BAMs as a model for intramuscular drug injection. In Chapter 5, several parameters such as compound toxicity, retention, release and metabolism of injected test compounds were evaluated in micro-injected BAMs. We have used human myoblasts in this 3D muscle model to better mimic human muscle physiology. Use of a soft fibrin hydrogel allowed for injection with a micro-syringe and follow-up of injected compounds or their metabolites during several days. Skeletal muscle toxicity was measured by creatine kinase release in the medium, which increased with increasing toxic insult, showing the potential of the model to measure toxicity in a dose-response curve. Using spectrophotometry and measurement of luminescence, we confirmed release of the injected compounds and their metabolized products over 40 hours in contrast to 2D cell culture, showing the capacity of the BAM model to function as a drug depot. Taken together, we have shown that the BAM is an injectable human 3D model able to assess compound toxicity and release profile from muscle-like tissue and is capable of metabolizing the injected compounds. Further improvements are possible to implement the model in drug development pipelines. Firstly as discussed above, myotubes formed in BAM express a mixture of embryonic, neonatal and adult myosin forms. To obtain a model reflecting even better mature muscle tissue, BAMs could benefit from

perfusion, stimulation and addition of other cell types. Also, to be able to assess pharmacokinetics and toxicity of injected compounds in a rapid, reproducible and cost-effective way an automated high-throughput micro-injection set-up should be developed (6, 60). Finally translating *in vitro* obtained data to predict the exposure profiles *in vivo* can be achieved by *in vitro in vivo* extrapolation (IVIVE) linked to physiologically based pharmacokinetic (PBPK) modeling (61). To do so, besides pharmacokinetic data obtained from the BAM model, PBPK modeling requires scaling factors between *in vitro* and *in vivo* tissue and physiological parameters. Furthermore, to validate the IVIVE based PBPK model, pharmacokinetic data of IM injected drugs *in vivo* should be retrospectively paired to data obtained in the BAM model. For example *in vivo* pharmacokinetic data for intramuscular haloperidol decanoate administration could be used (62). Such an analysis could further advance the BAM model as a pre-clinical model for IM drug injection.

6.2 Future perspectives

In the translation to the clinic, tissue-engineered skeletal muscle still faces several challenges: translating results obtained in small animal models to human patients, scaling up the bioartificial muscle and increasing their force-generating capability.

Most SMTE constructs that are being developed are evaluated in small animals to explore their influence on muscle repair. These models are easily available and allow to compare results between different laboratories, but have some limitations in the translation into the clinic (63, 64). In this thesis, we have implanted bio-artificial muscle, developed with human myoblasts and endothelial cells, subcutaneously in immunodeficient NOD/SCID mice, lacking an adequate immune response. In most cases in SMTE research, immunodeficient models are used to bypass xenogeneic rejection and to allow for implant integration and maturation *in vivo* (39, 42, 65–67). Such models are used with the assumption that in subsequent human trials autologous cells and scaffolds could be used to avoid implant rejection (68). An autologous fibrin gel derived from the patient's own blood or already clinically approved fibrin sealants could substitute the current fibrin hydrogel used in our BAM model (69, 70). Another challenge in translating results from small animals into the clinic is related to the conditions present at the site of implantation. In our set-up, with the aim to study *in vivo* vascularization of the skeletal muscle construct, subcutaneous implantation was performed. However, to evaluate suitability of these SMTE constructs for muscle regeneration, implantation in injured skeletal muscle may be more relevant. Several approaches are described in inducing muscle injury and can differentially influence the regenerative outcome (71, 72). Furthermore, skeletal muscle

regeneration varies between rodents and humans (63, 73, 74), posing an extra challenge to extrapolation of results in animals to patients. Also working with immunodeficient animal models blunts the positive effects that a pro-regenerative immune response plays in skeletal muscle repair (75–77).

SMTE strategies of volumetric muscle loss are intrinsically dependent on the dimensions of the lesions to be treated. Injuries in volumetric muscle loss are extensive and require constructs with thicknesses that are currently not possible to engineer with current SMTE approaches. Current BAM size with a thickness of ~1 mm and a length of 2 cm limits the use for volumetric muscle loss repair. In Chapter 4, we have described a two stage approach of engineering a BAM. This approach allows stacking multiple BAM resulting in thicker tissue. Working with hydrogels alone may not be sufficient to withstand the high tensile stress present in human muscle without rupture of the construct (78, 79). Also skeletal muscle constructs should remain under tension to avoid atrophy upon implantation. The presence of engineered tendons that can be sutured in host tissue, resulting in construct tension, can meet this need (80). Therefore use of bioactive scaffolds having the necessary mechanical and elastic properties may provide the necessary support for the tissue-engineered constructs in large defects and provide anchor sites for implantation. Alternatively, a biological tendon can also be generated through tissue engineering (81). Furthermore, fibrin is sensitive to proteolytic degradation and is rapidly broken down *in vivo* as occurs naturally in the wound healing process (82, 83). Combination with a naturally derived scaffold will allow for a phased and ultimately complete degradation of the construct allowing initial support and subsequent ingrowth of host tissue. Additionally, the breakdown products may supply biological signals, further promoting integration of the construct into the host tissue (84–87). In this respect, decellularized extracellular matrices are an attractive source of scaffold and are already used in clinics for orthopaedic, dental and cardiovascular applications and in plastic and reconstructive surgery (88). ECM derived scaffolds have already been demonstrated to stimulate skeletal muscle repair in animal models as well as in patients (65, 67, 89). Nonetheless, concerns regarding decellularization of the materials are still present, as residual traces of cellular material can induce inflammatory reactions following implantation (90, 91). Also a challenge of ECM derived scaffolds, similar to other current SMTE approaches, is the insufficient level of skeletal muscle maturation and subsequent functional recovery following implantation. Engineering thick constructs brings also challenges regarding 3D visualization of tissue. A clearing method was recently developed in our lab to improve the depth of visualization of immunohistochemical stained muscle tissue

(114). However, the use of other scaffold materials may influence the clearing procedure. Also, solid scaffolds may pose technical challenges for sectioning with a microtome or vibratome.

Another important challenge in creating functional skeletal muscle, is innervation of regenerating myofibers. Stimulation of skeletal muscle is important for long-term survival, since denervation results in atrophy and functional loss (92, 93). In SMTE, two different approaches have been evaluated to mimic innervation: electrical stimulation (94, 95) or coculture with neurons or nerve explants (96, 97). Both approaches improve the cytoskeletal organization in the myofibers, but it is only the coculture approach that is able to develop skeletal muscle constructs with functional motor end plates containing nicotinic acetylcholine receptors (nAchRs) clustered on the skeletal muscle sarcolemma. Addition of agrin and laminin to the culture medium can stimulate AchR clustering *in vitro* as well (10). Following denervation of skeletal muscle, newly formed axons that grow into regenerating muscle generally form neuromuscular junctions with the original motor end plates on the muscle fibers (98). Therefore, *in vitro* formation of such clusters in skeletal muscle engineered constructs can be of interest to guide ingrowing axons *in vivo* and was already shown to improve *in vivo* innervation of implanted muscle constructs (99).

Next to the choice of scaffold and cell types, application of external stimuli can also further improve the SMTE construct. Examples thereof are the use of electrical stimulation, shear stress by flow perfusion or applying mechanical stimuli. The main goal is typically advancing myofiber maturity, however vascularization of the 3D bioengineered skeletal muscle may also be positively affected.

Electrical stimulation of SMTE constructs improves myogenic protein content in myofibers, sarcomeric organization and contractile force generation (94, 95, 100). Also enhancement of angiogenesis in electrically stimulated skeletal muscle has been described before (101, 102) and was shown to be mediated by an increased release of VEGF, which is a pro-angiogenic growth factor (103), by muscle fibers (104, 105). VEGF receptor activation resulted in enhanced reorientation, elongation and migration of endothelial cells through the PI3K-Akt and Rho-ROCK signaling pathways (101). These findings suggest electrical stimuli can play a direct role in angiogenesis *in vivo*. A direct effect of electrical stimulation was shown *in vitro* in endothelial cell cultures (101), but this has not yet been demonstrated in SMTE approaches.

For skeletal muscle it is known that exercise induces hypertrophy, whereas a lack of adequate load results in atrophy. Therefore, mechanical stimulation of myofibers *in vitro* is an appealing way to stimulate myofiber maturation in SMTE. In 2D myoblast culture, mechanical stimulation caused myoblasts to fuse into significantly longer myotubes compared to static

culture conditions (106). *In vitro* stimulated engineered skeletal muscle implanted onto the *latissimus dorsi* muscle of mice generated tetanic and twitch contractile responses in contrast to static cultured constructs (107) and shows the potential of mechanical stimulation in SMTE. In addition VEGF production in muscle was also upregulated in response to mechanical stimulation and shows an effect of mechanical stimulation broader than hypertrophy (108). Also endothelial cell activities, such as migration and tube formation, involved in angiogenesis are influenced by cyclic stretch (109–111). The importance of mechanical stimulation in vascular endothelial cell patterning and sprout formation has also been demonstrated *in vitro* for both 2D and 3D culture systems in which mechanical strain was found to regulate the spatial location of cell proliferation and the directionality of the sprout formation respectively (109). Identifying the biophysical aspects of angiogenesis regulation is therefore crucial to advance vascularization of tissue engineered products.

Fluidic flow and associated shear stress are known to be important in vasculogenesis (112–114), remodelling of immature vessels (115) and maintenance of blood vessels. Differences in blood flow in a branch point are suggested to play a role in blood vessel pruning (116). Also flow was suggested to be a regulator of arterial-venous differentiation in chick embryo yolk sac (117). One way to induce fluidic flow in an engineered construct *in vitro* is by using a bioreactor. It was demonstrated that bioreactors promote the viability and long-term maintenance of skeletal muscle precursor cells *in vitro* seeded and cultured on 3D porous collagen sponges (118). However skeletal muscle is shear-sensitive and high shear stress may therefore affect viability negatively (119). The equilibrium between a beneficial and a detrimental shear stress still needs to be thoroughly explored.

6.3 Conclusion

In conclusion, the research in this dissertation describes the characterization and optimization of tissue-engineered human skeletal muscle tissue. More specifically, we evaluated approaches for prevascularization. The skeletal muscle tissue engineering approach we used as a starting point allowed formation of multinucleated myotubes aligned in the direction of the passive tension. To further expand the 3D muscle tissue two prevascularization strategies were developed to introduce vascular networks *in vitro*. *In vivo* these vascular networks proved to be functional and showed anastomosis with host vessels. In addition we have discussed how prevascularization in turn influences the survival and integration of a tissue-engineered construct *in vivo*. Furthermore, we have shown that the BAM is an adequate pre-clinical model for intramuscular drug injections, allowing to assess compound toxicity, retention, release and

metabolization. To further translate the BAM model to clinical applications for regenerative medicine or towards drug testing assays, several challenges and opportunities need to be addressed.

6.4 References

1. Prothero JW (2015) Musculoskeletal system. *The Design of Mammals*, pp 142–156.
2. Frontera WR, Ochala J (2015) Skeletal muscle: a brief review of structure and function. *Calcif Tissue Int* 96(3):183–95.
3. Ostrovidov S, Hosseini V, Ahadian S, Fujie T, Parthiban SP, Ramalingam M, Bae H, Kaji H, Khademhosseini A (2014) Skeletal Muscle Tissue Engineering: Methods to Form Skeletal Myotubes and Their Applications. *Tissue Eng Part B Rev* 20(5):403–436.
4. Lee KT, Mun GH (2014) A Systematic Review of Functional Donor-Site Morbidity after Latissimus Dorsi Muscle Transfer. *Plast Reconstr Surg* 134(2):303–314.
5. Tabebordbar M, Wang ET, Wagers AJ (2013) Skeletal Muscle Degenerative Diseases and Strategies for Therapeutic Muscle Repair. *Annu Rev Pathol Mech Dis* 8(1):441–475.
6. Vandenburgh H, Shansky J, Benesch-Lee F, Barbata V, Reid J, Thorrez L, Valentini R, Crawford G (2008) Drug-screening platform based on the contractility of tissue-engineered muscle. *Muscle Nerve* 37(4):438–47.
7. Thorrez L, Vandenburgh H, Callewaert N, Mertens N, Shansky J, Wang L, Arnout J, Collen D, Chuah M, Vandendriessche T (2006) Angiogenesis enhances factor IX delivery and persistence from retrievable human bioengineered muscle implants. *Mol Ther* 14(3):442–51.
8. Powell CA, Smiley BL, Mills J, Vandenburgh HH (2002) Mechanical stimulation improves tissue-engineered human skeletal muscle. *Am J Physiol Cell Physiol* 283(5):1557–1565.
9. Thorrez L, DiSano K, Shansky J, Vandenburgh H (2018) Engineering of human skeletal muscle with an autologous deposited extracellular matrix. *Front Physiol* 9(Aug):1–11.
10. Wang L, Shansky J, Vandenburgh H (2013) Induced formation and maturation of acetylcholine receptor clusters in a defined 3D bio-artificial muscle. *Mol Neurobiol* 48(3):397–403.
11. Madden L, Juhas M, Kraus WE, Truskey GA, Bursac N (2015) Bioengineered human myobundles mimic clinical responses of skeletal muscle to drugs. *Elife* 4:1–14.
12. Martin NRW, Passey SL, Player DJ, Khodabukus A, Ferguson R a, Sharples AP, Mudera V, Baar K, Lewis MP (2013) Factors affecting the structure and maturation of human tissue engineered skeletal muscle. *Biomaterials* 34(23):5759–65.
13. Heher P, Maleiner B, Prüller J, Teuschl AH, Kollmitzer J, Monforte X, Wolbank S, Redl H, Rünzler D, Fuchs C (2015) A novel bioreactor for the generation of highly aligned 3D skeletal muscle-like constructs through orientation of fibrin via application of static strain. *Acta Biomater* 24:251–265.
14. Gholobova D, Decroix L, Van Muylder V, Desender L, Gerard M, Carpentier G, Vandenburgh H, Thorrez L (2015) Endothelial Network Formation Within Human Tissue-Engineered Skeletal Muscle. *Tissue Eng Part A* 21(19–20):2548–2558.
15. Vandenburgh H, Shansky J, Benesch-Lee F, Skelly K, Spinazzola JM, Saponjian Y, Tseng BS (2009) Automated drug screening with contractile muscle tissue engineered from dystrophic myoblasts. *FASEB J* 23(10):3325–34.
16. Chen S, Nakamoto T, Kawazoe N, Chen G (2015) Engineering multi-layered skeletal muscle tissue by using 3D microgrooved collagen scaffolds. *Biomaterials* 73:23–31.
17. Sun Y, Duffy R, Lee A, Feinberg AW (2013) Optimizing the structure and contractility of engineered skeletal muscle thin films. *Acta Biomater* 9:7885–7894.
18. Takahashi H, Shimizu T, Nakayama M, Yamato M, Okano T (2013) The use of anisotropic cell sheets to control orientation during the self-organization of 3D muscle tissue. *Biomaterials* 34(30):7372–80.
19. Hinds S, Bian W, Dennis RG, Bursac N (2011) The role of extracellular matrix composition in structure and function of bioengineered skeletal muscle. *Biomaterials* 32(14):3575–83.
20. Morin KT, Tranquillo RT (2013) In vitro models of angiogenesis and vasculogenesis in fibrin gel. *Exp Cell Res* 319(16):2409–17.
21. Gholobova D, Gerard M, Decroix L, Desender L, Callewaert N, Annaert P, Thorrez L (2018) Human tissue-engineered skeletal muscle: a novel 3D in vitro model for drug disposition and toxicity after intramuscular injection. *Sci Rep* 8(1):12206.
22. Roman W, Gomes ER (2018) Nuclear positioning in skeletal muscle. *Semin Cell Dev Biol* 82:51–56.

23. Scott IC, Tomlinson W, Walding A, Isherwood B, Dougall IG (2013) Large-scale isolation of human skeletal muscle satellite cells from post-mortem tissue and development of quantitative assays to evaluate modulators of myogenesis. 4:157–169.
24. Gholobova D, Gerard M, Terrie L, Desender L, Shansky J, Vandenburgh H, Thorrez L (2019) Coculture Method to Obtain Endothelial Networks Within Human Tissue-Engineered Skeletal Muscle. *Methods in Molecular Biology (Clifton, N.J.)*, pp 169–183.
25. Sousa-Victor P, et al. (2014) Geriatric muscle stem cells switch reversible quiescence into senescence. *Nature* 506(7488):316–321.
26. García-Prat L, et al. (2016) Autophagy maintains stemness by preventing senescence. *Nature* 529(7584):37–42.
27. Bengal E, Perdiguero E, Serrano AL, Muñoz-cánoves P (2017) Rejuvenating stem cells to restore muscle regeneration in aging. *F1000Research* 6:1–10.
28. Collins CA, Olsen I, Zammit PS, Heslop L, Petrie A, Partridge TA, Morgan JE (2005) Stem cell function, self-renewal, and behavioral heterogeneity of cells from the adult muscle satellite cell niche. *Cell* 122(2):289–301.
29. Ceafalan LC, Popescu BO, Hinescu ME (2014) Cellular Players in Skeletal Muscle Regeneration. *Biomed Res Int* 2014:1–21.
30. Dennis RG, Kosnik PE, Gilbert ME, Faulkner JA (2001) Excitability and contractility of skeletal muscle engineered from primary cultures and cell lines. *Am J Physiol Physiol* 280(2):C288–C295.
31. Brady MA, Lewis MP, Mudera V (2008) Synergy between myogenic and non-myogenic cells in a 3D tissue-engineered craniofacial skeletal muscle construct. *J Tissue Eng Regen Med* 2:408–417.
32. Carosio S, Barberi L, Rizzuto E, Nicoletti C, Del Prete Z, Musarò A (2013) Generation of eX vivo-vascularized Muscle Engineered Tissue (X-MET). *Sci Rep* 3:1420.
33. Akhmedov D, Berdeaux R (2013) The effects of obesity on skeletal muscle regeneration. *Front Physiol* 4(Dec):1–12.
34. Osaki T, Sivathanu V, Kamm RD (2018) Crosstalk between developing vasculature and optogenetically engineered skeletal muscle improves muscle contraction and angiogenesis. *Biomaterials* 156:65–76.
35. Jeon JS, Bersini S, Whisler J a, Chen MB, Dubini G, Charest JL, Moretti M, Kamm RD (2014) Generation of 3D functional microvascular networks with human mesenchymal stem cells in microfluidic systems. *Integr Biol (Camb)* 6(5):555–63.
36. Tiruvannamalai Annamalai R, Rioja AY, Putnam AJ, Stegemann JP (2016) Vascular Network Formation by Human Microvascular Endothelial Cells in Modular Fibrin Microtissues. *ACS Biomater Sci Eng* 2(11):1914–1925.
37. Shandalov Y, Egozi D, Koffler J, Dado-Rosenfeld D, Ben-Shimol D, Freiman A, Shor E, Kabala A, Levenberg S (2014) An engineered muscle flap for reconstruction of large soft tissue defects. *Proc Natl Acad Sci U S A* 111(16):6010–6015.
38. Rosenfeld D, Landau S, Shandalov Y, Raindel N, Freiman A, Shor E, Blinder Y, Vandenburgh HH, Mooney DJ, Levenberg S (2016) Morphogenesis of 3D vascular networks is regulated by tensile forces. *Proc Natl Acad Sci* 113(12):201522273.
39. Juhas M, Engelmayr GC, Fontanella AN, Palmer GM, Bursac N (2014) Biomimetic engineered muscle with capacity for vascular integration and functional maturation in vivo. *Proc Natl Acad Sci U S A* 111(15):1–6.
40. Terramani T, Eton D, Bui PA, Wang Y, Weaver F, Yu H (2000) Human macrovascular endothelial cells: optimization of culture conditions. *Vitr Cell Dev Biol - Anim* 36(2):125.
41. Relou IAM, Damen CA, Van Der Schaft DWJ, Groenewegen G, Griffioen AW (1998) Effect of culture conditions on endothelial cell growth and responsiveness. *Tissue Cell* 30(5):525–530.
42. Levenberg S, Rouwkema J, Macdonald M, Garfein ESS, Kohane DSS, Darland DCC, Marini R, Van Blitterswijk CAA, Mulligan RCC, D'Amore PAA, Langer R (2005) Engineering vascularized skeletal muscle tissue. *Nat Biotechnol* 23(7):879–84.
43. Sacharidou A, Stratman AN, Davis GE (2011) Molecular mechanisms controlling vascular lumen formation in three-dimensional extracellular matrices. *Cells Tissues Organs* 195(1–2):122–143.

44. Gökçinar-Yagci B, Uçkan-Çetinkaya D, Çelebi-Saltik B (2015) Pericytes: Properties, Functions and Applications in Tissue Engineering. *Stem Cell Rev Reports* 11(4):549–559.
45. Ding R, Darland DC, Parmacek MS, D'amore PA (2004) Endothelial–Mesenchymal Interactions In Vitro Reveal Molecular Mechanisms of Smooth Muscle/Pericyte Differentiation. *Stem Cells Dev* 13(5):509–520.
46. Lesman A, Koffler J, Atlas R, Blinder YJ, Kam Z, Levenberg S (2011) Engineering vessel-like networks within multicellular fibrin-based constructs. *Biomaterials* 32:7856–7869.
47. Stratman AN, Malotte KM, Mahan RD, Davis MJ, Davis GE (2009) Pericyte recruitment during vasculogenic tube assembly stimulates endothelial basement membrane matrix formation. *Blood* 114(24):5091–101.
48. Newman AC, Nakatsu MN, Chou W, Gershon PD, Hughes CCW (2011) The requirement for fibroblasts in angiogenesis: fibroblast-derived matrix proteins are essential for endothelial cell lumen formation. *Mol Biol Cell* 22:3791–3800.
49. Nakatsu MN, Sainson RCA, Aoto JN, Taylor KL, Aitkenhead M, Pérez-del-Pulgar S, Carpenter PM, Hughes CCW (2003) Angiogenic sprouting and capillary lumen formation modeled by human umbilical vein endothelial cells (HUVEC) in fibrin gels: the role of fibroblasts and Angiopoietin-1. *Microvasc Res* 66(2):102–12.
50. Alekseeva T, Unger RE, Brochhausen C, Brown RD, Kirkpatrick JC (2013) Engineering a micro-vascular capillary bed in a tissue-like collagen construct. *Tissue Eng Part A*:1–36.
51. Blinder YJ, Freiman A, Raindel N, Mooney DJ, Levenberg S (2016) Vasculogenic dynamics in 3D engineered tissue constructs. *Sci Rep* 5(1):17840.
52. Martino MM, et al. (2015) Extracellular Matrix and Growth Factor Engineering for Controlled Angiogenesis in Regenerative Medicine. *Front Bioeng Biotechnol* 3:45.
53. Bach AD, Arkudas A, Tjiawi J, Polykandriotis E, Kneser U, Horch RE, Beier JP (2006) A new approach to tissue engineering of vascularized skeletal muscle. *J Cell Mol Med* 10(3):716–726.
54. Grasman JM, Do DM, Page RL, Pins GD (2015) Rapid release of growth factors regenerates force output in volumetric muscle loss injuries. *Biomaterials* 72:49–60.
55. Sicari BM, et al. (2014) An Acellular Biologic Scaffold Promotes Skeletal Muscle Formation in Mice and Humans with Volumetric Muscle Loss. *Sci Transl Med* 6(234):234ra58.
56. Rao L, Qian Y, Khodabukus A, Ribar T, Bursac N (2018) Engineering human pluripotent stem cells into a functional skeletal muscle tissue. *Nat Commun* 9(1):126.
57. Vandenburgh HH, Karlisch P, Farr L (1988) Maintenance of highly contractile tissue-cultured avian skeletal myotubes in collagen gel. *In Vitro Cell Dev Biol* 24(3):166–74.
58. Simon A, de Almeida Borges VR, Cabral LM, de Sousa VP (2013) Development and validation of a discriminative dissolution test for betamethasone sodium phosphate and betamethasone dipropionate intramuscular injectable suspension. *AAPS Pharm Sci Tech* 14(1):425–34.
59. Seidlitz A, Weitschies W (2012) In-vitro dissolution methods for controlled release parenterals and their applicability to drug-eluting stent testing. *J Pharm Pharmacol* 64(7):969–85.
60. Vandenburgh H (2010) High-content drug screening with engineered musculoskeletal tissues. *Tissue Eng Part B Rev* 16(1):55–64.
61. Chen Y, Jin JY, Mukadam S, Malhi V, Kenny JR (2012) Application of IVIVE and PBPK modeling in prospective prediction of clinical pharmacokinetics: strategy and approach during the drug discovery phase with four case studies. *Biopharm Drug Dispos* 33(2):85–98.
62. Nayak RK, Doose DR, Nair NP (1987) The bioavailability and pharmacokinetics of oral and depot intramuscular haloperidol in schizophrenic patients. *J Clin Pharmacol* 27(2):144–150.
63. Bareja A, Holt JA, Luo G, Chang C, Lin J, Hinken AC, Freudenberg JM, Kraus WE, Evans WJ, Billin AN (2014) Human and Mouse Skeletal Muscle Stem Cells: Convergent and Divergent Mechanisms of Myogenesis. *PLoS One* 9(2):e90398.
64. Seok J, et al. (2013) Genomic responses in mouse models poorly mimic human inflammatory diseases. *Proc Natl Acad Sci* 110(9):3507–3512.
65. Koffler J, Kaufman-Francis K, Yulia S, Dana E, Daria AP, Landesberg A, Levenberg S (2011) Improved vascular organization enhances functional integration of engineered skeletal muscle grafts. *Proc Natl Acad Sci U S A* 108(36):14789–94.
66. Haraguchi Y, Shimizu T, Sasagawa T, Sekine H, Sakaguchi K, Kikuchi T, Sekine W, Sekiya S, Yamato M, Umezu M, Okano T (2012) Fabrication of functional three-dimensional tissues by

stacking cell sheets in vitro. *Nat Protoc* 7(5):850–858.
67. Criswell TL, Corona BT, Wang Z, Zhou Y, Niu G, Xu Y, Christ GJ, Soker S (2013) The role of endothelial cells in myofiber differentiation and the vascularization and innervation of bioengineered muscle tissue in vivo. *Biomaterials* 34(1):140–149.
68. Kazmi B, Inglefield CJ, Lewis MP (2009) Autologous cell therapy: current treatments and future prospects . *Wounds a Compend Clin Res Pract* 21(9):234–42.
69. Dietrich M, Heselhaus J, Wozniak J, Weinandy S, Mela P, Tschoeke B, Schmitz-Rode T, Jockenhoevel S (2013) Fibrin-based tissue engineering: comparison of different methods of autologous fibrinogen isolation. *Tissue Eng Part C Methods* 19(3):216–26.
70. Spotnitz WD (2014) Fibrin Sealant: The Only Approved Hemostat, Sealant, and Adhesive—a Laboratory and Clinical Perspective. *ISRN Surg* 2014:1–28.
71. Pereira T, et al. (2013) Biomaterials and Stem Cell Therapies for Injuries Associated to Skeletal Muscular Tissues. *Advances in Biomaterials Science and Biomedical Applications* (InTech), p 64.
72. Hardy D, et al. (2016) Comparative Study of Injury Models for Studying Muscle Regeneration in Mice. *PLoS One* 11(1):e0147198.
73. Borisov AB (1999) Regeneration of skeletal and cardiac muscle in mammals: Do nonprimate models resemble human pathology? *Wound Repair Regen* 7(1):26–35.
74. Khodabukus A, Prabhu N, Wang J, Bursac N (2018) In Vitro Tissue-Engineered Skeletal Muscle Models for Studying Muscle Physiology and Disease. *Adv Healthc Mater* 1701498:1–20.
75. Sadtler K, et al. (2016) Developing a pro-regenerative biomaterial scaffold microenvironment requires T helper 2 cells. *Science (80-)* 352(6283):366–370.
76. Juhas M, Abutaleb N, Wang JT, Ye J, Shaikh Z, Sriworarat C, Qian Y, Bursac N (2018) Incorporation of macrophages into engineered skeletal muscle enables enhanced muscle regeneration. *Nat Biomed Eng* 2(12):942–954.
77. Laumonier T, Menetrey J (2016) Muscle injuries and strategies for improving their repair. *J Exp Orthop* 3(1):15.
78. Garrett WE (1996) Muscle strain injuries. *Am J Sport Med* 24(24):S2–S8.
79. Weaver DS (2000) Skeletal tissue mechanics. *Am J Phys Anthropol* 112(3):435–436.
80. Larkin LM, Calve S, Kostrominova TY, Arruda EM (2006) Structure and functional evaluation of tendon-skeletal muscle constructs engineered in vitro. *Tissue Eng* 12(11):3149–3158.
81. Moshiri A, Oryan A (2012) Role of tissue engineering in tendon reconstructive surgery and regenerative medicine: Current concepts, approaches and concerns. *Hard Tissue* 1(2):1–11.
82. Wolbank S, Pichler V, Crawford JF, Meinl A, van Griensven M, Goppelt A, Redl H (2015) Non-invasive in vivo tracking of fibrin degradation by fluorescence imaging. *J Tissue Eng Regen Med* 9:973–976.
83. Lorentz KM, Kontos S, Frey P, Hubbell JA (2011) Engineered aprotinin for improved stability of fibrin biomaterials. *Biomaterials* 32(2):430–438.
84. Vorotnikova E, et al. (2010) Extracellular matrix-derived products modulate endothelial and progenitor cell migration and proliferation in vitro and stimulate regenerative healing in vivo. *Matrix Biol* 29(8):690–700.
85. Conconi MT, Coppi P De, Bellini S, Zara G, Sabatti M, Marzaro M, Franco Zanon G, Gamba PG, Parnigotto PP, Nussdorfer GG (2005) Homologous muscle acellular matrix seeded with autologous myoblasts as a tissue-engineering approach to abdominal wall-defect repair. *Biomaterials* 26(15):2567–2574.
86. Badylak SF, Kropp B, McPherson T, Liang H, Snyder PW (1998) Small Intestinal Submucosa: A Rapidly Resorbed Bioscaffold for Augmentation Cystoplasty in a Dog Model. *Tissue Eng* 4(4):379–387.
87. Sicari BM, et al. (2014) An Acellular Biologic Scaffold Promotes Skeletal Muscle Formation in Mice and Humans with Volumetric Muscle Loss. *Sci Transl Med* 6(234):234ra58.
88. Parmaksiz M, Dogan A, Odabas S, Elçin AE, Elçin YM (2016) Clinical applications of decellularized extracellular matrices for tissue engineering and regenerative medicine. *Biomed Mater* 11(2):022003.

89. Corona BT, Ward CL, Baker HB, Walters TJ, Christ GJ (2014) Implantation of In Vitro Tissue Engineered Muscle Repair Constructs and Bladder Acellular Matrices Partially Restore In Vivo Skeletal Muscle Function in a Rat Model of Volumetric Muscle Loss Injury. *Tissue Eng Part A* 20(3–4):705–715.
90. Keane TJ, Londono R, Turner NJ, Badylak SF (2012) Consequences of ineffective decellularization of biologic scaffolds on the host response. *Biomaterials* 33(6):1771–1781.
91. Zheng MH, Chen J, Kirilak Y, Willers C, Xu J, Wood D (2005) Porcine small intestine submucosa (SIS) is not an acellular collagenous matrix and contains porcine DNA: Possible implications in human implantation. *J Biomed Mater Res - Part B Appl Biomater* 73(1):61–67.
92. Carlson BM (2014) The biology of long-term denervated skeletal muscle. *Eur J Transl Myol* 24(1):5–11.
93. Boncompagni S, Kern H, Rossini K, Hofer C, Mayr W, Carraro U, Protasi F (2007) Structural differentiation of skeletal muscle fibers in the absence of innervation in humans. *Proc Natl Acad Sci U S A* 104(49):19339–44.
94. Donnelly K, Khodabukus A, Philp A, Deldicque L, Dennis RG, Baar K (2010) A Novel Bioreactor for Stimulating Skeletal Muscle In Vitro. *Tissue Eng Part C Methods* 16(4):711–718.
95. Ikeda K, Ito A, Sato M, Kawabe Y, Kamihira M (2016) Improved contractile force generation of tissue-engineered skeletal muscle constructs by IGF-I and Bcl-2 gene transfer with electrical pulse stimulation. *Regen Ther* 3:38–44.
96. Larkin LM, Van der Meulen JH, Dennis RG, Kennedy JB (2007) Functional evaluation of nerve-skeletal muscle constructs engineered in vitro. *In Vitro Cell Dev Biol Anim* 42(3–4):75–82.
97. Martin NRW, Passey SL, Player DJ, Mudera V, Baar K, Greensmith L, Lewis MP (2015) Neuromuscular Junction Formation in Tissue-Engineered Skeletal Muscle Augments Contractile Function and Improves Cytoskeletal Organization. *Tissue Eng Part A* 21(19–20):2595–2604.
98. Bodine-Fowler S (1994) Skeletal muscle regeneration after injury: An overview. *J Voice* 8(1):53–62.
99. Ko IK, Lee BK, Lee SJ, Andersson KE, Atala A, Yoo JJ (2013) The effect of in vitro formation of acetylcholine receptor (AChR) clusters in engineered muscle fibers on subsequent innervation of constructs in vivo. *Biomaterials* 34(13):3246–3255.
100. Langelaan MLP, Boonen KJM, Rosaria-Chak KY, Van der Schaft DWJ, Post MJ, Baaijens FPT (2011) Advanced maturation by electrical stimulation: Differences in response between C2C12 and primary muscle progenitor cells. *J Tissue Eng Regen Med* 5(7):529–539.
101. Zhao M (2003) Electrical stimulation directly induces pre-angiogenic responses in vascular endothelial cells by signaling through VEGF receptors. *J Cell Sci* 117(3):397–405.
102. Milkiewicz M, Hudlicka O, Brown MD, Silgram H (2005) Nitric oxide, VEGF, and VEGFR-2: interactions in activity-induced angiogenesis in rat skeletal muscle. *Am J Physiol Heart Circ Physiol* 289(1):H336-43.
103. Carmeliet P, Jain RK (2011) Molecular mechanisms and clinical applications of angiogenesis. *Nature* 473(7347):298–307.
104. Amaral SL, Linderman R, Morse MM, Greene AS (2001) Angiogenesis induced by electrical stimulation is mediated by angiotensin II and VEGF. *Microcirculation* 8(1):57–67.
105. Hang J, Kong L, Gu JW, Adair TH (1995) VEGF gene expression is upregulated in electrically stimulated rat skeletal muscle (Rapid Communication). *AmerJ Physiol-HeartCircPhy* 38:H1827–H1831.
106. Vandenburgh HH, Karlisch P (1989) Longitudinal growth of skeletal myotubes in vitro in a new horizontal mechanical cell stimulator. *In Vitro Cell Dev Biol* 25(7):607–16.
107. Moon DG, Christ G, Stitzel JD, Atala A, Yoo JJ (2008) Cyclic Mechanical Preconditioning Improves Engineered Muscle Contraction. *Tissue Eng Part A* 14(4):473–482.
108. Van der Schaft DW, Van Spreeuwel AC, Van Assen HC, Baaijens FP (2011) Mechanoregulation of Vascularization in Aligned Tissue-Engineered Muscle: A Role for Vascular Endothelial Growth Factor. *Tissue Eng Part A* 17(21–22):2857–2865.
109. Matsumoto T, Yung YC, Fischbach C, Kong HJ, Nakaoka R, Mooney DJ (2007) Mechanical Strain Regulates Endothelial Cell Patterning In Vitro. *Tissue Eng* 13(1):207–217.

110. Kou B, Zhang J, Singer DRJ (2009) Effects of cyclic strain on endothelial cell apoptosis and tubulogenesis are dependent on ROS production via NAD(P)H subunit p22phox. *Microvasc Res* 77(2):125–133.
111. Von Offenberg Sweeney N, Cummins PM, Cotter EJ, Fitzpatrick PA, Birney YA, Redmond EM, Cahill PA (2005) Cyclic strain-mediated regulation of vascular endothelial cell migration and tube formation. *Biochem Biophys Res Commun* 329(2):573–582.
112. Yu F, Li R, Jen N, Chi N, Lien C-L, Hsiai T (2013) Canonical Wnt/β-catenin Signaling Pathway mediates Shear Stress-Activated Angiopoeitin-2 expression and vasculogenesis. *FASEB J* 27:526.6.
113. Li R, et al. (2014) Shear Stress-Activated Wnt-Angiopoietin-2 Signaling Recapitulates Vascular Repair in Zebrafish Embryos. *Arterioscler Thromb Vasc Biol* 34(10):2268–2275.
114. Obi S, Masuda H, Shizuno T, Sato A, Yamamoto K, Ando J, Abe Y, Asahara T (2012) Fluid shear stress induces differentiation of circulating phenotype endothelial progenitor cells. *AJP Cell Physiol* 303(6):C595–C606.
115. Lucitti JL, Jones EA V., Huang C, Chen J, Fraser SE, Dickinson ME (2007) Vascular remodeling of the mouse yolk sac requires hemodynamic force. *Development* 134(18):3317–3326.
116. Kochhan E, Lenard A, Ellertsdottir E, Herwig L, Affolter M, Belting H-G, Siekmann AF (2013) Blood Flow Changes Coincide with Cellular Rearrangements during Blood Vessel Pruning in Zebrafish Embryos. *PLoS One* 8(10):e75060.
117. le Noble F (2003) Flow regulates arterial-venous differentiation in the chick embryo yolk sac. *Development* 131(2):361–375.
118. Cimetta E, Flaibani M, Mella M, Serena E, Boldrin L, De Coppi P, Elvassore N (2007) Enhancement of Viability of Muscle Precursor Cells on 3D Scaffold in a Perfusion Bioreactor. *Int J Artif Organs* 30(5):415–428.
119. Rangarajan S, Madden L, Bursac N (2014) Use of Flow, Electrical, and Mechanical Stimulation to Promote Engineering of Striated Muscles. *Ann Biomed Eng* 42(7):1391–1405.

APPENDIX

Author affiliations

Annaert Pieter

- Drug Delivery and Disposition, Department of Pharmaceutical and Pharmacological Sciences, KU Leuven, Leuven, Belgium

Callewaert Nico

- AZ Groeninge, Kortrijk, Belgium

Carpentier Gilles

- Laboratoire de Recherche sur la Croissance Cellulaire, la Réparation et la Régénération Tissulaires (CRRET), Faculté des Sciences et Technologie, Université Paris-Est, France

Decroix Lieselot

- Faculty of Physical Education and Physiotherapy, Department of Human Physiology and Sportsmedicine, Brussels, Belgium

Deprest Jan

- Centre for Surgical Technologies, Group Biomedical Sciences, KU Leuven, Leuven, Belgium
- Department of Development and Regeneration, Woman and Child, Group Biomedical Sciences, KU Leuven, Leuven, Belgium
- Pelvic Floor Unit, University Hospitals KU Leuven, Leuven, Belgium

Desender Linda

- Tissue Engineering Lab, Department of Development and Regeneration, KU Leuven, Kortrijk, Belgium

Gerard Melanie

- Tissue Engineering Lab, Department of Development and Regeneration, KU Leuven, Kortrijk, Belgium

Gholobova Dacha

- Tissue Engineering Lab, Department of Development and Regeneration, KU Leuven, Kortrijk, Belgium

Hympanova Lucie

- Centre for Surgical Technologies, Group Biomedical Sciences, KU Leuven, Leuven, Belgium
- Department of Development and Regeneration, Woman and Child, Group Biomedical Sciences, KU Leuven, Leuven, Belgium
- Pelvic Floor Unit, University Hospitals KU Leuven, Leuven, Belgium
- Institute for the Care of Mother and Child, Third Faculty of Medicine, Charles University, Prague, Czech Republic

-

Mackova Katerina

- Centre for Surgical Technologies, Group Biomedical Sciences, KU Leuven, Leuven, Belgium
- Department of Development and Regeneration, Woman and Child, Group Biomedical Sciences, KU Leuven, Leuven, Belgium
- Pelvic Floor Unit, University Hospitals KU Leuven, Leuven, Belgium
- Institute for the Care of Mother and Child, Third Faculty of Medicine, Charles University, Prague, Czech Republic

Terrie Lisanne

- Tissue Engineering Lab, Department of Development and Regeneration, KU Leuven, Kortrijk, Belgium

Thorrez Lieven

- Tissue Engineering Lab, Department of Development and Regeneration, KU Leuven, Kortrijk, Belgium

Van Muylder Vicky

- Tissue Engineering Lab, Department of Development and Regeneration, KU Leuven, Kortrijk, Belgium

Vandenburgh Herman

- Department of Pathology and Laboratory Medicine, Brown University, Providence, USA

Biography

Dacha Gholobova werd geboren op 4 maart 1992 te Chelkino, Oekraïne. In 1999 verhuisde zij samen met haar broer en ouders naar België. In 2009 behaalde zij haar diploma Algemeen Secundair Onderwijs (ASO) in de afstudeerrichting Latijn-Wiskunde aan de Instituut van Gent school te Gent. Vervolgens startte zij haar opleiding Biomedische Wetenschappen aan de Universiteit van Gent, waar zij in 2012 haar diploma bachelor in de Biomedische Wetenschappen behaalde. Aansluitend behaalde zij haar diploma master in de Biomedische Wetenschappen (specialiteit Degeneratie & Regeneratie) in 2014. Haar eindwerk, getiteld "De rol van c-Myb in de embryonale hematopoëtische ontwikkeling" werd uitgevoerd aan het departement van klinische chemie, microbiologie en immunologie in de groep van Prof. Dr. Bart Vandekerckhove. In oktober startte zij haar doctoraat aan de KU Leuven, campus Kortrijk, in de groep van Prof. Dr. Lieven Thorrez, Weefselengineering Laboratorium. Gedurende deze periode van 4,5 jaar verrichtte zij haar onderzoek naar het ontwikkelen van een humaan bio-artificieel spierconstruct.

Bibliography

Publications

- Gholobova D*, Decroix L*, Van Mulyder V, Desender L, Gerard M, Carpentier G, Vandenburgh H, Thorrez L (2015) Endothelial network formation within human tissue-engineered skeletal muscle. *Tissue Eng Part A. 2015 Oct;21(19-20):2548-58.*
  * equally contributing authors

- Gholobova D*, Gerard M*, Decroix L, Desender L, Callewaert N, Annaert P, Thorrez L (2018) Human tissue-engineered skeletal muscle: a novel 3D in vitro model for drug disposition and toxicity after intramuscular injection. *Sci Rep. 2018 Aug 15;8(1):12206.*
  * equally contributing authors

- Gholobova D, Gerard M, Terrie L, Desender L, Shansky J, Vandenburgh H, Thorrez L (2019) Coculture Method to Obtain Endothelial Networks Within Human Tissue-Engineered Skeletal Muscle. *Methods Mol Biol. 1889:169-183.*

- Gholobova D, Mackova K, Desender L, Carpentier G, Terrie L, Gerard M, Hympanova L, Deprest J, Thorrez L (2019). Functional evaluation of prevascularization in one-stage versus two- stage tissue engineering approach of human bio-artificial muscle. *Biomaterials* (submitted).

- Gholobova D, Terrie L, Gerard M, Thorrez L (2019) Vascularization of tissue-engineered skeletal muscle constructs. *Biomaterials* (submitted).

Oral presentations

- Human bio-artificial muscle as preclinical *in vitro* model

  BSTE 2016, April 14 – 15, Leuven, Belgium

- Comparison of tissue-specific microvascular endothelial cells to HUVECs for skeletal muscle tissue engineering

  BSTE 2017, May 4 – 5, Leuven, Belgium

Poster presentations

- Endothelial network formation within human tissue-engineered skeletal muscle
  BSTE 2015, March 19 - 20, Leuven, Belgium
  ESAO 2015, September 4th, Leuven, Belgium
- Vascularization of human bio-artificial muscles (BAM)
  TERMIS 2017, June 26 – 30, Davos, Switzerland
  BSTE 2018, November 24th, Ghent, Belgium
- Vasculogenic properties of HUVECs versus micro-vascular endothelial cells in skeletal muscle tissue engineering
  BSTE 2018, November 24th, Ghent, Belgium
- Human tissue-engineered skeletal muscle: a novel 3D in vitro model for drug disposition and toxicity after intramuscular injection
  BSTE 2018, November 24th, Ghent, Belgium

Travel grants

- FWO travel grant (transport)
  Awarded for the poster presentation at TERMIS 2017, Davos, Switzerland

- ASL travel grant (transport)
  Awarded for the poster presentation at TERMIS 2017, Davos, Switzerland

Contribution to teaching

Courses

- Histology practical sessions (B-KUL-U02E6A)
  2014-2019

- Osteology practical sessions (B-KUL-U01E0A)
  2014-2019

Guidance master students

Master in Sciences - Biomedical Sciences

- Skeletal muscle tissue engineering: *in vivo* evaluation of a prevascularization strategy and exploration of novel synthetic scaffolds (Lisanne Terrie)
  09.2017 - 06.2018

Guidance bachelor students

Bachelor in Sciences - Biotechnology

- Isolatie en karakterisatie van humane myoblasten (Kimberly Vandaele)
  02.2015 – 06.2015
- Evaluatie van samenstellende componenten voor spierweefsel engineering (Joyce Vanderveken)
  02.2016 – 06.2016
- Vascularisatie van bioartificiële spieren (Stijn Maes)
  02.2017 – 06.2017
- Karakterisatie technieken van bioartificiële spieren (Stijn Desnijder)
  02.2017 – 06.2018

Guidance summer interns

- Gael Vermeersch 2015
- Anke Vandekeere 2016
- Eline Declerk 2016
- Laurens Willaert 2017 & 2018
- Lisa Dewitte 2017
- Rune Peyskens 2018

Acknowledgments / Dankwoord

Na een intensieve periode van 4 dikke jaren is het zover. Met het schrijven van dit dankwoord leg ik de laatste hand aan mijn scriptie. Het was een periode waarin ik veel heb geleerd, op wetenschappelijk gebied, maar ook op persoonlijk vlak. Ik wil graag stil staan bij de mensen die mij de afgelopen periode enorm hebben gesteund en geholpen.

Eerst en vooral wil ik Lieven en Melanie bedanken. Jullie hebben me de kans gegeven om te doctoreren en hebben me doorheen mijn thesis jaren veel steun geboden. Lieven, bedankt om steeds zo toegankelijk te zijn. Menig malen op een dag, soms op een uur, sprong ik binnen op je bureau om snel advies te vragen rond een experiment, feedback te krijgen of je te doen herinneren aan bepaalde deadlines. Steeds werd ik met een welkom gevoel ontvangen, af en toe gepaard gaand met een chocolaatje of een nootje. Je enthousiasme voor het onderzoek rond spier weefselengineering is besmettelijk. Veel succes nog met je carrière en het onderzoek. Melanie, bedankt om er steeds te zijn. Ik kon menigmaal op je rekenen, op je uitgebreide kennis, je ervaringen. Ook als het even niet meezat kon ik bij je terecht en zochten we samen naar oplossingen. De micro-injecties, die zullen me zeker bijblijven, lachen met de miserie is toch fijn. Ook aan jou nog veel geluk gewenst aan de Kulak, met Hans en de kindjes.

Verder zou ik Prof. dr. Annaert, Pieter, willen bedanken voor de fijne en opbouwende samenwerking omtrent de micro-injecties, de jaarlijkse collageen bevoorrading en de interesse. Daaruit is een mooie publicatie gevloeid. I would also like to thank Prof. dr. Sampaolesi, Maurilio, for the valuable suggestions and the instructive experience during the meetings in Leuven.

Verder wil ik de leescommissie, Prof. dr. De Bock, Prof. dr. Vereecke, Prof. dr. Van Oosterwyck en dr. Declercq bedanken voor het uitvoerig lezen van de thesis, voor de uitvoer van de belangrijke taak om dit proefschrift te beoordelen en menig opbouwende tips te geven. Mede door jullie snelle actie en adequate feedback heb ik deze thesis tot een mooi einde kunnen brengen. Evenzeer dank ik jullie om hier allen aanwezig te zijn. Ook Prof. Simon De Meyer, dank ik om hier vandaag als voorzitter aanwezig te zijn.
Ook zou ik graag mijn interne juryleden, Evie en Hans, willen bedanken om er steeds aanwezig te zijn op de kritieke momenten. Jullie hebben mijn doctoraat kunnen opvolgen doorheen de jaren en hebben dit telkens opnieuw gedaan met nuttige feedback en helpvolle suggesties. In

het specifiek zou ik Evie nog willen bedanken, om me deel te laten uit maken van het ‘Anatomie-team’, met allemaal heel fijne mensen en studenten.

Verder zou ik mijn lieve collegaatjes willen bedanken voor de sfeer en gezelligheid. Elise en Faes, het olijke duo van de Anatomie. Menig maal hebben jullie me tot tranen toe doen lachen. Jullie inzichten in het leven waren zeker geestverruimend. Niemand bleef gespaard, inclusief mezelf: ahum, 8 km lopen voor de eerste maal met serieuze hellingen met Faes; de ongevraagde stijladviezen en de ‘good girl, gone bad’- invloed. Altijd lachen! Faes, ik wens je super veel succes toe in de States, jammer dat je er niet bij kan zijn. Elise, ik wens je nog veel liefde toe met je kindjes en Ines, and don’t stop wearing AcTiVeWeAr. Bedankt ook Timo, Marie en Maarten voor de gezellige babbeltjes en advies. Ik wens jullie dan ook veel succes toe met jullie doctoraat. Merci jongens, om me op te nemen in jullie leuk team! Vincent, meermaals heb je me door paar dalletjes weer boven geholpen. Steeds met een luisterend oor en een grapje, die ik wel niet altijd begreep, kon ik bij je terecht. ’t Beste met Tine en veel plezier op jullie trouw. We drinken er nog één op! Mijn burogenootje, Joke, merci voor de vele gesprekken over het leven. Jouw hulpvaardigheid is een heel mooie eigenschap. Liesbeth, de eerste keer dat we elkaar zagen was in het ‘bokaal’, en het zag er niet al te goed uit voor je. Mercikes, voor je wijze raad en daad. Lisanne, wat een fijne thesis studente was je, een droom voor elke begeleider. Zo ijverig en volhardend. Verlies die motivatie niet, en je zal nog grootse dingen bereiken. Bedankt voor je hulp met de initiële proefdierexperimenten. Ik wens je het allerbeste toe. Bedankt Linda, voor de nauwe samenwerking. Je eindeloze liefde voor weefselcoupes, heeft me heel erg geholpen. Sandrine, bedankt voor de fijne babbels. Dat koffietje in Gent, heb je nog tegoed! Eva, bedankt voor de gezellige pizzalunches en je oprechte goedheid. Kulak moet je koesteren. Ester, Christele en Sigrid, bedankt om alles in goede banen te houden en dat ik steeds terecht kon voor bestellingen, praktisch advies en het veranderen van de lessenrooster. Erly, bedankt voor de fijne quizz-avonden. Bedankt Hans voor je adviezen, de verhalen over het bedrijfsleven en om mij een paar nieuwe inzichten te doen verwerven over de politiek van universiteiten. Bedankt aan Charlotte, Elien, Petra en Celine voor de gezellige lunches in ’t zonnetje en om te dromen van wilde plannen voor onze cafetaria. Kostas, thank you for being such a tolerable desk mate, your silly jokes and funny stories. Alireza, thank you for learning me more about the Islamic culture and customs. Bedankt ook aan alle overige collega’s, Prof. dr. Dewaele, Prof. dr. Callewaert, Jasper, Felipe, Cien, Maarten (Mees), Jonas, Caroline, Alican, Salvatore, Ann-Sophie, Lore, Gertrude, Katleen, Elodie, Prof. Dudal, Bert voor de leuke sfeer binnen de Geneeskunde en het IRF.

Furthermore I would like to thank the many people, who made this research possible. I would like to express my sincere gratitude towards Gilles. Your analyses were of great value for my research. I really enjoyed to practice my French as well. Merci beaucoup! I would also like to thank Prof. dr. Deprest, for the opportunity to collaborate regarding *in vivo* studies. Thank you, Lucie and Katerina for your insights and the help during *in vivo* experiments. Ook bedankt aan alle medewerkers, Stephanie, Marleen en Erna in het bijzonder, van de dierenfaciliteit te Gasthuisberg voor de vele tips en hulp. Ook oprechte dank aan Prof. dr. Luttun en Sander voor jullie tijd en de opleiding Laser Doppler imaging. Verder wil ik graag de mensen aan AZ Groeninge, Prof. dr. Callewaert en dr. Katleen Croes willen bedanken voor het meten van de micro-injectie stalen. At last, thank you Prof. dr. Vandenburgh for the critical reading of all my papers and the suggestions.

Liefste vriendinnetjes, wat zou ik een humeurig persoontje geweest zijn zonder jullie goede zorgen en eindeloos plezier. Margaux en Eveline, topvriendinnen zijn jullie. Na een weekendje weg met jullie, was ik weer helemaal opgeladen. Dit BMW verhaal ben ik gestart met Jits, Irene, Laura en Mali. Alle steun van de wereld krijg ik van jullie, bedankt ervoor. Isa, jij bent één en al brok vrolijkheid, alle zorgen en cellen van de wereld kon ik vergeten met jou op stap. Emke, Lee, Eva, Lolo de voorbije jaren zijn jullie hartsvriendinnen geworden, ik zou niet weten wat te doen zonder jullie toewijding, overheerlijke dinertjes en amusement. De boykes, Alex, Otto, RJ, Emiel wat hebben we een geluk met zo gekke, toegewijde vrienden. Ook Marco en Arthur staan er altijd voor ons klaar! Ook zou ik graag Rein willen bedanken voor het openstellen van zijn collectie etsen, met een prachtige cover tot resultaat. Thank you, Hanns, for your kindness and beautiful artwork.

De allerbelangrijkste mensen moet ik nog bedanken. Hadden mijn ouders er niet geweest om me van mijn impulsieve ideeën te behoeden, was ik nu olifanten feces aan het rapen in de zoo van Antwerpen. Bedankt mama en papa voor alle goede raad, het meegeven van volharden tot het einde en alle liefde. Liefste broer, ik geniet heel veel van onze wandelingetjes met de nodige gezever en het filosoferen. Wat een beetje frisse lucht kan doen.

En allerlaatst dit eindwerk was niet mogelijk zonder de steun en het begrip van mijn grootste fan, Greg. Je maakt het allemaal zoveel gemakkelijker en betekent veel voor me. Het waren drukke tijden, het doctoraat buiten beschouwing genomen, maar zoals altijd valt alles mooi in de plooi en ben ik niet enkel een diploma rijker (laten we toch hopen), maar ook een hond, een huis en een getrouwde man. Je motiveert en inspireert.
Dacha

Personal contributions

The doctoral thesis was written by Dacha Gholobova, and corrected by the promoter Prof. Dr. Lieven Thorrez, and co-promoters Prof. Dr. Pieter Annaert and Prof. Dr. Maurilio Sampaolesi.

All experiments were performed by the PhD candidate with technical support from Dr. Melanie Gerard (microinjection, spectrophotometric analysis and statistics) and lab technician Linda Desender (histology, RNA isolation, spectrophotometric analysis). All other contributions are mentioned in the acknowledgments section of each chapter.

The data published in the journal 'Tissue Engineering part A' were generated and written by the PhD candidate together with Dr. Lieselot Decroix and with the support and feedback from the co-authors.
The data published in the journal 'Scientific Reports' were generated and written by the PhD candidate together with Dr. Melanie Gerard and with the support and feedback from the co-authors.
The data submitted in the journal 'Biomaterials' were generated and written by the PhD candidate and with the support and feedback from the co-authors.
The review submitted in the journal 'Biomaterials' was written by the PhD candidate with support from the co-authors and corrected by the senior author.
The book chapter published in 'Methods in Molecular Biology' was written by the PhD candidate with support from the co-authors.
For the cover image an etching of Hanns Schimansky was used. Written permission from the artist was granted.

Images without citations were made by the PhD candidate. Images with citations were adapted from the cited paper.